

A person wearing a white lab coat and white gloves is holding a rectangular soil sample. The background is a laboratory setting with various pieces of equipment, including a large metal frame. The image is partially covered by an orange diagonal shape in the bottom-left corner.

CIVIL ENGINEERING, SCIENCE AND TECHNOLOGY CHALLENGES: GEOTECHNICAL AND GEOENVIRONMENTAL ENGINEERING

EDITED BY

**WAN HASHIM WAN IBRAHIM
SITI NOOR LINDA TAIB
NORSUZAILINA MOHAMED SUTAN**

**CIVIL ENGINEERING, SCIENCE AND
TECHNOLOGY CHALLENGES:
GEOTECHNICAL AND GEOENVIRONMENTAL
ENGINEERING**

© Wan Hashim Wan Ibrahim, Siti Noor Linda Taib, Norsuzailina Mohamed Sutan

2022

All rights reserved. No part of this publication may be reproduced, stored in a retrieval system, or transmitted, in any form or by any means, electronic, mechanical, photocopying, recording or otherwise, without the prior permission of the publisher.

Published in Malaysia by
UNIMAS Publisher,
Universiti Malaysia Sarawak,
94300 Kota Samarahan,
Sarawak, Malaysia.

Perpustakaan Negara Malaysia

Cataloguing-in-Publication Data

CIVIL ENGINEERING, SCIENCE AND TECHNOLOGY CHALLENGES: GEOTECHNICAL AND GEOENVIRONMENTAL ENGINEERING / EDITED BY WAN HASHIM WAN IBRAHIM, SITI NOOR LINDA TAIB, NORSUZAILINA MOHAMED SUTAN.

Mode of access: Internet

e ISBN 978-967-2298-94-6

1. Geotechnical engineering.
2. Environmental geotechnology.
3. Government publications--Malaysia.
4. Electronic books.

I. Wan Hashim Wan Ibrahim. II. Siti Noor Linda Taib.

III. Norsuzailina Mohamed Sutan.

624.151

The book is based on scientific and technological advances in various Geotechnical and Geoenvironmental Engineering areas of Civil Engineering. It nurtures therefore the exchange of discoveries among research workforces worldwide including those focusing on the vast variety of facets of the fundamentals and applications within the Geotechnical and Geoenvironmental Engineering area. To offer novel and rapid developments, this book contains original contributions covering theoretical, physical experimental, and/or field works that incite and promote new understandings while elevating advancement in the Geotechnical and Geoenvironmental Engineering fields. Works in closing the gap between the theories and applications, which are beneficial to both academicians and practicing engineers, are particularly of interest to this book that paves the intellectual route to navigate new areas and frontiers of scholarly studies in Geotechnical and Geoenvironmental Engineering area.

CIVIL ENGINEERING, SCIENCE AND TECHNOLOGY CHALLENGES: GEOTECHNICAL AND GEOENVIRONMENTAL ENGINEERING

Editors in Chief

Wan Hashim Wan Ibrahim
Siti Noor Linda Taib
Norsuzailina Mohamed Sutan

Editors

Raudhah Ahmadi
Idawati Ismail
Abdul Razak Abdul Karim
Azida Rashidi
Delsye Teo Ching Lee
Mohd Raduan Kabit
Mohammad Ibrahim Safawi bin Mohammad Zain
Ahmad Kueh Beng Hong
Mohammad Abdul Mannan
Ng Chee Khoo
Leonard Lim Lik Pueh
Alsidqi Hasan
Charles Bong Hin Joo
Mah Yau Seng
Norazzlina bt M. Sa'don

Advisory Editors

Vishwas A Sawant
Prabir Kolay
Bishwajit Bhattacharjee
Sanjeev Kumar
Marlinda Bte Abdul Malek
Megat Azmi Megat Johari
Zainah Ibrahim
Mohd Saleh Jaafar
Farah Nora Aznieta Abd. Aziz
Fadzli Mohamed Nazri
Ahmad Baharuddin Abd.Rahman
Md. Habibur Rahman Sobuz

Copy Editors/Proofreaders

Chuah Kee Man
Zayn Al-Abideen Gregory
Helmy Hazmi
Annisa Jamali

Layout Editor

Freddy Yeo Kuok San
Rose Sima Anak Ikau

TABLE OF CONTENTS

CHAPTER	TITLE OF CHAPTERS	PAGE NO
1	Predicting Hydraulic Conductivity (k) of Tropical Soils by using Artificial Neural Network (ANN)	1
2	Peat Stabilization with Carbide Lime	7
3	Catchment Size, Soil Type and Land Use to Determine the Amount and Likelihood of Flood in the Sarawak Corridor of Renewable Energy (SCORE) Region	13
4	A Review of Soil Nailing Design Approaches	19
5	Geotechnical Properties of Fly Ash and its Application on Soft Soil Stabilization	26
6	Peat Stabilization using Gypsum and Fly Ash	32
7	Soil Erosion and Sediment Yield of a Sanitary Landfill Site – A Case Study	38
8	A Study on Factors Influencing the Determination of Moisture Content of Fibrous Peat	50
9	Stabilization of Indian Fly Ashes with Soils, Cement, and Randomly Oriented Fibers	59
10	Study of Soil Erosion at a Site Near Chemical Engineering Laboratory in UNIMAS	62
11	Strength And Durability Effect On Stabilized Subgrade Soil	68
12	Analysis Of Combined Footings On Extensible Geosynthetic Stone Column Improved Ground	79
13	Assessment Of Soil Erosion By Simulating Rainfall On An Equatorial Organic Soil	95
14	Comparison Of The Behavior Of Fiber And Mesh Reinforced Soils	105
15	Uplift Capacity Of Single And Group Of Granular Anchor Pile System	111
16	Refinement Of Topographical Factor For Estimating Soil Loss And Sediment Yield In Equatorial Regions	118
17	Effect Of Wall Inclination On Dynamic Active Thrust For Cohesive Soil Backfill	138
18	Prediction Of California Bearing Ratio Of FineGrained Soil Stabilized With Admixtures Using Soft Computing Systems	143

CHAPTER 1

PREDICTING HYDRAULIC CONDUCTIVITY (k) OF TROPICAL SOILS BY USING ARTIFICIAL NEURAL NETWORK (ANN)

Lim, D.K.H¹. and Kolay, P.K².

Abstract

Hydraulic conductivity of tropical soils is very complex. Several hydraulic conductivity prediction methods have focused on laboratory and field tests, such as the Constant Head Test, Falling Head Test, Ring Infiltrometer, Instantaneous profile method and Test Basins. In the present study, Artificial Neural Network (ANN) has been used as a tool for predicting the hydraulic conductivity (k) of some tropical soils. ANN is potentially useful in situations where the underlying physical process relationships are not fully understood and well-suited in modeling dynamic systems on a real-time basis. The hydraulic conductivity of tropical soil can be predicted by using ANN, if the physical properties of the soil e.g., moisture content, specific gravity, void ratio etc. are known. This study demonstrates the comparison between the conventional estimation of k by using Shepard's equation for approximating k and the predicted k from ANN. A programme was written by using MATLAB 6.5.1 and eight different training algorithms, namely Resilient Backpropagation (rp), Levenberg-Marquardt algorithm (lm), Conjugate Gradient Polak-Ribière algorithm (cgp), Scale Conjugate Gradient (scg), BFGS Quasi-Newton (bfg), Conjugate Gradient with Powell/Beale Restarts (cgb), Fletcher-Powell Conjugate Gradient (cgf), and One-step Secant (oss) have been compared to produce the best prediction of k . The result shows that the network trained with Resilient Backpropagation (rp) consistently produces the most accurate results with a value of $R = 0.8493$ and $E^2 = 0.7209$.

Keywords: Tropical Soils, Hydraulic Conductivity, Artificial Neural Network (ANN)

1. INTRODUCTION

Soils are extremely heterogeneous and the magnitude of its hydraulic conductivity is very complex. In general, the hydraulic conductivity of the soil depends on several factors, including the particle size, porosity and the bulk density of the soil. Hydraulic conductivity of soils is divided into saturated hydraulic conductivity, k_s , and unsaturated hydraulic conductivity, k_u . It is measured in horizontal permeability, k_H and vertical permeability, k_V . Overall permeability is then then obtained by

$$k = \sqrt{k_H \cdot k_V} \quad (1)$$

Many hydraulic conductivity prediction methods have focused on correlations with laboratory and field tests, such as Constant Head Test, Falling Head Test, Ring Infiltrometer, Instantaneous profile method and Test Basins [1]. Field test gives advantages as the soil profile is often undisturbed but we are unable to control the soil environment. For laboratory tests, obtaining an undisturbed sample is difficult but we could test the soil in a controlled environment. However, most of the available methods are restricted by simplification of the problem by incorporating several assumptions for the factors that determine the hydraulic conductivity of the soil. Sometimes, these methods are quite costly as well.

There were several attempts to predict the hydraulic conductivity of soils from its physical characteristics in the literature. Cronican and Gribb produced equations for predicting hydraulic conductivity based on grain-size data [2]. Nemati et al. came out with another method to predict hydraulic conductivity changes from aggregate mean weight diameter based on the study of the decrease in mean weight diameter of aggregates exposed to different rates of wetting [3]. Poulsen et al. did a study on predicting saturated and unsaturated hydraulic conductivity in undisturbed soils from soil water characteristics [4]. Each of these methods is of great practical importance, because it permits the prediction of the hydraulic conductivity of the soil, without conducting field and or laboratory tests. It seems, however, that very few universally accepted methods that have been proposed for predicting the hydraulic conductivity of the soil.

1 Student, Department of Civil Engineering, Faculty of Engineering, Universiti Malaysia Sarawak, Sarawak, Malaysia, godspilla@gmail.com

2 Senior Lecturer, Department of Civil Engineering, Faculty of Engineering, , Universiti Malaysia Sarawak, Sarawak, Malaysia, kkprabir@feng.unimas.my or, pkolay2001@yahoo.com,

Hydraulic conductivity of soils (k) can be determined for various types of soils. Several equations are available by various researchers [5-9] for calculating the k from the physical properties of the soil.

Hydraulic conductivity prediction is one of the most challenging geotechnical engineering problems because a considerable level of uncertainty often affects it which in turn influences designs. Several researchers [4, 10-13] have predicted hydraulic conductivity by considering different uncertainty parameters, neural networks, analytical methods, regression analysis and simplified methods.

Each soil has unique properties that differentiate it from the others. An estimation of the hydraulic conductivity (k) by using tests in laboratory takes long time and also sample disturbance may occur while conducting the test. In that situation, Artificial Neural Network (ANN) is potentially useful, where the underlying physical process relationships are not fully understood and well-suited in modelling dynamic systems on a real-time basis, for predicting the hydraulic conductivity characteristics of the soft soil. The hydraulic conductivity characteristics of the tropical soils can be predicted by using ANN, if the physical properties of the soils are known. It will be much more convenient and economical compared to even laboratory tests for calculating and predicting the hydraulic conductivity characteristics of tropical soils. Hence, in this paper an attempt has been made to predict the hydraulic conductivity of tropical soils by using ANN.

2. ARTIFICIAL NEURAL NETWORK (ANN)

Artificial neural network (ANN) is a form of artificial intelligence (AI), which attempts to simulate the biological structure of the human brain and nervous system in their architecture. The key element of this paradigm is the novel structure of the information processing system. It is composed of a large number of highly interconnected processing elements (neurons), working together to solve a particular problems. Like human beings, ANNs also learn by example. An ANN is set for a specific application, such as pattern recognition or data classification, through a learning process.

There are various sorts of artificial neural networks which differ in their functions, such as data prediction, data classification, data association, data conceptualization, and data filtering. The common type of ANN consists of three interconnected layers: input layer, hidden layer and output layer. Multi-layered networks use a variety of learning techniques; the most popular is back-propagation. In this method, the output values are compared with the correct answer to compute the value of some predefined error-functions. By various techniques, the error is then fed back through the network. Using this information, the algorithm adjusts the weights of each connection in order to reduce the value of the error function by some small amount.

Back-propagation networks are probably the most well known and widely applied of the neural networks today. In essence, the back-propagation network is a perceptron with multiple layers, a different threshold function in the artificial neuron, and a more robust and capable learning rule. ANNs do not have any prior knowledge about the existing problem. Therefore, training is required to make the network more intelligent. The ANN is trained with a set of input and known output pairs known as the training set. At the beginning of the training process, the network is initialised with the data provided from the laboratory. The weights are optimised to gain a specific response from the ANN. The process of optimisation or training is essential in ANN models. This is because when these weights are modified, data transfer through the ANN changes and the overall network performance alters.

The most important step in designing an ANN is the determination of the ANN architecture and the selection of the training algorithm. An optimal architecture is able to obtain good performance with minimal resulting errors. It must also retain a simple and compact structure.

No unified theory exists to determine which optimal architecture best suits a project and very often, more than one ANN can produce similar results. The numbers of input and output nodes are problem dependent. The main problem is the difficulty in selecting the number of hidden layers and in assigning the number of nodes to each of these layers. A trial-and-error procedure is generally adopted to determine the optimal architecture.

3. APPLICATION OF ANN IN GEOTECHNICAL ENGINEERING

Over the past decades, ANNs have been applied to various geotechnical engineering applications. For example, Lee and Sterling produced a neural network for identification of probable failure modes for underground openings from prior case history information [14]. Besides that, Penumadu et al. have attempted to model the stress-strain behaviour of clays, incorporating rate dependant behaviour [15]. Lee and Lee study utilised neural networks to predict the ultimate bearing capacity of piles [16]. Sivakugan et al. studied the possibility of using neural networks to predict the settlement of shallow foundations on granular soils [17]. Kolay et al. have used a back-propagation method for neural networks in predicting settlement of tropical soft soil [18]. Apart from that, there was also involvement of ANNs in seismic liquefaction assessment [19].

Several researchers, as mentioned above, have studied the different aspects in geotechnical engineering by using ANN modelling. However, the application of ANN in predicting the hydraulic conductivity of tropical soils in Sarawak, Malaysia is not available. Thus, the present study concentrates on predicting the hydraulic conductivity of tropical soils by using ANN programming.

4. METHODOLOGY

In this research, 8 different MATLAB 6.5.1 training algorithms have been applied to the network, namely Resilient Backpropagation (rp), Levenberg-Marquardt algorithm (lm), Conjugate Gradient Polak-Ribière algorithm (cgp), Scale Conjugate Gradient (scg), BFGS Quasi-Newton (bfg), Conjugate Gradient with Powell/Beale Restarts (cgb), Fletcher-Powell Conjugate Gradient (cgf), and One-step Secant (oss). Every training algorithm has its own special characteristics towards the network and differs in its simulated results.

In any training algorithm, the aim is to reduce the global error, E which is defined as

$$E = \frac{1}{P} \sum_{p=1}^P E_p \quad (2)$$

Where, P = total number of training patterns; and E_p = error for training pattern, p

$$E_p = \frac{1}{2} \sum_{k=0}^N (o_k - t_k)^2 \quad (3)$$

Where, N = total number of output nodes; o_k = network output at the k th output node; and t_k = target output at the k th output node.

In the present study, feed-forward back-propagation neural network with 1 hidden layer is utilised for data prediction. The network was trained using 8 different patterns of back-propagation algorithms. A different number of neurons in the hidden layer of the neural network will result in a different simulated result. Therefore, in this study, 2, 4, 6, 8, 10, 20, and 30 neurons have been used in the program. Learning rates were also applied to the network so that a better training could be achieved. The training rates of the networks examined are 0.01, 0.03, 0.05, 0.07, and 0.09.

MATLAB 6.5.1 is utilised in training and simulation of data. The parameters that have been investigated and analysed are (a) Number of neurons in the hidden layer; (b) Learning algorithms; (c) Learning rates.

The performances of the networks were measured by coefficient of correlation, R , and coefficient of efficiency (Nash-Sutcliffe equation), E^2 . Value of R is given by the following equation:

$$R = \frac{\sum_{i=1}^{i=n} [Q_m(t_i) - \overline{Q_m(t_i)}][Q_s(t_i) - \overline{Q_s(t_i)}]}{\sqrt{\sum_{i=1}^{i=n} [Q_m(t_i) - \overline{Q_m(t_i)}]^2 \sum_{i=1}^{i=n} [Q_s(t_i) - \overline{Q_s(t_i)}]^2}} \quad (4)$$

Where, subscript m and s represent the observed and simulated C_c respectively while $\overline{Q_m}$ and $\overline{Q_s}$ are average of the observed and simulated C_c . Nash-Sutcliffe coefficient, E^2 is expressed as:

$$E^2 = 1 - \frac{\sum_{i=1}^{i=n} [Q_m(t_i) - Q_s(t_i)]^2}{\sum_{i=1}^{i=n} [Q_m(t_i) - \overline{Q_m}]^2} \quad (5)$$

It should be noted that an R and E^2 value of 1.0 implies a perfect fit.

Disturbed and undisturbed soil sample data from boreholes were collected from Geospec Sdn. Bhd., Kuching, Sarawak, Malaysia. A total of 144 sample data were used to calculate the hydraulic conductivity of the soil. The most important property of soil for indirectly determining the hydraulic conductivity, k , is the D_{10} value from the particle size distribution graph. Hence in this study, the hydraulic conductivity values have been deduced from the empirical formula given by Shepherd [9].

5. RESULTS AND DISCUSSION

There are a few important parameters, which contributes to the value of k of the samples, which are moisture content (w), bulk density (Mg/m^3), dry density (Mg/m^3), void ratio (e), liquid limit (%), plastic limit (%), gravel (%), sand (%), silt (%) and clay (%) and hydraulic conductivity (cm/s).

These parameters have been used in training and testing of the ANN models. Firstly, 100 data values have been used to train the network and the remaining 44 data have been used for testing purposes. The following parameters were analysed and the results are as follows:

Table 1 shows different learning algorithms and their efficiencies. It can be observed from Table 1 that the coefficient of correlation R of testing for rp is the highest, with a value of 0.8493. Observing from the variation of R and E^2 values of training, R and E^2 are correlated to each other. A higher R value will contribute to a higher E^2 value. Observing the value of E^2 , rp also has the highest value with 0.7209. Therefore, it can be concluded that the rp algorithm yields the best model.

Table 1. Correlation values of different algorithms with 5000 epochs, 10 neurons in the hidden layer and learning rate 0.03

Training Algorithm	Testing	
	Coefficient of Correlation, R (testing)	Coefficient of Efficiency, E^2 (testing)
<i>rp</i>	0.8493	0.7209
<i>lm</i>	0.7140	0.4836
<i>cgp</i>	0.6988	0.2679
<i>scg</i>	0.6952	0.2081
<i>bfg</i>	0.6988	0.4682
<i>cgb</i>	0.6988	0.4630
<i>cgf</i>	0.6988	0.3624
<i>oss</i>	0.2618	0.0198

The overall performances of the 8 training algorithms are with respect to the training and testing coefficients. rp is the training algorithm that yields the best result. The oss algorithm performs poorly and produced the least accurate results in training and testing.

The aim of this study is to find out the optimum number neurons that best suit the network. Figures 1(a) and 1(b) show the performance of R testing and E^2 testing for networks with epoch 5000 and learning rate 0.03. As observed from Figure 1(a) and 1(b), low number of neurons may lead to lesser precision of simulated results because like human being, neural network learns by example. Therefore, the larger the number of neurons is “equal” to more people giving feedbacks to the network. This phenomenon creates a network with more learned examples and increases the precision of the simulated results. As of this, number of neurons of 8, 10, 20 and 30 will be more suitable because they perform consistently above 50%.

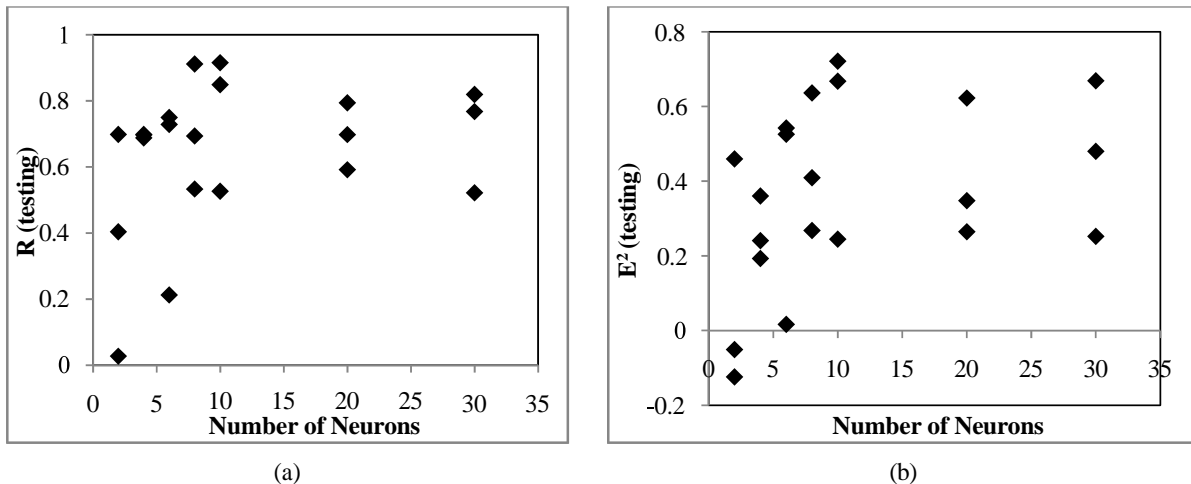


Figure 1. Performance of neural networks in (a) R for testing and (b) E^2 for testing using trainrp, with epoch 5000 and learning rate 0.03

The ratio of R testing ranges from 0.03 to 0.91 whereas, the ratio of E^2 testing ranges from -0.12 to 0.72. Comparing both R testing values and E^2 testing values, we can deduce that the efficiency of E^2 is lower. The number of neurons which perform at higher efficiency of E^2 testing will be the suitable for this network. As observed from Figure 1(a) and 1(b), number of neurons of 10 gives the highest percentage in E^2 testing. Therefore, 10 neurons will be suitable for this network.

Learning rates are utilized in the network to ensure a better training algorithm. Figure 2 compares the performance of different learning rates with number of neurons. Generally, different learning rates do not contribute to any significant differences in training and testing of the network. The larger the learning rate, the bigger the step. However, if the learning rate is set too high, the algorithm may oscillate and become unstable. If the learning rate is too small, the algorithm will take too long to converge. In this study, most learning rates are able to converge in simulating the networks. Learning rate of 0.01, 0.03, 0.05, 0.07 and 0.09 shows a wide range of R values from 0.21 to 0.92. Out of these values, learning rate of 0.03 is most suitable as it produces the highest R value of 0.92. Figure 3 shows the results of simulated and calculated hydraulic conductivity, k , values trained with *trainrp*.

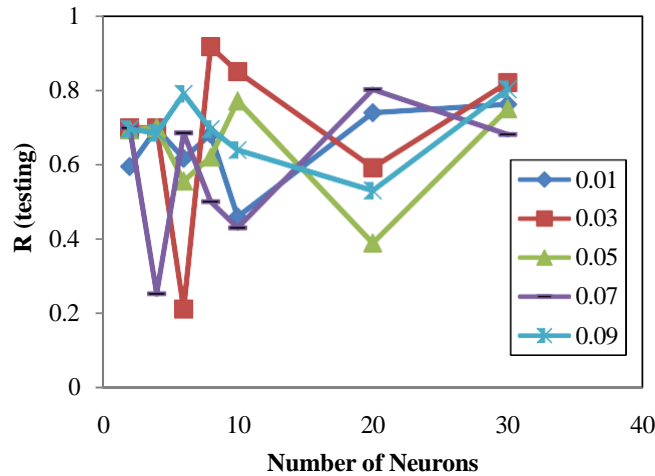


Figure 2. Testing of data according to learning rate.

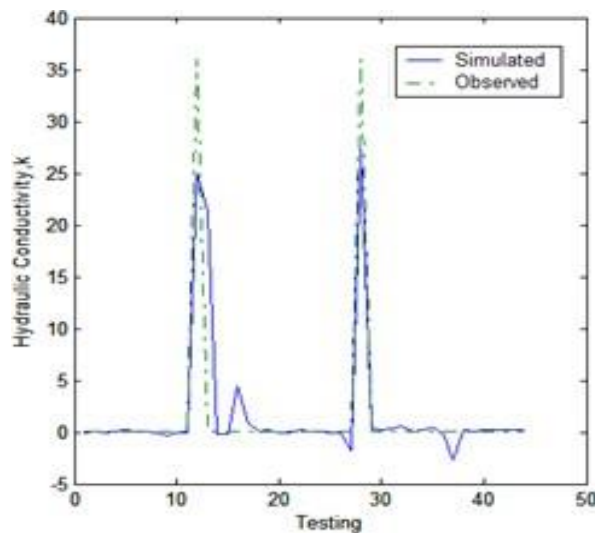


Figure 3. Comparison between simulated and calculated hydraulic conductivity, k trained with *trainrp*.

6. CONCLUSIONS

In this study an attempt has been made to predict the hydraulic conductivity (k) of tropical soils using the neural network simulation based on the geotechnical properties of various soil types from different borehole testing data. Based on the neural network simulated by MATLAB 6.5.1, the following conclusions can be made:

- i. Network trained with Resilient Backpropagation algorithm (*trainrp*) consistently simulates the most precise result. Networks trained with One-step Secant (*trainoss*) algorithm simulate the results with least accurate precision.
- ii. A simulation with a bigger number of neurons in the hidden layer shows a better result than simulation with a lower number of neurons.
- iii. Different learning rates do not contribute to any significant differences in training and testing of the network. Most values of the learning rates are able to converge in simulating the networks.

ACKNOWLEDGMENT

The authors are thankful to Mr. Kelvin Huong Tuong Yu, General Manager of Geospec Sdn. Bhd., and Miss Wong for allocating time and providing invaluable borehole data. The authors also thank Bustami, R.A. and Hong, C.C.C. Faculty of Engineering, UNIMAS for their help.

REFERENCES

- [1] Das, B.M. "Principles of Foundation Engineering", 5th Edition, Brooks/Cole. 2004, United States.
- [2] Cronican, A.E. and Gribb, M.M. "Hydraulic Conductivity Predicting for Sandy Soils", *Ground Water*, Vol. 42, No. 3, 2004, pp. 459-464.
- [3] Nemati, M.R., Caron, J. and Gallichand, J. "Predicting hydraulic conductivity changes from aggregate mean weight diameter", *Water Resources Research*, Vol. 38, No. 9, 2002, 1170.
- [4] Poulsen, T.G., Moldrup, P., Yamaguchi, T. and Jacobsen, O. H. "Predicting saturated and unsaturated hydraulic conductivity in undisturbed soils from soil water characteristics", *Soil science*, Vol.164, No. 12, 1999, pp. 877-887.
- [5] Darcy, H. *Les Fontaines Publiques de la Ville de Dijon*, 1856, Paris.
- [6] Richards, L.A. "Capillary conduction of liquids through porous media", *Physics*, Vol. 1, 1931, pp. 318-333.
- [7] Samarashinghe, A.M., Huang, Y.H., and Drnevich, V.P. "Permeability and Consolidation of Normally Consolidated Soils," *Journal of the Geotechnical Engineering Division, ASCE*, Vol. 108, No. GT6, 1982, pp. 835-850.
- [8] Tavenas, F., Jean, P., Leblond, P., and Leroueil, S. "The Permeability of Natural Soft Clays, Part II: Permeability Characteristics," *Canadian Geotechnical Journal*, Vol. 20, No. 4, 1983, pp. 645-660.
- [9] Shepherd, R.G. "Correlations of permeability and grain-size", *Ground Water*, Vol. 27, No. 5, 1989, pp. 633-638.
- [10] Filz, G.M., Henry, L.B., Heslin, G.M., and Davidson, R.R. "Determining Hydraulic Conductivity of Soil-Bentonite Using the API Filter Press", *Geotechnical Testing Journal*, Vol. 24, Issue 1, 2001.
- [11] Gribb, M.M. and Gribb, G.W. "Use of Neural Networks For Hydraulic Conductivity Determination in Unsaturated Soil", *Proc. 2nd International Conference on Ground Water Ecology*, Atlanta (eds. Stanford, J.A., Valett, H.M.), Bethesda MD: Amer. Water Resources Assoc., 1994, pp. 155-163.
- [12] Najjar, Y.M. and Basheer, I.A. "Utilizing Computational Neural Networks for Evaluating the Permeability of Compacted Clay Liners", *Geotechnical & Geological Engineering*, Vol. 14, No. 3, 1996, pp. 193-212.
- [13] Boadu F.K. "Hydraulic Conductivity of Soils from Grain-Size Distribution: New Models", *J. Geotech. and Geoenviron. Engrg.*, Vol. 126, Issue 8, 2000, pp. 739-746
- [14] Lee, C. and Sterling, R. "Identifying Probable Failure Modes for Underground Openings using a Neural Network", *International Journal of Rock Mechanics and Mining Sciences & Geomechanics Abstracts*, Vol. 29, No. 1, 1992, pp. 49-67.
- [15] Penumadu, D., Jin-Nan, L., Chameau, J-L. and Arumugam, S. "Rate Dependant Behavior of Clays Using Neural Networks, Proc. 13th Conference of Int. Soc. Soil Mechanics and Foundation Engineering, New Delhi: New Delhi, Oxford & IBH Publ. Co., Vol. 4, 1994, pp. 1445-1448.
- [16] Lee, I. and Lee, J. "Prediction of Pile Bearing Capacity Using Artificial Neural Networks." *Computers and Geotechnics*, Vol. 18, No.3, 1996, pp. 189 - 200.
- [17] Sivakugan, N., Eckersley, J.D., and Li, H. "Settlement predictions using neural networks." *Australian Civil Engineering Transactions*, CE40, 1998, pp. 49-52.
- [18] Kolay, P.K., Bustami, R.A. and Ling, N.W. "Settlement Prediction of Tropical Peat Soil by Artificial Neural Network (ANN)", *12th International Association for Computer Methods and Advances in Geomechanics (IACMAG)*, Goa, 1-6 Oct 2008, pp. 1843-1849.
- [19] Goh, A.T.C. "Seismic Liquefaction Potential Assessed by Neural Networks", *Journal of Geotechnical Engineering - ASCE*, Vol. 120, No. 9, 1994, pp. 1467-1480.

CHAPTER 2

PEAT STABILIZATION WITH CARBIDE LIME

Said, J.M.¹, Taib, S.N.L.²

Abstract

Peat is in the category of problematic soil because it has low shear strength and high compressibility, which are not suitable for construction. Peat lands can be found in various parts of the world; therefore, it is essential to find an alternative to improve the strength since nowadays lands are very expensive and very limited. This paper presents a research on peat stabilization with objectives that are to improve the soil to be more stable and to have higher strength and to find a cheap alternative material that can be used as a stabilizing agent. In this research, an admixture, which is carbide lime, a by-product of acetylene is used to stabilize the peat soil. Laboratory tests on physical properties and shear strength are done. The research is done on peat soil that is collected from Matang area in Kuching, Sarawak. Investigation on the effects of various percentages of carbide lime added to the soil at different curing time on the soil strength is performed. The changes in strength gained are also compared with the natural soil sample. The unconfined compressive strength test results are analyzed and show that, with the increase of percentages of carbide lime added and the increase of curing time, the strength of the peat soil sample is increased.

Keywords: Peat stabilization, carbide lime, unconfined compressive strength

1. INTRODUCTION

Stabilization of soil is one of the most important criteria that should be considered for construction on soft soil. It is well known that stability of ground will affect the stability of the structure above it and there are many types of soil to deal with, depending on the area, its location, its surroundings and various other factors. Peat soil is an extremely soft soil and often referred to as problematic soil by engineers. Peat soil is not only soft, it is compressible too where this characteristic will lead to excessive settlement which is a very serious problem. There are about 2.7 million ha of peat and organic soils in Malaysia accounting for about 8% of the total land area of the country. In Sarawak, peat lands are in abundance and Sarawak has the largest area of peat in the country, covering about 1.66 million ha and constituting 13% of the state [1]. Today, lands are very expensive and very limited and due to this, constructions on peat soil cannot be avoided. Maintenance works on damages caused by peat soil would be the next arising problem if matters are not resolved and this can affect the safety of the occupants and can be costly. There are many researches on improving peat soil. The methods are mostly concentrating on modifying and stabilizing the soil. Stabilization of peat soil focuses on increasing the strength of this soft and highly compressible soil. It is done to improve the ability of the soil to perform well by increasing its strength and decreasing the excessive settlement when soil is subjected to loads. According to Jarrett (1997), peat soils experience instability and massive primary and long term consolidation settlements when subjected to even moderate load increases [2].

There are various methods of stabilization and one of them is using admixture. Different types of admixtures are available. Chemical admixtures or chemical stabilization always involve treatment of the soil with some kind of chemical compound, which when added to the soil, would result in a chemical reaction. The chemical reaction modifies or enhances the physical and engineering aspects of a soil, such as, volume stability and strength [3]. Replacing peat with good quality soil is still a common practice when construction has to take place on peat deposit even though most probably, this effort will lead to uneconomical design because it requires transportation of large amount of good quality soil. Hence, cheaper alternatives or cheaper improvement method is to be found. An admixture, which is carbide lime, a by-product of acetylene, and a stabilizer, is used in this research of peat soil stabilization.

2. OBJECTIVES OF THE RESEARCH

The main aim of conducting this study is to do stabilization of peat using admixture which is carbide lime. The specific objectives of this study are to stabilize peat soil and to improve the strength of peat soil.

¹Said, J.M., Student of Civil Engineering Department, Universiti Malaysia Sarawak (e-mail: fuzzypeach_03@yahoo.com)

²Taib, S.N.L., Senior Lecturer of Civil Engineering Department, Universiti Malaysia Sarawak (e-mail: linda@feng.unimas.my) (Corresponding Author)

3. EXPERIMENTAL WORK

The peat soil samples used in this study were collected from Matang area at a depth of approximately 0.25m – 0.30m below the ground surface. The laboratory works are divided into two categories, which are laboratory works that determine physical and compaction properties, and laboratory works, which test the strength of the peat soil. The former laboratory works are particle size analysis (sieve analysis), moisture content, degree of decomposition, specific gravity, compaction test (Standard Proctor Test) and organic, fiber and ash content. For the latter laboratory works, samples were oven dried, grinded and the samples passing sieve size 1.18mm were used for testing and mixing. Unconfined compressive strength test (UCS) was done to test the strength gained and to make strength comparison between peat soil without carbide lime and peat soil with different percentages of carbide lime, which are 3%, 6%, 9%, and 12% of total mixing weight. This test was conducted on the soil sample after curing period of 7, 14, and 28 days.

4. RESULTS AND DISCUSSION

Particle size analysis

Particle size analysis was done on both peat soil and carbide lime used in this study. The size distributions of peat soil particle and carbide lime particle that will be used in the mixing are analyzed. It is found that the distribution for Carbide Lime is similar to peat distribution for the same range of sieve size. No further hydrometer testing was performed on Carbide Lime as it is feared that hazardous reaction might occur with the reagent used for the hydrometer test. However, it was observed about 3.05 g of Carbide Lime passed through the smallest sieve size.

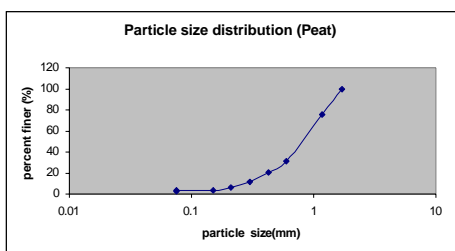


Figure 1 Particle size distribution of peat soil

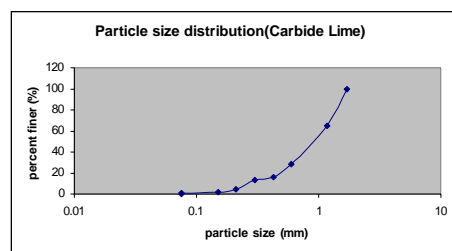


Figure 2 Particle size analysis of Carbide Lime

Moisture Content

There are three soil samples taken which are from the surface, middle and bottom parts respectively for 0.25-0.30 m depth. Each sample was prepared for three sets and average value was determined. The first collection results indicate that the moisture content increases proportional to the soil depth. Moisture content of soil for the first collection is higher for the second collection. This is because it was raining during the collection and the water table was high. Carbide Lime sample was collected from Eastern Oxygen Sdn. Bhd. factory. The carbide lime collected was in slurry form and the moisture content of it is 86.18%.

Table 1 Moisture content of soil (First collection)

Sample	Surface	Middle	Bottom
Moisture content (%)	472.99	517.50	785.87
Average Moisture content (%)	592.12		

Table 2 Moisture content of soil (Second collection)

Sample	Surface	Middle	Bottom
Moisture content (%)	415.54	393.40	529.21
Average Moisture content (%)	446.05		

Table 3 Moisture content of Carbide Lime

Sample	1	2	3
Moisture content (%)	84.17	86.00	88.38
Average Moisture content (%)	86.18		

Degree of Decomposition

Degree of decomposition of the soil is the measure of the organic remains that have decayed. Degree of decomposition of peat soil was done by referring to the Von Post scale that consists of 10 scales that are H1 to H10. In this study, the soil collected in Matang falls in the category of H5 and H6 that is hemic or moderately decomposed.

Specific Gravity Test

The specific gravity (G_s) of the highly organic or peat soil was determined based on the procedure stated in BS 1377: Part 2: 1990 [4]. In this test, specific gravity was measured using small pyknometer. For maintaining accuracy, the average specific gravity is obtained from the results of three tests. The soil must be heated to avoid entrapped air that will affect the results because of the test sensitivity. Two tests were done that is specific gravity (not heated) and specific gravity (heated) for comparison purpose. From the results, it can be concluded that the sample must be heated in order to obtain more accurate results.

Table 4 Specific Gravity (not heated)

Sample	1	2	3
Specific gravity	0.85	0.76	0.92
Average Specific gravity	0.84		

Table 5 Specific Gravity (heated)

Sample	1	2	3
Specific gravity	1.45	1.39	1.38
Average Specific gravity	1.41		

Compaction (Standard Proctor Test)

Compaction test or Standard Proctor test was conducted by referring to BS 1377-1990: Part 4 [4]. This is done to determine the maximum dry density (MDD) (γ_d) and the optimum moisture content (OMC) of the peat soil sample that will be used in the mixing. This test was done in three sets. The first test results could not give the expected dry density-moisture content curve. The problem was the soil used during compaction test was not totally dried. To overcome this problem, the soil was dried under the sun for 3 days until it was totally dried and the compaction test was repeated. In the first compaction test, particles larger than 1.18 mm were removed before testing.

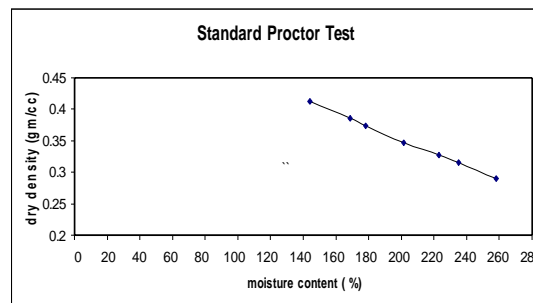


Figure 3 Standard Proctor Test 1

The second compaction used bigger particle size that was 6.3mm. Assumption was made in which it could give similar results as testing 1.18mm particle size as the soil used was taken from the same location. The maximum dry density from the second compaction is 0.56gm/cc and the optimum moisture content is 80% (Figure 4).

The third compaction effort used soil particles passing 1.18mm sieve. The maximum dry density from the third compaction is 0.51gm/cc and the optimum moisture content is 82% (Figure 5). The results of the second and the third compaction results do not differ much but for more accurate mixing, the third compaction results is used as the particle size that will be used in the mixing for shear strength test is of <1.18mm.

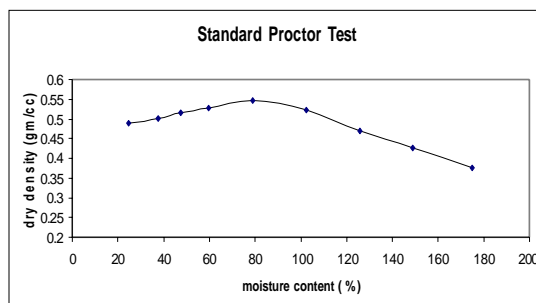


Figure 4 Standard Proctor Test 2

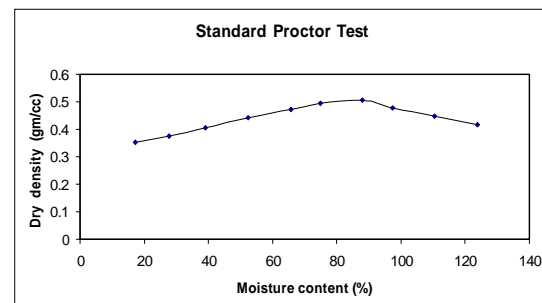


Figure 5 Standard Proctor Test 3

Organic, fibers and ash content

Organic content of the soil sample depends on the ash content. Organic content is inversely proportional to ash content. Ash content (as measured by test methods D2974 [5]):

- Low ash – Peat with less than 5% ash
- Medium ash – Peat with between 5 and 15% ash
- High ash – Peat with more than 15% ash

Table 6 Ash content, loss in ignition and organic content (1 hour in muffle furnace)

Sample	Surface	Middle	Bottom	Average
Ash content (%)	12.27	9.12	6.52	9.30
Loss on ignition (%)	87.70	90.90	93.50	90.70
Organic Content (%)	87.20	90.50	93.20	90.30

Table 7 Ash content, loss in ignition and organic content (5 hours in muffle furnace)

Sample	Surface	Middle	Bottom	Average
Ash content (%)	20.56	27.42	22.04	23.34
Loss on ignition (%)	79.40	72.60	78.00	76.66
Organic Content (%)	78.60	71.50	77.10	75.73

Table 6 shows the results of ash content, loss in ignition and organic content (1 hour in muffle furnace) and Table 7 shows the results of ash content, loss in ignition and organic content (5 hour in muffle furnace). The results of 5 hours in muffle furnace is more accurate since the heating duration is longer and the soil was totally ashed compared to the results of 1 hour in muffle furnace in which some of the soil was only partially ashed. This can be known by comparing the soil color after the soil sample is taken out from the muffle furnace.

The fiber content is the dry weight of fibers retained on ASTM sieve no. 100 (>0.15 mm opening size) as a percentage of oven dried mass (ASTM D1997) [6]. The first fiber content test was done by dry sieving on 425µm sieve. From this test, the fiber content is 80.27%. The second fiber content test was conducted by wet sieving the soil sample on sieve no. 100 (>0.15 mm opening size). From this test, the fiber content is 25%. The second fiber content test result is used in order to obtain more accurate result in which the soil was wetted in order to further break the soil particles into smaller size.

Unconfined compressive strength

There were 2 mixing done for the same type of soil (particle sizes < 1.18mm) and percentage of lime. Mixing 1 is not as good as Mixing 2 because the sample taken out from the pipe was not as perfect and smooth as samples in Mixing 2. Some of the soil surface was peeled off, retained on the pipe because of excessive used of grease. There were 3 layers of compacted soil prepared in the sample. After the first layer had been compacted, another layer was placed and this was repeated until the final layer.

Table 8 Results of Unconfined Compressive Strength Test of Soil Before Stabilized

Sample (0% Lime)	1	2	Average
Unconfined Compressive Strength (kPa)	38.33	38.33	38.33

From Table 8, it can be noticed that the unconfined compressive strength of soil before stabilized or before adding Carbide Lime is 38.33 kPa. Table 9 shows the results of unconfined compressive strength test of Mixing 1 that is in average value. From the values, it can be seen that strength is gained after stabilization. The longer the curing time, the higher strength gained. For sample of 7 days and 14 days curing, 3% and 6% lime added shows increment of strength but the strength decreases in the 9% lime added and it increases again in 12% lime added. For sample of 28 days, percentage lime added is directly proportional to the strength gained. Figure 6 shows the results of unconfined compressive strength test of Mixing 1. From the plot it can be concluded that with the increase of different percentages of carbide lime added, and with the increase in curing periods, the strength of the original soil is increased.

Table 9 Results of Unconfined Compressive Strength Test of Mixing 1

Percentage Lime (%)	Unconfined Compressive Strength (kPa)		
	Curing Time (days)		
	7	14	28
3	42.58	54.10	60.63
6	50.23	66.66	63.81
9	41.89	60.38	73.36
12	51.79	62.15	74.50

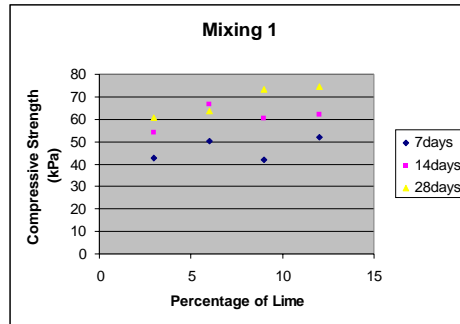


Figure 6 Results of Unconfined Compressive Strength Test of Mixing 1

Table 10 shows the results of unconfined compressive strength test of Mixing 2. Mixing 2 was cured up to 14 days. From the results, it can be seen that there is gain in strength. Strength gained for sample cured for 14 days is higher than the sample cured for 7 days. Strength increases with the increase of carbide lime added but there is a little bit of decrease for the 12% lime added sample. Figure 7 shows the same trend with Figure 6 at which strength is increased by time and by increment of lime percentage. Mixing 2 shows higher value of strength because the condition of the sample before testing was good and none of the surface was peeled off or remained on the pipe.

Table 10 Results of Unconfined Compressive Strength Test of Mixing 2

Percentage Lime (%)	Unconfined Compressive Strength (kPa)	
	Curing Time (days)	
	7	14
3	72.32	86.94
6	76.2	114.8
9	90.93	123.45
12	89.03	115.30

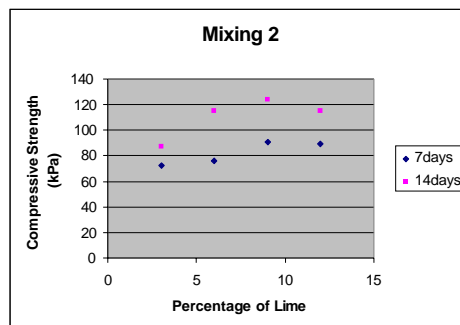


Figure 7 Results of Unconfined Compressive Strength Test of Mixing 2

5. CONCLUSIONS

The main observations and findings are concluded as follows:

- Soil collected from Matang area falls in the category of H5 and H6, that is, hemic or moderately decomposed.
- Moisture content of peat soil is very high and the moisture of the soil used in this research that is collected in Matang area falls in the range of 400% to 600% for the depth of 0.25 to 0.3m.
- The unconfined compressive strength test results shows that with the increase of percentages of carbide lime added, the strength of the peat soil sample is increased.
- The unconfined compressive strength test results shows that with the increase curing time, the strength of the peat soil sample is increased.
- Carbide Lime that is a by-product of acetylene can be used as a stabilizer since it can increase the strength of the peat soil when added to the soil.

6. ACKNOWLEDGMENT

Authors would like to thank UNIMAS Civil Engineering Department for providing the experimental facilities and guidance.

7. REFERENCES

- [1] Wong, M.H.(1991). The distribution, characteristics and agricultural utilization of peat in Sarawak. Department of Agriculture, Sarawak.
- [2] Jarrett P.M. (1997), *Recent Developments in Design and Construction on Peat and Organic Soils*. Proceeding of Conference on Recent Advances in Soft Soil Engineering volume 1, 1997 Kuching Sarawak, Malaysia.
- [3] Van Impe, W. F., (1989) “ Soils Improvement Techniques and their Evolution” , A.A. Balkema.
- [4] British Standards Institution, (1981). “ Methods of test for soils for Civil Engineering Purposes” . London: BS 1377
- [5] ASTM D 2974 - 87 (1987) *Standard Test Method for Moisture, Ash, and Organic matter of Peat and other Organic soils*. Annual Book of ASTM Standards, Philadelphia, USA.
- [6] ASTM D 1997 - 91 (1996) *Standard Test Method for Laboratory determination of the fiber content of peat samples by dry mass*. Annual Book of ASTM Standards, Philadelphia, USA.

CHAPTER 3

CATCHMENT SIZE, SOIL TYPE AND LAND USE TO DETERMINE THE AMOUNT AND LIKELIHOOD OF FLOOD IN THE SARAWAK CORRIDOR OF RENEWABLE ENERGY (SCORE) REGION

Awang Abdillah, D.N.H.¹ and Selaman, O.S.²

Abstract

Size of catchment, soil types and land use are some of the factors that influence the flood phenomenon. Generally, the amount and behavior of the runoff from precipitation are analyzed to observe their effects on the catchment in terms of flood occurrence. This study measures the likelihood of flood event by comparing the peak flow rates at the pre development and post development stages of the major system. The approach used is by the most common practice in hydrology that is Rational Method. With a higher peak flow rate obtained at post development stage, it has been proven that as more urbanization takes place, there is the more flood occurrence. Similar results are obtained where the poorly-drained soils like peat and clay are present at certain area in the region. It has been verified that the size of catchment contributes the most on the flood risk.

Keywords: Catchment size, Soil types, Land use, Peak flow rate, Likelihood of flood occurrence

I. INTRODUCTION

LOOD occurs most commonly when there is excessive flow. Basically, the flow comes from heavy rainfall, from melting ice and snow, or from a combination of these, that exceeds the carrying capacity of the river system, lake, or the ocean where it is conveyed. Therefore, an apt analysis is needed to be carried out based on the catchment characteristics that contribute to this problem.

This study is to determine the likelihood of flooding on Sarawak SCORE watersheds at which the flooding gives impact on the project and also which the project impacts flooding based on analysis with the intention of considerations of size of catchment, land use and soil types in varying conditions that give effects towards the water volume and its travel behavior due to changes occur by doing comparisons at conditions of pre development and post development.

Urbanization is a primary cause of nonhomogeneity of flood records [1]. MSMA:2000 stated that urbanization is the conversion of natural or rural areas into a residential, commercial or industrial development. Generally, the flood occurs because there are changes being made to the particular place which is referred to as land use changes. This happened due to the land surface modification in order to fulfill the human needs to ease them doing their activities on land, which then affect the runoff behavior that leads to flooding. Also, changes of soil types due to cut and fill works and land's soil modifications too, contribute to the problem [2]. Consequently, urbanization areas that keep increasing over time change the frequency of flood occurrence. These soils may be quite productive, but they have a flooding hazard that seriously limits their use for urban development or agriculture [3].

The influence of catchment size increases basically related to the amount of precipitation. As the catchment gets larger, then, the precipitation area, regardless the differences in the amount of rain fall into the regions [1]. The water will run on the land, which is called runoff, to the drains and river. Therefore, when the catchment is bigger, the runoff would be greater because it collects runoff from the entire specified area. When the catchment size is considered as large, it might be a highly flood-potential area [1]. This corresponds to the amount of the runoff collected over a period of time.

¹ Student, Department of Civil Engineering, Faculty of Engineering, Universiti Malaysia Sarawak, Sarawak, Malaysia, no_rule007@hotmail.com

² Lecturer, Department of Civil Engineering, Faculty of Engineering, , Universiti Malaysia Sarawak, Sarawak, Malaysia , sosuhaiza@feng.unimas.my

2. METHODOLOGY

MSMA:2000 [4] stated that there are two ways to estimate peak flow, either by Rational Method or by hydrograph. The study comprises the pre development and post development stage. According to MSMA:2000, the peak flow at channel outlet at post development stage should not exceed the peak flow value of both minor and major system of pre development stage. The flood minor and major system flow is determined based on ARI values chosen. This is to ensure that the flood will not occur.

The peak flows, Q are compared to each other in its own development stage to see whether Q value is significant enough to cause flood based on the basins' flood history. Secondly, the Q value is compared among the same two basins, but at different development stages to see the impact of the SCORE development, by estimations.

MSMA:2000 stated that to Rational Formula is the most frequent approach used to do the flow peak computation and the formula is given as;

$$Q = CiA/360 \quad (1)$$

Where:

- Q = Peak rate of runoff in cubic meter per second
- C = Runoff coefficient, an empirical coefficient representing the relationship between rainfall and runoff
- i = Average intensity of rainfall for the time of concentration (t_c or t) for a selected design storm in mm/hr
- A = Drainage area in hectares

To obtain the runoff coefficient, C MSMA:2000 gives;

$$C_{avg} = \frac{\sum_{i=1}^m C_i A_i}{\sum_{i=1}^m A_i} \quad (2)$$

Whereby;

- C_{avg} = average runoff coefficient
- C_i = runoff coefficient for segment i
- A_i = area of segment i (ha)
- i = 1,2,...,m
- m = the number of different sub-catchment with different types of land use and soil type.

The land use map of scale 1:250,000 is obtained and downloaded from the website of www.library.wur.nl/isric/index2.html for the stage of pre development. The soil type data is obtained in the map form, purchased from the Agricultural Department of Sarawak. There are two sets of maps named Soil Map of Sarawak, Malaysia Timor 1968; Sheet A and Sheet B, of the scale of 1:500,000. For catchment size determination, the Department of Irrigation and Drainage Sarawak (DID) provides all the basin sizes in their website. Each basin have been prepared for their catchment characteristics whereby they are compiled in form of soil layers and land use layers to ease any task or comparison that is going to be performed, for that the data is gathered in a proper way.

As shown in figure 1, Sarawak consists of 21 river basins with different sizes and characteristics. Out of those, by referring to SCORE region as in figure 2, 10 river basins are used in this study namely; Baram, Niah, Suai, Similajau, Kemena, Rajang, Tatau, Balingian, Mukah and Oya.

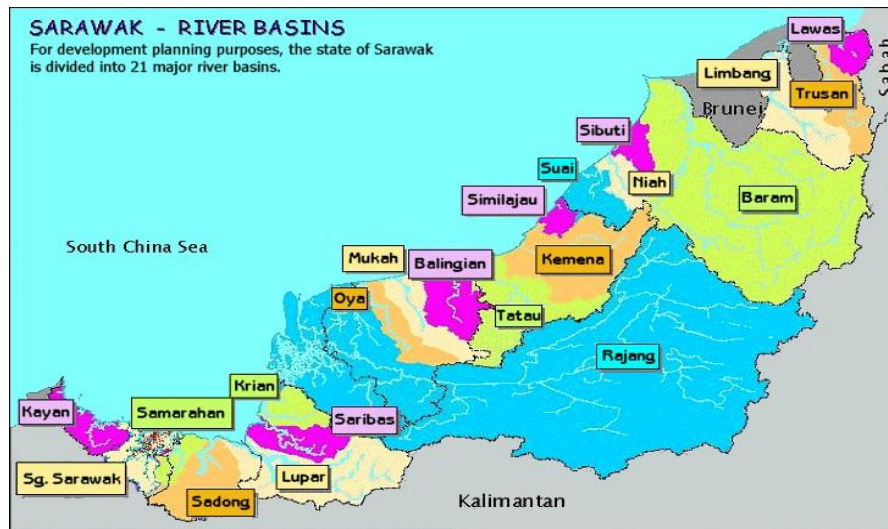


Figure 1: Sarawak River Basins Map. [5]

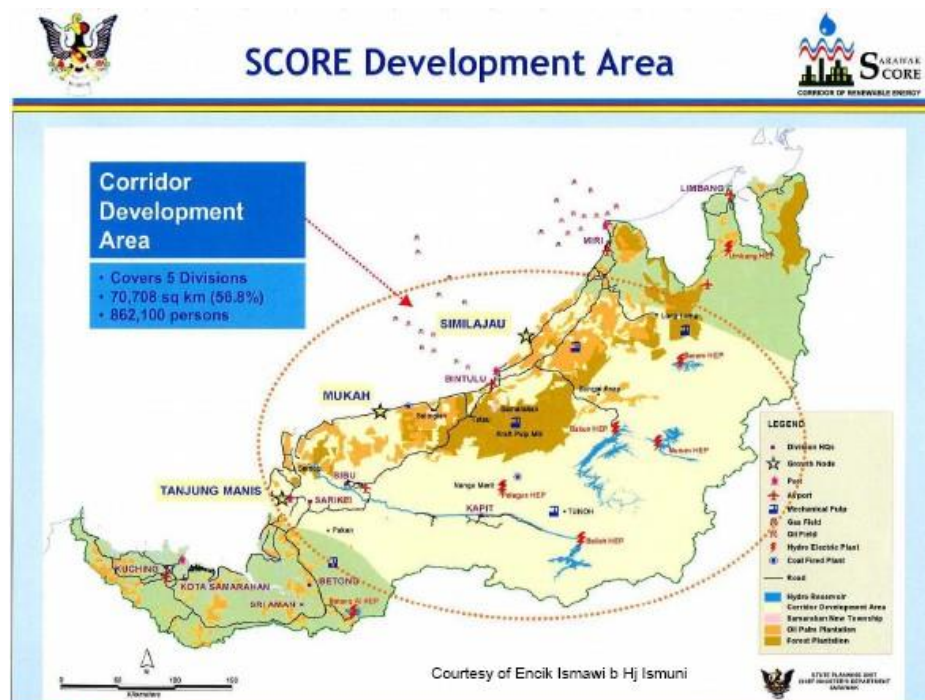
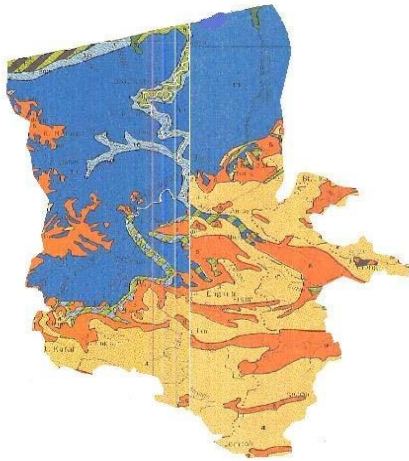


Figure 2: The scope of SCORE development area. [6]

3. RESULT AND ANALYSIS

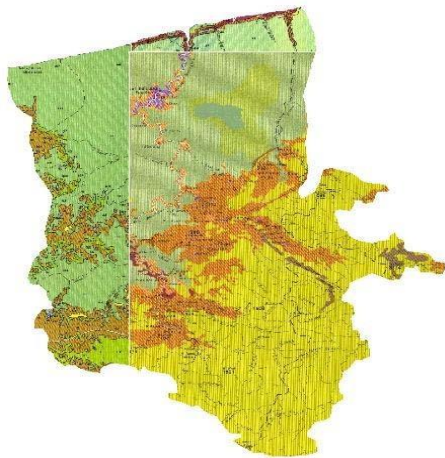
The results are obtained for each different catchment in the SCORE region which are then compared to each other respect to the influence of size of basin, soil type and land use. Furthermore, results are also being compared at pre development and post development stages.

The runoff coefficient, C is analyzed by considering both soil type and land use of the basin. Like in figure 3 and figure 4, the details of Balingian basin existing type of soil and land use are indicated by the colors and the conclusions are shown in the text box. The C average is obtained by using (2).



Catchment name: Balingian
Area : 262500 ha
Major soil type(s): Peat, sandy clay

Figure 3: Balingian Soil Map. [7]



Catchment name: Balingian
Area : 262500 ha
Major land use: Forest and open crop plantations

Figure 4: Balingian Land Use Map. [8]

Design rainfall intensity is tabulated in table 1 and it appears that the i values for post development are always higher than those for pre development. This is because the ARI used are higher for post development stage, which is 20-year ARI, and higher ARI means rainfall data consists of larger rainfall intensities.

Table 1: Design rainfall intensity

Catchment	i value (mm/hr)	
	Pre development Stage (5 years ARI)	Post development stage (20 years ARI)
Oya	111.337	140.685
Mukah	111.337	140.685
Balingian	111.337	140.685
Tatau	124.281	148.445
Kemena	124.281	148.445
Similajau	124.281	148.445
Suai	108.609	137.823
Niah	108.609	137.823
Baram	108.609	137.823
Upper Rajang	93.6489	110.965
Lower Rajang	111.337	140.685

A comparison is needed to be carried out to analyze which factor affects the Q value the most. Therefore, table 2 below is prepared. In the table, as the catchment size increases, the Q values increases proportionally. While for C values, gives varying amount of flow rate as the C value increases, or in other words, the increment of C values are disproportionate to the Q values. Based on Rational Formula in which C value is supposed to increase the Q value proportionally as catchment size does, the results turns not to be as expected. This is mainly because of the catchment is very large, making the A value governs the Q value. For this SCORE project, it is clear that between the three factors, catchment size affects the likelihood of flood the most, followed by C value, which is a combination of both soil type and land use.

Table 2: Comparison of Q value to A value and C value

No.	Catchment order (biggest to smallest size)	Q (10 ⁶ m ³ /s)		C	
		Pre development	Post development	Pre development	Post development
1	Rajang	449	624	0.79	0.87
2	Baram	179	231	0.74	0.76
3	Kemena	55.6	67.7	0.73	0.75
4	Tatau	48.2	58.7	0.73	0.75
5	Balingian	23.4	30.1	0.80	0.82
6	Mukah	20.5	28.5	0.81	0.89
7	Oya	19.2	24.7	0.80	0.82
8	Suai	15.2	19.7	0.73	0.74
9	Niah	10.5	13.6	0.72	0.74
10	Similajau	5.66	7.43	0.71	0.78

Due to lack of information regarding the areas of the development in SCORE project, the exact peak flow rate cannot be obtained simultaneously. Yet, there is still a way to simplify the determination for these discharges by deriving an equation for each catchment using the existing data. Derived from Rational Formula, these equations are easy to be used by any individual. Table 3 indicates the equations according to each basin concerned.

Table 3: Flow peak, Q equation

Catchment	Flow peak equation	
	pre development	post development
Oya	$0.309271(\sum c_i A_i)$	$0.390792(\sum c_i A_i)$
Mukah	$0.309271(\sum c_i A_i)$	$0.390792(\sum c_i A_i)$
Balingian	$0.309271(\sum c_i A_i)$	$0.390792(\sum c_i A_i)$
Tatau	$0.345225(\sum c_i A_i)$	$0.412346(\sum c_i A_i)$
Kemena	$0.345225(\sum c_i A_i)$	$0.412346(\sum c_i A_i)$
Similajau	$0.345225(\sum c_i A_i)$	$0.412346(\sum c_i A_i)$
Suai	$0.301692(\sum c_i A_i)$	$0.382842(\sum c_i A_i)$
Niah	$0.301692(\sum c_i A_i)$	$0.382842(\sum c_i A_i)$
Baram	$0.301692(\sum c_i A_i)$	$0.382842(\sum c_i A_i)$
Lower + Upper Rajang	$0.309271(\sum c_i A_i)$	$0.390792(\sum c_i A_i)$

4. CONCLUSIONS

From the Q values obtained, it is indicated that Rajang catchment has the highest risk of flood occurrence because the basin gives the greatest flow rate among all basin, at both development stages. This corresponds to the flood history on the area that flood occurred more frequently there compared to other basins. Moreover, with further development, impervious areas will increase and the area is certainly would get flooded. Rajang is one good example to indicate how the C values and A values influence the flood phenomenon. As from the data collected, Rajang has the largest portion of peat soil which does not permit good drainage for precipitation. Rajang also has the biggest catchment area which means to collect the largest amount of runoffs. In contrast, Similajau has the smallest portion of peat soil, is least developed and has the smallest area of catchment. Consequently, it gives the smallest Q. It has been proven that the bigger the value of the above factors the bigger the Q value. Tanjung Manis, the main growth nodes for this project, is located in Rajang basin. Thus, several features must be planned carefully in order to minimize the risk. This study concluded that the likelihood of flood in SCORE region is determined that, Rajang has the highest probability, followed by Baram, Kemena, Tatau, Balingian, Mukah, Oya, Suai, Niah and Similajau. As understood, flood is affected by several factors that are not included in this study. Further study is recommended to be implemented to obtain more accurate and complete results.

5. ACKNOWLEDGEMENT

Special thanks are due to the Department of Irrigation and Drainage (Sarawak), Land and Survey Department of Sarawak and Department of Agriculture (Sarawak) for providing very useful information in order to carry out this study. Round of applause is given to Prof. Dr Wang Yin Chai of Faculty Information and Technology for his kindness and being helpful.

6. REFERENCES

- [1] McCuen, Richard H.. (1989). *Hydrological Analysis And Design*. 1st ed. New Jersey: Prentice-Hall
- [2] Nelson, S.A. (2009). River Systems & Causes of Flooding. <http://www.tulane.edu/~sanelson/geol204/riversystems.htm/> 10 March 2009
- [3] Headrick, Nevelyn. (2006). <http://www.utahenvirothon.org/64.176.89.73/pdf/UTSoils.pdf/> 5 September 2008
- [4] MASMA:2000. Urban Stormwater Management Manual for Malaysia (*Manual Saliran Mesra Alam Malaysia*). (2000). Department of Irrigation and Drainage, Malaysia.
- [5] *Department of Irrigation and Drainage*. (2000). <http://www.did.sarawak.gov/> 7 November 2008
- [6] Mohamed, Murtedza. (2008). Participation of Sarawak Based Institutions of Higher Education in the Sarawak Corridor of Renewable Energy (SCORE) Development. <http://www.unimas.my/images/stories/score/U-ScoreWebsite.pdf/> 22 October 2008
- [7] Department of Agriculture Sarawak (2008). Soil Map of Sarawak, Malaysia Timor 1968; Sheet A and Sheet B. Malaysia.
- [8] WAGENINGEN. (2009). World Soil Information Database. <http://www.library.wur.nl/isric/index2.html/> 14 February 2009

CHAPTER 4

A REVIEW OF SOIL NAILING DESIGN APPROACHES

S.N.L. Taib¹

Abstract

A number of design manuals and recommendations; namely by the HA 68 [4] (U.K.), BS8006 [1] (U.K.), RDGC [7] (France) and FHWA [5] (USA) are available for soil nailing. This paper will focus on the different approaches, specifically on the assumptions made for the design of soil nailing structures.

Keywords: Soil nailing, BS8006, HA 68

I. INTRODUCTION

Soil nailing is a relatively new method, which has been used for over 3 decades for soil reinforcement purposes. It is an in-situ earth reinforcing method, in which the primary applications are to retain excavations or cuts and to stabilise slopes. The principal reinforcing materials, the nails, are inserted into the earth as passive inclusions providing reinforcement to the earth that help the earth structure to gain its overall strength. A factor, which makes soil nailing technique more desirable than other earth reinforcing methods when performed on cuttings or excavations, is its easy and flexible top-down construction (excavation, nail installation and placement of shotcrete) as shown in Figure 1.

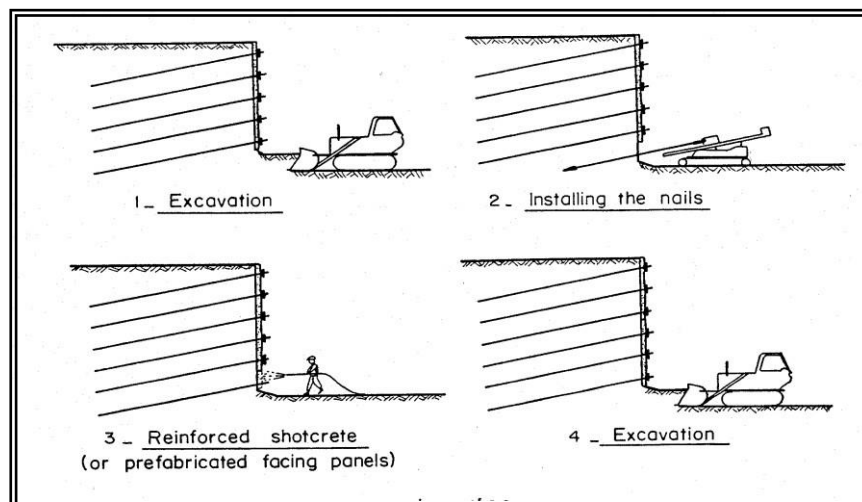


Figure 1 The three stages of soil nailing construction process [7].

¹Senior Lecturer, Department of Civil Engineering, Faculty of Engineering, Universiti Malaysia Sarawak.

2. DESIGN ACCORDING TO HA 68 [4]

The Department of Transport of the UK [4] employs the limit state principles incorporating partial safety factors as suggested by [3] for geotechnical engineering design. Any design is based on ultimate and serviceability limit states. The ultimate limit state occurs when a collapse mechanism forms, while, the serviceability limit state might occur during the working or service condition of the structure in which a situation such as movement in the structure may affect the functionality of the structure or of the adjacent structures or services.

HA 68 gives a single unified effective stress design approach for all types of reinforced highway earthworks with slope angles to the horizontal in the range 10° to 70° , and soil types in the strength range $\phi = 15^\circ$ to 50° . Values of c' may be included, as well as pore water pressures and limited uniform surcharge applied at the top of the slope.

A limit equilibrium approach is adopted based on a two-part wedge mechanism with the inclusion of partial safety factors. Figure 2 shows the geometry of HA 68's two-part wedge mechanism. Equilibrium is reached when the driving forces, which consist of the self weight of the structure and surcharge loads multiplied with the load partial factor (of predetermined value of unity) are in equilibrium with the resisting forces which are the shear strengths of soil and the reinforcement forces divided by the material partial safety factors of predetermined values suggested by Department of Transport. The assumption is made that the nails' contribution is purely axial. Shear stress and bending stiffness are ignored in this design.

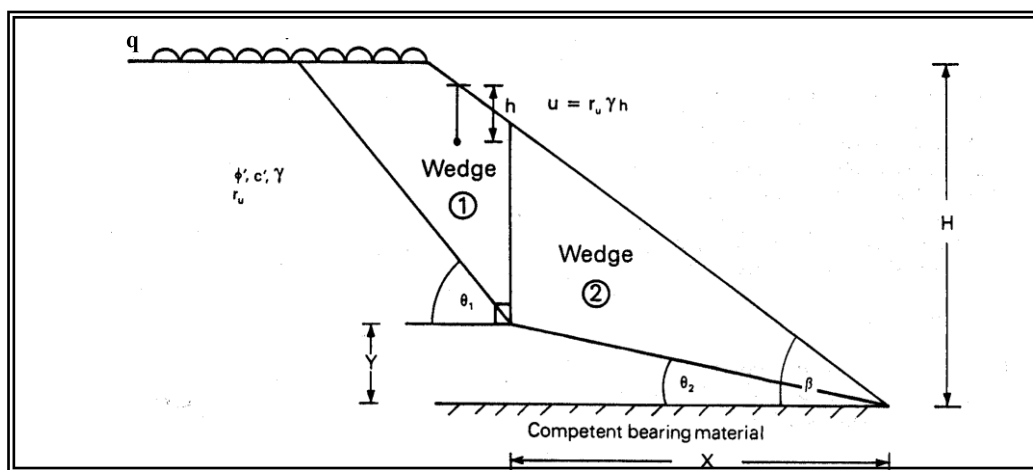


Figure 2: Geometry of HA68's two-part wedge mechanism [4].

According to Department of Transport, the two-part wedge mechanism is preferable to a log spiral mechanism because it provides a simple basis for obtaining safe and economical solutions and is particularly suitable for reinforced soil including soil nailed structures. It is inherently conservative when compared to more exact solutions but allows simple hand check calculations to be carried out. Two two-part wedges are introduced in this manual that are the T_{max} and T_o mechanisms. The T_{max} mechanism identifies the location in the structure, which needs the maximum total horizontal reinforcement, meanwhile, the T_o mechanism is one where no reinforcement is needed. For inclined reinforcement (when angle of nail inclination, $\delta \neq 0$) the variables for these mechanisms are presented as $T_{max\delta}$ and $T_{o\delta}$ (refer to Figure 3).

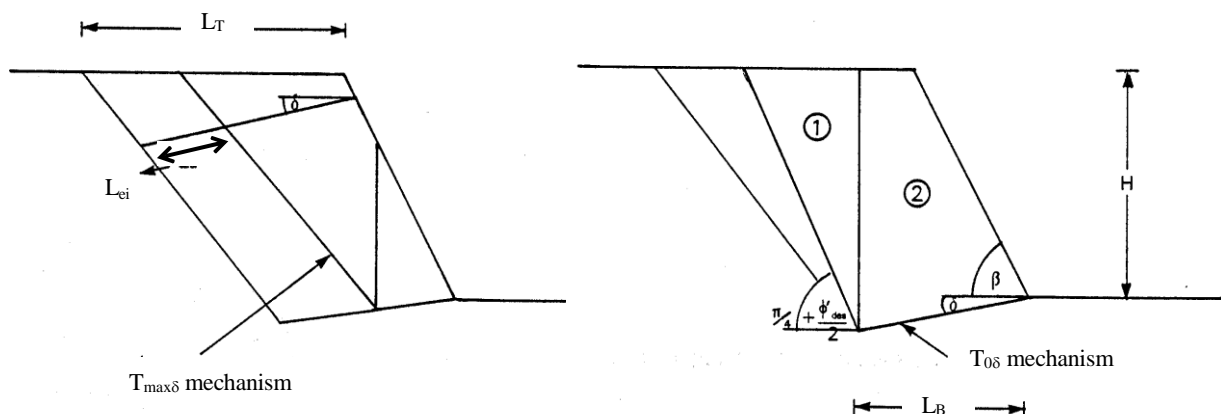


Figure 3: $T_{max\delta}$ and $T_{o\delta}$ mechanisms [4]

For inclined reinforcement, the values of $T_{\max\delta}$ and P_{des} shall be determined next. $T_{\max\delta}$ value is the total reinforcement force inclined at angle δ for most critical two-part wedge mechanism; while, P_{des} is the design nail capacity per metre length of slope, based on the rupture strength of the reinforcement or pullout capacity of the reinforcement. HA68 in Section 2.23 on page 2/4 comments that the strength mobilised in the reinforcement is taken to be the lesser of the design rupture strength and the design pullout resistance of the length of reinforcement beyond the failure surface (L_c) whenever the failure surface cuts a layer of reinforcement or row of nails. The lesser value is chosen to govern the design since this is the value that becomes critical at failure.

The Department of Transport suggests nails of the same strength capacity to be utilised for reinforcing the slope. The number of reinforcements per unit length, N_n , not including the basal layer is directly obtained from the values of $T_{\max\delta}$ and P_{des} , where

$$N_n = T_{\max\delta} / P_{\text{des}} \quad (\text{Equation 1})$$

Due to this assumption, of similar capacity to all the nails, the manual suggests optimum variable vertical layer spacing due to the requirement to avoid local over-stressing of any layer of reinforcement, which would later introduce progressive failure of the whole structure; especially for reinforcement having identical capacity. In HA68 designs, the total reinforcement force increases parabolically down to the bottom of the structure and the decrease in vertical spacing going down the slope is seen as desirable to avoid local instability. The equation that governs the spacing is

$$z_i = [\sqrt{(i-1)/N_n}] \times H \quad (\text{Equation 2})$$

where

z_i = depth of i th layer of reinforcement below crest of slope.

Now that once the $T_{\max\delta}$, T_{δ} mechanisms are located and total number of reinforcements (N_{n+1}) are obtained, a drawing of the soil nailed structure's profile can be designed. In general, HA 68 gives a step by step design procedure for soil nailing.

3. DESIGN ACCORDING TO BS 8006 [1]

In the design approach of BS 8006, the limit state principle is again adopted. The limit equilibrium approach is applied wherein the internal as well as the external stabilities of structure are checked against the limit states. As in HA68, in order to be consistent with suggestions in [3], partial safety factors are included in its design calculation. The design of soil nailed structure in existing ground is presented in Section 7 (Design of Reinforced Slopes) of the standard, while design of soil nailing wall is presented as part of Section 6. (Design of Walls and Abutments)

BS 8006 is more comprehensive than HA 68 in its explanation of the available approaches and assumptions from which the designer can choose. A comprehensive list of suitable load partial factors and material partial factors is given and these are related to different construction conditions and situations. Two methods of searching for the critical failure are presented - the two-part wedge (as in HA 68) and the log spiral method. BS 8006 advises its users to include shear resistance along with the known tensile reinforcement provided by the nails if the resistance is significant.

BS 8006 suggests the stages that designer can follow in soil nailed structures design; which are:

1. The determination of the position of the critical slip surface and the resisting force or moment to maintain equilibrium of the active zone.
2. The determination of the tensile and shear loads for an initial constant spacing and inclination of nails of constant stiffness and length.
3. A check for each level, allowing for stages of construction, against failure due to
 - a. tension in the nail at the slip surface,
 - b. pullout of the length of nail in the resistant zone,
 - c. bending and shear in the nail near the slip surface, and
 - d. bearing failure of soil against the nail.

The designer can now select a new and improved pattern and disposition of nails and re-analyse. It should be noted here that the shear loads in the nails can be obtained from [8] and [7] in which according to BS 8006, a *technique based on maximum plastic work with limits placed on the allowable lateral earth pressure on the nails and bond resistance* is applied. Another method to look for shear loads is introduced by [2] where they adopted the theory of deflection of laterally loaded narrow piles to determine nail deflections and kinematical compatibility to determine the value of resulting shear forces in the nails.

BS 8006 gives more freedom in many aspects of choosing the most suitable design approach rather than HA 68, which is more directive. It depends on the experience and the knowledge of the designer in choosing the appropriate approaches suitable design with guidance from the design manual.

4. RECOMMENDATIONS BY RDGC [7] (PROGRAM CLOUTERRE)

The French initiated the Clouterre program in 1986 [7], jointly funded by the French government and private industry, with a budget of the order of \$4 million and with 21 individual private and public participants. The program involved three large-scale experiments in a prepared fill of Fontainebleau sand and the monitoring of six full-scale in-service structures. The results of the Clouterre program have been published and form the basis for soil nailing design approach adopted in France.

The report by RDGC on the program does not specifically provide a step-by-step procedure to design a soil nailed structure as presented in HA68. It sets up guidance on design and special criteria that must be considered. A designer is recommended to start with a preliminary design that will enable him or her to later define essential characteristics of the structure, such as the resistance values, lengths and spacings required in the final design. Preliminary design charts are used to seek for the characteristics mentioned above at the simplest condition of the structure; for example, identical nails are evenly distributed, homogeneous soil and nails working only in tension. Several design charts are presented in the report i.e. [6].

The report elaborates on the principles used to assess stability of soil nailed structures. In accordance with [3], for geotechnical design, and as can be seen in HA 68 and BS 8006, the conventional global safety factor is replaced by partial resistance and load factors. Apart from that, suggestions on characteristic values of the loads and resistances are also presented. The characteristic value is defined as the ratio of average value and the distribution coefficient. The coefficient is applied to make sure that a minimal probability is not achieved. The report mentions that analysis of stability and design of soil nailing can be done at both the ultimate limit state and the serviceability limit state.

The limit equilibrium method and the finite element method are suggested as the basis for stability analysis and design of soil nailing. Limit equilibrium method includes an examination on the equilibrium between the soil and the strength of materials used in the slope, while the finite element method is used to calculate the amount of deformation that the structure will have (to check whether it is either below or beyond a certain acceptable threshold value). Due to unavailability of a mean to calculate the deformation in slope in this report, the design is limited to the limit equilibrium method which has to be checked not only when structure is completed but also during each phase of construction.

The report presents 4 types of failure modes based on scaled-down laboratory models tested to failure, which are breakage of the nails, lack of friction between the soil and nails, instability during excavation process and overall sliding of the reinforced soil mass. These failure modes which are observed in laboratory models, justified the use of limit equilibrium in designing soil nailed structures as all these failures involved slip surfaces (except for the lack of friction case). A second justification on the use of limit equilibrium method is given by two actual structures, which failed and exhibited pullout and tensile failures respectively. Safety factor was checked by analysing the potential failure surfaces and was found to be near unity.

An interesting point that is included in the report concerns the assumption made in any limit equilibrium calculation on the simultaneous mobilisation of resistances. These resistances are the resistances of the nail, particularly its tensile strength, shear resistance in the soil, pullout resistance of the nail (limit skin friction, f_{max}) and passive pressure at failure of the soil normal to the nail, which in actual condition do not act simultaneously in the structure. Further justification on this has to be done through experimental work in order to gain more confidence on the use of the limit equilibrium method in soil nailing design. However, according to the report, *the assumption on simultaneous mobilisation of resistances is, in spite of everything, still a good approximation of the actual-and complicated-behaviour of soil nailed walls.*

5. DESIGN ACCORDING TO FHWA [5]

As with other design approaches, the FHWA also applies limiting equilibrium method in its soil nailing design. Specifically, the manual utilises the slip surface limiting equilibrium method which is used by all current practical design methods of soil nailing. Two limit states, as with the other design recommendations, are considered, namely, the strength limit state (ultimate limit state) and the service limit state. Another limit state known as extreme limit state, which belongs to the strength limit state, recognises structure under extreme loads such as seismic loading.

The manual recognises the benefits of utilising the slip surface limiting equilibrium method compared to the earth pressure method and these are summarised as below;

To date, virtually all designers have utilised the approach and there are no current empirical earth pressure recommendations sufficient to handle the variety of conditions faced in soil nailing such as soil types, geometries and loading.

Several factors inherited by soil nailing technique; for example, heterogeneity of soils introduces complexity in the use of earth pressure method in soil nailing.

Another drawback of using the earth pressure system is the definition of locations of the maximum tension line for each of the reinforcements. Again, it is particularly complex to define these locations due to the variety of conditions encountered in soil nailing since the definition of these locations is dependent on the geometry of the system, character of reinforcements and distribution of applied loading. A soil nailed structure, will have a wide range of soil shear strengths and soil / grout bond capacities.

The manual introduces two approaches to design, which are the Service Load Design (SLD) and the Load and Resistance Factor Design (LRFD), which consider both limit states in their calculations. In SLD, allowable nail loads (tendon strength and pullout resistance of nail) are suggested for the reinforcement strength and recommended factors of safety are applied to the soil strength at both limit states in which the allowable nail loads and factored soil strengths exceed the applied loads. In contrast, in LRFD, at strength limit state, the soil and nail design strengths which are obtained by applying resistance factors to their ultimate strengths, exceed the applied loads which are multiplied by load factors. In service limit state analysis for both designs, overall displacement of the structure is recognised and in certain cases, on the facing, the crack width has to be observed to be within specified limits. This manual provides guidance on finding the displacements (i.e. maximum lateral movements in different soil types) for consideration in the service limit state analysis.

To consider the strength limit state, all potential modes should be considered; the external modes (that do not specifically intersect the reinforcement), the internal modes (i.e. failure either due to rupture of reinforcement or failure of facing) in which the global failure surface intersects the reinforcement and the mixed modes which includes internal mode failure and where some part of the failure surface does not touch the reinforcement. The local stability of the facing during excavation is also highlighted in the manual since this failure cannot be directly assessed using the conventional stability analysis.

A matter to point out from this manual is the reinforcing effect of the nail. The nail is seen to contribute three reinforcing effects which are the rupture strength of the tendon, the pullout resistance and an additional effect not considered in other design manuals, which is the nail head connection to the facing. The manual continues to state that the nail contribution to the stability of the structure must be the least of three values namely, the tensile strength of the nail, pullout resistance of the length of the nail beyond the slip surface, and the nail head strength plus the pullout resistance of nail's length between the head and the slip surface.

Design of soil nails and wall facing is treated as a *combined integrated soil-nail-wall "system"*. This is an effort to ensure that the design could suffice for long-term usage. This manual does not include the shear and bending contributions of the nail and only considers the tensile strength. The other contributions are neglected due to the reason that their mobilisations only after significant deformation in the structure and this assumption, according to the manual, is conservative.

Before establishing detailed design calculations, the designer has to choose the wall layout and dimensions (i.e. considering the environment in the vicinity of the location) together with the ground material properties and the subsurface properties in order to determine the preliminary nail pattern which includes nail lengths, locations, spacings, strengths and inclinations. As a starting point, a uniform inclination of 15° is suggested for nails installed in predrilled holes (inclination of lower than 5° should not be used since grouting will be particularly difficult). Uniformity also applies to the spacings, length (normally in the range of 0.6 to 1 times the height of the wall for cut slopes with modest backslopes and minimal surcharge loadings) and size of the nails. The nail lengths and required strengths are exposed to the same limiting factors as the nail spacing. They will increase in the presence of lower soil strengths, lower nail-ground pullout resistances, steeper face and backslope angle and higher surcharge loadings, which will alter the preliminary pattern. With the preliminary design, designer can check for stability and make necessary alterations in order to obtain a more satisfactory detailed design.

6. CONCLUSIONS

This paper reviews soil nailing design suggestions and manuals [HA68 [4] (U.K.), BS8006 [1](U.K.), RDGC [7] (France) and FHWA [5] (USA)]. Theories on the mechanics of the technique were presented. General conclusions of this paper are:

- All methods employ the limiting equilibrium analysis and in some methods, use of partial safety factors is evident.
- In the limiting equilibrium analysis, concern on the assumption made on the simultaneous mobilisation of resistances should be addressed.
- HA 68 allows the users to follow step by step procedures in designing a soil nailed structure as opposed to the other manuals (i.e. BS 8006 in which users are given various design suggestions for them to consider).
- The straightforward approach in HA 68, allows a spreadsheet program for designing to be produced. The design was applicable for up to ten reinforcements and for simple design of soil nailing. A proper method of finding the T_0 mechanism still needs to be established for program HA 68 Design.
- It would be beneficial if more empirical data (i.e. pullout tests on nails) are included in these manuals for reference.

- The general failure mechanisms in soil nailing as provided in the manuals are tensile failure in the nail at the slip surface, pullout of the length of nail in the resistant zone, bending and shear in the nail near the slip surface, bearing failure of soil against the nail, instability during excavation process and overall sliding of the reinforced soil mass. However, FHWA does not include the shear and bending contributions of the nail and only considers the tensile strength. The other contributions are neglected due to their mobilisations only after significant deformation in the structure and this assumption, according to the manual, is conservative.
- Clouterre recommends that limit equilibrium method has to be checked not only when structure is completed but also during each phase of construction.
- FHWA includes extreme limit state which belongs to the strength limit state, recognises structure under extreme loads such as seismic loading.
- An additional effect not considered in other design manuals, which is the nail head connection to the facing, is included in FHWA manual.
- Further work on estimating amount of displacements on soil nailing structure is recommended and shall complement the limiting equilibrium analysis.

REFERENCES

- [1] BSI (1995), BS 8006, British Standard Code of Practice for Strengthened/Reinforced Soils and Other Fills.
- [2] Bridle, R.J. and Barr, B.I.G. (1990), The Analysis and Design of Soil Nails, Proceedings of the International Reinforced Soil Conference, Glasgow, 10-12 September 1990, Thomas Telford, London, pp. 249-254.
- [3] CEN (1999), Eurocode 7: Geotechnical Design, ENV 1997-1:1999 – Part 1, General Rules, European Committee of Standardisation.
- [4] Department of Transport, HA 68, Design Methods for the Reinforcement of Highway Slopes by Reinforced Soil and Soil Nailing Techniques. (1994)
- [5] FHWA (1996), FHWA/SA-96/069 Manual For Design and Construction Monitoring of Soil Nail Walls (Technical Manual 1994-1996), Redmond, Washington.
- [6] Juran, I., Baudrand, G., Farrag, K. and Elias, V. (1990), Design of Soil Nailed Retaining Structures, Design and Performance of Earth Retaining Structures, ASCE Geotechnical Special Publication, No.25, pp. 645-659.
- [7] RDGC, Renforcement des Sols par Clouage: Programme Clouterre, Projets Nationaux de Recherche Developpement en Genie Civil, Paris, February. French National Research Project CLOUTERRE (1991) “Recommendations CLOUTERRE 1991 – Soil Nailing Recommendations 1991” Presses de l’Ecole Nationale des Ponts et Claussees” English Translation, July 1993. (1991)
- [8] Schlosser, F., Behaviour and Design of Soil Nailing, Proceedings of Symposium on Soil and Rock Improvement Techniques, Bangkok, Thailand, 29 November –3 December 1982, pp. 399-413. (1982)

CHAPTER 5

GEOTECHNICAL PROPERTIES OF FLY ASH AND ITS APPLICATION ON SOFT SOIL STABILIZATION

Emilliani Anak Geliga¹ and Dygku Salma Awg Ismail²

Abstract

Soil stabilization has become the major issue in construction engineering and the researches regarding the effectiveness of using industrial wastes as a stabilizer are rapidly increasing. This paper briefly describes the suitability of the local fly ash to be used in the local construction industry in a way to minimize the amount of waste to be disposed to the environment causing environmental pollution. Several civil engineering laboratory tests are conducted to study the geotechnical properties of fly ash and strength gain when mixed with local clay sample. A different proportion of fly ash and soil sample cured for 7 days results in a strength gain. A better understanding of the properties of fly ash is gained from the study and the tests indicates an improved strength and better properties of soft soil sample when stabilized.

Keywords: fly ash, soft soil, stabilization

1. INTRODUCTION

Civil engineering projects located in areas with soft or weak soils have traditionally incorporated improvement of soil properties by using cement and lime. Use of fly ash as a ground improvement soil admixture, when found viable, will be effective in terms of cost and a good approach to the environment to preserve and minimize accumulation of industrial waste. This study is performed to obtain geotechnical properties of fly ash for its application in the stabilization of soft soil. The geotechnical properties of fly ash will be evaluated with various laboratory tests to investigate the feasibility of using fly ash in soft soil stabilization. Constructions over soft soil are one of the most frequent problems in many parts of the world. The typical approach to soil stabilization is to remove the soft soil, and substitute it with a stronger material of crushed rock. Due to substantial cost of replacement, alternative methods to the problems are assessed. The study of using coal combustion residues, fly ash, is carried out to observe the effectiveness of its addition on stabilization of soft soil. This is one of the approaches to overcome the increasing amount of solid waste generated by the population. As land is a very valuable commodity and landfills are fast diminishing, the disposal of the ash generated from solid waste incineration poses increasingly difficult problems for the municipalities. A practicable solution to the disposal problems would be the reuse of solid waste ash for civil engineering applications. A research study of the geotechnical properties of the incinerator fly ash derived from solid waste incineration is investigated. The objectives of the study are to determine the geotechnical properties of fly ash and to investigate the effects of fly ash addition for strength of stabilized soft soil. Scope of this study is to analyze the consequences of the application of fly ash in soft soil stabilization. It covers methods for determining the geotechnical properties of fly ash to assess its suitability for soft soil stabilization. The fly ash is taken from Sejingkat Thermal Plant, Kuching.

2. LITERATURE REVIEW

Fly ash is one of the most plentiful and industrial by-products. It is generated in vast quantities as a by-product of burning coal at electric power plants (Senol et al., 2006). Electric utility companies in many parts of the world generate electricity by burning coal which generate an amount of fly and bottom ash. Fly ash generated by coal combustion based power plants typically fall within the ASTM fly ash classes C and F (Reyes and Pando, 2007). Fly ash consists of inorganic matter present in the coal that has been fused during coal combustion. This material is solidified while suspended in the exhaust gases and is collected from the exhaust gases by electrostatic precipitators. Since the particles solidify while suspended in the exhaust gases, fly ash particles are generally spherical in shape (Ferguson et. al., 1999). Fly ash particles those are collected in electrostatic precipitators are usually silt size (0.074 - 0.005 mm). Making a more productive use of fly ash would have considerable environmental benefits, reducing air and water pollution. Increased use as a partial cement or lime replacement would also represent savings in energy because fly ash has been called a high-energy-based material (Hausmann, 1990). Fly ash utilization, especially in concrete, has significant environmental benefits including (FHWA, 2006):

- i. Increasing the life of concrete roads and structures by improving concrete durability,

¹Student, Department of Civil Engineering, Faculty of Engineering, Universiti Malaysia Sarawak, 94300-Kota Samarahan, Sarawak, Malaysia.

²Lecturer, Department of Civil Engineering, Faculty of Engineering, Universiti Malaysia Sarawak, 94300-Kota Samarahan, Sarawak, Malaysia, +6082583268

- ii. Net reduction in energy use and greenhouse gas and other adverse air emissions when fly ash is used to replace or displace manufactured cement,
- iii. Reduction in amount of coal combustion products that must be disposed in landfills,
- iv. Conservation of other natural resources and materials.

Atterberg Limits

Soils containing fines display the properties of plasticity and cohesiveness where a lump of soil can have its shape changed or remolded without the soil changing in volume or breaking up. This property depends on the amount and mineralogy of the fines and the amounts of water present, or generally known as moisture content. As the moisture content increases clayey soil will become softer and stickier until it cannot retain its shape when it is described as being in a liquid state. If the moisture content is decreased, the soil becomes stiffer until there is insufficient moisture to provide cohesiveness when the soil becomes friable and cracks or breaks up easily if remolded. This is described as semi-plastic solid or semi-solid. If the moisture content decreased further there is a stage where the forces between the soil particles will not permit them to move closer and now the soil is described as a solid. It is very useful to define the moisture content at these transitions between above states. They are determined as liquid limit, plastic limit and shrinkage limit. A Swedish soil scientist named Atterberg, thus the tests now known as Atterberg Limits devised the tests for liquid and plastic limit. Both tests are carried out on the portion of a soil finer than 425 μm .

Specific Gravity

The variation of specific gravity of fly ash is the result of a combination of many factors such as gradation, particle shape and chemical composition (Gray and Lin, 1972). This low specific gravity of fly ash results in low dry density. This is because of micro bubbles of air entrapped in ash particles. The trapping of air increases the surface area hence the volume of fly ash. The breaking of fly ash particles increases specific gravity that may be because of release of entrapped gas when ash ground by mortar and pestle (WEBB, 1973). According to Pandian et al., (1998) the low specific gravity could be either the presence of more hollow cenospheres from which the entrapped air cannot be removed or the variation in the chemical composition (in particular, iron content) or both.

Mechanical Properties

Compaction Characteristics

Compaction characteristics of soil-fly ash mixes were studied by several investigators since they are very important in the construction of embankments, roads, and backfilling of retaining walls. Several investigators reported that the maximum dry unit weight increases and the optimum moisture content decreases due to addition of fly ash (Basavanna and Ravi Kumar 1990, Choudhary 1994, Pandian 2004, Prabakar 2004)

The compaction tests were performed to get the optimum water content and maximum dry unit weight of fly ash sample.

Table 2: Geotechnical Properties of Fly Ash (Gupta, 2008)

No	Property Name	Value
1	Grain size distribution % of Gravel % of sand % of silt + clay	Nil 6 94
2	Coefficient of Uniformity, C_u	2
3	Coefficient of Curvature, C_c	1.13
4	Specific Gravity	1.95-2.2
5	Direct shear test Cohesion Angle of Shear resistance	0.0 27°
6	Proctor's Density Optimum Moisture Content Max. Dry Density	18% 1.29 g/cc
7	Permeability Test Coefficient of Permeability	1.3×10^{-4} cm/sec

Compressive strength

Based on Reyes and Pando (2007), the compressive strength of tested plain fly ash for 7 days curing period gives 4754 kN/m². The compressive strength values indicate that all admixture treatment types resulted in strength gains and that most of the gain occurred within the first seven days of curing. The fast strength gain is believed to be related to the initial rapid

hydration that takes place with the admixture. The strength gain due to stabilization depends mainly upon three factors; ash content, molding water content and compaction delay (Senol et al 2006).

Fly ash has been used successfully in many projects to improve the strength characteristics of soils. Fly ash can be used to stabilize bases or subgrades, to stabilize backfill to reduce lateral earth pressures and to stabilize embankments to improve slope stability. Typical stabilized soil depths are 15 to 46 centimeters (6 to 18 inches). The primary reason fly ash is used in soil stabilization applications is to improve the compressive and shearing strength of soils. The compressive strength of fly ash treated soils is dependent on:

- In-place soil properties
- Delay time
- Moisture content at time of compaction
- Fly ash addition ratio

Hydration of Fly Ash

Formation of cementitious material by the reaction of free lime (CaO) with the pozzolans (AlO_3 , SiO_2 , Fe_2O_3) in the presence of water is known as hydration. The hydrated calcium silicate gel or calcium aluminate gel (cementitious material) can bind inert material together. Hydration of tricalcium aluminate in the ash provides one of the primary cementitious products in many ashes. The rapid rate at which hydration of the tricalcium aluminate occurs results in the rapid set of these materials, and is the reason why delays in compaction result in lower strengths of the stabilized materials. The hydration chemistry of fly ash is very complex in nature. So the stabilization application must be based on the physical properties of the ash treated stabilized soil and cannot be predicted based on the chemical composition of the fly ash (Wikipedia, 2008)

3. METHODOLOGY

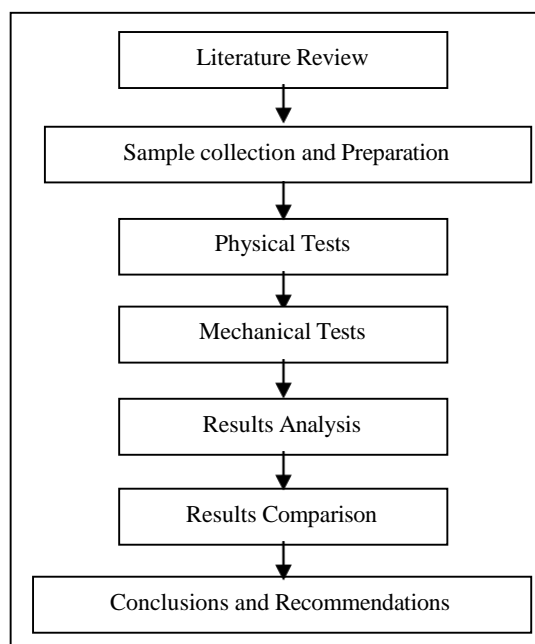


Figure 1: Flowchart of Methodology

The overall flow of research is as illustrated in Figure 1. The tests were conducted in accordance with British Standard 1377. Several physical tests had been conducted for clay sample, fly ash sample and mixes of clay and fly ash. The tests mentioned were Atterberg Limits test, Specific Gravity test, sieving and hydrometer test. In Atterberg Limit tests, Liquid Limit (LL) and Plastic Limit (PL) were obtained. Then, Plasticity Index was determined based on Plasticity chart (BS 5930:1981). The LL of clay and fly ash mixes is obtained by testing varies of fly ash percentage. Specific gravity and particle size distribution are obtained for original fly ash and clay sample. In addition, Standard Proctor and Unconfined Compressive Tests were conducted in order to obtain geotechnical properties of the sample. Unconfined compressive strength for clay and fly ash mixes is obtained based on cured sample for 7 days.

4. RESULTS AND DISCUSSIONS

In Table 3, the values were obtained from laboratory tests indicate the geotechnical properties of Fly ash, the physical properties and mechanical properties.

Table 3 : Engineering Properties of Fly ash

Geotechnical Properties	Value
Liquid Limit	22.5
Plastic Limit	6.17
Plasticity Index	16.33
Specific Gravity	2.17
Optimum Moisture Content	15.4%,
Maximum Dry Density	1.51 kg/m ³
7 Days Compressive Strength	82.53 kPa

Figure 2 show the particle size distribution of clay sample and Fly ash. It shows that the Clay sample fall under the silt category and is gap graded i.e the particle size is a combination of 2 or more uniformly graded fraction. While Fly ash is of a poorly graded fine particles i.e the particle of Fly ash is of the same size.

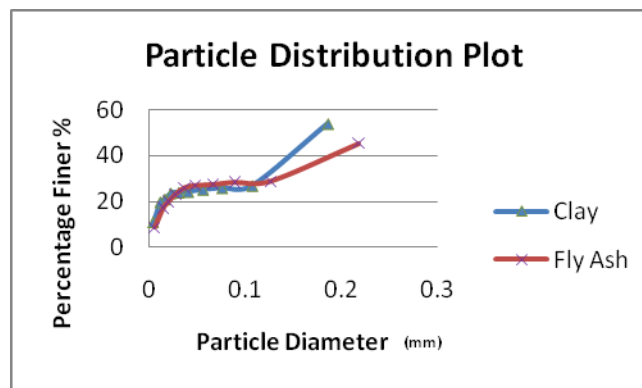


Figure 2: Particle Size Distribution of Clay sample and Fly Ash

From Table 4 it can be seen that the liquid limit of the sample is decreasing with the increasing amount of Fly Ash with the percentage of 0%, 5%, 10%, 15% and 20 %.

Table 4: Liquid Limit of different Percentage of Fly Ash by weight in Clay

Percentage of Fly Ash by weight in Clay	Liquid Limit , %
0%	60
5%	57.5
10%	55
15%	56
20%	51

The sample of clay and Fly Ash mixes of 0%, 60% 80% and 100% were cured for seven (7) days. Figure 3 shows the stress strain characteristics of the samples observed in Unconfined Compressive strength test. The 60 % Fly Ash by weight of clay results is the highest value of compressive strength, while Fly Ash alone is not a very strong material.

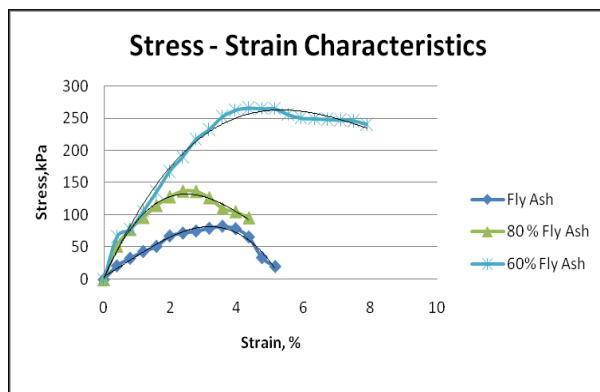


Figure 3: Stress - Strain Characteristics

Figure 4 shows the shear stress with respect to percentage of fly ash in clay sample. From Figure 4, the declined line shows that when there is too much amount of fly ash added, the shear stress is decreased as the sample was not able to stand the amount of stress applied. 60% of fly ash by weight of clay in the clay mixture gave the highest value of axial stress exerted. The fly ash alone is not a very strong material. The shear strength of cured sample tested was within the limitation based on the dry density and optimum moisture content of the fly ash which is 1.51 kg/m^3 .

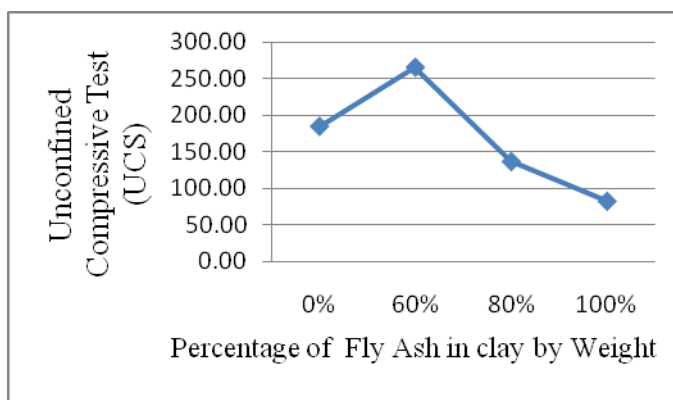


Figure 4: Unconfined Compressive Test versus different percentage of fly ash and clay mixes.

5. CONCLUSION

1. From the study, finally the basic Geotechnical Properties of Fly Ash can be concluded in the following table of 5.1. From the classification tests, the clay is classified as Gravelly clay. The Fly Ash is ashes with very fine particles slightly smaller than the particle size of clay. The different size can create a good bonding between the clay particle and Fly Ash particles. This type of clay is suitable to be stabilized with Fly Ash.

2. Addition of Fly Ash does have effects on the strength of clay. The shear strength observed of sample mixtures cured for 7 days were decreasing when amount of fly ash governed 80% of the total weight of mixture. Besides that, 60% of fly ash by weight and clay mixture gave the highest value of axial stress exerted. The fly ash alone is not a very strong material. Therefore in this scope of study, the most suitable amount of fly ash to be added in fly ash and clay mixes is between 50% - 60%. Besides the shear strength, the addition of fly ash also does improve other properties such as the dry density of mixture soil and the optimum moisture content of soil.

6. RECOMMENDATIONS

- i. It is recommended that a longer curing period should be done for 7, 14, 21 & 28 days in order to observe the shear strength pattern of fly ash and clay mixture of different mixture.
- ii. It is also recommended that the liquid limit of cured samples should be done since in this study only the liquid limits of uncured treated samples were done.

- iii. For further study it is suggested that the Consolidation Test to be performed to attain the compressibility of samples and to obtain soil data which is used in predicting the rate and amount of settlement of structures founded on clay.
- iv. It is also proposed to run the X-ray diffraction (XRD) to obtain the chemical composition of FA in order to determine the type of Fly Ash accurately.
- v. For advance research, it is recommended that the effect of combining two stabilizing agents in the stabilization of soft soil to be investigated to see whether it can improve the properties of soil better than fly ash alone.

ACKNOWLEDGMENT

The authors wish to thank Laboratory Assistances, Faculty of Engineering, UNIMAS Geotechnical Engineering Lecturers and fellow coursemates.

REFERENCES

- [1] American Society of Civil Engineers (ASCE) (2003), "Fly Ash" <http://engineers.ihs.com/pdf/abstact-navigation.html>, September 17 2008.
- [2] Basavanna, B.M. and Itagi Ravi Kumar (1990) 'Use of Coal Ash to Improve Some Properties of Black Cotton Soil,' Indian Geotechnical Conference-1990 on Advances in Geotechnical Engineering, Indian Geotechnical Society, Bombay, India, pp. 185 – 188.
- [3] Das, B.M., (2002), Principles of Geotechnical Engineering, Fifth Edition, Australia; Brooks/Cole.
- [4] Ferguson, G. (1993). "Use of self-cementing fly ashes as a soil stabilization agent." *Fly ash for soil improvement, Geotechnical Special Publication No. 36*, ASCE, New York, 1–14.
- [5] Ferguson, G., (1990) Aggregate Bases Constructed with Self Cementing Fly Ash, 9th international Ash Utilization Symposium, Washington, D.C.
- [6] Ferguson, G.,(1987) Ferguson, G(1987) Aggregate Bases Constructed with Self Cementing Fly Ash, 8th international Ash Utilization Symposium, Washington, D.C.
- [7] FHWA, 2006 FHWA (2006) – US Department of Transportation, Federal Highway Administration, Chapter 1 - Fly Ash Facts for Highway Engineers - Recycling – Pavements.
- [8] Gray and Lin, 1972 Gray, D.H., and Lin, Y.K., (1972), 'Engineering Properties of Compacted Fly Ash.' Journal Soil Mechanics Foundation Engineering, ASCE, Vol. 98, pp.361-380.
- [9] Gupta, 2008 Gupta, R.D., Alam, J., Mohd. Ahmadullah Farooqi (2008), Elsevier Ltd. 'Effect On CBR Value And Other Geotechnical Properties Of Fly Ash Mixed With Lime And Non-Woven Geofibres'
- [10] Hausmann, M.R.(1990), Engineering Principles Of Ground Modification, Singapore: McGraw-Hill,
- [11] Johnson et al. Johnson, W.A., m.Herrin, D.T. Davidson and R.L. Handy, 1988. Soil Stabilization in Highway Design Reference Guide. 5th Edition, McGraw Hill Book New York, pp: 501-548.
- [12] Koliass et al., Koliass, S., V. Kasselouri-Rigopoulou, and Karahalio, A., (2004) 'Stabilization Of Clayey Soils With High Calcium Fly Ash And Cement
- [13] Naik et al. Naik T.R., Ramme B.W, Kraus R.N., and Siddique, R., (2003). 'Long Term
- [14] Pandian et al., Pandian, N.S., RajaSekhar, C., and Sridharan, A., (1998) ' Studies on the Specific Gravity of some Indian Coal Ashes,' Journal of TESTING AND Evaluation, JTEVA. Vol. 26, No.3, pp. 177-186.
- [15] Phanikumar and Sharma (2004) "Effect of flyash on Engg properties of Expansive Soil" Journal of Geotechnical and Geoenvironmental Engineering Vol. 130, No7, July, pp. 764-767.
- [16] Reyes, A. and Pando, M. (2007). ' Evaluation of CFBC fly ash for Improvement of Soft Clays' World of Coal Ash (WOCA), Covington, Kentucky, USA, May 7 – 10.
- [17] Scott et. al, 2008"Scott M. Mackiewicz, E. Glen Ferguson"; Stabilization of Soil with Self-Cementing Coal Ashes
- [18] Senol et al., Senol, A., Edil, T.C., Md. Sazzad Bin Shafique, Hector, A.A., Benson. C.H.(2006). 'Soft Subgrades' Stabilization by Using Various Fly Ashes'. Resources, Conservation and Recycling, 46 (4); 365 – 376.
- [19] TPUB(2008),Chapter 18 Soil Stabilization TPUB, 2008 http://www.tpub.com/content/engineering/14070/css/14070_424.htm, Integrated Publishing Inc.,(September, 2008)
- [20] WEBB, 1973 Webb, D. L., (1973), The use of Pulverized Fuel Ash in Reclamation Fills.' Proceedings, 8th International Conference on Soil Mechanics and Foundation Engineering (ICSMFE), Vol. 1.2, Moscow, pp. 471 – 474.
- [21] Wikipedia (2008), www.wikipedia.com/Fly Ash, September 15 2008.

CHAPTER 6

PEAT STABILIZATION USING GYPSUM AND FLY ASH

Kolay, P.K. and Pui, M.P.

Abstract

This paper presents the stabilization of local peat soil from Matang, Sarawak, using gypsum and fly ash. Peat soil has been identified as one of the major groups of soils found in Malaysia, which has high compressibility and low shear strength. Presence of soft or peaty soil is a major problem encountered by civil engineers in Sarawak. Different percentages of gypsum (i.e., 2, 4, 6 and 8%) and fly ash (i.e., 5, 10, 15, 20 and 25%) were added into peat soil at optimum moisture content and its maximum dry density determined by standard Proctor test. Unconfined compressive strength (UCS) test were conducted to determine the strength gain after 7, 14 and 28 days of curing periods. Physical properties of the peat soil have also been studied for identification and classification purposes. The unconfined compressive strength test results show that the peat soil gained strength due to the addition of different percentages of admixtures such as gypsum and fly ash and the strength also increases with the increase of curing periods.

Keywords: Peat Soil, Stabilization, Gypsum, Fly Ash, Unconfined Compressive Strength (UCS)

1. INTRODUCTION

Peat soil is soft, wet and contains very high percentages of organic matter from plant materials. Peat covers a major area in Malaysia especially in the land of Sarawak. Peat soil usually is black to dark brown in color. The presence of organic matter in peat leads to high potential for further decomposition as a result of changing environment conditions. Peat also exhibit high natural moisture content (up to 800%) [1]. As demand for lands goes up with the increase of population causes engineers to think about the future development of peat land. Due to the very low shear strength and high compressibility of peat soil, engineers need alternative ways to develop a peat land for construction. Different approaches are used for the improvement of peat soil. Soil stabilization such as compaction and soil mixing with the addition of chemicals is to modify the soil condition so that construction can be done easily without any risk [2]. Most common way for soft or peat soil treatment is by excavating the soft or peat soil and replacing it with good granular or sandy soil but this way of soil treatment is not encouraged because of the uneconomical design. If heavy loaded buildings are to be constructed on a soft peat soil layers, piled foundations can be used to transfer the loading to the rock. But if lightly loaded buildings or a road are to be constructed, it is not economical to construct the structures on a piled foundation. The method of pre-consolidation by preloading is the most widely used method by the engineers to improve the soil. But the one of the disadvantage of preloading method is it requires a long period of time. Soil stabilization is very important to strengthen the peat soil. Therefore, it is more economical to improve the strength and stiffness of the soil so that the structures can be built on top of soft soil. Soil stabilization by using chemical admixtures involves the treatment of the structures and fabric of the soil. The chemical reaction that occurs within the soil will results in changes in moisture content, shear strength, compressibility, pH values and other physical, chemical and engineering properties of the soil. The chemical stabilizer will accelerate the bonding in the soil but the bonding and the rate of the bonding depends on the type of stabilizer used. Several researchers have done researches on the use of fly ash and gypsum on soft soil stabilization [3-13]. However, the study of possible improvement of soft or peat soil stabilization by using different types of admixtures seems to be limited in Sarawak, Malaysia. The objective of this paper is to demonstrate the feasibility of stabilizing peat soil with fly ash and gypsum as admixtures and to evaluate the response of peat for soil improvement for construction on it.

2. PHYSICAL PROPERTIES OF PEAT

Peat is a product of decomposition of organic matter from plants and animals. It has a great capacity for taking up and holding water. High water content results in high pore volume leading to low bulk density and low bearing capacity [14, 15]. Void ratio is an indicator for the compressibility of the material. Void ratios of peats and organic soils are generally higher

than for inorganic soils. For submerged peats and organic soils void ratio linearly varies with water content. The higher specific gravity indicates a higher degree of decomposition and low mineral content. An approximate and easier method of determining specific gravity is to use ash content or organic content. The ash content is an indication of the organic content in the peat. The unit weight is influenced by the water content and organic content of the peat. Unit weights will increase with the increment of specific gravity. Unit weight of peat is typically lower compared to inorganic soils. Peat will shrink extensively when dried.

3. ENGINEERING PROPERTIES OF PEAT

The shear strength of peat soil is very low; however, the strength could increase significantly upon consolidation [16]. Shear strength is associated with several variables such as the origin of soil, water content, organic content, and degree of decomposition. The shear strength of peat is determined based on drained condition. Considering the presence of peat soil is almost always below the groundwater level, the determination of undrained shear strength is also important. The compression behavior of fibrous peat is different from clay soil. Initial compression occurs instantaneously after the load being applied; the primary and secondary compressions are time dependent. Primary consolidation is due to dissipation of excess pore water pressure caused by an increase in effective stress whereas secondary compression takes place under constant effective stress after the completion of dissipation of excess pore water pressure [14]. Compression of fibrous peat continues at a gradually decreasing rate under constant effective stress, and this is termed as the secondary compression. The secondary compression of peat is thought to be due to further decomposition of fiber which is conveniently assumed to occur at a slower rate after the end of primary consolidation [17]. Permeability is one of the important properties of peat because it controls the rate of consolidation and increase in the shear strength of the soil [18]. Previous studies indicated that the peat is averagely porous, and certifies the fact that fibrous peat has a medium degree of permeability [19].

4. METHODOLOGY

Physical properties such as moisture content, specific gravity, particle size and liquid limit are determined to establish the basic characteristics of the peat soil. The peat soil was classified based on von Post scale for degree of decomposition, fiber content, loss on ignition and organic content. Engineering property such as standard Proctor test and unconfined compressive strength also has been studied.

After the soil sample collected from Matang, Sarawak, approximately at the depth of 0.5 to 1.0 m, at first sun-dried followed by grinding and sieving. The soil particles that passed through 1.18 mm sieve are collected to conduct different test with different percentage of admixtures. The procedure for conducting the experimental investigation is based on the British Standard BS 1377:1990 and ASTM standard. Tests on different proportion of fly ash and gypsum are designed to obtain the most suitable proportion of stabilizer that will improve the peat soil sample most in term of strength and other physical and engineering properties. Tests on original peat soil alone also been conducted in order to access the improvement made on the peat soil samples.

After obtaining the value of maximum dry density and optimum moisture content of the sample from standard Proctor test, the specimens were tested using stabilized agents such as gypsum of 2, 4, 6, and 8%; and fly ash of 5, 10, 15, 20, and 25% of dry weight of the sample. To prepare a cylindrical sample for UCS test, a poly vinyl chloride (PVC) pipe with 50 mm diameter and 100 mm height has been used. As shown in Figure 1, a PVC pipe cut into half so that the soil sample can be easily extracted without disturbing the structure of the soil was used as a mould. Two cap (top and bottom) is used to seal the soil sample once the sample is filled into the PVC pipe. After sample preparation, the sample has been kept for approximately 24 hours before it being immersed in the water tank for curing. The unconfined compressive strength tests were conducted after curing period for 7, 14 and 28 days to investigate the strength of treated soil.

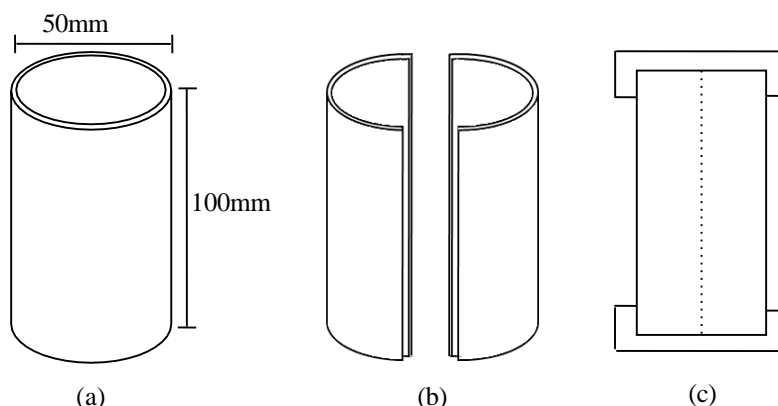


Figure 1: Mould for UCS soil samples preparation

5. SOIL PROPERTIES' TEST RESULTS

The physical and geotechnical properties of the soil samples were shown in Table 1. The preliminary identification of the soil was made based on the index properties testes conducted on the peat soil sample. The peat can be considered as very soft and dark brown peat which contained a large amount of fiber by using visual identification. There were lots of plant structures such as roots in the soil. The texture is quite coarse and may results in large permeability.

The peat was classified based on the degree of humification known as von Post scale and the organic and the fiber content in the soil sample. The degree of humification test was done by based on the appearance of soil water that is extruded when a sample of soil is squeezed in the hand.

Loss on ignition test has been conducted on the samples collected to obtain the organic content of the samples. From the Table 1 it can be observed that the sample has very high value of loss of ignition and organic content. The value of liquid limit is high because the sample contains lots of fiber which results in high water absorption capacity. Standard Proctor test was carried out for soil sample in order to find out the compaction characteristics such as the optimum moisture content (OMC) and maximum dry density (MDD) for the sample.

Table 1. Physical and geotechnical properties of peat soil

Parameters	Results
Natural moisture content, MC (%)	678.47
Von Post humification for peat	H4
Fiber content (%)	70.83
Specific gravity, G_s	1.21
Loss on Ignition, LOI (%)	95.21
Organic content, OC (%)	94.47
Liquid Limit, LL	150
Maximum Dry Density, MDD, γ_d (gm/cc)	0.56
Optimum Moisture Content, OMC (%)	95.17

6. UNCONFINED COMPRESSIVE STRENGTH

Unconfined compressive strength (UCS) test was performed on the cured peat soil sample with different percentages of stabilizers and the results are presented in Figure 2 and 3. UCS test is the most common test to determine the strength of stabilized soil. For each UCS test, the stress – strain relationships was determined. The sample was mixed with various percentages of gypsum (i.e. 2, 4, 6 and 8%) and fly ash (5, 10, 15, 20 and 25%). Figure 2 shows the gain in UCS with respect to various percentages of gypsum added and to different curing periods, where as Figure 3 shows the similar test results with respect to various percentages of fly ash added to peat soil with different curing periods.

In general, the compressive strength value indicates that all admixture treatment types resulted in strength gain. It can be noticed that the strength of treated soil increased with curing time. Most of the strength gain occurred within the first seven days of curing. The results show that higher strength was achieved for the sample mixed with fly ash. This fast gain of strength is believed to be related to the initial rapid hydration that takes place with these admixtures. The UCS strength value for peat treated with fly ash has the highest level of strength gain and these seem to be a slower rate of strength gain after 14 days of curing. This trend is the same with the sample mixed with gypsum where the UCS values for gypsum seem to stabilize after 14 days of curing, the strength only increase slightly compared with 14 days of curing and 28 days of curing. The UCS value increases constantly for the sample mixed with gypsum and fly ash. But for the sample mixed with 25% of fly ash, the samples have higher gain of strength when compared to samples mixed with other percentages of fly ash.

The results show that soil treatments were effective in increasing the strength of the samples. The UCS values increase with addition of gypsum and fly ash to its maximum at 6% of gypsum and 20% of fly ash after that it dropped at 8% of gypsum and 25% of fly ash. This decrease in the UCS value after the addition of 8% gypsum may be due to the excess gypsum added to the soil and therefore formed weak bonds between the soil particle and the cementitious compound formed. The reason for the fly ash added soil' strength drop is not certain, but it could be related to sample degradation during the curing. But after 28 days of curing, the sample treated with 25% of fly ash gain more strength when compared with the sample treated with 20% of fly ash. Strength improvement levels were observed to be highest for fly ash treated soil where most improvement was achieved with 20%.

In general, the UCS increases with the increase of percentages of gypsum added to the soil sample, but the UCS values starts to decrease after 6%. The strength increases with the period of curing for all percentages of gypsum added. The

maximum strength obtained is from the sample with 6% gypsum added with 28 days of curing which is 44.94 kPa. For Fly Ash, the UCS values increase with the increases of percentage of fly ash added to the soil sample except for 25% fly ash with curing time of 7 days and 14 days. The sample with 25% fly ash added to the soil sample has slightly higher value than 20% fly ash added. The maximum strength obtain is from the sample with 25% fly ash added with 28 days of curing which is 109.69 kPa. For minor percentages of stabilizer added to the sample, gypsum shows high gain of strength even though the highest strength is only 44.94 kPa. The strength gains in samples with fly ash are the highest when highest percentages of stabilizer are added. In comparison by curing time, the samples increase in strength with the increase in curing time. In general, the soil samples gain more strength with addition of fly ash as compared to gypsum.

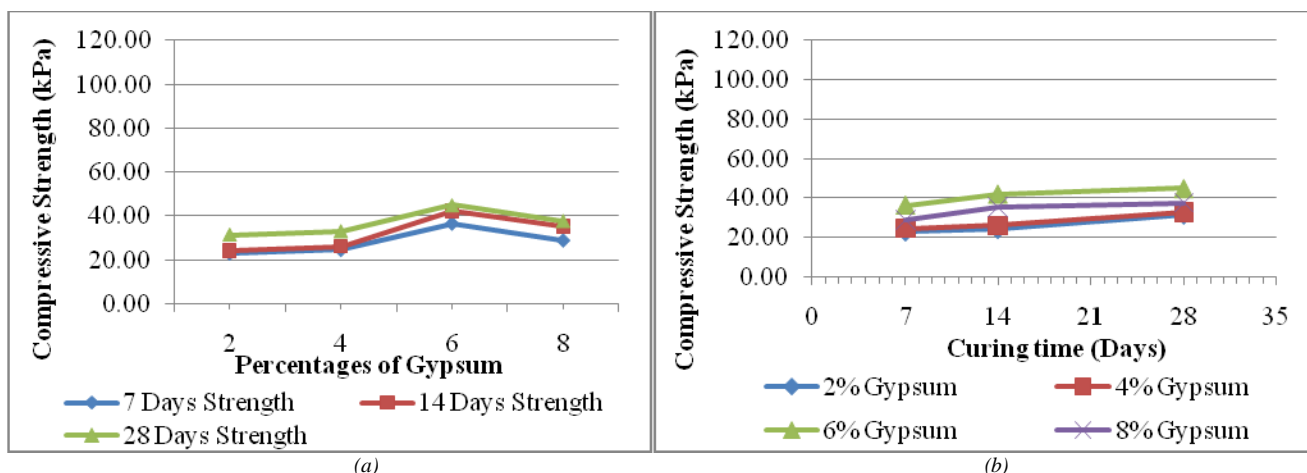


Figure 2. UCS test results for sample with respect to various (a) percentages of gypsum added (b) curing periods

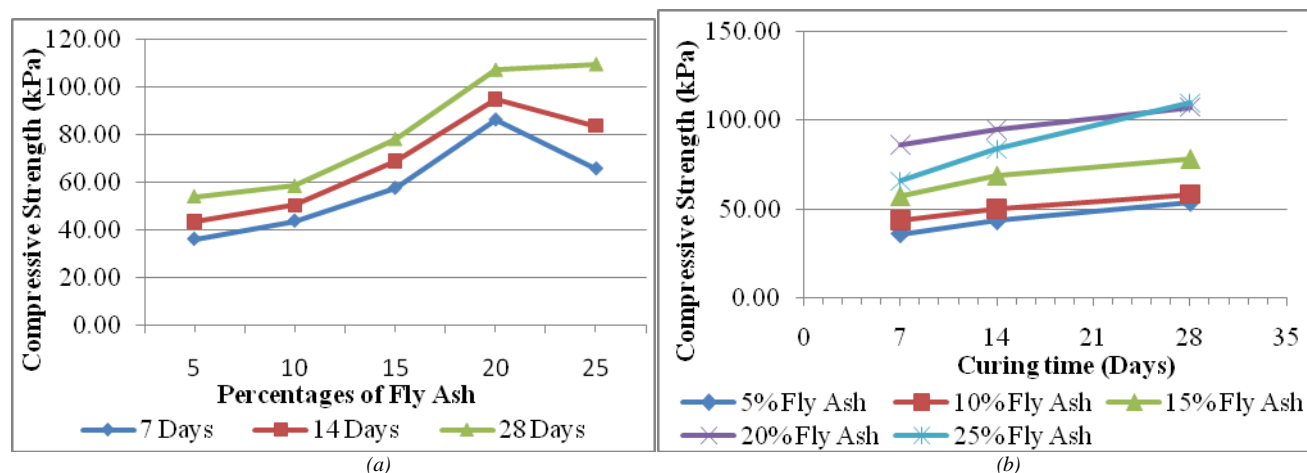


Figure 3. UCS test results for sample with respect to various (a) percentages of fly ash added (b) curing periods

7. CONCLUSIONS

In the present study, a laboratory investigation involving use of gypsum and fly ash for the improvement of strength of peat soil was carried out. In general, the test results indicate that peat soil treated with gypsum and fly ash result in improvement of strength of the soil as measured from unconfined compressive tests. In general the compressive strength gain was observed primarily in the first 14 days of curing and then had a tendency to slow down the rate of strength gain afterwards. For 8% gypsum treated soil, drop in strength was observed when compared to 6% gypsum treated soil. Similar trend has been observed with 25% fly ash treated soil (compared to 20% fly ash) except for 28 days of curing, where slightly drop in strength was observed.

From the series of laboratory investigation carried out, the following conclusions can be made:

- The soil sample collected from Matang is categorized as peat soil.
- The unconfined compressive strength (UCS) values increase as the percentages of gypsum and fly ash added increase except for 8% of gypsum and 25% of fly ash.
- The unconfined compressive strength (UCS) values increase as the curing period increase for all percentages of stabilizer added.
- The average value of unconfined compressive strength (UCS) from test results are 31.37, 32.92, 44.94 and 37.70 kPa for 2, 4, 6 and 8% gypsum added respectively for 28 days curing.

- The average value of unconfined compressive strength (UCS) from test results are 54.01, 58.47, 78.17, 107.35 and 109.69 kPa for 5, 10, 15, 20 and 25% fly ash added, respectively for 28 days curing.

This improvement favorably indicates the use of cheaply available local fly ash in stabilization of peat in sub-grade, embankment etc.

ACKNOWLEDGMENTS

The authors would like to express deep gratitude for the technical supports offered by the Geotechnical laboratory staff and the Construction on Soft Soil Group members, Universiti Malaysia Sarawak (UNIMAS), Sarawak, Malaysia.

REFERENCES

- [1] Deboucha, S., Hashim, R. & Alwi, A. Engineering Properties of Stabilized Tropical Peat Soils. *EJGE*, Vol. 13, Bund. E, 2008, pp. 1-9.
- [2] Kawamura, M. *Fundamental Studies on the Fabric of Soil Cement Mixture and Its Mechanical Properties*, Kyoto University, 1970, Japan.
- [3] Hughes, P., Glendinning, S. "Deep dry mix ground improvement of a soft peaty clay using blast furnace slag and red gypsum". *Quarterly Journal of Engineering Geology and Hydrogeology*, Vol. 37, No. 3, 2004, pp. 205-216.
- [4] Degirmenci, N., Okucu, A., and Turabi, A. "Application of phosphogypsum in soil stabilization". *Building and Environment*, Vol. 42, No. 9, 2007, pp. 3393-3398.
- [5] Ameta, N. K., Purohit, D.G.M., Wayal, A.S. and Sandeep D. "Economics of Stabilizing Bentonite Soil with Lime-Gypsum". *Electronic Journal of Geotechnical Engineering*, 2007, Vol. 12, Bundle E.
- [6] Anil, M. (2006). CBR and DCP Correlation for Class C Fly Ash-Stabilized Soil, *Geotechnical Testing Journal*, Vol. 29, No. 1, pp. 30-36.
- [7] Edil, T.B. and Acosta, H.A. Stabilizing Soft Fine-Grained Soils with Fly Ash. *Journal Material in Civil Engineering*, Vol. 18, No. 2, 2006, pp. 283-294.
- [8] Dutta, R.K. and Sarda, V.K. CBR Behaviour of waste plastic strip-reinforced stone dust/fly ash overlying saturated clay. *Turkish Journal of Engineering and Environmental Science*, Vol. 31, 2007, pp. 171-182.
- [9] Hughes, P., Glendinning, S. "Deep dry mix ground improvement of a soft peaty clay using blast furnace slag and red gypsum". *Quarterly Journal of Engineering Geology and Hydrogeology*, Vol. 37, No. 3, 2004, pp. 205-216.
- [10] Indraratna, B., Utilization of lime, slag and fly ash for improvement of a colluvial soil in New South Wales, Australia, *Geotechnical and Geological Engineering*, Vol. 14, 1996, pp. 169-191.
- [11] Kolay P.K, and Romali N.S.B. Stabilization of organic soil by different types of stabilizer. *International Conference on Civil Engineering in the New Millennium: Opportunities and Challenges*, Bengal Engineering and Science University, Shibpur, India, Vol. III, 2007, pp. 1394-1400.
- [12] Singh, S.P., Tripathi, D.P. and Ranjith, P.G. Performance of evaluation of cement stabilized fly ash-GBFS mixes as a highway construction material. *Waste Management*, Vol. 28, 2008, pp. 1331-1337.
- [13] Trzebiatowski BD, Edil TB, Benson CH Case study of subgrade stabilization using fly ash. *State Highway 32, Port Washington, Wisconsin*, 2000, pp. 123-136.
- [14] Gofar, N. *Fundamental studies on compressibility of peat soil using large strain*. Fundamental research report, 2005, Universiti Teknologi Malaysia.
- [15] Huat, B.B.K. *Organic and Peat Soils Engineering*. Malaysian Book Publishers Association, 2004, UPM Press.
- [16] Noto, S. *Peat Engineering Handbook*. Civil engineering Research Institute, 1991.
- [17] Mesri, G., Stark, T. D., Ajlouni, M. A. & Chen, C. S. "Secondary compression of peat with or without surcharging." *Journal of Geotechnical and Geo-environmental Engineering*. Vol. 123, No. 5, 1997, pp. 411-421.
- [18] Hobbs, N. B. "Mire morphology and the properties and behavior of some British and foreign peats." *Engineering. Geology*, Vol. 19, No. 1, 1986, pp. 7-80.
- [19] Macfarlane, I. C. *Engineering Characteristics of Peat*. In *Muskeg Engineering Handbook*. Proc., Ottawa, Canada, 1969, pp. 3-30.

CHAPTER 7

SOIL EROSION AND SEDIMENT YIELD OF A SANITARY LANDFILL SITE – A CASE STUDY

Oon, Y.W.¹, Chin, N.J.² and Law, P.L.³

Abstract - This research presents the results of a study on soil erosion rates and sediment yields of a proposed Level 4 Sanitary Landfill construction site located in Sibul, Sarawak. Assessments on potential soil erosion rates and sediment yields during pre-construction, construction and operation stages were carried out using the Revised Universal Soil Loss Equation (RUSLE) and Modified Universal Soil Loss Equation (MUSLE), respectively. It was found that soil erosion rates during construction and operation stages fell under “Moderately High” category, whereby highest sediment yield occurred during construction and operation stages. Comparative analysis on with and without Best Management Practices (BMPs) during construction stage demonstrated that BMPs could significantly reduce the rate of soil erosion, and thus sediment yields.

Keywords: Soil erosion rate, sediment yield, construction, RUSLE, MUSLE, BMPs

1. INTRODUCTION

In Malaysia, there has been an increasing concern over soil erosion due to deforestation, land conversion for highway, logging activities, industrial or urbanization purposes [1]. Runoff erosivity has been the most significant erosion factor due to high mean of annual rainfall, storm frequency and density [2]. The objectives of this research are to estimate and compare soil erosion rates and sediment yields during pre-construction, construction, and operation stages of a sanitary landfill at Sibul, Sarawak.

The proposed Level 4 Sanitary Landfill is located approximately 26 km from Sibul Town centre (Figure 1). It is a Level 4 Sanitary Landfill located at Jalan Kemuyang, Sibul, Sarawak. Comprehensive assessments on the rates of erosion and sediment yields were carried out during pre-construction, construction and post-construction stages. The topography of the region comprises of generally rolling and flat lands, well-drained by tributaries of Sg. Lukut running along the northeast boundary of the proposed landfill site (Figure 1). There are relatively lower spots at the north part of the landfill site, mainly swampy land. The landfill area is predominantly underlain by Tertiary Eocene sediments; namely Pelagus Formation and a small portion by Pleistocene-Holocene sediments.

The two main streams draining the site catchment are Sungai Lukut and Sungai Pasai, whereby Sungai Lukut is the tributary of Sungai Pasai. The annual rainfall pattern varies from year-to-year with distinct dry and wet seasons, which shows the characteristic influence of the monsoon seasons. The region experiences rather heavy rainfall during the peak of the Northeast monsoon, receiving more than 400 mm in December and 500 mm in January. The total annual rainfall is relatively high that varies between 110.2 mm during the El Nino years to above 4,500 mm during the wet years.

¹ Oon, Y.W., Student of Civil Engineering Department, Universiti Malaysia Sarawak (e-mail: yinwee3@yahoo.com)

² Chin, N.J., Student of Civil Engineering Department, Universiti Malaysia Sarawak (e-mail: chin_17@live.com)

³ Law, P.L., Prof. Civil Engineering Department, Universiti Malaysia Sarawak (e-mail: puonglaw@feng.unimas.my)

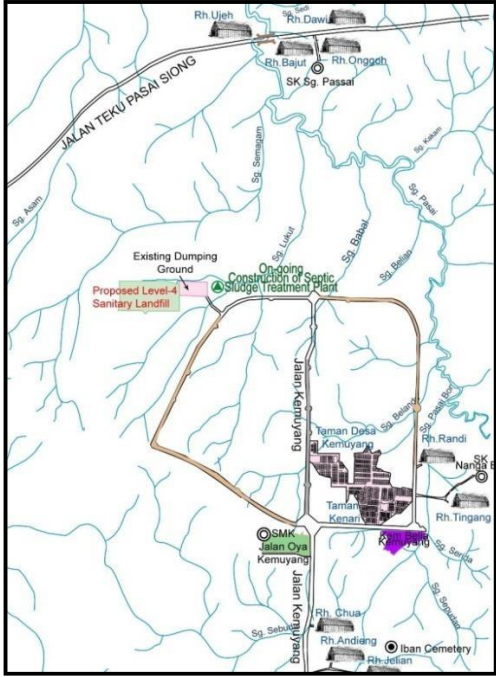


Figure 1: Locality of Proposed Level 4 Sanitary Landfill, Jln Kemuyang, Sibul

Since the early 1980s, the United States Department of Agriculture (USDA) has used the Universal Soil-Loss Equation (USLE) to estimate the severity of soil and sediment yield from disturbed land surface. Lately, a refined and revised equation called Revised Universal Soil-Loss Equation (RUSLE) that can be applied to many more field conditions, provides much more site-specific value than does the USLE, and to overcome major limitations of the USLE for predicting rainfall erosion losses. Generally, the RUSLE equation can be written as follow:

$$RUSLE = R \times K \times LS \times C \times P \tag{1}$$

- where, RUSLE = Average annual soil loss in unit $[tons.(ha.yr)^{-1}]$
- R = Rainfall/runoff erosivity in unit $[Mj.mm.(ha.h.yr)^{-1}]$
- K = Soil erodibility in unit $[tons.ha.h.(ha.Mj.mm)^{-1}]$
- LS = Slope length and steepness factor
- C = Cover-management factor
- P = Erosion control practice factor

In this study, the R factor was estimated using Foster’s Method according to the following equation [4]:

$$R = 0.276P \times \left(\frac{I_{30}}{173} \cdot 6 \right) \tag{2}$$

- where, P = mean annual rainfall in mm, and
- I_{30} = maximum 30-minute rainfall intensity.

Appropriate LS value could be obtained from the following equation:

$$LS = (0.065 + 0.045S + 0.0065S^2) \times \sqrt{\frac{L}{22} \cdot 13} \tag{3}$$

where, *L* is in metre (m) and *S* in percent (%).

In addition to RUSLE equation, another soil loss equation was established in 1975, namely the Modified Universal Soil Loss Equation (MUSLE) or also called Single Event Sediment Yields [5]. In this equation, the rainfall energy or runoff erosivity factor, R in the USLE was replaced with a term that includes both the peak discharge and total amount volume of runoff applied to the field to determine the sediment yield during a specific storm event [5]. Generally, the MUSLE equation is expressed as:

$$\text{MUSLE} = 11.8 \times \left((V \times Q_p)^{0.56} \right) \times K \times LS \times C \times P \quad (4)$$

where MUSLE = Sediment yield (tons)
V = Runoff volume (m³)
Q_p = Peak runoff rate (m³.sec⁻¹)

The peak runoff rate can be determined by using rational formula with the equation described as follow:

$$Q_p = \frac{CIA}{360} \quad (5)$$

The runoff coefficient, C, represents the percentage of rainfall which is related to multiple hydrologic processes. In a non-homogeneous drainage area, C should be calculated as an area-weighted composite of the different land uses in the watershed. The intensity, I can be obtained from Rainfall Intensity, Duration and Frequency Curve (IDF Curves) [6]. A is the drainage area. The IDF curve summarizes the conditional probabilities or frequencies of rainfall depth or average intensities at a particular location. These variables, i.e. intensity, duration and frequency are all related to each other [7].

The SCS Curve Number Runoff relates a calculated Runoff Curve Number (CN) to runoff, accounting for initial abstraction losses and infiltration rates of soils. The fundamentals rainfall-runoff equations are as follows [8]:

$$Q_p = \frac{((P - I_a))^2}{(P - I_a) + S} \quad (6)$$

Initial abstraction (I_a) is all losses before runoff begins, which includes water retained in surface depressions, water intercepted by vegetation, evaporation, and infiltration. I_a is highly variable but generally is correlated with soil and cover factors. From the previous studies on small agricultural watersheds, I_a can be approximated by the following empirical equation:

$$I_a = 0.2S \quad (7)$$

While I_a is an independent parameter, this approximation allows the use of a combination of S and P to produce a unique runoff amount. Substituting (7) into (6) gives:

$$Q_p = \frac{(P - 0.2S)^2}{P + 0.8S} \quad (8)$$

S is related to the soil and cover conditions of the watershed as represented by the value of Runoff Curve Number (CN). Generally, CN values range from 0 to 100, and S is related to CN by:

$$S = \left(\frac{1000}{CN} \right) - 10 \quad (9)$$

For a given CN and precipitation depth, the volume of runoff can be calculated using Equation 8 and Equation 9. The CN value can be expressed as a function of soil characteristics, hydrologic condition and cover or land use. For watersheds with multiple soil types or land uses, an area-weighted CN should be used. When significant differences in land use or natural control points exist, the watershed should be divided up into smaller drainage areas for modeling purposes. Many factors can affect the erosion and sedimentation processes especially in construction development. In this study, the RUSLE and MUSLE concepts were used as measurements of soil erosion for specific combinations of physical and

management conditions in the proposed landfill site, in addition to taking into consideration the suitability and data dependant factors.

During construction stage, the Erosion and Sedimentation Control Plan (ESCP) is generally regarded as a comprehensive plan designed to address the temporary and permanent mitigation of erosion and sedimentation hazards on disturbed soil surfaces. The objectives of ESCP are to implement temporary or permanent erosion and sedimentation mitigation measures. The plans also aim to identify, reduce, eliminate, or prevent the pollution of stormwater as well as the water quality of nearby watercourses by controlling peak rates and volumes of runoff outfalls and downstream of the outfalls.

II. MATERIALS AND METHOD

An integrated approach for the assessment of the soil erosion rate and sediment yield for different construction stages, and recommended appropriate mitigation measures for the project site is shown in Figure 2. Preliminary investigation and identification of the study area were carried out prior to the erosion analysis. In this study, RUSLE and MUSLE equations were used to estimate the soil erosion rates and sediment yields at the project site. The equations and the relevant factors are shown in Equation 1 to Equation 9.

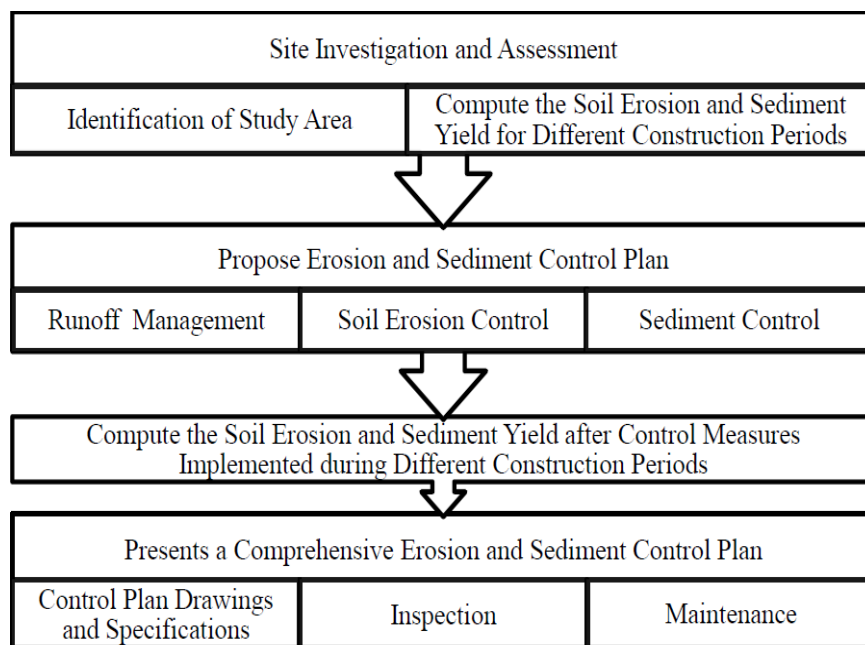


Figure 2: Erosion Rate and Sediment Yield and Mitigation Measures

Since comprehensive rainfall records are not available, the rainfall observations obtained from Jabatan Kerja Raya, Sibul, Sarawak was used to represent the rainfall condition at the landfill site, as it is the nearest rainfall station in Sibul Division or Central Zone of Sarawak. The R factor was estimated using Foster's Method as shown in Equation 2 [4]. The monthly average rainfall was used to determine the mean annual rainfall and the *Rainfall Intensity-Duration-Frequency Curve* for 30 minute in 5 years return period was used to estimate the R factor [6].

Due to the absence of empirical value, the K factor of a soil was determined from *USDA Soil Erodibility Nomograph* during pre-construction, construction, and operation stages [9]. The K factor is related to the class of land-component map on the basis of percentages of sand, silt, very fine sand, organic matters, soil structure and permeability [9]. The basis of percent of sand, percent of silt plus very fine sand parameters was determined from the soil particle size distribution analysis for the landfill site. The percentage of organic matters was obtained from the *Test Report* of the landfill site by taking the average percentage of organic matters content of the 16 borehole log data in the disturbed samples. The soil structure categories were determined from the *USDA Soil Structure Classes* [9]. The permeability value

was estimated using borehole drilling test method and the results were compared to the *USDA Soil Permeability Classes* [9].

The landfill site is located on existing ground levels between 8.5–16.0 meters contour levels, and the site will be elevated to a design elevations ranging from 10.0 – 22.5 meters contour level. Site stripping, excavation, and grading on exposes soil shall alter slope gradient and slope length. Therefore, the potential erosion and sedimentation shall most likely to occur along the project alignments during construction stage. During operation stage, slope length is generally not significant as the elevation is same as the design level. Therefore, the slope length (LS) during construction stage and operation stage shall be considered the same.

As shown in Figure 4 and Figure 5, a total of 13 different slope lengths for the individual “micro-catchments” had been estimated in the process of determining the value of C during pre-construction, construction, and operation stages with reference to *Cover Management Factor (C) for Construction Sites* [10]. However, the P value was determined by using the *Surface Condition for Construction Sites* [10].

The peak flow, Q_p was determined using *Rational Formula* by delineating the watershed boundary and computing the landfill area. Then the rainfall intensity, i for the 5-Yr design storm was determined with reference to the *IDF Curve* [6]. The runoff coefficient was adopted from the *Runoff Coefficients for Rational Equation* to determine the peak flowrate, Q_p [11].

Additionally, the *SCS Curve Number Runoff Method* was used to determine the volume of runoff by using the *Runoff Curve Numbers for Undeveloped Land* [10]. The *Hydrologic Soil Groups (HSGs)* in *USDA Manual, 1986* describes the water absorption in soil after a period of prolonged wetting and the data were used to determine the CN values [10].

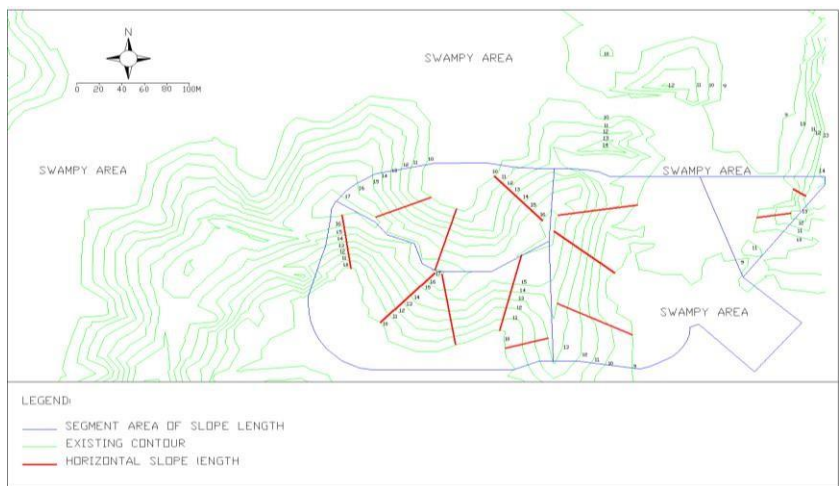


Figure 3: Estimated Slope Lengths during Pre-Construction Stage

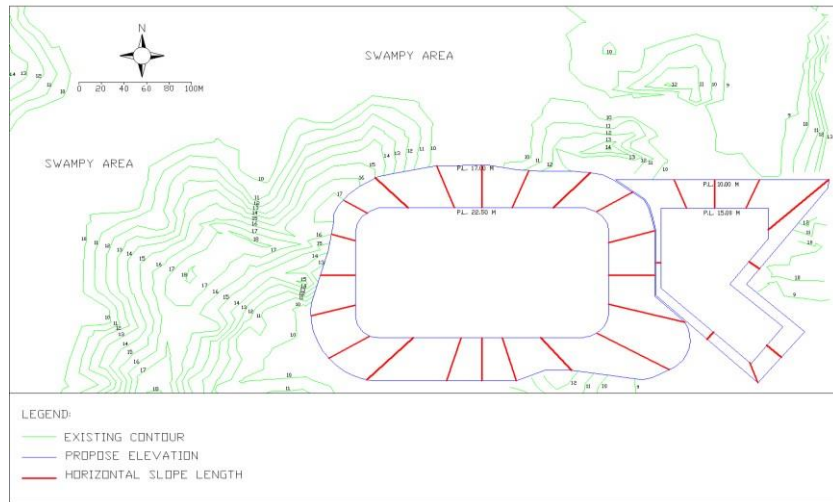


Figure 4: Estimated Slope Lengths during Construction Stage

III. RESULTS AND DISCUSSION

Soil erosion rates were estimated using the Revised Universal Soil Loss Equation (RUSLE), while sediment yields were predicted using the Modified Universal Soil Loss Equation (MUSLE). The mean annual rainfall in Year 2003 recorded at *Sibu JKR Water Board Station* was 270.54 mm for the region [6]. From the *Rainfall Intensity-Duration-Frequency Curve*, it was determined that the value of rainfall intensity, I for 30-minute 5 years return period was approximately 99 mm.hr^{-1} . From Equation 2, the rainfall runoff erosivity, R was found to be $42.58 \text{ Mj.mm.(ha.h.yr)}^{-1}$.

Analysis on the soil samples collected from project site showed that the soil types ranged from very soft clay, clayed silt to firm sandy silt. The particle size distribution analysis showed that the average percentage of silt (including very fine sand), sand and organic matters were 78.59%, 1.22% and 0.128%, respectively. The average soil permeability at landfill site was found to be $1.15 \times 10^{-5} \text{ cm.s}^{-1}$, and the K factor for the landfill site was $0.46 \text{ tons.ha.h.(ha.Mj.mm)}^{-1}$.

The maximum LS values at site were found to be 3.16 during pre-construction stage and 3.59 during construction and operation stages. The soil at site would be disturbed during earthwork and the existing vegetation would have to be cleared and removed for cut-and-fill activities. Based on the *Cover Management Factor (C) for Construction Sites*, the C value of 0.01 would be used during pre-construction stage as an undisturbed condition [10]. During construction and operation stages, C value of 1.0 would be used for cleared or bare soil surfaces and no re-vegetation conditions.

Based on the *Surface Condition for Construction Sites*, when no activities are carried out on the landfill site, a default P value of 1.0 would be used [10]. During construction stage, construction activities such as grading, excavating, cutting and filling would disturb the soil by loosening the particles of soil and thus reducing the soil's shear strength, which may lead to surface runoff caused by heavy rain water. Thus, a P value of 1.3 would be used. After the construction period, considering the project site is rough, irregular surface equipment tracks in all directions, P value of 0.9 would be used.

The runoff coefficient, C and the peak flow, Q_p used in the Rational Formula was computed in Table 1 whilst the Runoff Curve Number, CN and Runoff Volume, V were calculated in Table 2 for different construction stages. Table 3 and Table 4 show the predicted soil erosion rates and sediment yields without control measures onsite during different construction stages, whilst Table 5 and Table 6 show the estimated soil erosion rates and sediment yields with BMP control measures onsite. The BMP control measures proposed for this research are stated in Table 7 for different construction stages whilst the proposed locations and methods of application are shown in Figures 5, 6, 7, 8 and 9.

As shown in Tables 2, 3, 4, 5 and 6, the potential soil erosion rates and sediment yields after implementation of BMPs control measures during different construction stages could effectively reduce the impacts from 91.4 and 954.8 to 1.62 and 24.8 tons.(ha.yr)^{-1} , respectively. During operation stage, the

soil erosion rates and sediment yields would decrease from 63.3 and 1042.4 to 0.54 and 14.9 tons.(ha.yr)⁻¹, respectively. According to the *Classification of Soil Erosion Risk under Department of Environment* [12], BMP is very effective and able to reduce the potential soil loss from Moderate-High Soil Loss Risk to Low Risk, as shown in Table 8. With BMP onsite, it was showed that a decrease of 97.4% in soil erosion rate and more than 98% sediment reduction during both the construction and operation stages.

Table 1: Runoff Coefficient, C and Peak Flow, Q_p vs Construction Stage

Stage	Area (m ²)	Area (ha)	Average slope	Coefficient, C	Rainfall Intensity, I (mm.hr ⁻¹)	Peak Flow, Q _p (m ³ .s ⁻¹)	Total
Pre -Construction	14720.64	1.472	0.11	0.2	99	0.081	0.415
	24302.70	2.430	0.10	0.2	99	0.134	
	36493.17	3.649	0.12	0.2	99	0.201	
Construction	17426.68	1.743	0.17	0.5	99	0.240	1.038
	58089.83	5.809	0.17	0.5	99	0.799	
Operation	17426.68	1.743	0.17	0.6	99	0.288	1.246
	58089.83	5.809	0.17	0.6	99	0.958	

Table 2: Runoff Curve Number, CN and Runoff Volume, V vs Construction Stage

Stage	Rainfall Depth (mm)	Rainfall Depth (in)	HSGs	CN	S	Runoff Depth, Q (in)	Runoff Depth (m)	Area of Site (m ²)	Runoff Volume (m ³)
Pre-Construction	49.5	1.95	D	86	1.628	0.811	0.021	75516.51	1556.24
During Construction	49.5	1.95	D	74	3.514	0.327	0.008	75516.51	626.81
Operation	49.5	1.95	D	82	2.195	0.616	0.016	75516.51	1181.61

Table 3: Predicted Soil Erosion Rates vs Construction Stages (without Control Measures)

Stage	R [Mj.mm.(ha.h.yr) ⁻¹]	K [tons.ha.h.(ha.Mj.mm) ⁻¹]	LS	C	P	RUSLE (tons.{h a.yr} ⁻¹)
Pre-construction	42.58	0.46	3.16	0.01	1	0.619
During Construction Without Control	42.58	0.46	3.59	1.0	1.3	91.412
Operation Stage	42.58	0.46	3.59	1.0	0.9	63.285

Table 4: Predicted Sediment Yields vs Construction Stages (Without Control Measures)

Stage	Q _p (m ³ .s ⁻¹)	V, (m ³)	K [tons.ha.h.(ha.Mj.mm) ⁻¹]	LS	C	P	MUSLE (tons)
Pre-construction	0.415	1556.24	0.46	3.16	0.01	1	6.43
During Construction Without Control	1.038	628.81	0.46	3.59	1.0	1.3	954.81
Operation Stage	1.246	1181.61	0.46	3.59	1.0	0.9	1042.44

Table 5: Soil Erosion Rates with Implementation of BMP Control Measures

Stage	R	K	LS	C	P	Effectiveness of Sediment Control Factor					RUSLE (tons.{ha .yr} ⁻¹)
						Earth Bund	Silt Fence	Silt Trap	Check dams	Stabilized Construction Exit	
During Construction Without Control	42.58	0.46	3.59	0.1	1.0	0.95	0.95	0.85	0.4	0.75	1.618
Operation Stage	42.58	0.46	3.59	0.01	0.9	-	-	0.85	-	-	0.538

Table 6: Sediment Yields with Implementation of BMP Control Measures

Stage	Q _p	V	K	LS	C	P	Effectiveness of Sediment Control Factor					MUSLE (tons)
							Earth Bund	Silt Fence	Silt Trap	Check dams	Stabilized Construction Exit	
During Construction Without Control	1.038	628.81	0.46	3.59	0.1	1.0	0.95	0.95	0.85	0.4	0.75	24.806
Operation Stage	1.246	1181.61	0.46	3.59	0.01	0.9	-	-	0.85	-	-	14.928

Table 7: Proposed Erosion and Sediment Control Measures

BMPs Control Measures	Construction Stage	Operation Stage
<u>Sediment Control</u>		
Silt Fence	√	
Check Dams	√	
Silt Trap	√	√
Stabilized Construction Exits	√	
<u>Erosion Prevention Controls</u>		
Seeding / re-vegetation / turfing	√	√
Appropriate Earthwork Operation	√	

Table 8: Classification of Potential Soil Loss

Classification of Soil Loss	Potential Soil Loss/Erosion Rate (tons/ha/yr)
Low	0 – 10
Moderate	10 – 50
Moderate High	50 – 100
High	100 – 150
Very High	Above 150

Source: State Environmental Conservation Department (ECD), Sabah, Malaysia

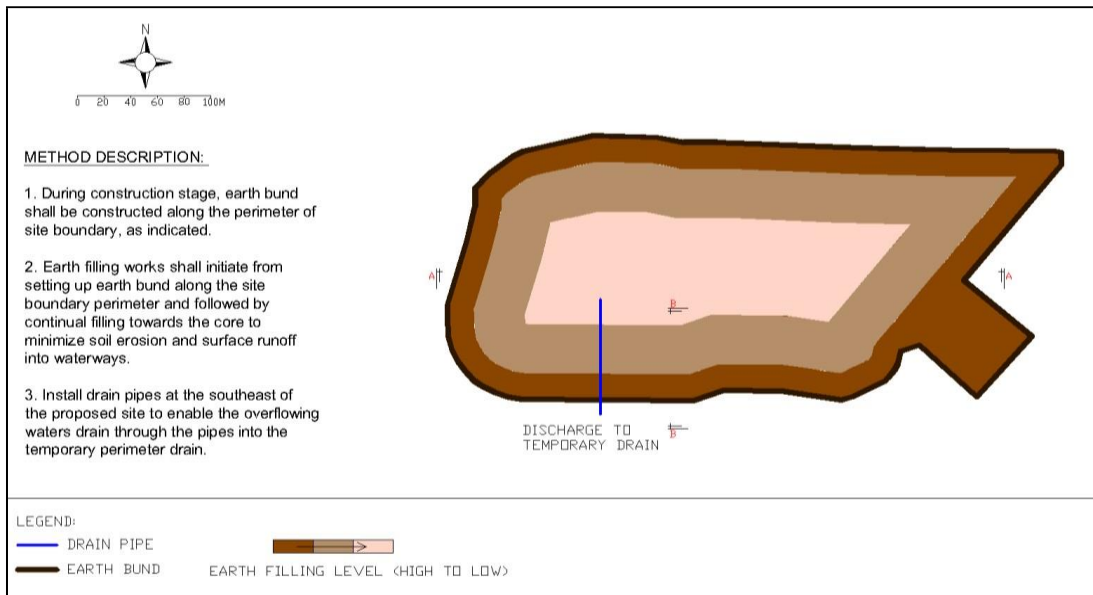


Figure 5: Temporary Earth Filling Method

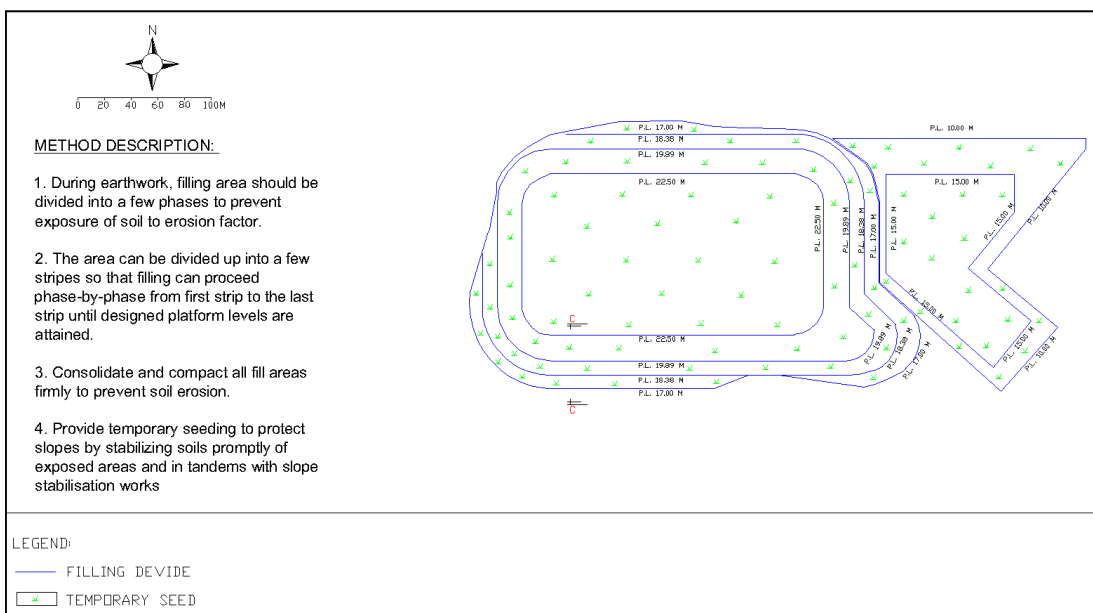


Figure 6: Temporary Phasing of Filling & Seeding Area

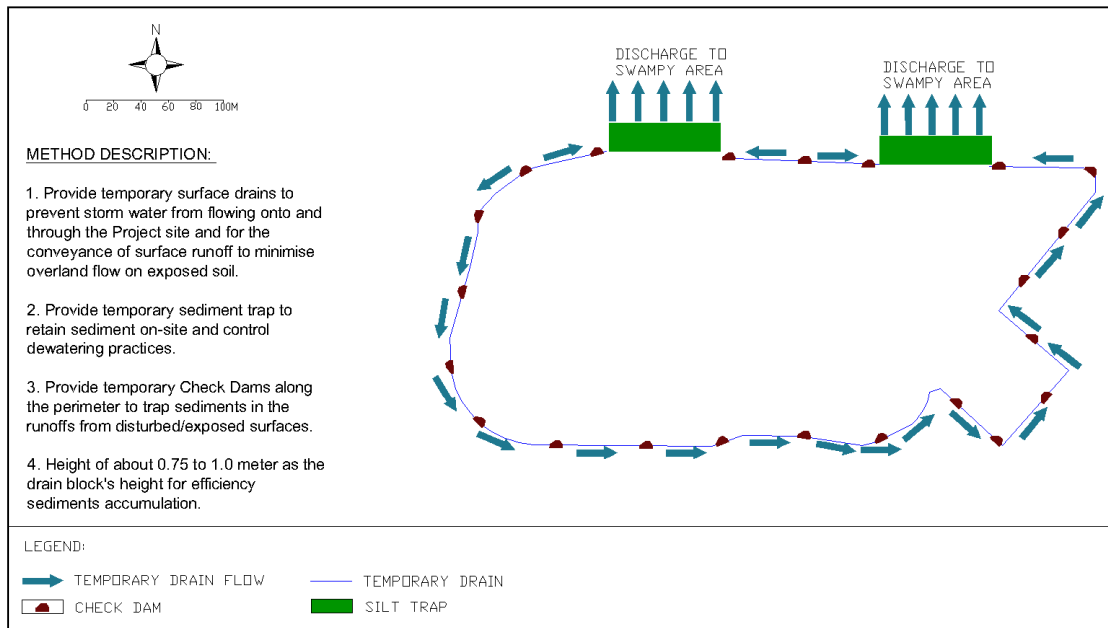


Figure 7: Temporary Earth drain, Silt Trap and Check Dams

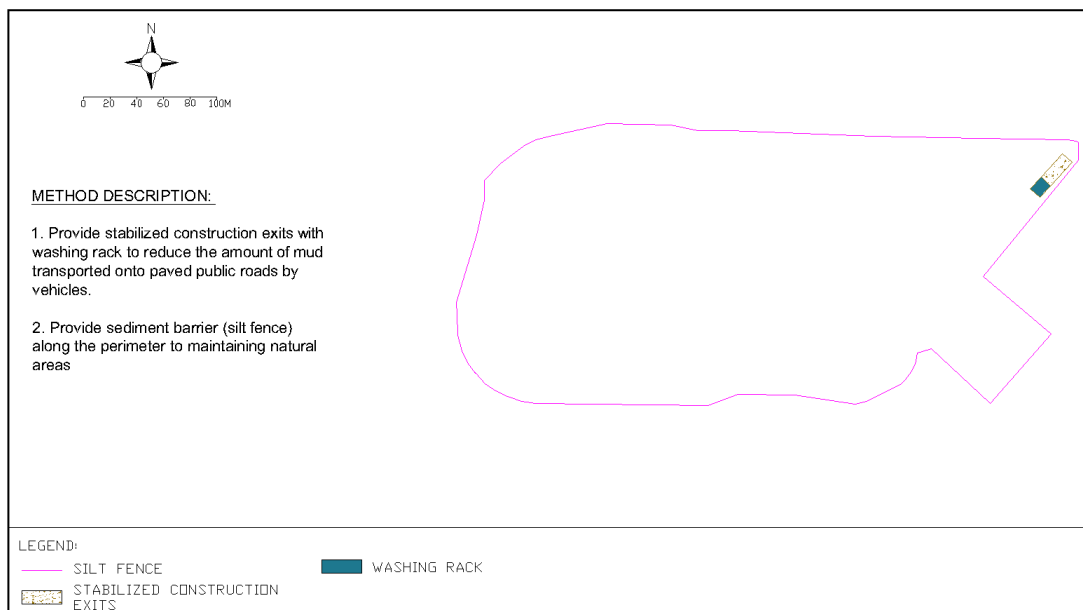


Figure 8: Temporary Stabilized Construction Exits and Silt Fence along Site Boundary

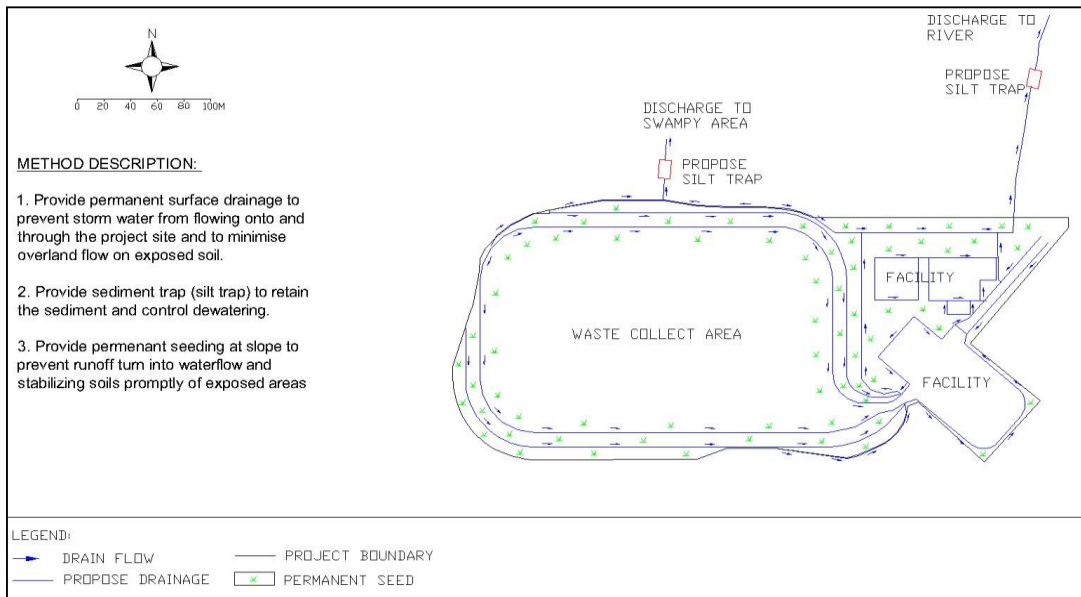


Figure 9: Permanent Seeding, Drainage, and Silt Trap Systems

IV. CONCLUSIONS

With BMP control measures onsite, the soil erosion rates during construction and operation stages could be reduced from “Moderate-High Soil Loss Class” (between 50 – 100 tons. {ha.yr} ⁻¹) to “Low Soil Loss Class” (between 0 – 10 tons. {ha.yr} ⁻¹). Similarly, after implementing BMP control measures onsite, sediments yields on a single storm event during construction can be reduced from 954.81 to 16.90 tons/storm event, and during operation stage from 1,042.44 to 8.86 tons/storm event. It can also be concluded that the most effective factor to reduce the potential of soil erosion rates and sediment yields was proper cover management. The implementation of seeding has shown a significant decrease in soil erosion rate and sediment yield due to its effectiveness in resisting rainfall impact through soil stabilizing effects caused by roots, and thus enhance sediment trapping capability and finally slowing down the runoff of both water and sediments.

ACKNOWLEDGMENT

The authors wish express their gratitude to Universiti Malaysia Sarawak for the support in this research.

REFERENCES

- [1] Brooks, S.R. and Spencer, T. (1993). Tropical Rain Forest Logging: Modeling Slope Processes and Soil Erosion in Sabah, East Malaysia. *Journal of Tropical Geography*, 15-27.
- [2] Department of Irrigation and Drainage (DID). (2001). *Urban Stormwater Management Manual for Malaysia*. Department of Irrigation and Drainage.
- [3] Wischmeier, W. and Smith, D. (1978). Predicting rainfall erosion-losses. In *A guide to Conservation Planning* (pp. 58). Washington, D.C: Agricultural Handbook No. 537.
- [4] Foster, G.R. and Lane, L.J. (1981). Erosion and Sediment Yield on Field-Sized Areas. *Transactions of the ASAE*, 24.
- [5] Williams, J. (1975). Sediment Yield Prediction with Universal Equation Using Runoff Energy Factor. In *Present and Prospective Technology for Predicting Sediment Yields and Source* (pp. 244-252). Washinton D.C.: ARS-S-40, 1976.
- [6] Department of Irrigation and Drainage (DID). (2003). *Sarawak Hydrology Year Book*, Malaysia.
- [7] Prodanovic, P. and Simonovic, S. (2007). *Water Resources Research Report*. London: The University of Western Ontario, Department of Civil and Environmental Engineering.
- [8] Missouri. (2007). *Drainage Criteria Manual*. City of Springfield: Missouri, USA

- [9] Wishmeier, W. H. and Johnson, C. B. (1971). A Soil Erodibility Nomograph for Farmland and Construction Sites. *Journal of Soil and Water Conservation*, 26 , 189- 192.
- [10] Certified Professional in Erosion and Sediment Control (CPESC). (2010). Environmental Institute of Malaysia (EiMAS), Department of Environmental, Ministry of Natural Resources and Environment, Universiti Kebangsaan Malaysia, Malaysia.
- [11] Bureau of Watershed Management. (2000). Erosion and Sediment Pollution Control Program Manual. Department of Environmental Protection Office. California Stormwater Quality Association, California, USA.
- [12] Environmental Impact Assessment (EIA) Guidelines Oil Palm Plantation Development (2000). 3rd Draft. State Environmental Conservation Department (ECD), Sabah, Malaysia

CHAPTER 8

A STUDY ON FACTORS INFLUENCING THE DETERMINATION OF MOISTURE CONTENT OF FIBROUS PEAT

Pui Tau Shien, Seneviratne, H.N. and Dygku Salma Awg Ismail

Abstract- Fibrous peat is an undrained peat that usually possesses very high moisture content. However, not all experimental procedures are applicable for determination of moisture content of fibrous peat. This research is aimed at examining the determination of insitu moisture content of fibrous peat using field measurements. The peat soil samples were collected at shallow depths from Asajaya at Kota Samarahan and Taman Kopodims at Matang, Kuching Sarawak by using peat auger. The laboratory tests such as determination of moisture content, fiber content, particle density and ash content were conducted on the collected samples in order to establish relationships between the parameters. Undisturbed peat samples from Matang were subjected to falling head permeability test to determine the saturated permeability. The saturated sample were then allowed to drain freely to simulate the moisture loss possible during sampling when samples were brought out of boreholes. The test results showed that moisture content varies according to the drying temperature and position of the soil sample (top, middle and bottom) during sampling. Comparing samples from both locations, peat soil from Kota Samarahan possessed higher moisture content. The saturated permeability of peat sample was in the range of 2.62 – 3.05 cm/s. The free draining trial showed that moisture loss during sampling significantly influence the moisture content measurement. The variation in value of moisture content for fibrous peat may occur due to several factors such as existing ground water table, sampling method by boring, existing standard test procedure which is not suitable for peat soils requirement and also because of the physical properties which varied according to depth of soil.

Keywords: Moisture content, fibrous peat, permeability, field measurement

I. INTRODUCTION

MOISTURE or water content is one of the most distinctive properties of peat as most of the physical characteristics of the peat are related to the amount of moisture present. There are many methods available for determination of moisture content of soils. However, not all test equipment and experimental procedures used with these methods are applicable in the case of fibrous peat soil as they are normally designed considering inorganic soils. Fibrous peat, which is also known as fibrist, is an undrained peat that usually possesses very high moisture content due to its high organic content and void ratio. Most of the peat materials are in fully saturated state as the ground water table is at a shallow depth.

The most common laboratory test for determination of moisture content of soil is the oven-drying method complying with British Standard (BS 1377 – 2: 1990) or American Society for Testing and Materials (ASTM D 2216). ASTM method D- 2216 which determines the free water or pore water content as a percentage based on moist and oven dried soil weight differences may generate erroneous information for soils with a high organic material content [1]. The BS 1377 – 2: 1990 also states that a microwave oven should not be used as definitive method in determining the moisture content of soils containing organic matter such as peat. This is caused by the difficulty in ensuring temperature of soil does not exceeds 110 °C. However, peat soil samples may experience particle burning even at temperatures well below 110 °C.

Another factor of importance is the method of sampling by boring which may affect the measurement of field moisture content. This is because once a sample is taken at the particular point, the soil has been disturbed and its properties may be altered. This introduces another variable, the heterogeneity of the soil into the moisture measurements; also there may be internal migration of water or moisture loss during sampling. The loss of moisture due to free draining during removal of the sample from the borehole also may be of importance. As a result of the above, factors that will significantly affect the determination of moisture content of fibrous peat must be identified. The use of present testing techniques for peat moisture is unsatisfactory, and therefore it is necessary to establish more reliable methods for obtaining the moisture content of fibrous peat in the field.

Dygku Salma Awg Ismail is a lecturer with the Department of Civil Engineering, Faculty of Engineering, Universiti Malaysia Sarawak, Kota Samarahan, 94300 Kota Samarahan, Sarawak, Malaysia (phone: +60 82 58 3268; fax: +60 82 583410; e-mail: aidsalma@feng.unimas.my).

*Nimal Seneviratne is a Professor with the Department of Civil Engineering, Faculty of Engineering, University of Peradeniya, Sri Lanka.
T.S.Pui, Undergraduate student, Department of Civil Engineering, UNIMAS, Kota Samarahan 94300 Malaysia (e-mail: allyxian87@gmail.com)*

II. LITERATURE REVIEW

Malaysia has a total 2.7 million ha of peat land and among its thirteen states, Sarawak the largest state comprises the biggest reserve of peat land of 1.66 million ha or 13% of the state ([2] and [3]). According to Malaysian Soil Classification system for organic soils, peats are defined as organic soils having an organic content more than 75%. Fibrous peat is characterized by a fibrous structure which consists of easily recognizable plant remains and retains some strength [4]. It is able to hold considerably amount of water due to the hollow, spongy and coarse nature of the organic particles [5]. Von Post scale is a well established field method to indicate the stages of decomposition of peat. It recognizes 10 degrees of humification from H1 which indicates little decomposed fibrous and light-coloured peat to H10 at the end of the scale for well decomposed, colloidal, dark-coloured material.

Peat soil has very high moisture content compared to common mineral soil. Field moisture content varies according to the type of peat where it may as low as 500 % in some amorphous granular peat and up to 3000 % had been recorded for the coarse fibrous material [6]. The occurrence of water present in the peat soil can be classified into physically and chemically bound water, capillary and film water, and immobilized water [7]. First stage of drying involves the removal of free water and water from large pores. The forces of capillary contraction increase and weakly bound intracellular and immobilized water is squeezed out on further drying; this is followed by the removal of physic-chemically bound water ultimately.

III. PRESENT STUDY

The peat samples were collected from two locations which are Taman Kopodims at Matang (N 01°35.466', E 110°16.464') and Asajaya at Kota Samarahan (N 01°25.751', E 110°32.476'), in state of Sarawak, Malaysia.

Method of Sampling

There are two types of samples collected from the both of the locations, namely, borehole samples and undisturbed samples. 50 cm high × 50 mm diameter borehole samples were obtained by using a hand auger specially suited for sampling peat, at 0.5 meter and 1.0 meter depth. The sample was divided into three parts: top, middle and bottom immediately after it is brought to ground surface. A trial pit was excavated to a depth just below the ground water table for undisturbed sampling purpose. Two cylindrical moulds were used: permeability mould (95.58 mm diameter × 130 mm height) and CBR mould (149.1 mm diameter × 132.72 mm height) were used to obtain undisturbed samples. These moulds were pushed into the trial pit to obtain the undisturbed peat samples.

Field Investigation and Laboratory Tests

The condition of the peat soil was investigated based on its degree of decomposition and classified according to the Von Post scale. Besides, depth of the existing ground water table was recorded on site. In order to identify the factors influencing the determination of fibrous peat, several tests had been conducted. Measurement of peat moisture content for both disturbed and undisturbed sample was carried out in two stages drying at 60°C and 100°C. At each temperature the specimens were kept in the oven until a constant weight was recorded.

The present laboratory test available for determination of fiber content is the ASTM D1997 – 91 (2008) Standard Test Method for Laboratory Determination of the Fiber Content of Peat Sample by Dry Mass. This test method is used to quantify the fiber content present in the peat soil sample. The specific gravity test of the peat soil sample was measured using 50 ml density bottle. Test specimen for specific gravity required to be ground to smaller size and sieving through the 425 µm sieve. Meanwhile, determination of ash content is carried out in accordance to ASTM D-2974 Standard Test Methods for Moisture, Ash and Organic Matter of Peat and Other Organic Soils. Ash content of the peat is determined by igniting the oven-dried (100 °C) sample in a muffle furnace at 550 °C according to Method C in ASTM standards.

The undisturbed peat soil sample was allowed to saturate by immersion in a water bath prior to laboratory testing. Two re-saturation methods were used: falling head permeability apparatus and immersion in a water bath. The water was allowed to flow through the sample in permeability mould while the permeability was measured during partially and fully saturated stages. Another undisturbed sample was soaked in the water for a period of time for it to become saturated. Then, testing is carried out to determine the rate of moisture loss of the sample by allowing it to drain freely under gravity. This test method is used to simulate the loss of moisture during the field sampling of the peat soil. The initial saturated weight of the sample is

recorded and the water in the sample is allowed to drip freely. The mass of the sample is recorded for every 5 minutes interval for the first half an hour followed by every 30 minutes interval thereafter.

IV. RESULT AND ANALYSIS

Table 1 shows the soil condition and water table based on the field investigation conducted at the two locations where the peat soil sample is collected.

Table 1: Field Investigation of Sampling Location.

Location	Kota Samarahan		Matang	
Soil condition (Von Post scale) Degree of humification	Depth of sampling		Depth of sampling	
	0.5 m	1.0 m	0.5 m	1.0 m
	H ₄	H ₂	H ₄	H ₃
Water table from ground level	0.38 m		0.70 m	

Measurement of Moisture Content

Moisture content was determined for both borehole and undisturbed peat soil samples. For the disturbed sample, determination of moisture content is carried out immediately at laboratory after field sampling. Moisture content is calculated according to (1).

$$\text{Moisture content, } w = [(m_2 - m_3) / (m_3 - m_1)] \times 100\% \quad (1)$$

Where; m_1 = Weight of the empty container

m_2 = Weight of container + saturated peat soil sample

m_3 = Weight of container + dried peat soil sample

Disturbed Sample

Two samples are obtained at a borehole and labeled as B1S1 and B1S2. B1 indicates the first borehole while S1 and S2 are samples at 0.5 m and 1.0 m depth respectively from ground surface. Each sample is then divided into three parts: top, middle and bottom as shown in Figure 1. For the test specimen of moisture content, each part of the soil sample is subdivided into three containers.



Figure 1: Peat soil sample divided into three parts; top, middle and bottom.

The peat soil sample undergoes two stages drying in this moisture content test; it is first oven-dried at 60°C until the mass of dry soil become stable and then transferred to oven with temperature of 100°C. The bar charts in Figure 2 and Figure 3

show that the moisture content values of peat soil increases with the increase of drying temperature from 60°C to 100°C. This result conforms with the similar studies done previously. Samples from Kota Samarahan have the average increase in moisture content of 37.4 % compared to that for sample from Matang which has a value of only 11.9%. Moreover, the overall moisture content for peat soil in Kota Samarahan area is higher than that in Matang area.

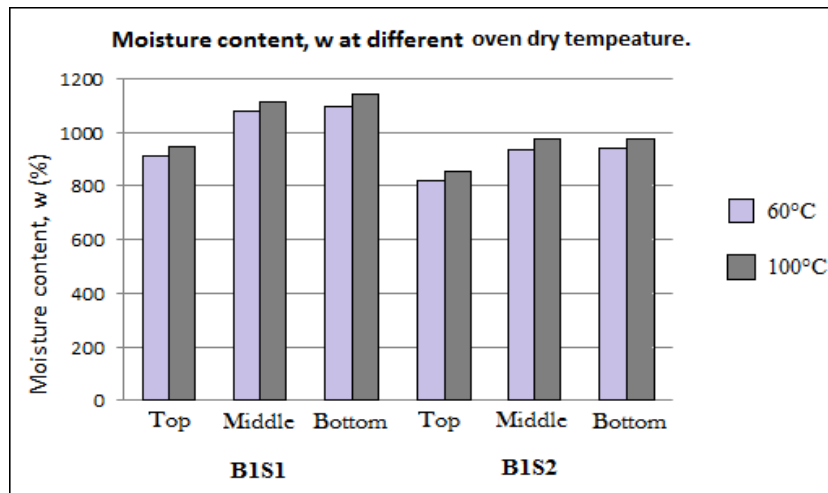


Figure 2: Graph of moisture content for Kota Samarahan area at different temperature.

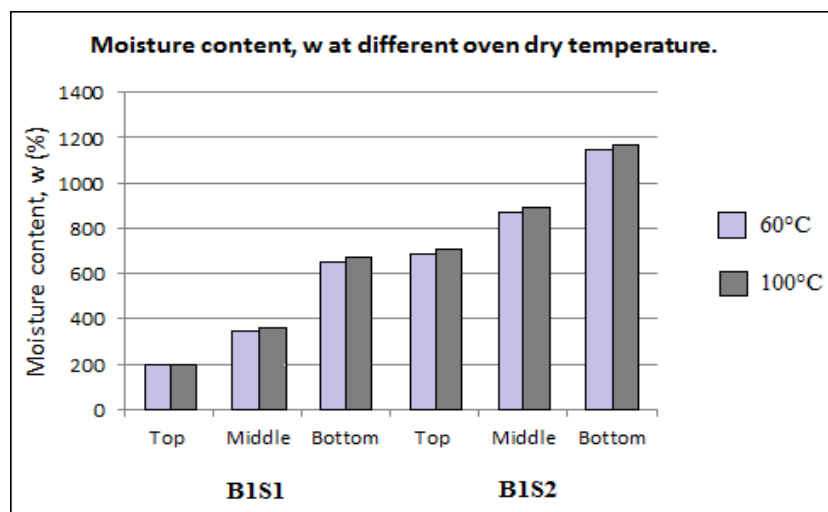


Figure 3: Graph of moisture content for Matang area at different temperature.

The moisture content of peat soil varies with depth in relation to ground water table. As shown in the bar charts, the soil below ground water table has a higher moisture content value. The sample B1S1 (0.5 m depth) from Kota Samarahan has higher moisture content as compared to sample B1S2 (1.0 m depth) as the first sample is taken just below the ground water table (0.38 m depth). Meanwhile for sample from Matang area, the moisture content for the top part of sample B1S1 is the lowest as compared to other five parts of the peat soil sample in same borehole. This is because the ground water table is located at 0.70 m depth. Therefore, the moisture content of peat soil sample below 0.70 m is gradually increasing.

The result shows that bottom part for each sample possesses the highest moisture content when compared with top and middle part. This situation occurs as the water in the peat soil sample will flow migrate downwards to the bottom part of sampler when it is taken out from the borehole.

Undisturbed Sample

The determination of moisture content for the undisturbed sample is carried out after re-saturation. A portion of sample was taken for measurement of moisture content. The sample oven dried at 100 °C gave moisture content for peat soil in Kota Samarahan area (902.6%) and that at Matang area (374.2%).

Fiber Content

The fiber content of peat soil was determined for both borehole and undisturbed sample by using equation (2). Each borehole sample is divided into top and bottom part. The sample is taken from the same location as moisture content samples but at a different borehole nearby, thus it is labeled as B2S1 (0.5 m depth) and B2S2 (1.0 m depth).

$$\text{Fiber content} = [(M_2 - M_1) / M_0] \times 100\% \quad (2)$$

Where; M_1 = Mass of empty 150 μm sieve

M_2 = Mass of 150 μm sieve + dry retained fiber

M_0 = Mass of original soil sample

Result has indicates that there are more fiber in the deeper soil at both locations. Fiber content obtained from Kota Samarahan and Matang at 1.0 m depth are 85.7% and 88.3% respectively. For the classification based on fiber content [8], the fibrous peat should consist of more than 66% fiber content to have a Von Post class of H4 or less. Based on Von Post scale all sample tested can be classified as fibrous peat. However, only sample at 1.0 m depth can be classified as fibrous peat according to the fiber content in the soil as the sample at 0.5 m depth consists of less than 66 % fiber content (56.4% for Matang area and 41.6% for Kota Samarahan).

Specific Gravity

Specific gravity (particle density) test is performed for both borehole and undisturbed peat soil samples. Equation (3) is used to compute the particle density. Two test specimens are prepared from the top, middle and bottom parts of borehole sample. The value of particle density for sample from Kota Samarahan ranges between 1.42 to 1.64 Mg/m^3 while that from Matang ranges from 1.32 to 1.66 Mg/m^3 . Thus, comparing the particle density in both locations, it suggests that the particle density for peat soil in these locations is similar to each other.

Based on the data obtained from the laboratory test, the decrease in particle density will leads to the increase in moisture content. For example, the moisture content will keep on increasing as the particle density decrease from the top to bottom part of the sample at Matang.

Particle density

$$\rho_s = \frac{(m_2 - m_1)}{[(m_4 - m_1) - (m_3 - m_2)]}$$

Where; m_1 is the mass of density bottle (in g);

m_2 is the mass of bottle and dry soil (in g);

m_3 is the mass of bottle, soil and water (in g);

m_4 is the mass of bottle when full of water only (in g).

Loss of Ignition/ Organic Matter Content

Loss of ignition test is only conducted for the undisturbed sample at Kota Samarahan and Matang. Peat soil sample is dried at 100 °C before placing in the muffle furnace with temperature at 550 °C for a 4 hours duration.

The results on the undisturbed sample verified that the lower value of particle density indicates low mineral content whereby the lower value of particle density (1.5 Mg/m^3) for peat soil at Kota Samarahan gives the lower ash content (mineral content) of 30.0 %. These values were within the range stated by researcher [9] which is from 20% to 80 %. Undisturbed sample from Matang on the other hand has particle density of 1.65 Mg/m^3 with ash content of 37.4%. Moreover, the lower ash content or higher organic matter content of sample is also related to the higher moisture content. The moisture content for undisturbed sample from Kota Samarahan is much higher as compared to sample from Matang.

$$\text{Ash content, N (\%)} = [(m_2 - m_c) / (m_1 - m_c)] \times 100 \quad (4)$$

$$\text{Organic matter content (\%)} = 100 - N \quad (5)$$

Where; m_c = Mass of empty crucible

m_1 = Mass of crucible + oven dried sample

m_2 = Mass of crucible + remaining sample after ignition

Falling Head Permeability Test

This test is carried out in order to saturate the undisturbed peat soil sample collected from Matang area. The sample is placed in the permeability mould with internal diameter of 95.58 mm and length of 130 mm. During the process of saturation, unsaturated and saturated permeability of the sample can be determined. The sample is assumed to be saturated when the permeability, K becomes constant. The data collected is used to plot the graph for $\log (h_1/h_2)$ against time, t . From the gradient of each run of test, the permeability can be computed. The sample is saturated for three consecutive days. Figure 4, Figure 5 and Figure 6 show the experimental data while Figure 7 and Figure 8 depict the variation of partially saturated and fully saturated permeability with time. The permeability values become constant at the end of the test.

The value of permeability, K is decreasing as the soil sample becomes fully saturated. The coefficient of fully saturated permeability for the peat soil ranges from 10^{-07} to 10^{-06} cm/s. The previous study [10] indicated that the fibrous peat soil is averagely porous and has a medium range of permeability from 10^{-6} to 10^{-3} cm/s. The hydraulic conductivity for undisturbed peat soils from present tests is in a range of 4×10^{-2} to 9×10^{-8} cm/s. The permeability of peat depends on the void ratio, mineral content, degree of decomposition, chemistry and the presence of gas in soil. In general, a clear tendency of decreasing value with increasing decomposition had been established [11].

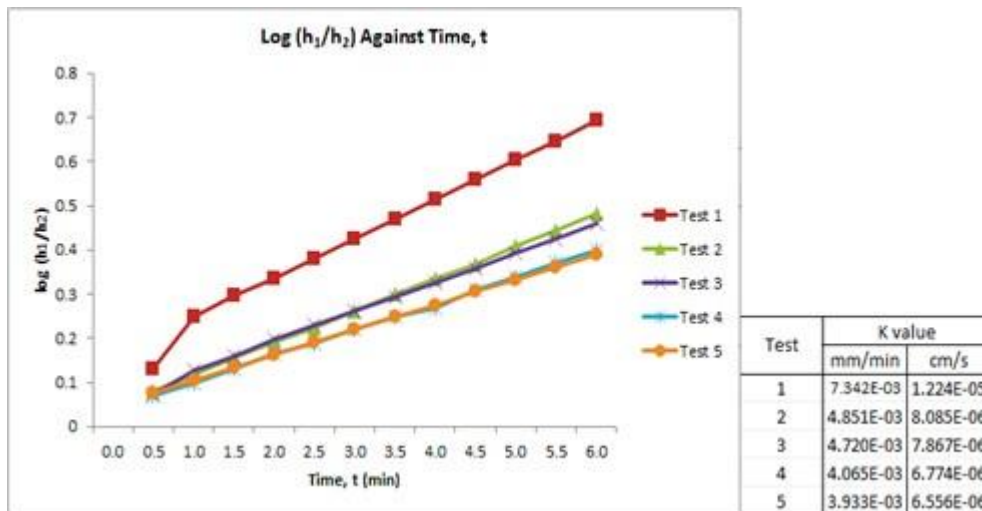


Figure 4: Graph of $\log (h_1/h_2)$ against time and the unsaturated permeability for first day.

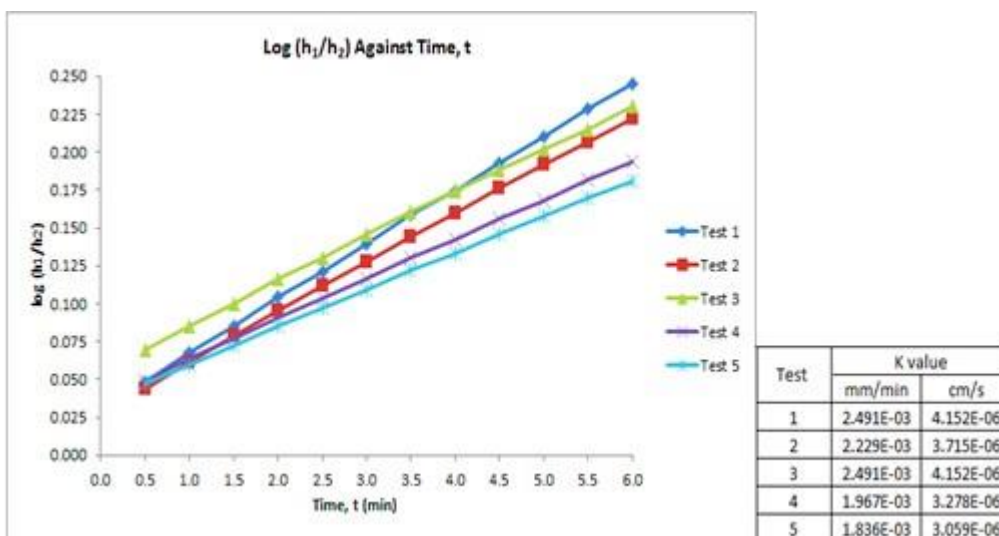


Figure 5: Graph of $\log (h_1/h_2)$ against time and the unsaturated permeability for second day.

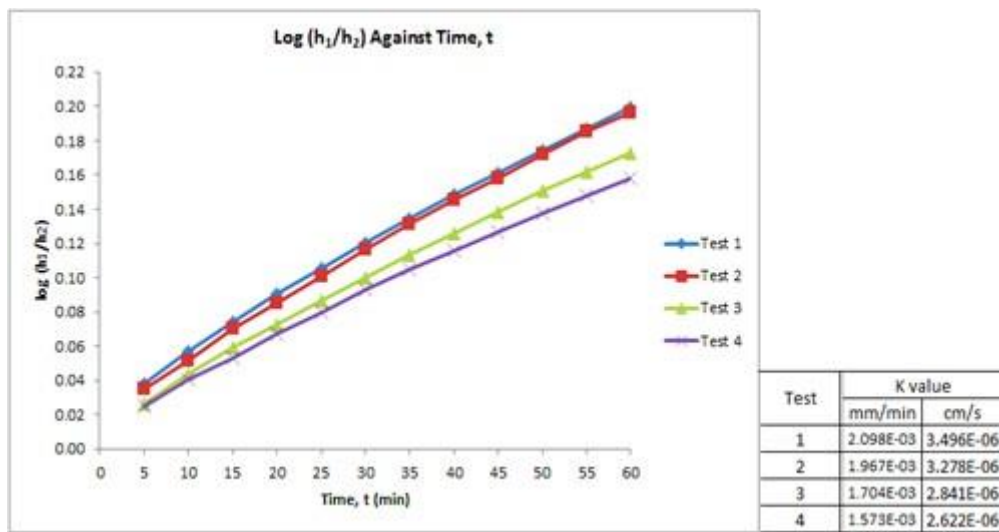


Figure 6: Graph of $\log (h_1/h_2)$ against time and the unsaturated permeability for third day.

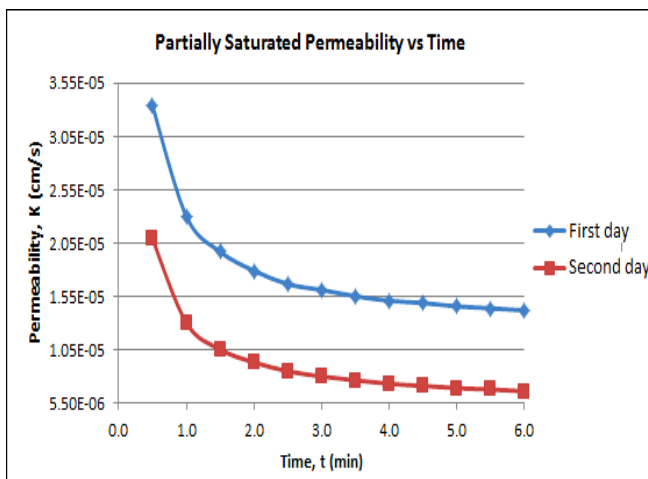


Figure 7: Partially saturated permeability.

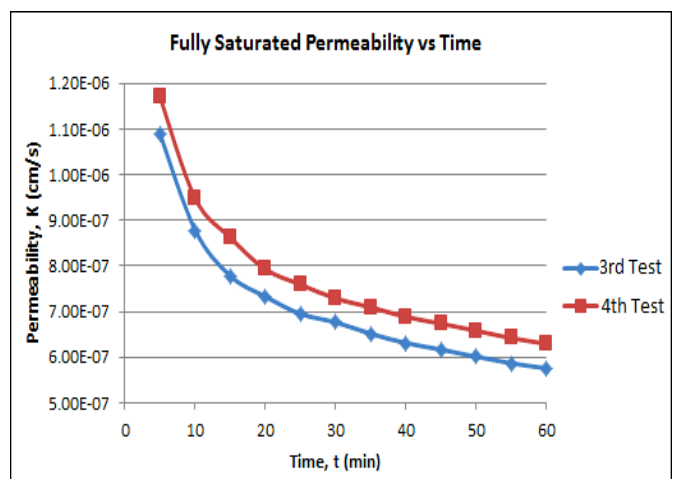


Figure 8: Fully saturated permeability.

Rate of Moisture Loss for Peat Soil

An undisturbed sample from Matang area is placed in the mould and then the whole sample is immersed in the water to simulate the peat soil condition under ground water table. The sample is allowed to saturate in the water. After sufficient time allowed for saturation, the testing for the rate of moisture loss is conducted. The moisture loss for the first 30 minutes is considered as the natural flow of water through the soil sample (free water or water from large pores) which is similar to the real condition of sampling. Thus, the graph of moisture loss is plotted for this duration of time (Figure 9). The test is repeated for another two times and the average rate of moisture loss obtained is 0.293 g/s. In terms of moisture content, i.e. moisture loss loss over the mass of dry soil of the sample, the moisture loss is about 0.06 % per second. Moisture content loss within one minute is 3.53 %.

The moisture loss for the following 2.5 hour is considered as the loss due to draining of micro pores governed by permeability. The permeability calculated at this stage is 2.982×10^{-4} cm/s and it is considered as the partially saturated permeability of the peat soil. Since most of the water had been flow out during the first half an hour, the soil sample is thus becomes unsaturated at the moment. The average loss of moisture at this stage is 0.052 g/s which is considerably small.

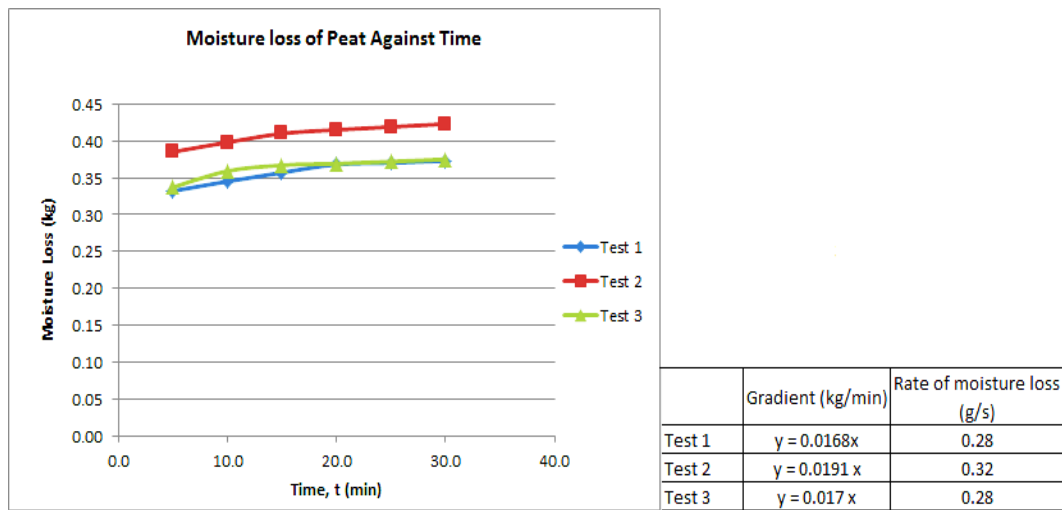


Figure 9: Graph of moisture loss against time for the first 30 minutes.

However, this test only involves sample in the mould, the data does not represent the actual condition of sampling by using peat auger since both sampler size were not same. The results only demonstrate the possibility of significant loss of moisture during the sampling process.

V. CONCLUSION

This study was conducted to identify the factors influencing the determination of moisture content of fibrous peat. A series of laboratory testing had been carried out during the study and the following conclusions are made based on result and analysis that had been carried out.

- i. The moisture content for Kota Samarahan fibrous peat is ranged from 853 % to 1138 % meanwhile for Matang sample it is ranged from 201 % to 1168 %. Hence, the sample from Kota Samarahan had higher average moisture content as compared to that of Matang.
- ii. There are several factors that had been identified to affect the determination of moisture content for fibrous peat:
 - The existing ground water table at location of sampling will influence the moisture content of the fibrous peat soil.
 - The measurement of moisture content becomes inaccurate due to the possibility of significant amount of moisture loss when using boring method of sampling.
 - Some parts of the existing standard procedures for determination of moisture content which developed based on mineral soil requirement may not be suitable for fibrous peat soil due to its high moisture and organic content.
 - The physical properties of the fibrous peat soil such as particle density and organic matter content also influenced the determination of moisture content.
- iii. The method of re-saturate the soil sample after sampling is necessary to regain the moisture loss. Besides, extend the drying time of the peat soil and using two stages drying will be able to make sure the moisture is totally squeezed out from the soil sample.

ACKNOWLEDGMENTS

The authors would like to express deep gratitude for the technical supports offered by the Geotechnical laboratory staff, Universiti Malaysia Sarawak (UNIMAS), Sarawak, Malaysia.

REFERENCES

- [1] Martin N. Sara (1994). *Standard Handbook for Solid and Hazardous Waste Facility Assessments*. Lewis Publishers, an imprint of CRC Press, Inc., Florida.
- [2] Mutalib A.A; Lim, J S; Wong, M H And Koonvai, L (1991). "Characterization, distribution and utilization of peat in Malaysia." Proc. of the International Symposium on Tropical Peatland (B Y Aminuddin; S L Tan; B Aziz; J Samy; Z Salmah; H Siti Petimah Choo eds.). MARDI, Kuala Lumpur. p. 7-16
- [3] Jamaludin Bin Jaya (2002). *Sarawak: Peat Agricultural Use*, MARDI, Malaysia.
- [4] Myslinska E. (2003). "Classification of organic soils for engineering geology." *Geol. Quart.*, 47 (1): 39-42. Warszawa

- [5] Faisal Haji Ali, Wong, Leong Sing and Roslan Hashim (2009). “*Engineering Properties of Improved Fibrous Peat.*” Scientific Research and Essay Vol. 5 (2). Pp. 154 -169
- [6] F.G. Bell (1993). *Engineering Geology*. Butterworth-Heinemann, Burlington, USA. p.247 & 248
- [7] J. P. Andriess (1988), *Nature and Management of Tropical Peat Soils*, FAO SOILS BULLETIN 59.
<http://www.fao.org/docrep/x5872e/x5872e08.htm>, 12th August 2010
- [8] Harwant Singh, Hufdi M. Bahia and Bujang B.K. Huat (2003). “*Varying Perspective on Peat, It’s Occurrence in Sarawak and Some Geotechnical Properties.*” Conference on Recent Advances in Soft Soil Engineering and Technology, 2 –4 July, 2003. Sibul, Sarawak, MALAYSIA
- [9] Håkan Rydin, J. K. Jeglum, Aljosja Hooijer (2006). *The Biology of Peatlands*. Oxford University Press Inc, New York. p.79 & 80.
- [10] Nurly Gofar (2006). “*Determination of Coefficient of Rate of Horizontal Consolidation of Peat Soil.*” <http://eprints.utm.my/2772/1/75210.pdf>, 3rd April 2011.
- [11] E. Paavilainen, Juhani Paivanen (1995). *Peatland Forestry: Ecology and Principles*. Springer-Verlag Berlin Heidelberg, Germany. p.46 & 47.

CHAPTER 9

STABILIZATION OF INDIAN FLY ASHES WITH SOILS, CEMENT, AND RANDOMLY ORIENTED FIBERS

Shenbaga R. Kaniraj, V. Gayathri and V.G. Havanagi

Abstract - Experimental studies were carried out on fly ashes from two Indian thermal power plants, namely Rajghat and Dadri, with the aim of improving the utilization of fly ash in geotechnical engineering applications. It was attempted to improve the engineering performance of fly ash by several means such as by mixing fly ash with soils, cement, and polyester fibers. The research program included the study of: a) physical properties, chemical composition and morphology of the fly ashes; b) compaction, strength, and permeability characteristics of the fly ashes and fly ash-soil mixtures; c) compaction and strength characteristics of fly ash-soil mixtures stabilized with fibers alone, with cement alone, and with both cement and fibers. Results showed that addition of fly ash to soils would result in lighter and stronger fills. Fiber inclusions increased the strength of fly ash-soil specimens significantly and altered their behaviour from brittle to ductile. Even small cement contents increased the strength of the fly ash-soil mixtures significantly. With higher cement contents of up to 18% it was possible to prepare fly ash-cement design mixes that satisfied the strength criteria for pavement base courses.

Keywords: Fiber reinforcement, Fly ash, Stabilization, Waste utilization

I. INTRODUCTION

India is heavily dependent on thermal power generation for electricity. The coal used as fuel has high ash content. India currently produces more than 130 MT of fly ash annually which in another ten years could rise to 600 MT. To improve the utilization of fly ash, India first commenced a Fly Ash Mission and then a Fly Ash Utilization Program. Utilization of fly ash increased from 1 MT in 1993-94 to 60 MT in 2006-07. The authors carried out a series of experimental studies on fly ashes from two Indian thermal power plants, namely Rajghat and Dadri, with the broad aim of improving the utilization of fly ash in geotechnical engineering applications. The behavior of fiber reinforced coarse grained soils has been investigated by several researchers. According to Gray [1], Brown and Sheu [2], Waldron [3], Wu and Erb [4], and Wu et al [5], plant roots increase the shear strength of the soil significantly and also increase the stability of natural slopes. The root concentration varies from 0.2% to 1% depending on the plant type and the increase in strength varies from 29% to 98%. According to McGown et al [6] the fiber reinforced soil comes under the category of ply soil in which the inclusions are extensible and the ratio of the reinforcement modulus to the unreinforced soil modulus is less than 3000. The other category called the reinforced earth, has inextensible inclusions and modulus ratio more than 3000. Fibers are of two types namely, natural and synthetic. The important properties of fibers are tensile strength, modulus of elasticity, elongation at break, and specific gravity. The thickness, length, and aspect ratio of fibers are the other important parameters in fiber reinforced soil. Rehsi [7] and Vasani [8] have summarized the properties of different synthetic and natural fibers. In oriented fiber reinforced soil, the fibers are placed in specific direction or at specific inclination to the plane of shear failure. Gray and Ohashi [9], Shewbridge and Sitar [10], and Bauer and Fatani [11] have carried out laboratory tests on oriented fiber reinforced sands and silty sands. In randomly distributed fiber reinforced soil, the fibers are mixed with the soil and compacted in a way that the fibers are oriented in various directions randomly. Hoare [12], Maher [13], Gray and Maher [14], Maher and Gray [15], and Charan [16], have carried out triaxial compression tests on randomly oriented fiber reinforced soil. The information available on the effect of fibers on the behaviour of fly ashes is scanty. Chakraborty and Dasgupta [17] carried out experiments on fly ash collected from Kolaghat thermal power station. The authors attempted to improve the engineering behavior of the fly ashes by several means such as mixing fly ash with other soils, cement, and fibers. The paper presents the salient features and results of the different aspects of the studies: a) physical properties of the fly ashes; b) compaction, strength, and permeability characteristics of the fly ashes and fly ash-soil mixtures; c) compaction and strength characteristics of fly ashes stabilized with polyester fibers alone, with cement alone, and with both cement and fibers. More details can be obtained from the authors' other publications [18]-[26].

Shenbaga R. Kaniraj is with the Universiti Malaysia Sarawak, 94300, Kota Samarahan, Sarawak, Malaysia. (phone: +6082583225; fax: +6082583410; e-mail: rkjshenbaga@feng.unimas.my).

V. Gayathri is with the itm University, Sector 23A, Gurgaon, 122017, India. (email: vgayathri@itmindia.edu)

V.G. Havanagi is with the Central Road Research Institute, Mathura Road, New Delhi, 110020, India. (email: vasant.crii@nic.in)

II. FLY ASHES

Fly ashes were collected in dry condition from the electrostatic precipitators of the Rajghat and Dadri thermal power stations in New Delhi. The scanning electron micrographs (SEM) of the two fly ashes are shown in Figure 1. The fly ashes consisted of spherical particles and had a porous structure. Table 1 shows the results of the tests for physical properties, geotechnical classification, and chemical composition of the two fly ashes. Based on their chemical composition and ASTM C 618 specifications [27], the two the fly ashes were classified as class *F* and pozzolanic materials.

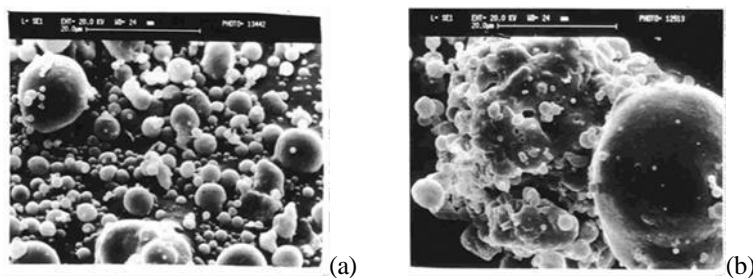


Figure 1 SEM of (a) Dadri and (b) Rajghat fly ashes [23]

Table 1 Physical properties, grain size, Atterberg limits and chemical composition of the fly ashes [26]

Properties	Fly ash		Composition	Fly ash	
	Dadri	Rajghat		Dadri	Rajghat
Specific gravity, G	2.2	2.19	Silica (SiO_2)	60.12	61.21
Loss on ignition, %	0.4	1.4	Alumina (Al_2O_3)	30.16	30.07
Specific surface area, cm^2/g	3520	4020	Iron oxide (Fe_2O_3)	6.36	4.17
<i>Grain size distribution</i>			Lime (CaO)	1.00	0.10
Fine sand, 0.475-0.075 mm, %	5	20	Magnesia (MgO)	0.53	0.40
Silt size, 0.075-0.002 mm, %	82	77	Titania (TiO_2)	---	2.60
Clay size, < 0.002 mm, %	13	3	Soda (Na_2O)	0.06	< 0.01
Uniformity coefficient, C_u	4.82	5.65	Potash (K_2O)	0.007	0.02
<i>Atterberg limits</i>			Sulphates (SO_3)	0.10	< 0.01
Liquid limit, w_p , %	30.5	48-50			
Plastic limit, w_l , %	NP	NP			

From the results of grain size distribution and Atterberg limits, both the fly ashes were classified as ML type belonging to the non-plastic silt category.

III. FLY ASH–SOIL MIXTURES

A. Rajghat Fly Ash–Soil Mixture

The Rajghat fly ash was mixed with locally available soils silt and sand separately in different proportions. The details of specific gravity and grain sizes of the two soils are shown in Table 2. Light weight (Proctor) compaction tests were carried out to determine the optimum moisture content (OMC) and maximum dry density (MDD) of the fly ash-soil mixtures. Unconfined compression tests (on 37.7 x 73.5 mm cylindrical samples) and direct shear tests (on 60 x 60 x 20 mm samples) were carried out on fly ash-soil mixture samples prepared at their respective OMC and MDD. Table 3 shows the results of the compaction tests, unconfined compressive strength (UCS) and direct shear tests (c , ϕ). The results showed the beneficial effects of addition of fly ash to silt and sand. Addition of fly ash decreased the MDD of the soil. A fly ash–soil fill would therefore be lighter than a soil fill. The shear strength parameters of the fly ash–soil specimens were generally more than those of the soils. The fly ash–soil fill would therefore be stronger than the soil fill.

Table 2 Specific gravity and grain sizes of sand and silt [18]

Properties	Silt	Sand
Specific gravity	2.64	2.66
<i>Particle size</i>		
Fine sand size, 0.475-0.075 mm	14%	94%
Silt size, 0.075-0.002 mm	73%	6%
Clay size, less than 0.002 mm	13%	-

Triaxial shear tests were carried out on OMC-MDD Dadri fly ash specimens also. The results of these tests were: $UCS = 116.7$ kPa; $c_{uu} = 12.6$ kPa, $\phi_{uu} = 31^\circ$; and $c' = 0$, $\phi' = 29.3^\circ$ [21].

Consolidation test and falling head permeability test were carried out on the same OMC-MDD Dadri fly ash specimen in a Casagrande type consolidometer. This experiment facilitated the investigation of the consolidation characteristics and the influence of the head loss across the specimen, effective stress, and void ratio on the coefficient of permeability (k). Figure 2 shows the variation of k_{av} with vertical effective stress (σ'). k decreased by 21.6% when σ' varied from 9.81 to 1255.68 kPa [25]. However, k was still in the range for non-plastic silts. This showed that fly ash embankments and fills would be moderately permeable over their entire height.

Table 3 Results of compaction, unconfined compression, and direct shear tests on fly ash–soil mixtures [18]

Mix designation	Fly ash-soil mixture	<i>MDD</i> kN/m ³	<i>OMC</i> %	UCS kPa	<i>c</i> kPa	ϕ^o
<i>R</i>	Rajghat fly ash	10.52	36.5	65.7	19.6	37.5
<i>RM1</i>	75% <i>R</i> + 25% <i>M</i>	12.21	26.6	61.7	13.7	37.0
<i>RM2</i>	50% <i>R</i> + 50% <i>M</i>	13.54	22.6	47.1	14.7	36.0
<i>RM3</i>	25% <i>R</i> + 75% <i>M</i>	15.40	18.0	50.6	22.6	30.5
<i>M</i>	Silt	17.66	14.0	36.3	15.7	29.5
<i>RS1</i>	75% <i>R</i> + 25% <i>S</i>	11.92	28.6	44.1	18.6	34.0
<i>RS2</i>	50% <i>R</i> + 50% <i>S</i>	13.64	22.6	33.3	9.8	33.0
<i>RS3</i>	25% <i>R</i> + 75% <i>S</i>	15.11	17.5	20.6	21.6	31.5

No tests were carried out on sand as compaction tests are not applicable to sands.

B. Baumineral Fly Ash–Rhine Sand Mixtures

Experiments were also carried out on mixtures of a German fly ash and Rhine sand. The fly from a chemical manufacturing industry Baumineral near Bochum was mixed with fine sand deposited by Rhine River. The specific gravity of the Baumineral fly ash $G = 2.36$, was higher than the G of the two Indian fly ashes, probably due to the higher iron oxide content (7.66%) of the Baumineral fly ash. The Baumineral fly ash too was a class *F* fly ash as its lime (CaO) content was only 0.21%. The Rhine sand was slightly coarser than the sand used with the Rajghat fly ash. It had coarse sand size, medium sand size, fine sand size, and silt size contents of 1%, 16%, 82%, and 1%, respectively. Table 4 shows the results of experiments carried out on Baumineral fly ash–Rhine sand mixtures. The results show that Baumineral fly ash–Rhine sand mixtures had significantly greater *MDD* values than the Rajghat fly ash–soil mixtures, probably due to the higher specific gravity of the Baumineral fly ash. As a result of this, the Baumineral fly ash–Rhine sand mixtures also had significantly greater *UCS* values than the Rajghat fly ash–soil mixtures.

Table 4 Results of tests carried out on Baumineral fly ash–Rhine sand mixtures [18]

Mix designation	Fly ash-soil mixture	<i>MDD</i> kN/m ³	<i>OMC</i> %	UCS kPa	<i>c</i> kPa	ϕ^o
<i>B</i>	Baumineral fly ash	14.18	18.4	165.5	28.4	30.0
<i>BS1</i>	75% <i>B</i> + 25% <i>S</i>	16.09	13.0	146.4	26.5	38.0
<i>BS2</i>	50% <i>B</i> + 50% <i>S</i>	17.95	10.0	133.7	23.5	37.0
<i>BS3</i>	25% <i>B</i> + 75% <i>S</i>	18.98	8.2	50.6	11.8	34.0
<i>S</i>	Rhine sand	No tests were carried out on Rhine sand				

III. FLY ASHES STABILIZED WITH FIBERS

Experiments were carried out to investigate the influence of randomly oriented fiber inclusions on the geotechnical behavior of Rajghat and Dadri fly ashes. Figure 3 shows the scanning electron micrograph of the 6 mm long polyester fiber. Table 5 shows the other details of the fibers. Fiber content, f_c , in a fly ash–fiber mixture is defined as $f_c = W_f/W_s$, where W_f = weight of fiber and W_s = weight of dry fly ash. In Rajghat fly ash specimens $f_c = 0.5$ and 1% were used whereas only $f_c = 1\%$ was used in Dadri fly ash specimens. Similarly, both 6 and 20 mm long fibers were used in Rajghat fly ash and only 6 mm long fibers were used in Dadri fly ash. Standard Proctor compaction tests, unconfined compression tests and triaxial shear tests, on OMC-MDD fly ash–fiber specimens, were conducted. Table 6 shows the results of the various tests.

Table 5 Characteristics of fibers [23]

Type and color	Diameter mm	Length mm	Aspect ratio	Specific gravity	Tensile strength Mpa	Tensile modulus Mpa
Polyester (Black)	0.0203	6	313	1.38	510	-
Polyester (Grey)	≈ 0.075	20	267	1.30	80-170	1450-2500

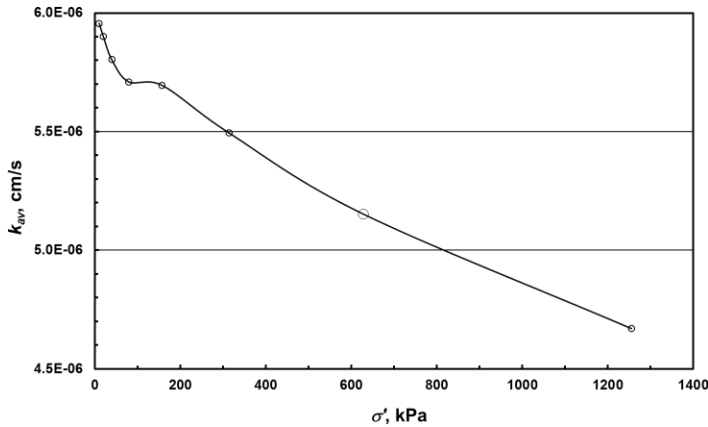


Figure 2 Variation of k_{av} with σ' [25]

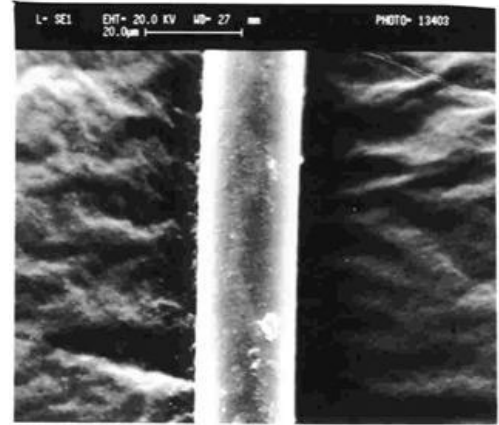


Figure 3 SEM of 6 mm polyester fiber [23]

Table 6 Results of compaction, unconfined compression, and triaxial shear tests on fly ash–fiber mixtures [23]

Fly ash	f_c %	Fiber length mm	MDD kN/m^3	OMC %	UCS kPa	c_{uu} kPa	ϕ_{uu}°	c' kPa	ϕ°
Dadri	-	-	13.8	21	116.7	12.6	31	0	29.3
Rajghat	-	-	10.5	37	65.7	43.2	30.1	-	-
Dadri	1	6	13.8	22	181	93.7	32.5	55.9	33.6
Rajghat	1	6	10.7	34	180.2	102.8	36	-	-
Rajghat	1	20	11.0	33	157.9	128.6	36	-	-
Rajghat	0.5	20	11.0	32	-	-	-	-	-

The small fiber content did not affect the MDD and OMC of Dadri fly ash appreciably. In Rajghat fly ash, however, the effect was a little more marked; the fibers increased the MDD and decreased the OMC. The fiber inclusions had a highly favorable effect on shear strength of the raw fly ashes. They increased the UCS as well as the shear strength parameters c and ϕ in the triaxial shear tests. The most significant effect of the fibers was on the stress-strain behavior of the fly ashes. Figure 4 shows the stress-strain curves in unconfined compression tests. Similar behavior was seen in other triaxial shear tests also. The fibers changed the brittle behavior of the raw fly ashes to ductile behavior.

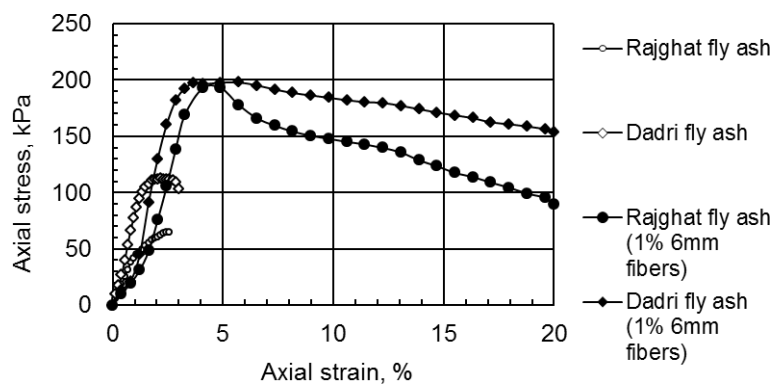


Figure 4 Stress-strain curves of fly ash-fiber specimens in unconfined compression tests [23]

IV. RAJGHAT FLY ASH – SOIL MIXTURES STABILIZED WITH FIBERS

Experiments were carried out to study the influence of randomly oriented fiber inclusions on the geotechnical behavior of selected Rajghat fly ash–soil mixtures. 20 mm long fibers (Table 5) and $f_c = 1\%$ were used. Table 7 shows the results of the compaction tests, unconfined compressive strength (UCS) and direct shear tests (c , ϕ) for the fiber reinforced fly ash–soil mixtures. The corresponding results for fly ash–soil mixtures without fibers are shown in Table 3. The results of unconsolidated undrained tests for the fiber reinforced fly ash–soil mixtures are also shown in Table 7. The corresponding values for fly ash–soil mixtures without fibers are shown alongside within parentheses.

Table 7 Results of compaction, unconfined compression, and direct shear tests on fiber reinforced fly ash–soil mixtures [22]

Mix designation	Fly ash-soil mixture	MDD kN/m ³	OMC %	UCS kPa	c kPa	ϕ	c_{uu} kPa	ϕ_{uu}°
RM2	50% R + 50% M	13.90	23.0	304.0	32.5	35.1	93.3 (25.8)	40.0 (30.2)
RS2	50% R + 50% S	13.60	23.5	436.4	17.4	39.4	160.0 (16.5)	32.9 (30.4)
M	Silt	17.60	14.5	411.9	21.3	38.4	-	-

Fibers did not have a significant effect on OMC and MDD of the fly ash–soil mixtures. However, they increased the shear strength of the fly ash–soil mixtures. The relative gain in UCS was defined as $G_f = (q_{fo} - q_o)/q_o$, where q_o and q_{fo} are the UCS of the unreinforced and fiber-reinforced specimens, respectively. The relative gain in UCS of RM2 and RS2 were as high as 546% and 1,211%, respectively. As in the case of raw fly ashes, the fibers changed the behavior of the fly ash–soil mixtures also from brittle to ductile.

V. FLY ASH – SOIL MIXTURES STABILIZED WITH CEMENT

Two series of investigations were carried out to study the effect of ordinary Portland cement as a stabilizing agent of fly ash–soil mixtures. Cement content, C_C , was defined as $C_C = W_C/W_{AS}$, where W_C = weight of cement and W_{AS} = weight of dry fly ash–soil mixture. In the first series (Series I) of experiments small cement contents of $C_C = 3\%$ and 6% were used. In general, 37.7 x 73.5 mm cylindrical specimens were prepared at the OMC-MDD state of the fly ash–soil mixtures, wrapped individually in a polyethylene bag, and kept inside a desiccator with a little quantity of water at the bottom of the desiccator and the temperature maintained around 21° C, for curing of the specimens. At the end of the specified curing period, unconfined compression tests were carried out. Table 8 shows the results for Series I experiments. The cement content did not influence the initial ($t = 0$) UCS of the specimens. The initial values of UCS can be referred to in Table 3. Even small cement contents increased the UCS of all fly ash–soil specimens significantly. The cement stabilized fly ash–soil specimens showed brittle behavior and the failure strain was in the range of 1-2%.

Table 8 UCS (kPa) of fly ash–soil mixtures stabilized with cement and fibers - Series I [22]

Mix designation	Fly ash-soil mixture	Curing period (days)					
		$C_C = 3\%$ $f_c = 0$		$C_C = 6\%$ $f_c = 0$		$C_C = 3\%$ $f_c = 1\%^a$	
		7	28	7	28	7	28
R	Rajghat fly ash	138.3	271.7	483.5	918.9	218.7	389.3
RM1	75% R + 25% M	219.7	251.1	589.5	893.4	-	-
RM2	50% R + 50% M	310.9	394.5	724.2	1,127.5	769.8	866.9
RM3	25% R + 75% M	433.5	750.3	821.1	1,155.5	-	-
M	Silt	650.5	931.6	1,013.3	1,678.2	1,220	1,350
RS1	75% R + 25% S	123.6	211.8	259.9	728.6	-	-
RS2	50% R + 50% S	135.3	270.7	272.6	822.8	482.5	680.6
RS3	25% R + 75% S	115.7	341.3	291.3	753.2	687.5	757.1

^a20 mm long polyester fibers (Table 5)

A fly ash-stabilizer design mix for base courses is one that complies with the prescribed strength criteria. In the second series (Series II) of experiments, utilization of fly ash as a base course material in pavements was investigated. Larger cement contents complying with the criteria of Electric Power Research Institute (EPRI) [28] were used. The tests were carried out only on the two raw fly ashes. The EPRI criteria are: (1) the minimum UCS of the specimens after 7 days of curing should be in the range of 2760-3100 kPa and should not exceed 5500 kPa; (2) UCS must increase with time; the 28-day UCS is

approximately twice that of the 7-day UCS; and (3) during curing, the specimens are wrapped in moisture proof

bags and kept under $21 \pm 2^\circ\text{C}$. The design mix was determined by compaction tests and unconfined compression tests on trial mixes. The final design mix specifications were $C_c = 18\%$, water content (w) = OMC = 37% and dry unit weight (γ_d) = MDD = 11.7 kN/m^3 for Rajghat fly ash specimens and $C_c = 15\%$, $w = 0.85$ $S = 23.6\%$, and $\gamma_d = 0.95$ MDD = 13.74 kN/m^3 for Dadri fly ash specimens. S is the degree of saturation. The development of the cementation products in Dadri fly ash can be seen in the scanning electron micrographs in Figure 5. Table 9 shows the UCS values for the Rajghat and Dadri fly ash design mix specimens of above specifications. The specimens failed suddenly after reaching the peak stress. The average failure strain varied between 1 and 3.5%.

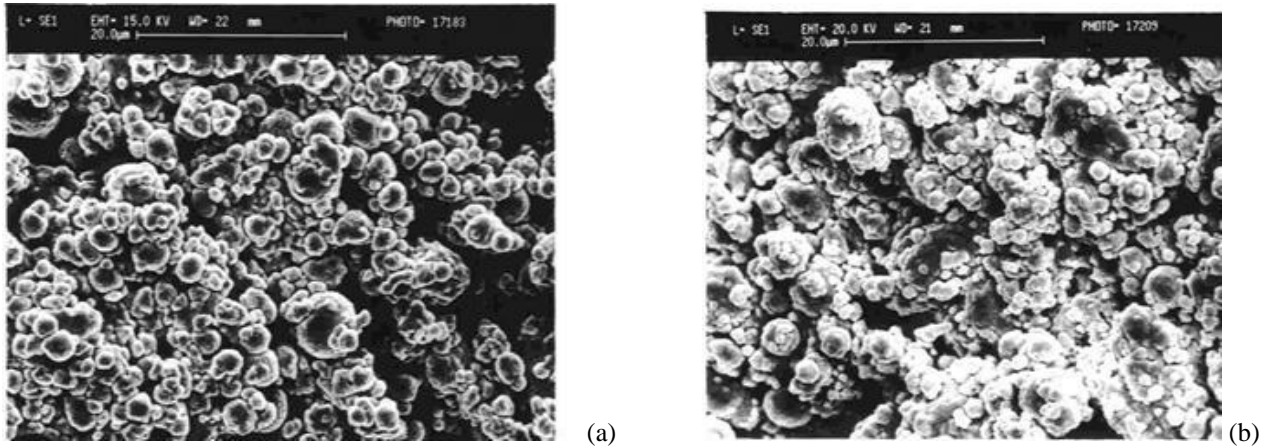


Figure 5 SEM of cement stabilized Dadri fly ash (Series II): (a) 7 days curing, and (b) 28 days curing [24]

Table 9 UCS (kPa) of fly ashes stabilized with cement and fibers - Series II [24]

Fly ash	Curing period (days)				
	0	$f_c = 0$		$f_c = 1\%^a$	
		7	28	7	28
Rajghat fly ash	120.6	3,843	7,453	3,389	7,749
Dadri fly ash	116.7	3,172	3,689	3,481	6,026

^a6 mm long polyester fibers (Table 5)

VI. FLY ASH – SOIL MIXTURES STABILIZED WITH CEMENT AND FIBERS

On the fly ash-soil mixtures stabilized with fibers alone and cement alone explained before, another set of experiments were done in which the fly ash-soil mixtures were stabilized with both cement and fibers. Figure 6 shows the scanning electron micrograph of Rajghat fly ash stabilized with both cement and fibers.



Figure 6 SEM of cement and fiber stabilized Rajghat fly ash – Series II (28 days curing) [24]

The UCS values of the cement and fiber stabilized specimens are shown alongside the respective UCS values of the specimens stabilized with cement alone in Tables 8 and 9 for Series I and Series II experiments, respectively. Some typical stress-strain curves of Series II experiments are shown in Figure 7. Each curve in the figure is for a particular combination of fly ash, cement content, and fiber length. RA and DA in the legend denote Rajghat fly ash and Dadri fly ash, respectively. The second figure of 18 and 15 denote the cement content. The third figure 06, 09, and 20 mm denote the length of fibers

used. The value of 00 in the third figure indicates that the specimen was stabilized only with cement and no fiber was used. The addition of fibers increased the UCS of cement stabilized Dadri fly ash significantly whereas it did not have a significant effect on the UCS of Rajghat fly ash. Like the cement stabilized fly ash specimens, the cement and fiber stabilized fly ash specimens of Series II too failed suddenly after reaching the peak stress. However, the fibers increased the failure strain; the average failure strain varied between 2.5 and 4.5%.

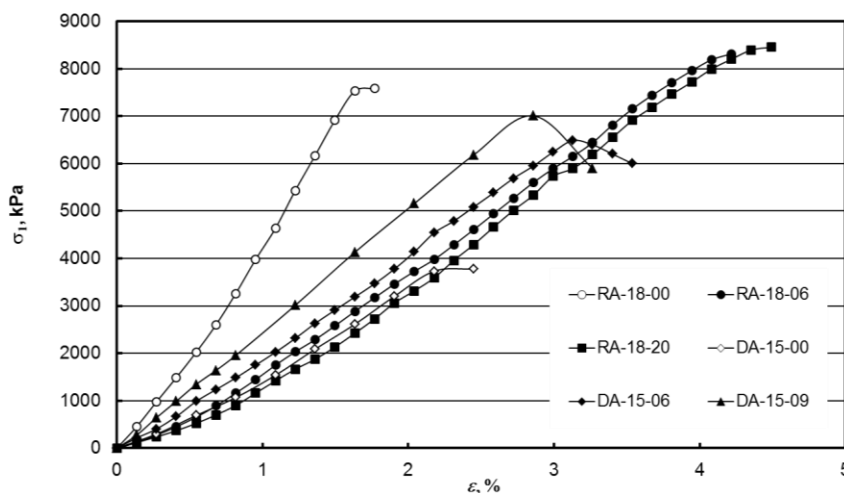


Figure 7 Axial stress-strain curves of cement and fiber stabilized fly ash specimens cured for 28 days [26]

VII. CONCLUSIONS

Following conclusions are arrived at from the experimental studies.

1. Mixing fly ash with soil decreased the MDD of soil. A fly ash–soil fill would therefore be lighter than a soil fill. The shear strength parameters of fly ash–soil fill were generally more than those of the soil fill. The fly ash–soil fill would therefore be stronger than the soil fill. Further, fly ash embankments and fills would be moderately permeable over their entire height.

2. In general, polyester fiber inclusions did not have a significant effect on the MDD and OMC of raw fly ashes and fly ash-soil mixtures. But, fiber inclusions had a highly favorable effect on shear strength and shear behavior. They increased the UCS as well as the shear strength parameters of the raw fly ashes and fly ash-soil mixtures. The fibers also changed the stress-strain behavior of the specimens from brittle to ductile.

3. Even small cement contents increased the UCS of the fly ash-soil specimens significantly. With higher cement contents of up to 18% it was possible to prepare fly ash-cement design mixes that satisfied the strength criteria for pavement base courses. All cement stabilized fly ash and fly ash-soil specimens failed suddenly after reaching the peak stress.

4. The addition of fibers increased the UCS of the cement stabilized Dadri fly ash significantly whereas it did not have a significant effect on the UCS of the cement stabilized Rajghat fly ash. The cement and fiber stabilized fly ash specimens too failed suddenly after reaching the peak stress. However, the fibers increased the failure strain.

ACKNOWLEDGMENT

The authors acknowledge with thanks the use of facilities at the Indian Institute of Technology, Delhi, where the experiments were carried out. The financial support provided by Universiti Malaysia Sarawak, Kota Samarahan, Sarawak, for this paper is also acknowledged with thanks.

REFERENCES

- [1] D. H. Gray, "Role of woody vegetation in reinforcing soils and stabilizing slopes," in *Proc. Symp. on Soil Reinforcement and Stabilizing Techniques*, Sydney, Australia, 1970, pp. 253-306.
- [2] C. B. Brown and M. S. Sheu, "Effect of deforestation on slopes," *J Geotech. Eng. Div.*, ASCE, vol. 101, GT1, pp. 147-165, 1975.
- [3] L. J. Waldron, "Shear resistance of root-permeated homogeneous and stratified soil," *Soil Science Society of America J.*, vol. 41, pp. 843-849, 1977.
- [4] T. H. Wu and R. T. Erb, "Study of soil-root interaction," *J Geotech. Eng. Div.*, ASCE, vol. 114, no. 12, pp. 1351-1375, 1988.
- [5] T. H. Wu, P. E. Beal and C. Lan, "In-situ shear test of soil-root system," *J Geotech. Eng. Div.*, ASCE, vol. 114, no. 12, pp. 1376-1394, 1988.
- [6] A. McGown, K. Z. Andrawes and M. M. Al-Hasani, "Effect of inclusion properties on the behaviour of sand," *Geotechnique*, vol. 28, no. 3, pp. 327-346, 1978.
- [7] S. S. Rehsi, "Use of natural fibre concrete in India," in *Natural Fibre Reinforced Cement and Concrete*, (ed) R.N. Swamy, Blackie-Glassy, 1988.
- [8] R. M. Vasan, "Investigations on fibre reinforced concrete pavements," *Ph.D. Thesis*, University of Roorkee, Roorkee, India, 1989.
- [9] D. H. Gray and H. Ohashi, "Mechanics of fiber reinforcing in sand," *J Geotech. Eng. Div.*, ASCE, vol. 109, no. 3, pp. 335-353, 1983.
- [10] S. E. Shewbridge and N. Sitar, "Deformation characteristics of reinforced soil in direct shear," *J Geotech. Eng. Div.*, ASCE, vol. 115, no. 8, pp. 1134-1147, 1989.

- [11] G. E. Bauer and M. N. Fatani, "Strength characteristics of sand reinforced with rigid and flexible elements," in *Proc. 9th Asian Regional. Conf. on Soil Mech. Found. Eng.*, Bangkok, vol. 1, pp. 471-474, 1991.
- [12] D. J. Hoare, "Laboratory study of granular soils reinforced with randomly oriented discrete fibers," in *Proc. Int. Conf. on Soil Reinforcement*, Paris, France, vol. 1, pp. 47-52, 1979.
- [13] M. H. Maher, "Static and dynamic response of sands reinforced with discrete randomly distributed fibers," *Ph.D. Thesis*, University of Michigan, Ann Arbor, U.S.A., 1988.
- [14] D. H. Gray and M. H. Maher, "Admixture stabilization of sand with discrete randomly distributed fibers," in *Proc. XII Int. Conf. on Soil Mech. Found. Eng.*, Rio de Janeiro, Brazil, pp. 1363-1366, 1989.
- [15] M. H. Maher and D. H. Gray, "Static response of sands reinforced with randomly distributed fibers," *J Geotech. Eng. Div.*, ASCE, vol. 116, no. 11, pp. 1661-1677, 1990.
- [16] H. D. Charan, "Probabilistic analysis of randomly distributed fibre reinforced soil," *Ph.D. Thesis*, University of Roorkee, Roorkee, India, 1995.
- [17] D. K. Chakraborty and S. P. Dasgupta, "Randomly reinforced fly ash foundation material," in *Indian Geotechnical Conference*, Madras, vol. 1, pp. 231-235, 1996
- [18] S. R. Kaniraj and V. G. Havanagi, "Geotechnical characteristics of fly ash-soil mixtures," *Geotechnical Eng. J.*, vol. 30, no. 2, pp. 129-147, Aug. 1999.
- [19] S. R. Kaniraj and V. G. Havanagi, "Compressive strength of cement stabilized fly ash-soil mixtures," *Concrete and Cement Research*, vol. 29, pp. 673-677, 1999.
- [20] S. R. Kaniraj and V. G. Havanagi, "Correlation analysis of laboratory compaction of fly ashes," *Practice Periodical of Hazardous, Toxic, and Radioactive Waste Management*, vo. 5, no. 1, Jan. 2001.
- [21] S. R. Kaniraj and V. Gayathri, "Geotechnical behavior of fiber reinforced fly ash," in *Landmarks in Earth Reinforcement*, Ochiai et al, Ed. 2001, pp. 61-65.
- [22] S. R. Kaniraj and V. G. Havanagi, "Behavior of cement-stabilized fiber-reinforced fly ash-soil mixtures," *J. Geotechnical and Geoenvironmental Eng.*, vo. 127, no. 7, pp. 574-584, July 2001.
- [23] S. R. Kaniraj and V. Gayathri, "Geotechnical behavior of fly ash mixed with randomly oriented fiber inclusions," *Geotextiles and Geomembranes*, vol. 21, pp. 123-149, 2003.
- [24] S. R. Kaniraj and V. Gayathri, "Factors influencing the strength of cement fly ash base courses," *J. Transp. Eng.*, vol. 129, no. 5, pp. 538-548, 2003.
- [25] S. R. Kaniraj and V. Gayathri, "Permeability and consolidation characteristics of compacted fly ash," *J. Energy Eng.*, vol. 130, no. 1, pp. 18-43, April 2004.
- [26] S. R. Kaniraj and V. Gayathri, "Behavior of fiber-reinforced cement-stabilized fly ashes," *J. Testing and Evaluation*, vol. 34, no. 4, pp. 290-297, July 2006.
- [27] *ASTM Standard C 618*, "Specification for fly ash and raw or calcined natural pozzolana for use as a mineral admixture in Portland cement concrete," in *Annual Book of ASTM Standards*, sec. 4, vol. 4.02, pp. 310-312, 1993.
- [28] P. E. Glogowski, J. M. Kelly, R. J. McLaren, and D. L. Burns, "Fly ash design manual for road and site application," *Final rep. prepared for Electric Power Research Institute, Palo Alto, Calif.*, 1992.

CHAPTER 10

STUDY OF SOIL EROSION AT A SITE NEAR CHEMICAL ENGINEERING LABORATORY IN UNIMAS

Fizzahutiah Binti Taha¹ and Shenbaga R. Kaniraj²

Abstract— Soil erosion is one of the problems of environmental concern. Natural causes such as rainfall and human development activities are the two main factors that can cause soil erosion. In order to control soil erosion, especially in urban areas, the bare soil surface needs to be covered by plants as much as possible. Re-vegetation, the best permanent erosion control measure, might take time to be complete. Therefore, some suitable temporary measures should be applied to minimize the amount of soil loss. Topographical features and climate are among the factors that determine the amount of soil erosion. In order to control the rate of erosion, it is important to estimate the amount of soil loss. Universal Soil Loss Equation (USLE) is one of the approaches to estimate the rate of soil loss. In this study, the topographical features of a site prone to erosion within University Malaysia Sarawak (UNIMAS), were investigated by field survey. Laboratory experiments were carried out on soil samples collected from the site. The parameters for use in USLE were evaluated. The soil loss at the site in 2011 was estimated as 52.85 t ha⁻¹ and the soil erosion risk at the site was categorized as moderately high.

Keywords: environmental issues, soil erosion, topographical features, Universal Soil Loss Equation (USLE), urban area

I. INTRODUCTION

URBAN areas have high potential for soil erosion due to developmental activities. The environmental impact due to soil erosion includes clogged drains, increased flooding, land degradation, etc. In order to minimize soil erosion, erosion risk analysis should be carried out. There are various techniques to analyze erosion risk. The most widely used mathematical model to estimate soil loss from an area is the Universal Soil Loss Equation (USLE). In Malaysia, USLE is commonly used in Environmental Impact Assessments (EIA) for predicting erosion and soil loss from land development sites [1]. Soil erosion is the removal of soil particles by wind, gravity, mass movement and water. There are many agents of erosion, but the most significant agent for soil erosion in the Malaysian environment is water. This is due to the high annual rainfall and storm events in Malaysia. The amount of soil loss will speed up in a short amount of time on the bare soil surface. Exposed soil surface will also increase the frequency of flood flows which will result in increased erosion and higher sediment concentration.

The most common soil erosion in Malaysia is rain splash erosion. Bare soil surface is extremely susceptible to rain splash erosion. Rain splash erosion occurs during high intensity rainstorms; the force of the falling raindrops dislodges the soil particles. Sheet erosion, rill erosion and gully erosion are the other common types of erosion. Sheet erosion, also known as inter-rill erosion, is the lateral transportation of loose soil in a uniform layer. Sheet erosion occurring during heavy rain can be interrupted by vegetation. Rill erosion results in the formation of shallow drainage lines particularly on short and steep slopes. Gully erosion occurs at sites of unstable exposed surfaces with high intensity rainfall producing high runoff rates. Gully erosion produces deeper and larger flow channels compared to rill erosion [1].

The amount of soil loss due to erosion is affected by soil characteristics, topography, climate and other factors. Soil texture, organic matter, moisture content and soil structure are the soil characteristics that affect the detachment and removal of the soil particles. Topographical features affecting the erosion rate are the gradient of slope, length of slope, elevation, and size and shape of the watershed. In steeper and longer slopes, higher runoff and soil erosion will occur. Annual rainfall is one of the climate factors that affect the amount of soil loss. Higher precipitation increases the amount of soil loss particularly on bare soil surfaces.

II. METHODOLOGY

The study explained in the paper was carried out at a site within UNIMAS, Kota Samarahan. The population of Kota Samarahan from the 2010 census was 87,923. As the population is more than 10,000, Kota Samarahan is classified as an urban area. Several areas in UNIMAS are experiencing soil erosion. However, most of them are not serious. But, there is serious soil erosion at one particular site near the Chemical Engineering Laboratory. Therefore, this site was chosen for the study. Figure 1 shows the location of the site in plan. Figure 2 shows the view of the site and the structures nearby.

¹Fizzahutiah Binti Taha is with the University College of Science and Technology, 96000 Sibul, Sarawak, Malaysia. She was a student in the Faculty of Engineering, Universiti Malaysia Sarawak, 94300 Kota Samarahan, Sarawak, Malaysia. (e-mail: switjan_0101@yahoo.com.my; phone: +6084 311 888 Ext 116; fax: +6084 322 323).

²S. R. Kaniraj, is with the Faculty of Engineering, Universiti Malaysia Sarawak, 94300 Kota Samarahan, Sarawak, Malaysia. (e-mail: rkjshenbaga@feng.unimas.my)

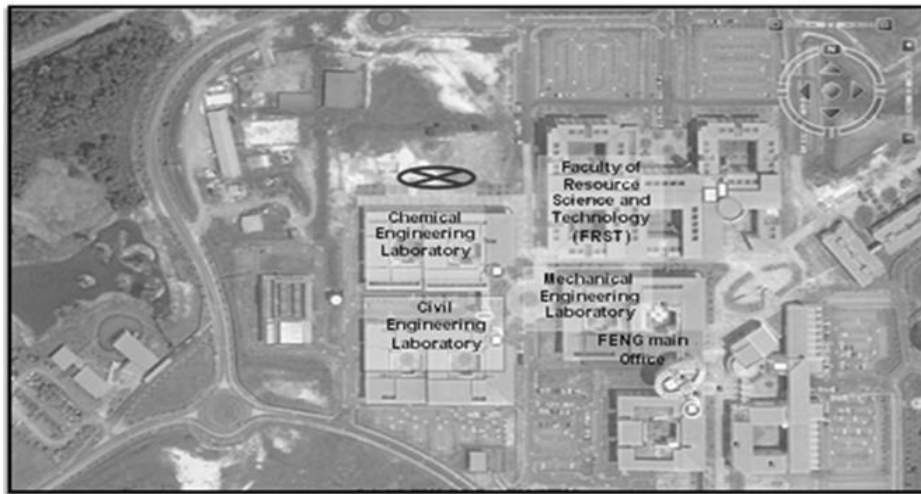


Figure 1: Study Site of Soil Erosion in UNIMAS



Figure 2: Soil Erosion Site Adjacent to the Chemical Engineering Laboratory

It was observed that the type of erosion at this site was gully erosion. Many deep and large flow channels were present in this area (Figure 3). The erosion in this area was associated with unstable exposed soil surfaces, high intensity rainfall events, and high runoff rates. The eroded soil was transported into the concrete drains. The concrete drains near this area were mostly choked with sediments (Figure 4). As a result, the efficiency of the drainage system had been affected and flooding occurred easily the vicinity of this area.

The soil erosion process at this site might have started with rain splash erosion. Since there were no measures for erosion control implemented at the site, the rain splash erosion eventually became gully erosion. Erosion and sedimentation result in depletion of river aquatic life and also affect the marine ecology as large sediment loads deposited along the coastline smother breeding grounds and coastal sea-beds. Inland, the sediments choke up culverts, river-beds and the drainage system. This will result in the increase in frequency of flash floods. Thus, there is a need to design and review an Erosion and Sediment Control Plan (ESCP) and supervise the implementation of Best Management Practices (BMPs) on-site. An integrated approach shown in Figure 5 was used to achieve the objective of the study systematically.

The amount of soil loss was estimated using USLE (Equation 1). Necessary field tests and site inspection were conducted to identify the USLE parameters for estimating the amount of soil loss at the site. Sieve analysis test was conducted to classify the soil at the site (type of soil, organic matter, size and percentage of different soil particles, etc.). To identify the topographical features of the site, namely, slope steepness and length of the slope, field surveying (leveling) was conducted. Others data such as, the annual precipitation at the site, were collected from the Department of Irrigation and Drainage (DID), Kota Samarahan.

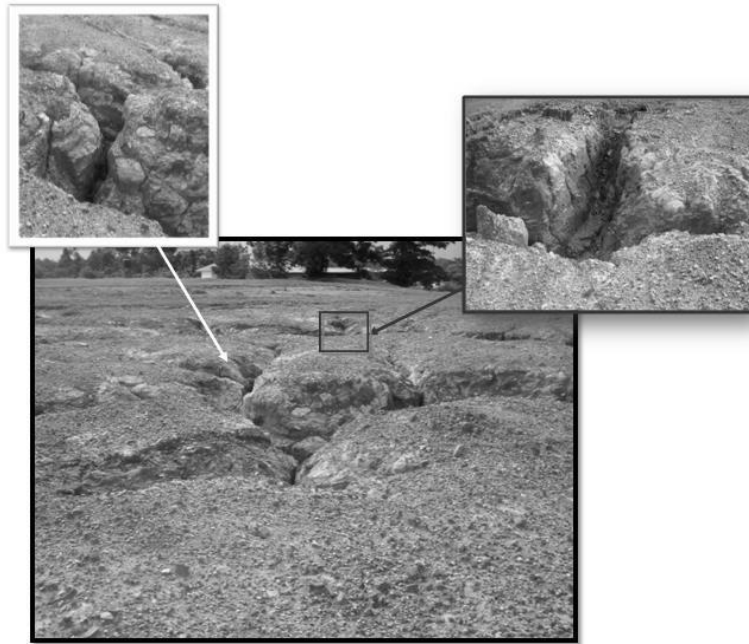


Figure 3: Gully Erosion at the Site near the Chemical Engineering Laboratory



Figure 4: Concrete Drains Choked with Sediments

$$A = R \times K \times LS \times C \times P \quad (1)$$

In Eq. 1, A = mean annual soil loss ($t \text{ ha}^{-1}$), R = rainfall erosivity index ($\text{Mg mm ha}^{-1} \text{ h}^{-1}$), K = soil erodibility factor, LS = topographical feature, C = cropping management factor, and P = erosion control management factor. Rainfall erosivity index (R) represents the erosion potential of rainstorms to be expected in a given locality. It is related to the kinetic energy and intensity of the rain. The product EI_{30} reflects the potential ability of rain to cause erosion, where E = total kinetic energy of rain, and I_{30} = peak 30 minutes intensity [2]. The equations suggested by Roose [1] and Morgan [3] to estimate R are shown in Equations 2 and 3, respectively.

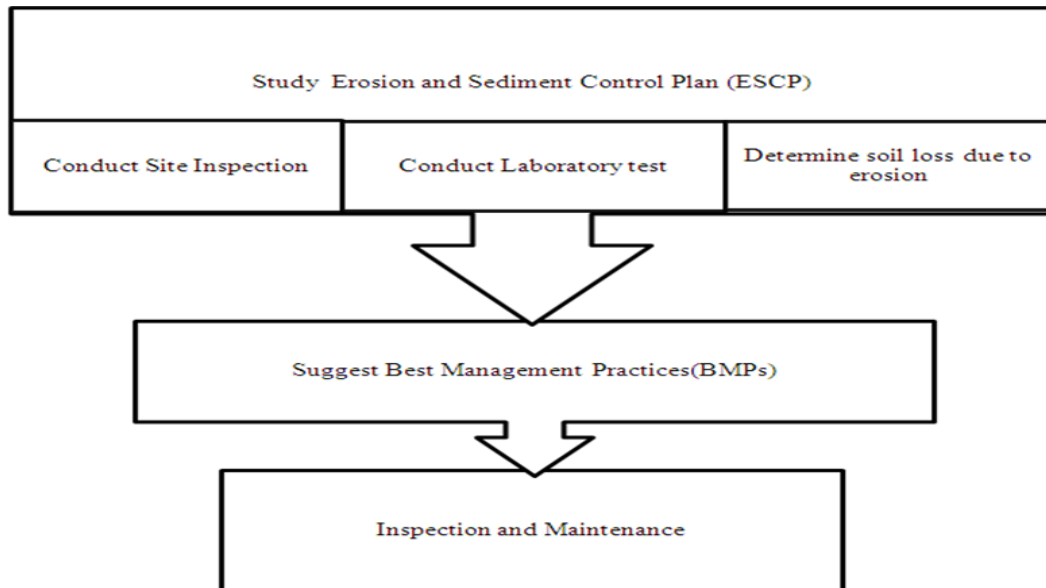


Figure 5: Flow Chart for Study of Controlling and Managing Erosion in Urban Areas

$$R = (EI_{30})/100 \quad (2)$$

In Equation 2, R is in $(\text{Mg mm ha}^{-1} \text{ h}^{-1})$, E = total kinetic energy of rain ($E = 9.28p - 8838$), p = mean annual precipitation (mm), and I_{30} = peak 30 minutes intensity (75 mm h^{-1}).

$$R = p \times 0.5 \times 17.3 \quad (3)$$

In Equation 3, R is in $(\text{Mg mm ha}^{-1} \text{ h}^{-1})$, and p = mean annual precipitation (mm). Soil erodibility factor, K , is the ability of the soil to be eroded by flowing water. It depends on the soil structure, organic matter, size composition of the soil particles, and soil permeability measured as hydraulic conductivity. The value of K can be obtained using a nomograph shown in Fig. 6 [4, 5].

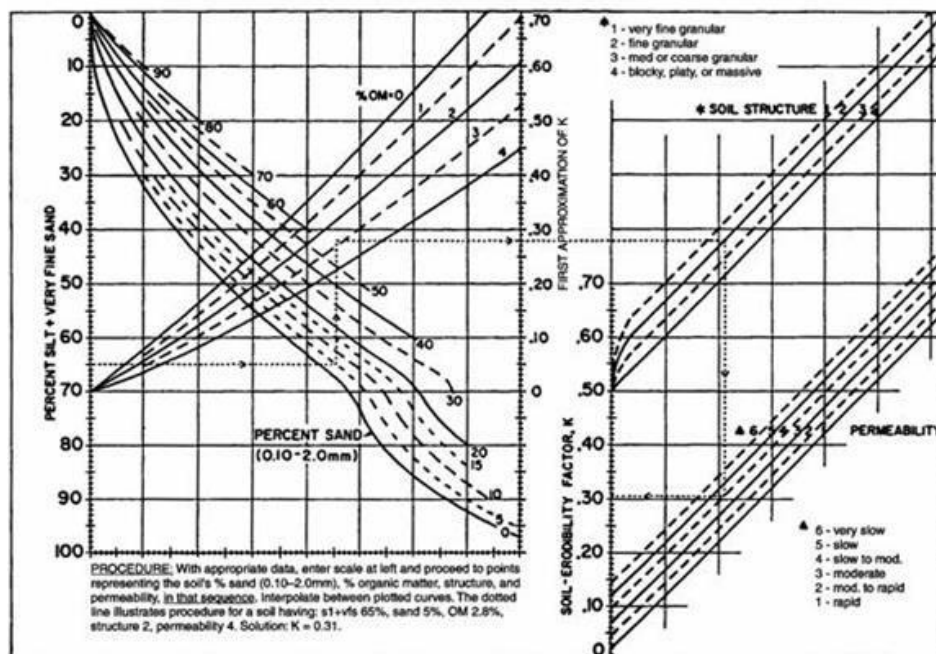


Figure 6: Nomograph for Soil Erodibility Factor, K [4, 5]

The value of topographical features factor, LS , can be obtained either by Equation 4 or by using a nomograph shown in Fig. 7 [6].

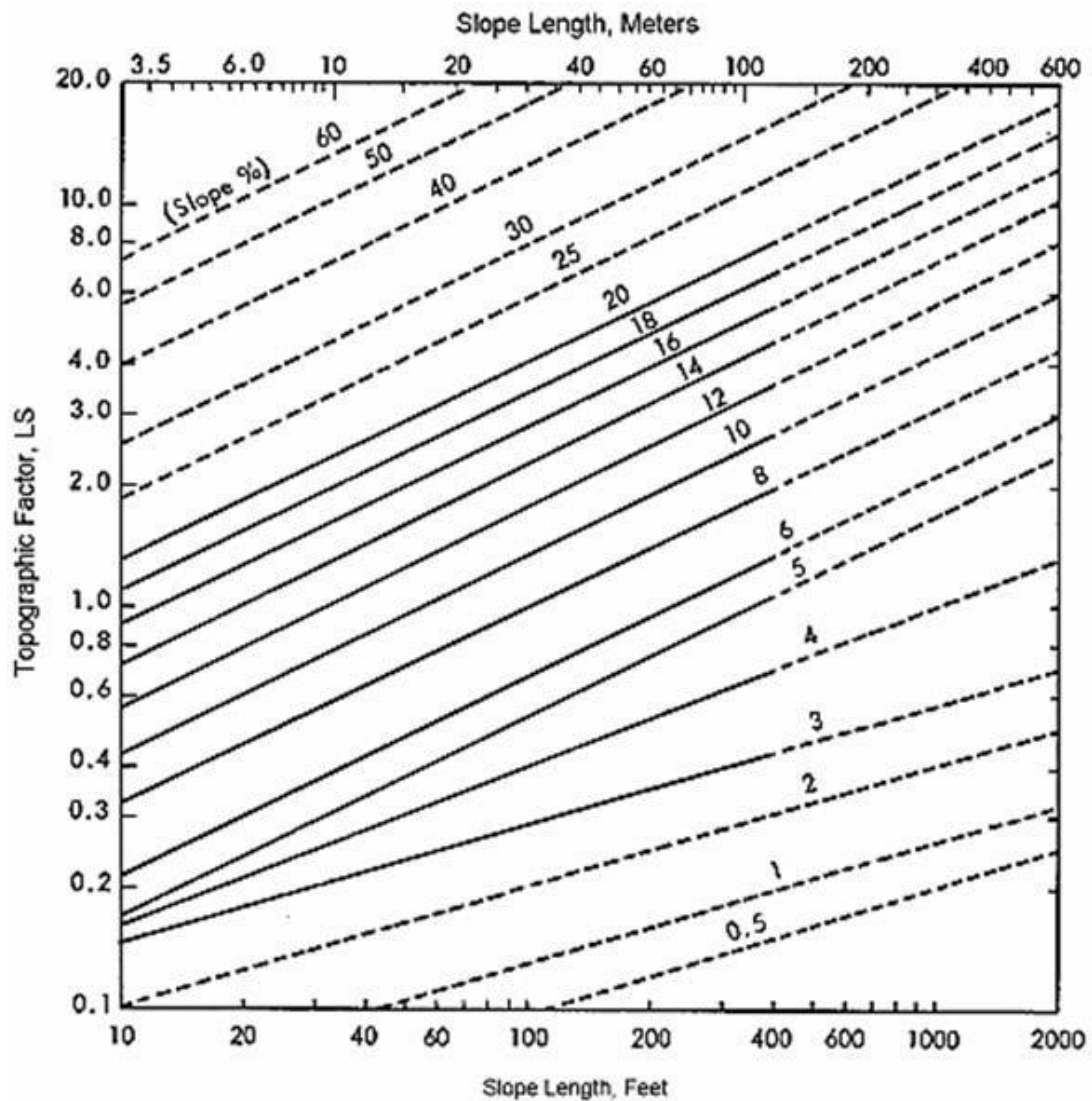
$$LS = (0.065 + 0.045 s + 0.0065 s^2) \times (l/22)^{0.5} \quad (4)$$

In Equation 4, l = length of the sloping ground (m), and s = slope gradient (%). Cropping management factor, C , and

erosion control management factor, P , are estimated according to the site characteristics by site inspection. Table 1 shows the summary of parameters in USLE and from where the values can be obtained.

Table 1: Sources for values of USLE parameters

USLE parameters	Sources
Rainfall erosivity index, R	Site inspection and related parties (e.g. DID, Meteorology department) <ul style="list-style-type: none"> • Precipitation value
Soil Erodibility factor, K	Nomograph (Fig. 6) and laboratory tests for: <ul style="list-style-type: none"> • Grain sizes in soil mass • Organic matter in soil
Topographical factor, LS	Nomograph (Fig. 7) and site survey (leveling) <ul style="list-style-type: none"> • Slope steepness • Slope length
Cropping management factor, C	Site inspection <ul style="list-style-type: none"> • Practice applied on the selected area
Erosion control management factor, P	Site inspection <ul style="list-style-type: none"> • Topographical information • Slope steepness



Dashed lines represent estimates for slope dimensions beyond the range of lengths and steepnesses for which data are available

Figure 7: Nomograph for Topographic Factor, LS [6]

III. RESULTS, ANALYSIS AND DISCUSSION

The amount of soil loss at the site was estimated using USLE. For rainfall erosivity index, R , the important data needed is the mean annual precipitation. The data for precipitation were taken from Department of Irrigation and Drainage (DID). In 2011, the precipitation at the site was about 4584.5 mm. The average value of R for the site from Equations 2 and 3 was $32467.8 \text{ Mg mm ha}^{-1} \text{ h}^{-1}$.

To determine soil erodibility factor, K , first sieve analysis test and organic content test were carried out in the laboratory on soil samples collected from the site. The type of soil at the site was poorly graded sand, SP . The organic content from loss-on-ignition method was 2.3%. The soil structure was medium granular and the permeability for this soil was rapid. Using all these data on the nomograph in Fig. 6, the value of K was estimated as 0.013.

From field survey, the slope length, l , and slope steepness, s , were estimated as 23.8 m and 2.27%, respectively. The value of topographic factor, LS , from both Equation 4 and nomograph in Fig. 7 was estimated as 0.21. Based on the field inspection, the cropping management factor, C , and erosion control practice factor, P , for the site were assigned as 1 and 0.6, respectively. Using the USLE parameters in USLE the amount of soil loss at the site in 2011 was estimated as 52.85 t ha^{-1} . Based on the criteria of Department of Agriculture [7] the soil erosion risk at the site was classified as moderately high.

Since the soil erosion risk is moderately high, proper management and controlling of erosion should be planned. To manage erosion, it is important to identify the suitable erosion and sediment controls for the site. These controls are based on the condition of soil loss, types of soil, topographical features, location of erosion, and the surrounding activities. The 9 steps for developing and implementing an erosion and sediment control plan are: *a)* identification of issues and concerns, *b)* development of goals and objectives, *c)* collection and analysis of data, *d)* development of BMP selection criteria, *e)* nomination of candidate BMPs, *f)* screening and selection of BMPs, *g)* development of ESPC, *h)* operation, monitoring, and maintaining the system, and *i)* updating the plan [6]. For selecting the best management practices (BMPs), the 5 recommended criteria are: *a)* temporary vs. permanent BMPs, *b)* availability, *c)* feasibility, *d)* suitability for the site, and *e)* cost effectiveness.

IV. CONCLUSION

The paper presents the study of erosion risk at a site in UNIMAS near Chemical Engineering Laboratory. The USLE parameters were determined and the amount of soil loss at the site was estimated using USLE. The amount of soil loss at the site in 2011 was estimated as 52.85 t ha^{-1} and categorized as moderately high risk erosion.

The environment impact due to the soil loss was the failure of drainage system at the site. The concrete drains at the roadside were fully choked with sediments. The parking spaces adjacent to the site area needed to be closed since the eroded soil had spread to the parking areas. In order to control erosion at the site, 9 important key steps of ESCP and 5 criteria for selection of BMPs had been outlined.

ACKNOWLEDGMENT

The authors express their gratitude to Universiti Malaysia Sarawak for the support to this research.

REFERENCES

- [1] Department of Environment, *Guidelines for Prevention and Control of Soil Erosion and Siltation in Malaysia*. Department of Environment, Ministry of Science, Technology and Environment, Malaysia, 1996.
- [2] S. I. Mir, M. B. Gasim, S. A. Rahim, and M. E. Toriman, "Soil loss assessment in the Tasik Chini catchment, Pahang, Malaysia," *Geological Society of Malaysia*, pp. 1-7, 2010.
- [3] R. P. C. Morgan, *Soil Conservation Problems and Prospects*. John Wiley & Sons Ltd, Toronto, 1980.
- [4] R. Morgan, *Soil Erosion and Conservation*. Australia: Blackwell Science Ltd, 2005.
- [5] "Erosion Mechanisms and the Revised Universal Soil Loss Equation (RUSLE)," Retrieved September 9, 2013, from <http://rpitt.eng.ua.edu/Class/Erosioncontrol/Module3/Module3.htm>
- [6] "Universal Soil Loss Equation: (Wischmeier and Smith)," (n.d.). Retrieved November 17, 2011, from <http://www.evsc.virginia.edu/~alm7d/soils/handouts/USLE.pdf>
- [7] "Soil Erosion Risk Map of Peninsular Malaysia," Department of Agriculture, Retrieved September 9, 2013, from <http://www.doa.gov.my/documents/10157/2ba95366-5f8a-416d-ae90-9fb016fa26eb>

CHAPTER 11

STRENGTH AND DURABILITY EFFECT ON STABILIZED SUBGRADE SOIL

Noraida binti Razali¹, Norazzlina binti M. Sa'don², and Abdul Razak bin Abdul Karim³

Abstract

This paper presents the development of strength and durability effect of stabilized soil. The clayey soil collected from Kota Samarahan, Sarawak was admixed with cement, fly ash and rubberchip as an additive for stabilization purposes. The optimum mixture determined was then used as a recommendation for the design guidelines of subgrade based on JKR Standard Specification for Road Works. The stabilized clay specimens were prepared with 5% cement and various fly ash and rubber chips contents, of 5%, 10% and 15%, respectively. The specimens were then cured for 7 and 28 days before subjected to Unconfined Compressive Strength (UCS) tests and California Bearing Ratio (CBR) tests. As observed, the stabilization improved the strength and stiffness of the soil properties significantly. However, the addition of 15% rubberchip shows a reduction in strength for both 7 and 28 days curing period. From the study, the optimum mixture, which fulfilled the JKR Standard Specification was the mixture of 5% cement and 15% fly ash. However, the mixture of 5% cement and 10% rubberchip is also recommended to be used as an alternative to stabilize the subgrade for low volume road.

Keywords: fly ash, rubberchip, subgrade

1.0 INTRODUCTION

In road and highway constructions, not only the pavement or premix quality is given serious scrutiny, but the substructure below the pavement is also equally vital. The stability of the underlying soils needs serious attention so as to ensure that the pavement structures that has been constructed can enhance the durability of the pavements. It is important to provide the optimum performance for the pavements because the pavement structures are significantly impacted by the direct loading of the traffic. Unfortunately, in Sarawak, some locations are frequently not adhered to the project requirements due to the availability of the soft soil and it is clearly inadequate for the traffic loading demands. In order to meet such requirements, the subgrade material requires a treatment to stabilize the soils in the specified area to provide a stable subgrade and also a suitable working platform for the needs of the pavement construction. As the materials used for road construction are getting more expensive, stabilizing the local soil and improved its physical properties through soil treatment is one of the alternatives.

The Portland cement, which is basically a compound of silica, alumina and iron has been widely used in order to stabilize soils especially in the highway construction [1], [2]. There are two basic reactions occur in cement stabilization which is hydration and pozzolanic reactions and it is well documented in the literature [3], [4]. As stated by [3], when cement is combined with water, the hydration reactions will occur and the cement-treated material will gain strength as well as the pozzolanic reactions that contribute to the strength of a specimen. An experimental work done by [5] shows that compressive strength development for 7 days soaked clay soil-cement mixture are 200 psi to 400 psi and for 28 days the results shows that it can reach 250 psi to 600 psi by using 9% to 16% of cement.

^{1,2,3}Fakulty of Engineering, Universiti Malaysia Sarawak, 94300 Kota Samarahan, Sarawak

However, [6] come out with a suggestion of the required cement quantity as 4% to 6% from the dry mass of the soil that can gain the strength of 100 psi (700 kPa) and they also concluded that the amount of 4% cement by dry weight of the soils are adequate for cement stabilization. [2] also stated that a reasonable criterion for soil stabilization is the increase of the strength of the untreated soil compared to the stabilized soil by 50 psi (350 kPa) or greater under the same condition of compaction and cure. The cement used in this study is Ordinary Portland cement produced by Cahaya Mata Sarawak Corporation (CMS).

The utilization of fly ash in stabilizing the clayey soil also has been studied by various researchers [2], [3], [7], [8], [9]. Fly Ash which is the product of the combustion of coal is one of the stabilizers used in subgrade soil stabilization for the construction of roads [7], [8]. It can provide the pozzolanic reactions to strengthen the clayey soils as the lack of silica and alumina in the soft soil will caused a failure. [9] pointed out that when exposed to water, fly ash will be hydrated and it can be used as a drying agent for wet soils and also acts as a weak cementing agent that increases the strength of the treated soil. In this study, the Class F fly ash was used as one of the stabilizing agent to strengthen the soil properties and the addition of 5% cement was used in order to enhance the ability of the fly ash to react with the pozzolanic activities as it contains very little amount of lime.

A study done by [10], shows that the strength improvement cannot be achieved by using rubberchip alone. However, the failure of the axial strain percentage was increased for the specimens with rubberchip as compared to the specimens without rubberchip as an additive. Regarding to [10], the soft soil that was stabilized with 5% mixture of cement together with rubber chips of various quantities of 5%, 10% and 15% from the soils dry weight can increase the cohesion value of the soft soil mixture from 0.06 to 0.70kN/m². From the study, it is shown that significant improvement in the undrained shear strength of the soft soil can be obtained from cement- rubberchip admixtures. From the previous study of [11], it has shown that the rubber can be a flexible filler material in the soft soil stabilization where 2% to 4% of rubbershred based on the dry weight of soil were prepared to the specimens. The study by [12] also agreed that the strength of naturally weak and soft soils like clay can be improved by stabilizing the soils with the mixture of cement-rubberchips. They also stated that it is practical to apply the rubberchips as one of the alternative material in order to improve the soft soil strength characteristics. The rubberchip that is used in this study is a product from Zhen Hak Ann Tyres Recycle Sdn Bhd located in Jalan Batu Kawa – Matang, Sarawak. The rubberchip is between 1 mm to 4 mm of particle sizes and it is taken from the raw material without sieving to the addition of the mix design. This paper presents an investigation to determine the strength development and durability effect of stabilized subgrade. This was conducted by performing Unconfined Compressive Strength (UCS) Tests, California Bearing Ratio (CBR) Tests, and Compaction by Standard Proctor Tests.

2.0 SOFT SOIL CHARACTERISTICS

A total 7 design mixtures were prepared in order to investigate the durability and strength development for the soft soil stabilization and 1 set of specimens is prepared for the untreated soil for comparison purposes. For each design mixture, there are 3 specimens prepared and the total specimens prepared were 96 specimens for UCS Tests and another 96 specimens for CBR Tests. The tests were conducted in two conditions namely, soaked and unsoaked and it is conducted in accordance to the British Standard 1377. The design mixture is indicated as follows:

1. 5% cement (5C)
2. 5% cement with 5% fly ash (5C_5FA)
3. 5% cement with 10% fly ash (5C_10FA)
4. 5% cement with 15% fly ash (5C_15FA)
5. 5% cement with 5% rubberchip (5C_5RC)
6. 5% cement with 10% rubberchip (5C_10RC)
7. 5% cement with 15% rubberchip (5C_15RC)

The tests is taken by two (2) phases which is to determine the soft soil characteristics and then to measure the engineering properties of the design mixtures. The soil characteristic that are being measured are the moisture content, specific gravity, Atterberg Limit and grain size distribution by conducting sieve analysis and hydrometer analysis tests. In Atterberg Limit tests, Liquid Limit (LL) and Plastic Limit (PL) were obtained before Plasticity Index (PI) was determined. The durability effect of the stabilized material is important for subgrade soil as the foundation of engineering structure [13]. In an effort to prevent subgrade failure, many studies with different protocols have been made in this study to evaluate the strength properties of the stabilized materials. Various laboratory tests of particular interest were conducted in this study namely Unconfined Compressive Strength Tests (UCS), California Bearing Ratio Tests (CBR) and Compaction Tests by Standard Proctor. Standard Proctor tests were conducted to obtain the optimum moisture content and dry unit weight of the clay sample and the mix designs. Unconfined compressive strength for clay with the various design mixes was obtained based on cured sample for 7 and 28 days. The tests were conducted in two conditions, which are soaked and unsoaked. California Bearing Ratio (CBR) tests were also being conducted to obtain the geotechnical properties of the mix design with soaked and unsoaked conditions for 7 and 28 days curing period.

3.0 SOIL PROPERTIES

Table 1 tabulated the general properties of the soil, as can be seen the moisture content is about 30.34%. The Atterberg limit value is 26.70% for LL whereas the plasticity index was 5.11%, respectively. Based on the plasticity chart the soil can be classified as low plasticity clayey silt, CL-ML.

Table 1: Geotechnical Properties of the Kota Samarahan Soft Clay

General Geotechnical Properties		
Water content, w_o	(%)	30.34
Liquid limit, LL	(%)	26.70
Plastic limit, PL	(%)	21.59
Plasticity Index, PI	(%)	5.11
Liquidity Index, LI	(%)	1.71
Shrinkage limit, SL	(%)	2.87
Specific gravity, G_s		2.35
Grain size distribution:	(%)	
Clay (<0.002 mm)		24.00
Silt (<0.075 mm)		34.00
Sand (>0.075 mm)		37.00
Gravel		5.00

4.0 COMPACTION EFFECT OF STABILIZED KOTA SAMARAHAN SOFT CLAY

Figure 1 illustrates the moisture-density relationship of the untreated and treated stabilized soil mixture, respectively. In general, the addition of cement, fly ash, and rubberchip for every soil mixture shows an increasing value in optimum moisture content and has different trends in their values by the increased fly ash and rubberchip amount along with 5% cement addition. However, the changes was considered small in the optimum moisture content and also in the maximum value of the dry unit weight due to the hydration process (from the addition of cement) that are not occurred in a short time period.

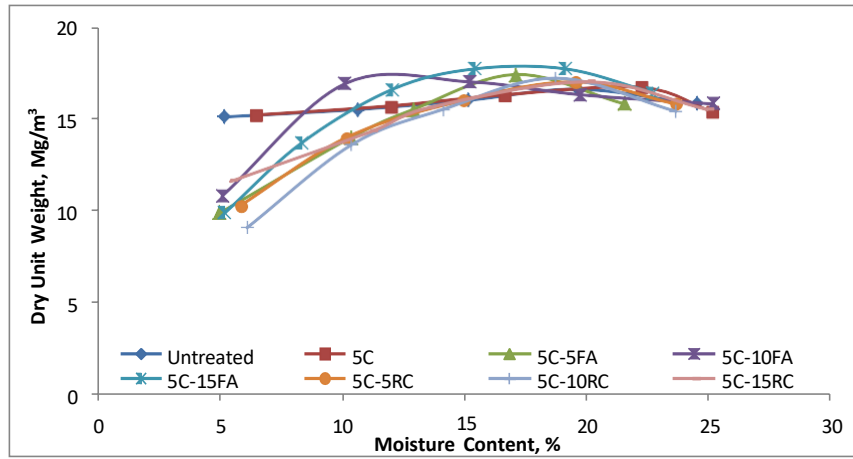


Figure 1: Relationship of dry unit weight versus optimum moisture content

5.0 STRENGTH DEVELOPMENT OF STABILIZED KOTA SAMARAHAN SOFT CLAY

The unconfined compressive strength (UCS) tests were conducted according to BS1377-7:1990 [14] in two conditions namely soaked and unsoaked. The soaked conditions represent the subgrade condition during heavy rainfall or drained condition while unsoaked represent normal rainfall or undrained condition. The stabilization of soil by using cement, fly ash and rubberchip generally increased the strength of the soil. However, the strength developments are dependent on the amount of stabilizers used. In order to get the best average value, three samples for each mixture were prepared for the purposes of the tests.

Figures 2 and 3 present the results obtained for 7- and 28-day curing time for all soil mixture samples. The highest strength was obtained from the mixture of the soil with 5% cement and 15% fly ash with the value of 941.69kPa which is 69.5% increase from the strength for 7-day curing period. The value obtained is greater than 0.8MPa required for the stabilized subgrade by [15]. The unconfined compressive strength values increased with continuous increasing of the fly ash content (from 5% to 15% fly ash). The highest strength gained for the soil mixture with cement and rubberchip is the mixture of 5% cement and 10% rubberchip in unsoaked condition where the strength gain about 50.7% value from 380.5kPa in 7-day curing period to 771.77kPa on 28th day. However, the rest of the mixture of rubberchip does not gain too much strength at the later age. Moreover, the strength value decreased for the rubberchip mixture of 15% rubberchip for both soaked and unsoaked conditions. From the findings, it can be concluded that the treated soil with rubberchip at early days curing period is characterized by a high strength but small strain at failure. Meanwhile, soil treated with fly ash shows larger strain before failure as it is stiffer than the rubberchip mixtures.

In addition, for the 7-day curing period, the untreated soil specimens had reach the strengths of 171.72kPa at optimum moisture content compaction while for 28th day of curing, the average value of the strength is 174.77kPa. According to [16], in the pavement applications, the strengths of the untreated soils that were compacted should be interpreted by general relationship between the soil consistency and its strength. Unfortunately, it is noted that untreated specimens were disintegrated after being submerged in water.

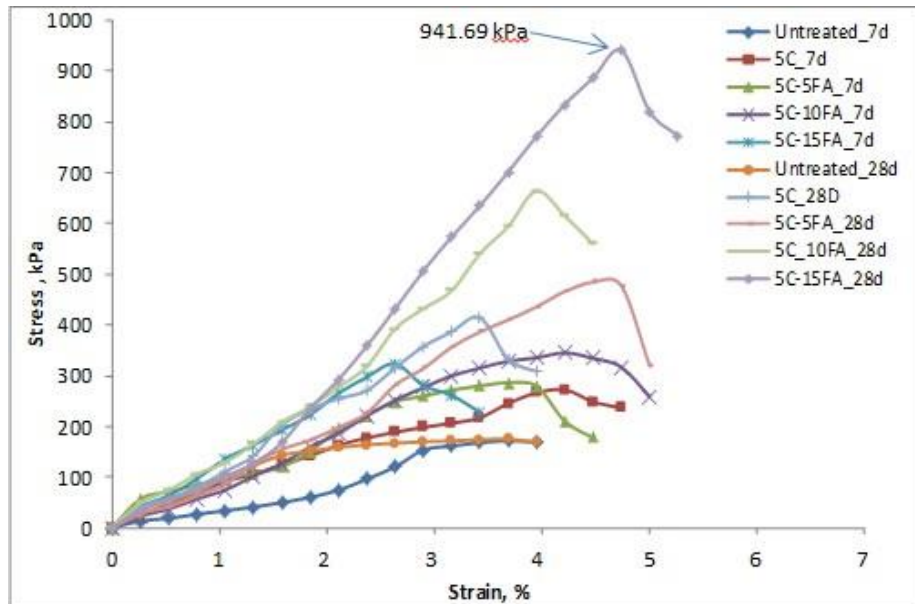


Figure 2: Unconfined compressive stress tests for fly ash

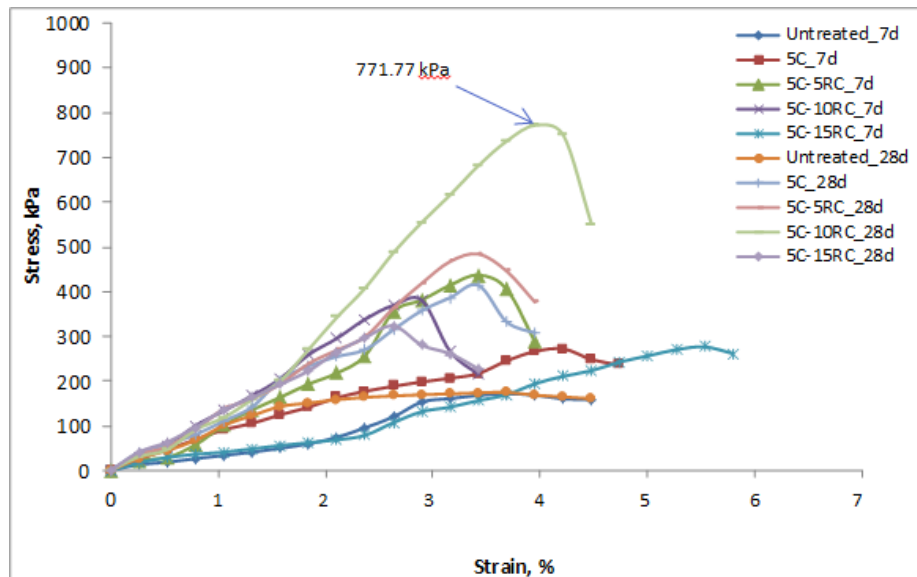


Figure 3: Unconfined compressive stress tests for rubberchip

6.0 DURABILITY EFFECT OF STABILIZED KOTA SAMARAHAN SOFT CLAY

The results of conducted CBR tests for soil samples with different percentages of stabilizers content are shown in Table 2. Based on the table, the value of the mixture to achieve 80% CBR value is obtained from the mixture of the soil with 5% cement and 15% fly ash.

It was also found that the percentage of CBR increases with strength due to the addition of stabilizers. The increasing trend of the CBR values by increasing the fly ash and rubberchip content is observed for all mixtures except for the mixture of 5% cement with 15% rubberchip. Surprisingly, the mixture shows the lowest CBR value for both soaked and unsoaked conditions as compared to other percentage of stabilizers.

Table 2: CBR value for unsoaked and soaked condition for Kota Samarahan soft clay

Admixture mixing			Curing Time	Unsoaked		Soaked	
Cement (%)	FA (%)	RC (%)	days	Penetration of 2.5mm,%	Penetration of 5 mm,%	Penetration of 2.5mm,%	Penetration of 5mm,%
Untreated soil			7	6.30	6.00	4.23	4.18
			28	19.80	6.26	29.28	13.37
5	0	0	7	16.59	48.52	29.90	20.65
			28	35.89	20.31	13.06	6.94
5	5	0	7	46.55	41.87	26.52	17.10
			28	54.00	51.35	36.22	35.77
5	10	0	7	30.92	30.81	14.56	9.65
			28	67.71	54.84	20.99	17.83
5	15	0	7	81.13	65.00	32.39	28.78
			28	82.60	78.77	72.28	71.55
5	0	5	7	28.86	14.90	24.38	16.59
			28	50.56	35.89	29.79	29.23
5	0	10	7	51.12	18.28	16.94	23.19
			28	64.66	61.28	9.82	4.74
5	0	15	7	5.59	13.54	2.37	9.25
			28	6.43	15.69	5.25	15.23

For the purpose of designing a stabilized subgrade according to [17], the mixture of 5% cement + 15% fly ash is sufficient to use for a high volume road while for designing a subgrade of low volume road, the mixture of 5% cement + 10% rubberchip can also be taken into consideration. The value gain is useful to determine the optimum additives content to be used for road construction when dealing with silty clayey subgrade for the local area. Table 2 also shows the effect of rubberchips of soaked and unsoaked CBR values of the mixtures of clay-cement-rubberchip. Both soaked and unsoaked values of these mixes initially increased up to 64.66% before they decreased when 15% rubberchip was added. The maximum value of CBR for the clay-rubberchip mixture was achieved with the addition of 10% rubberchip. The increasing value in CBR results was due to the characteristics of the rubberchips, which reinforced the mixture. The reinforcing characteristics prevent the cracks formation in the sample and binds together the soil particles which resulted in the increasing values of CBR. However, the increasing content of rubberchip decreases the distance of soil particles and the rubber chips, hence contributed to the increase in the volume but decreased the dry density. Hence, adding too much rubberchips could reduce the effectiveness of the improvement in the strength of the soil mixture, as fibres will adhere to form cluster and cannot be fully contacted with the soil particles [10],[18].



Figure 4: Examples of cracks formation in the mixture of clay-cement



Figure 5: Examples of cracks formation in the mixture of clay-cement-fly ash



Figure 6: Examples of cracks formation in the mixture of clay-cement-rubberchip

7.0 DESIGN GUIDELINES BASED ON JKR STANDARD

According to [17], both stabilized base materials and stabilized subgrade must have a minimum CBR of 80% and Unconfined Compressive Strength (UCS) of at least 0.8 MPa. From the laboratory experiments, the suitable design mixture that complies with this standard is the mixture of soil with 5% cement and 15% fly ash which the value of CBR was 82.6% and the UCS value was 941.69 kPa, respectively. The pavement design can be used as a guideline for a silty clayey soil in the local area of Kota Samarahan. The design mixture used minimum cement contents and optimum moisture contents to achieve the required strength for the traffic volume loading.

Based on the findings, the calculation for the pavement design was calculated using MathCad15 (PTC, 2010) by considering several input parameters such as Initial Daily Traffic Volume, the percentage of subgrade CBR value, etc. Then, the design of appropriate pavement structure was selected based on traffic category by using Manual for the Structural Design of Flexible Pavement produced by JKR. The Manual recommended a single tool that represents a design approach which combines the improved design data and methods of analysis and it present the predesigned pavement structures in the form of catalogue.

Several criteria or parameters have to be considered in order to design an appropriate flexible pavement for the selected area. The input parameters that will be used to design a stabilized subgrade thickness for a pavement are as follows:

1. Initial Daily Traffic Volume (ADT)
2. Percentage of commercial vehicle, P_c
3. Annual growth rate, r
4. Equivalent factor, e
5. Subgrade CBR value (%)
6. Equivalent Standard Axles (ESAL)
7. Reliability, R
8. Serviceability Index
9. Directional lane distribution
10. Lane distribution

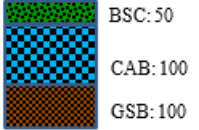
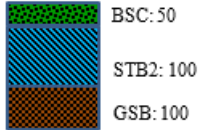

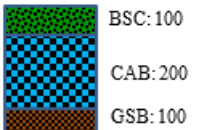
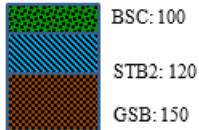

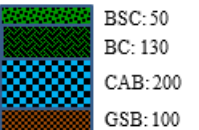
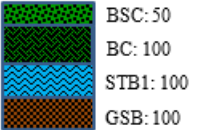


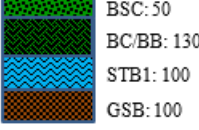
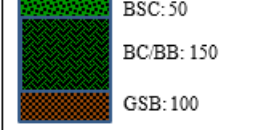
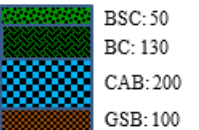
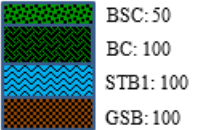


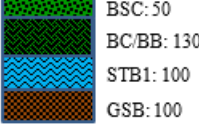
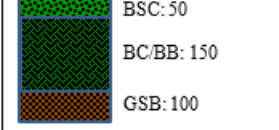
In designing an appropriate pavement structure, the first step is to calculate the design traffic by using parameters given by JKR and the Highway Planning Unit. The data is important in order to determine the loads that must be supported over the design life of the pavement. Then, the properties of subgrade are defined by using CBR tests result before determining the subgrade category that represents the subgrade strength. The subgrade category can be chosen by using Table 2 based on the percentage of CBR value. The last step is to select one of the pavement structures that can be selected in the catalogue contained in the Manual for the Structural Design of Flexible Pavement. The selected pavement structure depends on the subgrade category.

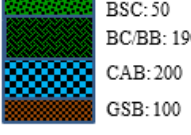

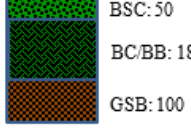

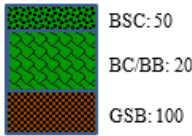
Table 3: Classes of Sub-Grade Strength (based on CBR) used as Input in the Pavement Catalogue
 (Manual for the Structural Design of Flexible Pavement, 2013)

Subgrade Category	CBR (%)	Elastic Modulus (MPa)	
		Range	Design Input Value
SG 1	5 to 12	50 to 120	60
SG 2	12.1 to 20	80 to 140	120
SG 3	20.1 to 30	100 to 160	140
SG 4	> 30	120 to 180	180

Based on the previous CBR results, Table 4 shows the alternative pavement structure based on the subgrade category for the optimum design mixtures.

Table 4: Alternative pavement structure based on traffic category for optimum design mixtures

No	Design Mixture	Stress (kPa)	Sub-grade Category	CBR (%)	Pavement Structure		
					Option 1 Conventional Flexible: Granular Base	Option 2 Deep Strength: Stabilized Base	Option 3 Stabilized Base with Surface Treatment
1.	5% Cement + 15% Fly Ash	941.69	SG 4	> 30	Traffic Category T1 		
					Traffic Category T2 		
3.	5% Cement + 15% Fly Ash	941.69	SG 4	> 30	Traffic Category T3 		
					Traffic Category T4 		
4.	5% Cement + 10% Rubberchip	771.77	SG 4	> 30	Traffic Category T3 		
					Traffic Category T4 		

No	Design Mixture	Stress (kPa)	Sub-grade Category	CBR (%)	Pavement Structure		
					Option 1 Conventional Flexible: Granular Base	Option 2 Deep Strength: Stabilized Base	Option 3 Stabilized Base with Surface Treatment
5.	5% Cement + 15% Fly Ash	941.69	SG 4	> 30	Traffic Category T5 		
6.	5% Cement + 10% Rubberchip	771.77	SG 4	> 30	Option 1 Special Purpose Surface Course Traffic Category T5 (Polymer Modified Asphalt) 	Option 2 Deep Strength High Modulus Base Course 	

GSB - Subbase Course: Crushed or natural granular material with maximum 10% fines

CAB - Road base course: Crushed granular material with maximum 10% fines

STB1 - Road base course: Stabilized base with at least 3% Portland cement

STB2 - Road base course: Stabilized base with bituminous emulsion and maximum of 2% Portland cement

BB - Road base course: Course bituminous mix, AC28

BC - Binder course: Course bituminous mix, AC28

BSC - Wearing Course: Asphaltic Concrete - Medium to fine bituminous mix, AC10 or AC14

PMA - Wearing Course: Polymer Modified Asphalt

SMA - Wearing Course: Stone Mastic Asphalt

PA - Wearing Course: Porous Asphalt

FC - Wearing Course: Gap-Graded Asphalt

8.0 CONCLUSIONS

This study has made a comprehensive examination of the effectiveness combination of cement, fly ash, and rubberchip as one of the options in stabilizing the geotechnical properties of soils encountered in Kota Samarahan, Sarawak. The results of the study provide valuable details on the properties, compaction and strength characteristics of the silty clayey soil as well as those mixed with 5% cement and different percentages of fly ash and rubberchip. The results obtained from the California Bearing Ratio (CBR) and Unconfined Compressive Strength (UCS) tests were thoroughly analyzed. The mixture that presents the best result in stabilizing subgrade and satisfied the requirement with JKR Specification was selected as the design value in the design for pavement. The strength increment was observed for both stabilized soils by the increasing amount of fly ash and rubberchip except for the addition of 15% rubberchip. The similar behaviours were then observed for the cement stabilized soil with fly ash but the addition of the soil-cement mixture with rubberchip above 10% shows a reduction in the strength of the stabilized soil. For durability (water-soaking) tests, both fly ash and rubberchip soil-cement mixtures have lost their strength due to the water soaking procedure. The percentage of reduction for soil-cement mixture with fly ash is 44% while 43% reduction can be seen from the mixture of soil-cement and rubberchip. Although the mixture of cement-fly ash used in this study was performed well with the silty clayey soil, further research on various types and sources of fly ash in treating subgrade soils is needed as the inherent in fly ash composition was basically different depends on the sources of the raw materials. Furthermore, a related research should be conducted in developing an appropriate connections for Unconfined Compressive Strength (UCS) and California Bearing Ratio (CBR) laboratory values for the long-term performance of in-situ stabilized soils with the durability of the treated specimens.

ACKNOWLEDGEMENT

The authors would like to thank the technical staff of Geotechnical Laboratory and lecturers of Faculty of Engineering, Universiti Malaysia Sarawak, and also to Ministry of Higher Education, Malaysia for the sponsorship of the first author.

REFERENCES

- [1] Little, D.N and Scullion, T., (2005), *Guidelines for Modification and Stabilization of Soils and Base for Use in Pavement Structures*. Construction Division, Materials & Pavements Section, Geotechnical, Soils & Aggregates Branch, Texas Department of Transportation (TxDot).
- [2] Little, D.N. and Nair, S., (2009), *Recommended Practice for Stabilization of Subgrade Soils and Base Materials*, Texas Transportation Institute, Texas A&M University College Station, Texas.
- [3] Parker, J.W., (2008), "Evaluation of Laboratory Durability Tests for Stabilized Subgrade Soils", Master Thesis. Brigham Young University, Utah.
- [4] Terrel, R.L., Epps, J.A., Barenberg, E.J., Mitchell, J.K., Thompson, M.R., (1979), "Soil Stabilization in Pavement Structures", *A User's Manual – Vol. 2: Mixture Design Consideration*, FHWA-IP-80-2, Federal Highway Administration, Washington, D.C.
- [5] Veisi, M., Chittoori, B., Celaya, M., Nazarian, S., Puppala, A. J., Solis, C., (2010), "Accelerated Stabilization Design of Subgrade Soils", *Center for Transportation Infrastructure Systems*, University of Texas.
- [6] Production Division, (2008), *Design Procedures for Soil Modification or Stabilization*, Office of Geotechnical Engineering, Indianapolis.
- [7] Patil, B.M. and Patil, K.A., (2013), "Improvement in Properties of Subgrade Soil By Using Pond Ash and Chemical Additive". *Indian Highways Technical Papers*, pp. 35-49.
- [8] Trivedi, J.S., Nair, S., Iyyunni, C., (2013), "Optimum Utilization of Fly Ash for Stabilization of Sub-grade Soil using Genetic Algorithm", *Chemical, Civil and Mechanical Engineering Tracks of 3rd Nirma University International Conference*, pp. 250-258.
- [9] Parsons, R. L. and Kneebone, E., (2005), "Field Performance of Fly Ash Stabilised Subgrade", *Ground Improvement*, No. 1, Department of Civil and Environmental Engineering, University of Kansas, Lawrence, USA , pp. 33–38.
- [10] Mokhtar, M. and Chan, C.M., (2012), "Effect of Using Cement Admixed With Rubberchip on the Undrained Shear Strength of Soft Soil", Master Thesis, Universiti Tun Hussien Onn, Malaysia.
- [11] Chan, C.M., (2012), "Mechanical Properties of Clayey Sand Treated", *CED*, Vol. 14, No. 1, pp. 7–12.
- [12] Robani, R. and Chan, C.M., (2008), "Unconfined Compressive Strength of Clay Stabilized with Cement–Rubberchips", Master Thesis, Universiti Tun Hussien Onn, Malaysia.
- [13] Parsons, R.L., and Milburn, J.P., (2003), "Engineering Behavior of Stabilized Soils", *Transportation Research Record: Journal of the Transportation Research Board*. No. 1837, TRB, National Research Council, Washington, DC, pp. 20-29.
- [14] British Standards Institution (BSI). (1990). BS1377: British Standard Methods of Test for Soils for Civil Engineering Purposes.
- [15] JKR Malaysia, (2008), *Standard Specification for Road Works, Section 4: Flexible Pavements*, Jabatan Kerja Raya, Malaysia.
- [16] Das, B. (1994): *Principles of Geotechnical Engineering*, PWS-Kent Publishing Company, Boston, 3rd Ed.
- [17] JKR Specification for Road Works, (2012), Jabatan Kerja Raya, Malaysia.
- [18] Ho, M.H., Chan, C.M., (2010), "The Potential of Using Rubberchips as a Soft Clay Stabilizer Enhancing Agent", *Modern Applied Science*, Vol. 4, No.10, pp. 122-131.

CHAPTER 12

ANALYSIS OF COMBINED FOOTINGS ON EXTENSIBLE GEOSYNTHETIC- STONE COLUMN IMPROVED GROUND

Priti Maheshwari¹

Abstract

Analysis of combined footings resting on an extensible geosynthetic reinforced granular bed on stone column improved ground has been carried out in the present work. Various components of soil-foundation system have been idealized using lumped parameter modeling approach as: combined footing as finite length beam, granular layer as nonlinear Pasternak shear layer, geosynthetic reinforcement as elastic extensible membrane, stone columns as nonlinear Winkler springs and foundation soil as nonlinear Kelvin body. Hyperbolic constitutive relationships have been adopted to represent the nonlinear behavior of various elements of a soil-foundation system. Finite difference method has been employed to solve developed governing differential equations with the help of appropriate boundary and continuity conditions. A detailed parametric study has been conducted to study the effect of model parameters like applied load, flexural rigidity of footing, configuration of stone columns, ultimate bearing resistance of foundation soil and stone columns, tensile stiffness of geosynthetics and degree of consolidation on response of soil-foundation system by means of deflection and bending moment in the footing and mobilized tension in geosynthetic layer. These parameters have been found to have significant influence on the response of footing and the geosynthetic reinforcement layer. To quantify this, results have been non-dimensionalized to produce design charts for ready use for the analysis of combined footings resting on such a soil-foundation system.

Keywords: Combined footings, extensible geosynthetic layer, stone columns, nonlinearity.

1.0 INTRODUCTION

Currently, various ground improvement measures have been adopted to enhance bearing capacity of foundations and reduce total as well as differential settlements. Use of stone columns and geosynthetics are some of the commonly adopted means for the improvement of earth beds. Various experimental, analytical and numerical studies have been conducted to study the response of such soil-foundation systems. Modeling of geosynthetics is done as an elastic membrane or as a beam possessing finite flexural rigidity. For geosynthetic reinforcement layers modelled as a membrane, if the modulus of elasticity of the reinforcement layer is very large in comparison to that of the soil, the reinforcement layer is treated to be inextensible. For such type of reinforcement, the compatibility of displacements requires that the displacements of the points in the soil along the interface are zero. For extensible reinforcement, the ratio of moduli of elasticity of reinforcement and the soil is moderate. Compatibility of deformations requires that displacements of reinforcement and the soil along the interface should be the same, i.e., no slip condition.

Some of the studies pertaining to analysis of stone columns that have dealt with soft soil foundation systems include Balaam and Booker [1], Alamgir et al. [2], Shahu et al. [3] etc. Analyses in which the ground was treated with the geosynthetic as a measure of ground improvement find mention in Madhav and Poorooshasb [4], Ghosh and Madhav [5], Shukla and Chandra [6], Yin [7], Maheshwari et al. [8] etc. A close look on these studies suggests that soft soil was either reinforced with stone columns or with geosynthetic layers. However, Deb et al. [9, 10] combined both the measures of ground improvement and presented simple models for analysis of geosynthetic – reinforced granular fill – soft soil with stone column systems by considering the inextensible and extensible nature of the geosynthetic layer respectively. However, the foundation was not modelled in the analysis. Only the load coming from the foundation was taken into account directly on the treated ground. To remove this limitation, Maheshwari and Khatri [11] modelled the combined footing as a beam resting on a geosynthetic – reinforced granular fill – stone column improved soft soil system.

¹Department of Civil Engineering, Indian Institute of Technology Roorkee, Roorkee 247667, India.

The geosynthetic layer was assumed to behave as an inextensible rough elastic membrane. Zhou et al. [12] proposed an analytical model for the analysis of geosynthetic reinforced embankment. Embankment fill was modeled as a Timoshenko beam imbedded with a geosynthetic layer and the pavement was idealized as an Euler-Bernoulli beam. Rajesh et al. [13] developed a foundation model for predicting the behavior of a geosynthetic reinforcement railway track system resting on soft clay subgrade. The geosynthetic layer was represented by a stretched rough elastic membrane. Burger model was used to characterize the soft clay subgrade. Zhao et al. [14] proposed a dual beam model for a geosynthetic-reinforced granular fill with an upper pavement. The upper pavement was modeled by an Euler–Bernoulli beam while the geosynthetic reinforced granular fill was simulated by a reinforced Timoshenko beam.

A critical review of literature suggests the absence of any study pertaining to settlement analysis of shallow foundations possessing finite flexural rigidity on extensible geosynthetic reinforced – granular fill – soft soil with stone columns system. A simple mechanical model has therefore been proposed in the present work for such an analysis. The governing differential equations have been derived considering free body diagrams of various components of a soil-foundation system. Further, these have been solved with appropriate boundary and compatibility conditions employing finite difference method.

2.0 ANALYSIS

2.1 Development of mathematical model

A combined footing subjected to column loads (Q_1 , Q_2 and Q_3) has been considered for the analysis. As shown in Fig. 1, the footing is resting on a geosynthetic reinforced granular layer. This layer is lying on soft foundation soil treated with stone columns. Length of footing has been considered as $2B$ while the extent of geosynthetic is up to $2L$. Diameter and spacing of stone columns has been represented as d and s respectively. Geosynthetic layer has been placed in between the granular layer with thicknesses and shear moduli as H_t , H_b and G_t , G_b respectively. As the geosynthetic has been assumed to be extensible in nature, its tensile stiffness is represented by E_g . This soil-foundation system has been modeled employing lumped parameter modeling and presented in Fig. 2. The footing has been modeled as a beam, the granular layer as a nonlinear Pasternak shear layer, the geosynthetic as a linear, rough, elastic, extensible membrane, the soft foundation soil as a nonlinear Kelvin body and the stone columns as nonlinear Winkler springs. The nonlinear nature has been modeled with the help of Kondner’s hyperbolic constitutive relationship.

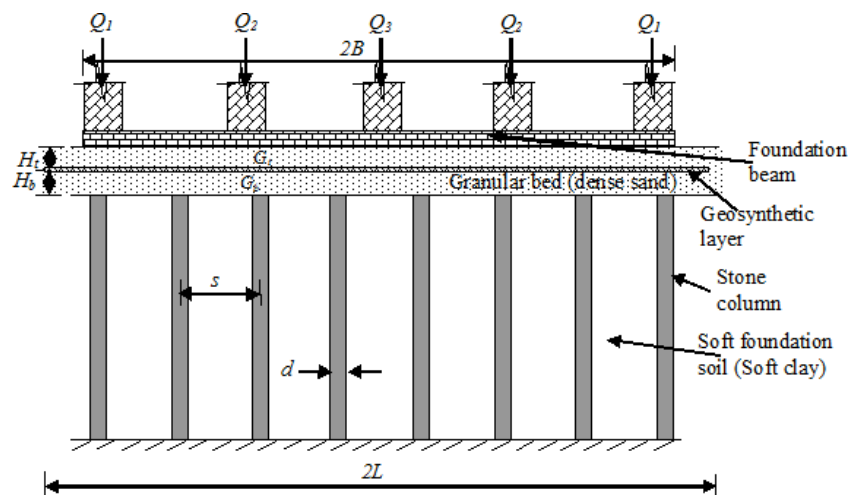


Figure 1 Definition sketch of the problem

Considering the equilibrium of free bodies of various components of the soil-foundation system and imposing the deformation compatibility conditions, the governing differential equations of the foundation

model can be expressed as [7] –

$$q = q_s - T \cos^3 \theta \frac{d^2 w}{dx^2} - \sin \theta \frac{dT}{dx} - (H_t G_t^1 + H_b G_b^1) \frac{d^2 w}{dx^2} \quad (1)$$

$$\begin{aligned} \frac{d^2 T}{dx^2} = & \sin \theta \cos \theta \frac{d^2 w}{dx^2} \frac{dT}{dx} + \frac{1}{\cos \theta} \left(\frac{G_t^o}{H_t} + \frac{G_b^o}{H_b} \right) \left[\sqrt{\left(\frac{T}{E_g} + 1 \right)^2 - \left(\frac{dw}{dx} \right)^2} - 1 \right] \\ & + \frac{H_b}{H_t} \left(\frac{G_t^o}{\tau_{ub}} - \frac{G_b^o}{\tau_{ut}} \frac{G_{to}}{G_{bo}} \frac{G_t^1}{G_b^1} \right) \frac{G_b^o H_t}{(G_t^o H_b + G_b^o H_t)} \frac{d^2 w}{dx^2} \frac{dT}{dx} \end{aligned} \quad (2)$$

where, q is the reaction of the soil on beam; q_s , the vertical reaction pressure of soft soil/stone column; T , the mobilised tension in geosynthetic layer; θ , the slope of geosynthetic layer element [7]; w , the vertical displacement of beam; dx , the projected element length in x direction; E_g , the tensile stiffness (N/m) of geosynthetic layer; G_{to} and G_{bo} , the initial shear modulus of top and bottom shear layers respectively; τ_{ut} and τ_{ub} , the ultimate shear resistance of the top and bottom shear layers respectively. G_t^o , G_b^o , G_t^1 , and G_b^1 are defined as follows:

$$G_t^o = \frac{G_{to}}{1 + \frac{G_{to}}{\tau_{ut}} \left| \frac{dw}{dx} \right|}; \quad G_b^o = \frac{G_{bo}}{1 + \frac{G_{bo}}{\tau_{ub}} \left| \frac{dw}{dx} \right|} \quad \text{and}$$

$$G_t^1 = \frac{G_{to}}{\left[1 + \frac{G_{to}}{\tau_{ut}} \left| \frac{dw}{dx} \right| \right]^2}; \quad G_b^1 = \frac{G_{bo}}{\left[1 + \frac{G_{bo}}{\tau_{ub}} \left| \frac{dw}{dx} \right| \right]^2}$$

The vertical reaction pressure, q_s can be written as [11]-

$$q_s = \frac{k_{so} w}{U [1 + k_{so} (w/q_u)]}, \quad \text{within the soft soil region} \quad (3a)$$

$$\text{and } q_s = \frac{k_{co} w}{1 + k_{co} (w/q_{cu})}, \quad \text{within the stone column region} \quad (3b)$$

where, k_{so} and k_{co} are the initial modulus of subgrade reaction for saturated soft soil and the stone columns respectively; q_u and q_{cu} , the ultimate bearing resistance of soft soil and the stone columns respectively and U , the average degree of consolidation at any time $t > 0$.

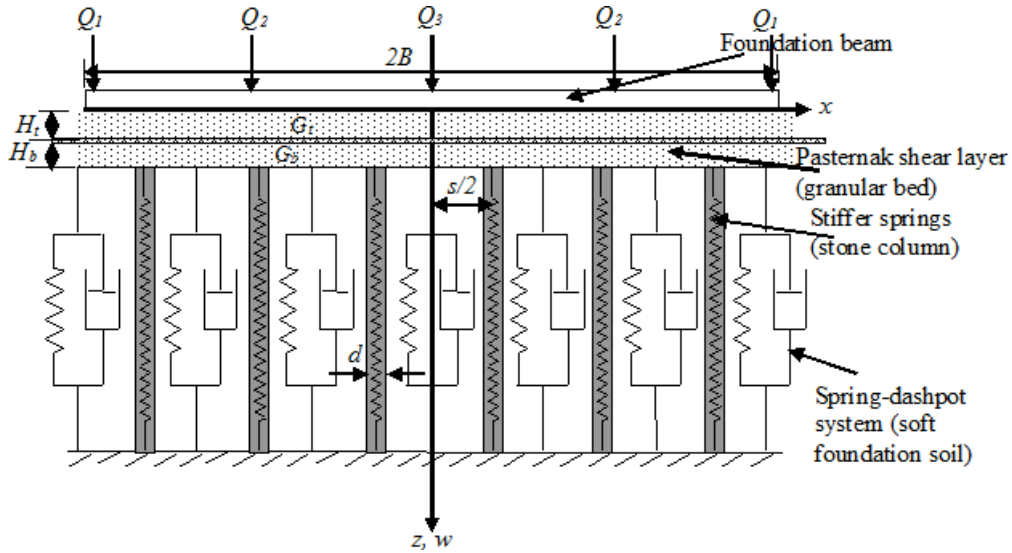


Figure 2 Idealization of proposed problem

Considering the bending of beam subjected to external load intensity, p , the governing equation can be written as:

$$EI \frac{d^4 w}{dx^4} + q = p \quad (4)$$

Combining the above equations yields the governing differential equations of the soil-foundation system below the footing.

2.2 Non-dimensionalization of proposed model

The governing differential equations have been nondimensionalized using the following parameters:

$$X=x/B, W=w/B, H_t^* = H_t/B, H_b^* = H_b/B, E_g^* = E_g / k_{so} B^2, q^* = q / k_{so} B, p^* = p / k_{so} B, q_u^* = q_u / k_{so} B, q_{cu}^* = q_{cu} / k_{co} B = q_{cu} / \alpha k_{so} B, \tau_{ut}^* = \tau_{ut} H_t / k_{so} B^2, \tau_{ub}^* = \tau_{ub} H_b / k_{so} B^2, T^* = T / k_{so} B^2, I^* = E I / k_{so} B^4, G_{to}^* = G_{to} H_t / k_{so} B^2, G_{bo}^* = G_{bo} H_b / k_{so} B^2, Q_1^* = Q_2^* = Q_3^* = Q^* = Q / k_{so} B^2 \text{ and } \alpha = k_{co} / k_{so}.$$

The equations below the footing have been written in nondimensional form as follows:

$$q^* = \frac{W}{U[1+(W/q_u^*)]} - T^* \cos^3 \theta \frac{d^2 W}{dX^2} - \sin \theta \frac{dT^*}{dX} - (G_t^{1*} + G_b^{1*}) \frac{d^2 W}{dX^2}, \text{ within soft soil region (5a)}$$

$$q^* = \left[\frac{\alpha W}{1+(W/q_{cu}^*)} \right] - T^* \cos^3 \theta \frac{d^2 W}{dX^2} - \sin \theta \frac{dT^*}{dX} - (G_t^{1*} + G_b^{1*}) \frac{d^2 W}{dX^2}, \text{ within stone column region (5b)}$$

$$\begin{aligned} \frac{d^2 T^*}{dX^2} = & \sin \theta \cos \theta \frac{d^2 W}{dX^2} \frac{dT^*}{dX} + \frac{1}{\cos \theta} \left(\frac{G_t^{o*}}{H_t^{*2}} + \frac{G_b^{o*}}{H_b^{*2}} \right) \left[\sqrt{\left(\frac{T^*}{E_g^*} + 1 \right)^2 - \left(\frac{dW}{dX} \right)^2} - 1 \right] \\ & + \frac{H_b^*}{H_t^*} \left(\frac{G_t^{o*}}{\tau_{ub}^*} - \frac{G_b^{o*}}{\tau_{ut}^*} \frac{G_{to}^*}{G_{bo}^*} \frac{G_t^{1*}}{G_b^{1*}} \right) \left(\frac{G_b^{o*}}{G_t^{o*} \frac{H_b^*}{H_t^*} + G_b^{o*} \frac{H_t^*}{H_b^*}} \right) \frac{d^2 W}{dX^2} \frac{dT^*}{dX} \end{aligned} \quad (6)$$

and

$$\frac{d^4 W}{dX^4} + \frac{q^*}{I^*} - \frac{p^*}{I^*} = 0 \quad (7)$$

2.3 Boundary conditions

Due to symmetry, half of the spatial domain has been considered in the analysis. The boundary conditions have been written as follows:

$$\text{At } x = 0, \frac{dw}{dx} = 0 ; -EI \frac{d^3w}{dx^3} = \frac{Q}{2} \text{ and } \frac{dT}{dx} = 0 \quad (8)$$

$$\text{At } x = B, \frac{d^2w}{dx^2} = 0 ; -EI \frac{d^3w}{dx^3} = -Q - (T \cos^3 \theta + G'_i H_i + G'_b H_b) \frac{dw}{dx} - T \sin \theta \quad (9)$$

$$\text{At } x = L, \frac{dw}{dx} = 0 \text{ and } T = 0 \quad (10)$$

2.4 Solution methodology and convergence criterion

A finite difference scheme has been adopted to obtain the solution of the soil-foundation system. The governing differential equations along with boundary conditions have been written in finite difference form and solution has been obtained by Gauss Siedel iterative scheme. The solution has been obtained with convergence criteria as

$$\left| \frac{W_i^k - W_i^{k-1}}{W_i^k} \right| < \varepsilon \text{ and } \left| \frac{T_i^{*k} - T_i^{*k-1}}{T_i^{*k}} \right| < \varepsilon$$

for all nodes i , where k and $k-1$ are the present and previous iterations respectively and ε is the specified tolerance which has been considered to be 10^{-8} in the present study.

3.0 RESULTS AND DISCUSSION

The above formulation has been programmed in C language and solution obtained by a finite difference scheme. Due to symmetry, only half of the spatial domain has been considered. It was observed that results corresponding to finite difference mesh with 401 and 501 nodes vary negligibly. In view of this, the whole spatial domain was discretized with 401 nodes for all parametric studies. After obtaining the deflection of the footing, bending moment and shear force have been obtained by taking appropriate derivative of the deflection.

3.1 Validation

Before the conduct of the detailed parametric study, the proposed mathematical model and developed computer program has been validated by comparing the results to those from Deb et al. [10]. A parameter, α was considered and defined as

$$\alpha = \frac{(1 + \nu_s)(1 - 2\nu_s) E_c}{(1 + \nu_c)(1 - 2\nu_c) E_s} = \frac{k_{co}}{k_{so}} \quad (11)$$

where (E_s, ν_s) and (E_c, ν_c) are elastic properties with respect to soil and the stone columns respectively. For the validation purpose, the input parameters have been considered as $\nu_s = \nu_c = 0.3$, $G_{to}^* = G_{bo}^* = 0.1$, $H_t^* = H_b^* = 0.25$, $q^* = 0.8$, $q_u^* = 10$, $E_g^* = 20$, $\tau_u^* = 10$, $U = 100\%$. Results from the present study for these parameters have been presented along with the results from Deb et al. [10] in Fig. 3. Perfect match between these results can be observed from Fig. 3 which validated the proposed model. RING

3.2 Range of values of input parameters

The range of values of input parameters considered in the present study has been mentioned in Table 1 in dimensional form [7, 15, 16, 17, 18]. These have been non-dimensionalized employing the above-mentioned parameters and used in the parametric study.

3.3 Influence of applied loads

The variation of deflection of combined footing along its length has been depicted in Fig. 4 for five different load levels. Further, the comparison has been made with inextensible geosynthetic reinforcement [11]. The input parameters have been considered as $I^* = 1.5 \times 10^{-4}$, $G_{to}^* = G_{bo}^* = 9.8 \times 10^{-5}$, $d/B = 0.05$, $s/d = 2.5$, $q_u^* = 4 \times 10^{-4}$, $q_{cu}^* = 1.5 \times 10^{-4}$, $\tau_{ut}^* = \tau_{ub}^* = 1.05 \times 10^{-6}$, $\alpha = 10$, $U = 90\%$. The deflection has not been found to be influenced by type of geosynthetics significantly. However, at higher load levels some marginal effect has been observed. The normalized maximum deflection has been found to reduce by 92% as the normalized load reduces from 2.25×10^{-4} to 1.0×10^{-4} .

The tension mobilized in the geosynthetic layer has been found to be significantly affected by type of geosynthetics (Fig. 5). In the case of extensible geosynthetics, the order of mobilized tension is much less than in the case of inextensible geosynthetic layer. The reduction in normalized tension mobilized in geosynthetics has been found to be about 97% for the corresponding reduction in normalized applied load from 2.25×10^{-4} to 1.0×10^{-4} . The variation of normalized bending moment in the combined footing along the length of footing has been presented in Fig. 6 for various load levels.

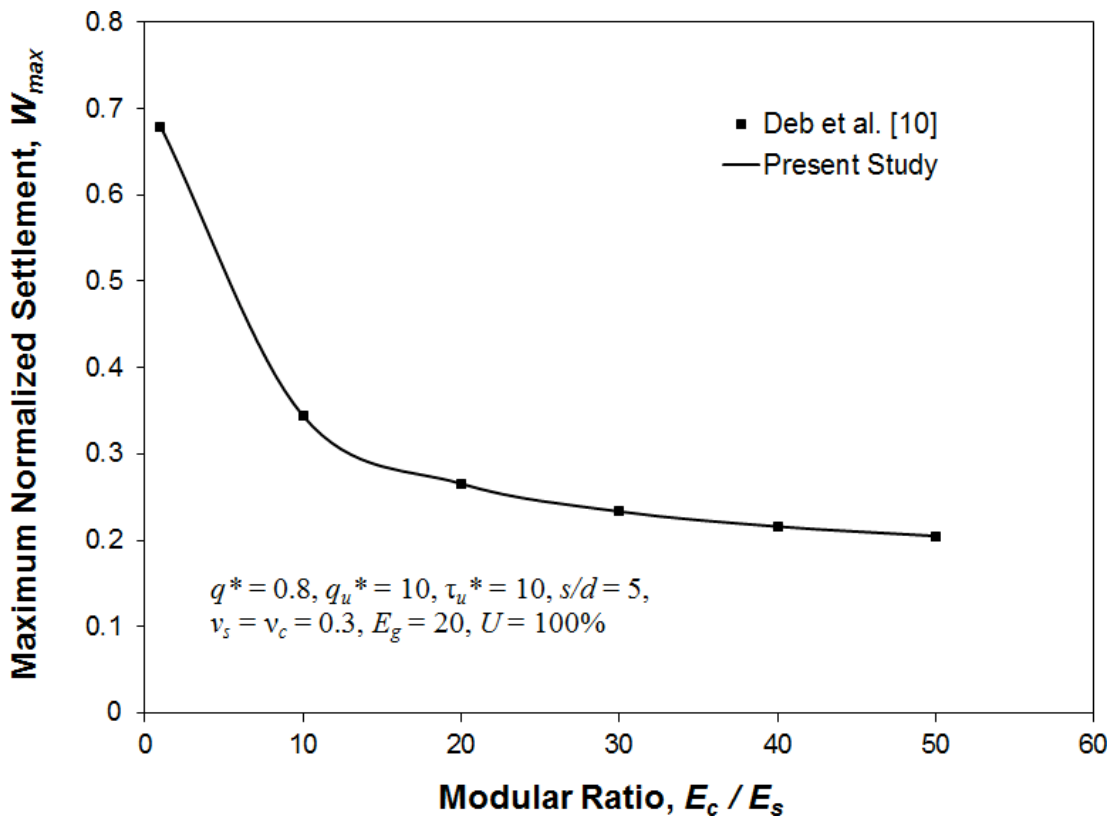


Figure 3 Maximum normalized settlement: validation

3.4 Influence of flexural rigidity of footing

To study the influence of flexural rigidity, EI of the footing, the values of input parameters have been taken as $Q^* = 2.0 \times 10^{-4}$, $G_{to}^* = G_{bo}^* = 9.8 \times 10^{-5}$, $d/B = 0.05$, $s/d = 2.5$, $q_u^* = 4 \times 10^{-4}$, $q_{cu}^* = 6 \times 10^{-5}$, $E_g^* = 0.025$, $\tau_{ut}^* = \tau_{ub}^* = 1.05 \times 10^{-6}$, $\alpha = 25$, $U = 90\%$. Figures 7 and 8 show the influence of flexural rigidity on deflection of the footing and mobilized tension in geosynthetics respectively. The maximum

normalized deflection has been found to reduce by 88% as the normalized flexural rigidity increases from 1.5×10^{-4} to 2.0×10^{-3} and the corresponding reduction in tension mobilized in geosynthetic has been found to be 96%. As the flexural rigidity of the footing increases, the footing exhibits resistance to deformation and bending and therefore the deflection of footing and tension mobilized in geosynthetic is lesser and more uniform.

Table 1 Range of values of input parameters considered for parametric study

Parameter	Symbol (unit)	Range of values
Applied load	Q (kN)	100 – 300
Flexural rigidity of footing	EI (MN-m ²)	15 – 200
Half-length of footing	B (m)	10.0
Thickness of granular fill layer	H (m)	0.3
Diameter of stone columns	d (m)	0.2 – 0.4
Spacing to diameter ratio for stone columns	s/d	2.5 – 4 [15]
Initial modulus of subgrade reaction for soft foundation soil	k_{so} (MN/m ² /m)	10 [16, 17]
Initial shear modulus of granular fill	G_o (kN/m ²)	652.4 [18]
Ultimate bearing resistance of soft foundation soil	q_u (kN/m ²)	20 – 60
Ultimate bearing resistance of stone column	q_{cu} (kN/m ²)	100 – 200
Ultimate shear resistance of granular fill layer	τ_u (kN/m ²)	4 – 10
Tensile stiffness of geosynthetics	E_g (MN/m ²) [7]	15 – 35
Relative stiffness of stone column	α	10 – 100
Average degree of consolidation	U	40 – 100%

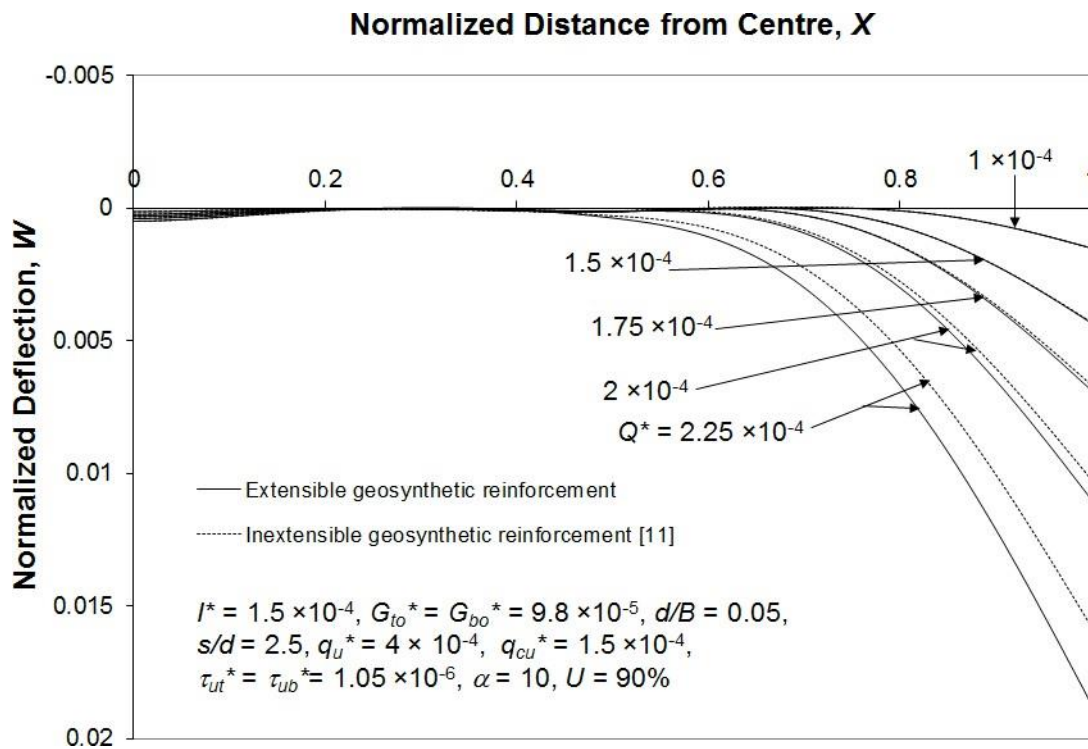


Figure 4 Variation of normalized deflection of combined footing: effect of applied load.

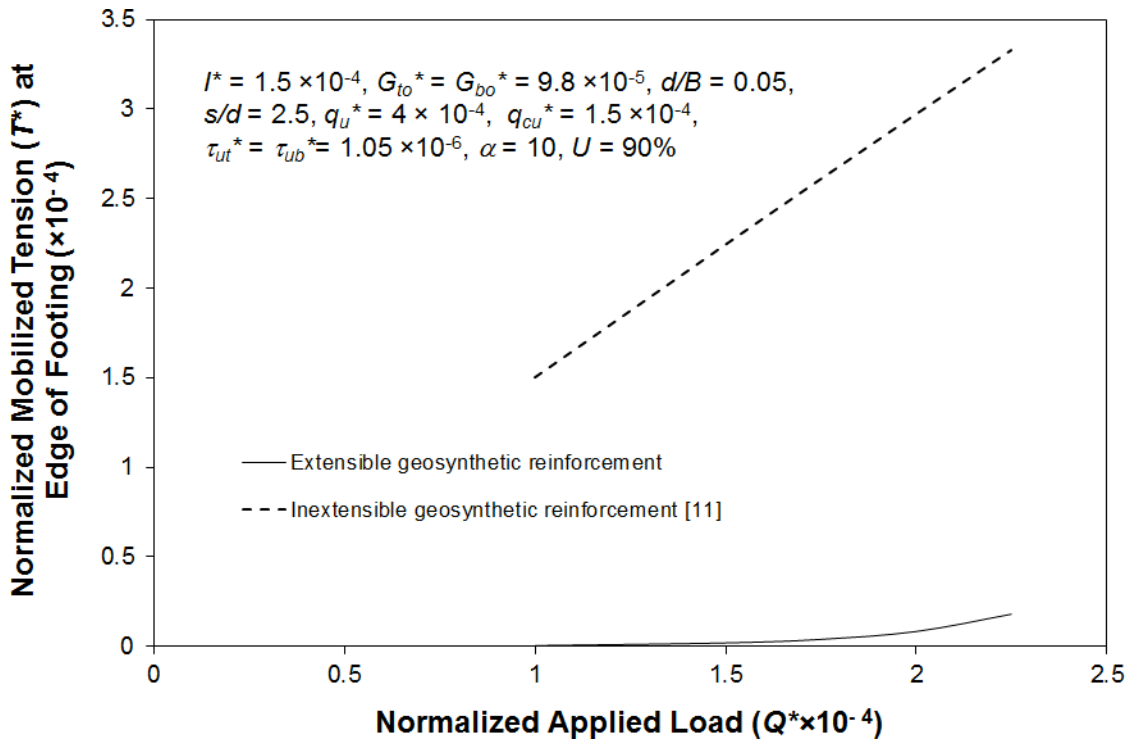


Figure 5 Variation of maximum normalized tension mobilized in geosynthetic: effect of applied load

3.5 Influence of configuration of stone columns

This section presents the influence of diameter and spacing of the stone columns on response of the soil-footing system for the input parameters. The normalized diameter of stone columns (d/B) has been varied from 0.02 to 0.1 while the variation in spacing to diameter ratio (s/d) has been considered as 2 – 4. Figures 9 and 10 exhibit the influence of normalized diameter on deflection of the footing and tension mobilized in the geosynthetic layer respectively. About 37% increase in maximum normalized deflection and 64% increase in mobilized tension has been observed as normalized diameter increases from 0.02 to 0.1. For lesser value of parameter d/B , more number of stone columns exist below the footing and therefore the deflection and mobilized tension is less.

Figure 11 depicts the effect of s/d on deflection of the footing for the input parameters as mentioned in the figure. There will be a lesser number of stone columns beneath the footings for higher values of the parameter s/d and therefore larger deflection has been observed for higher values of spacing to diameter ratio of stone columns. An optimum value of s/d can be observed as 2.5 – 3. Typical bending moment variation along the length of footing has been presented in Fig. 12 for different values of parameter s/d .

3.6 Influence of tensile stiffness of geosynthetic layer

Tensile stiffness of the geosynthetic layer has no influence on response of the footing. However, it significantly affects the tension mobilized in the geosynthetic layer. The variation of maximum normalized mobilized tension with normalized tensile stiffness of geosynthetic has been presented in Fig. 13. As expected, a reduction of about 34% is observed corresponding to the reduction in parameter E_g^* from 0.035 to 0.015.

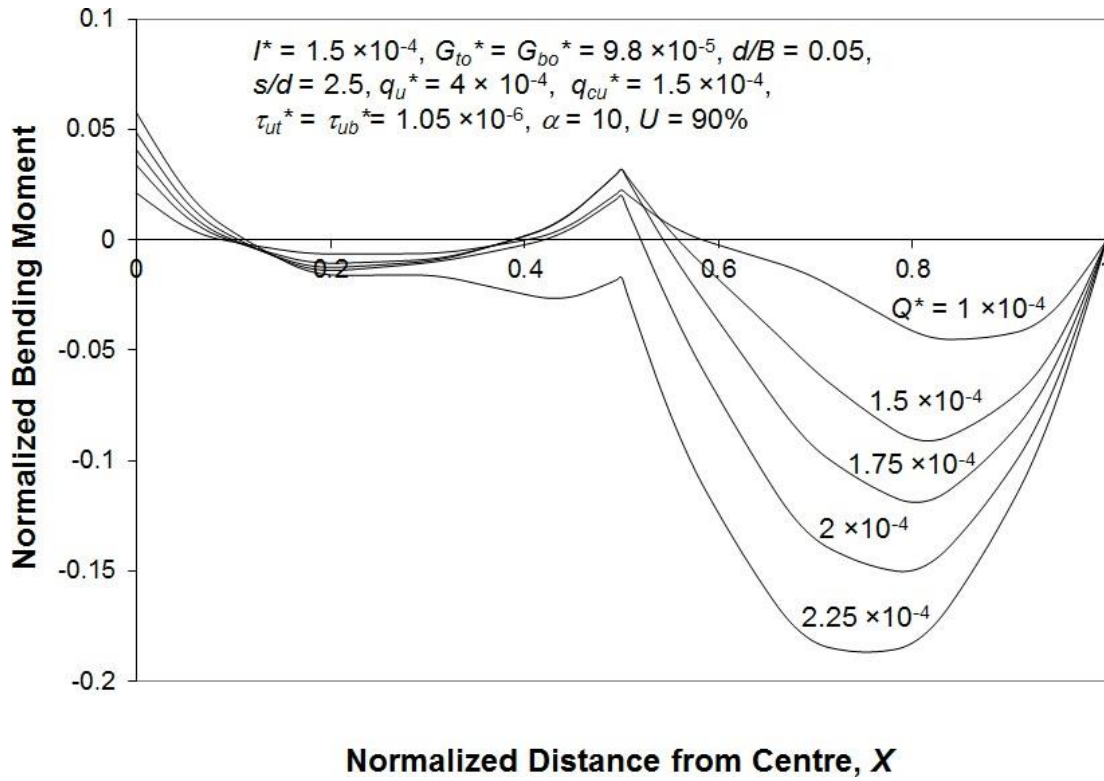


Figure 6 Variation of normalized bending moment in combined footing: effect of applied load

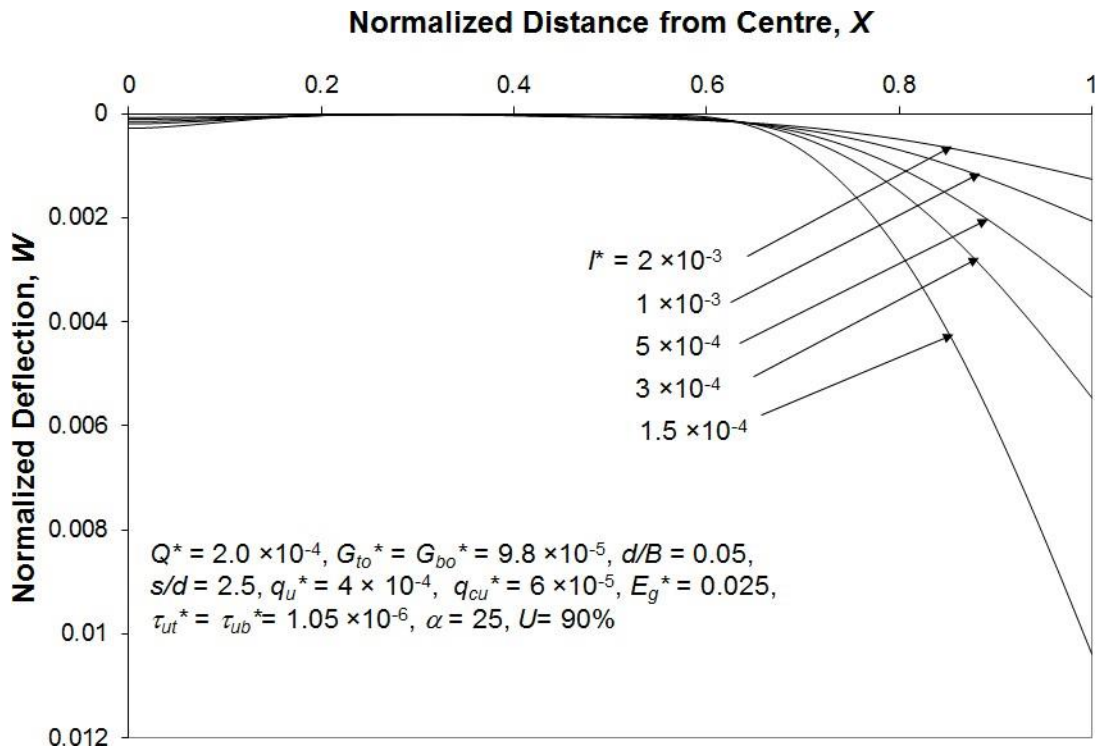


Figure 7 Variation of normalized deflection of combined footing: effect of flexural rigidity

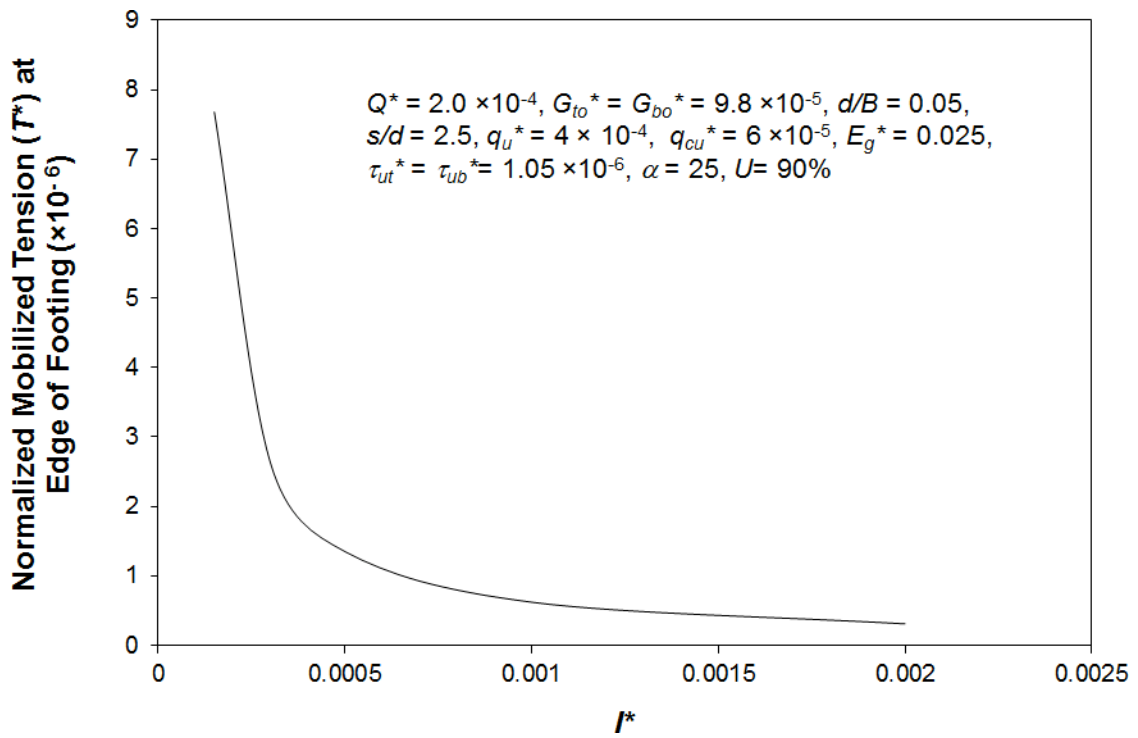


Figure 8 Variation of maximum normalized tension mobilized in geosynthetic: effect of flexural rigidity

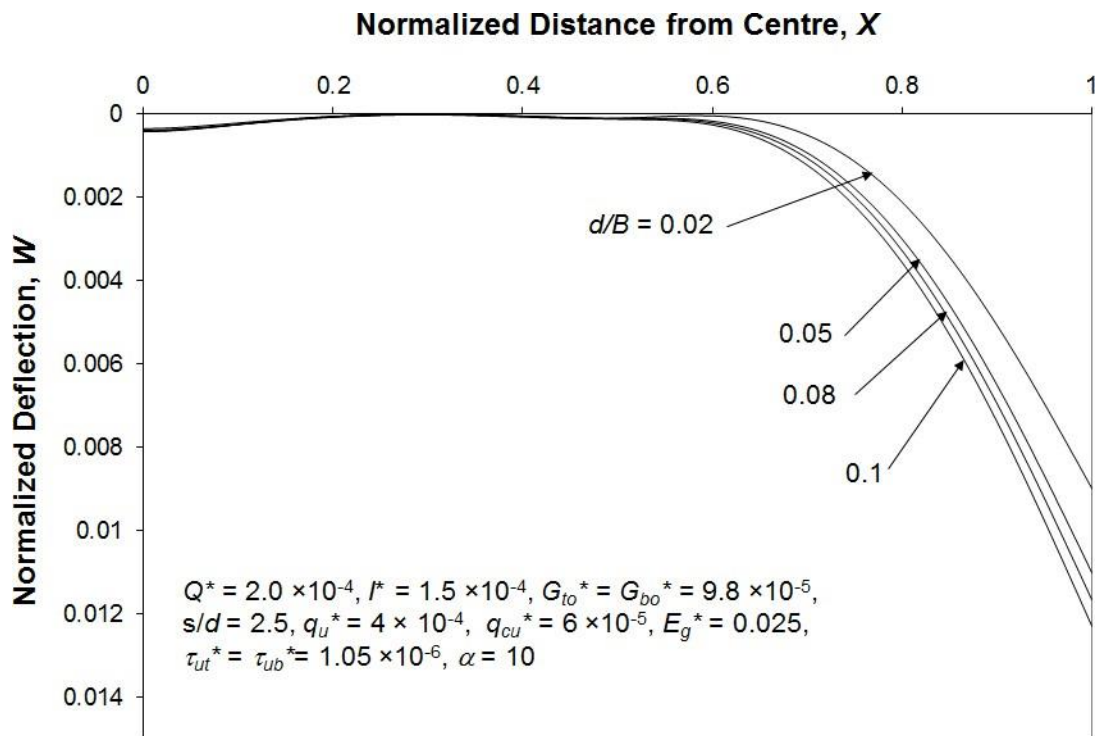


Figure 9 Variation of normalized deflection of combined footing: effect of parameter, d/B .

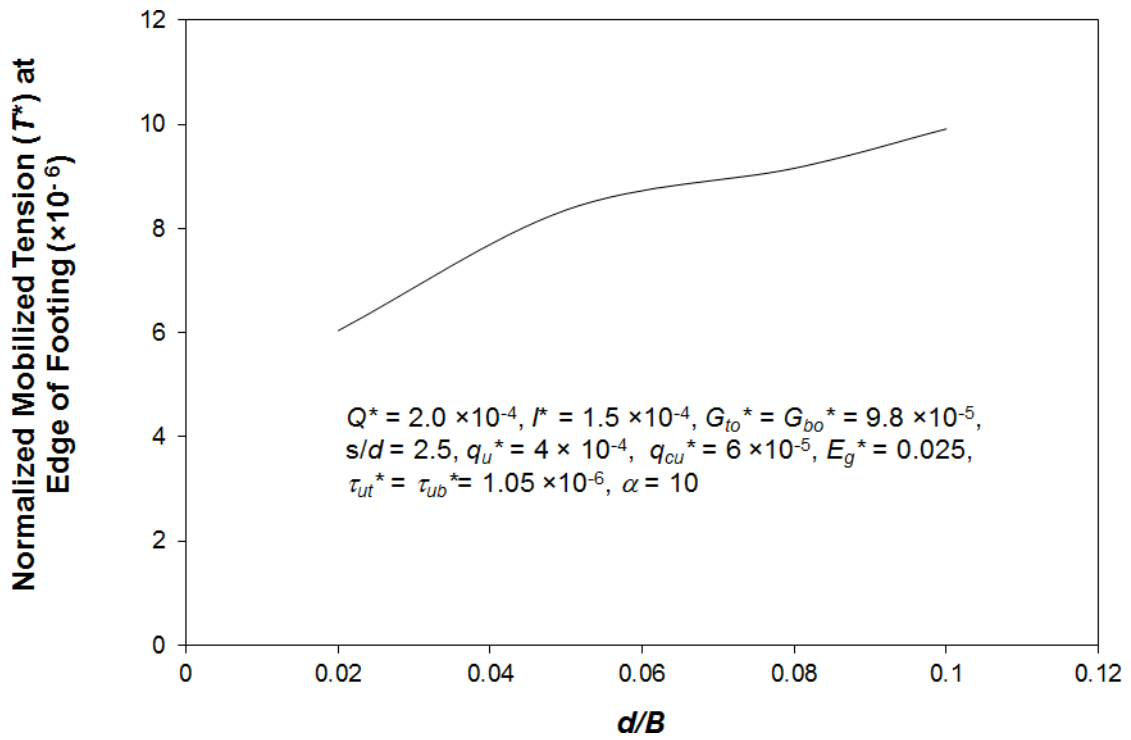


Figure 10 Variation of maximum normalized tension mobilized in geosynthetic: effect of parameter, d/B

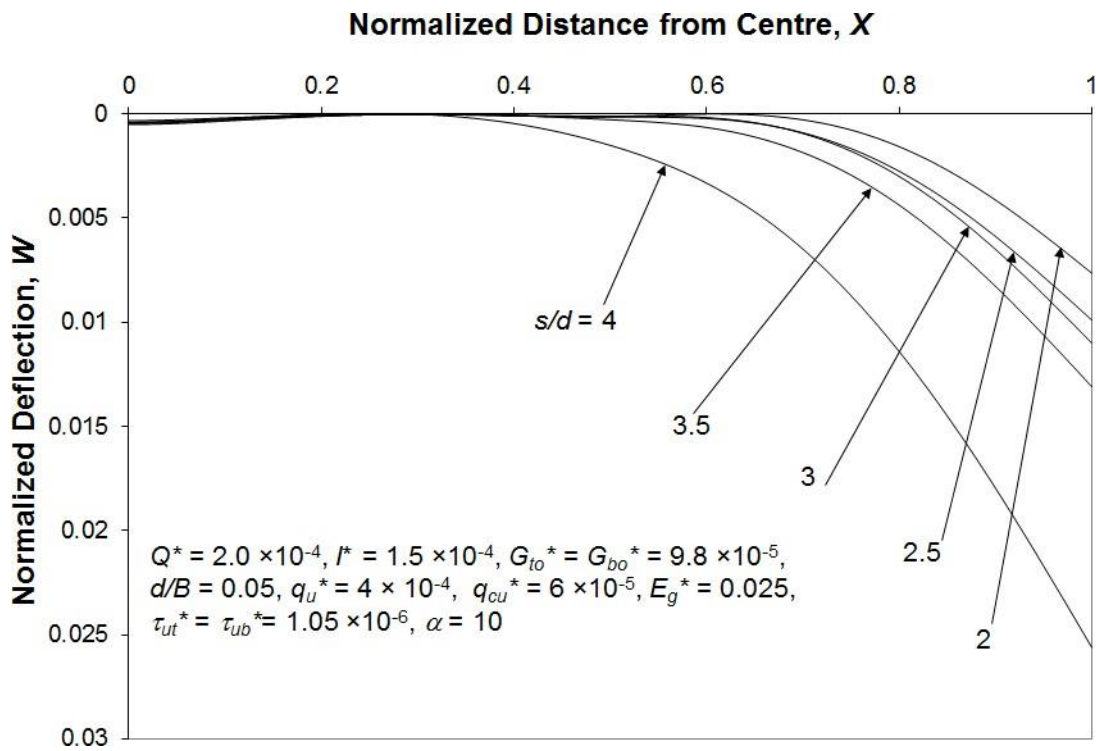


Figure 11 Variation of normalized deflection of combined footing: effect of parameter, s/d

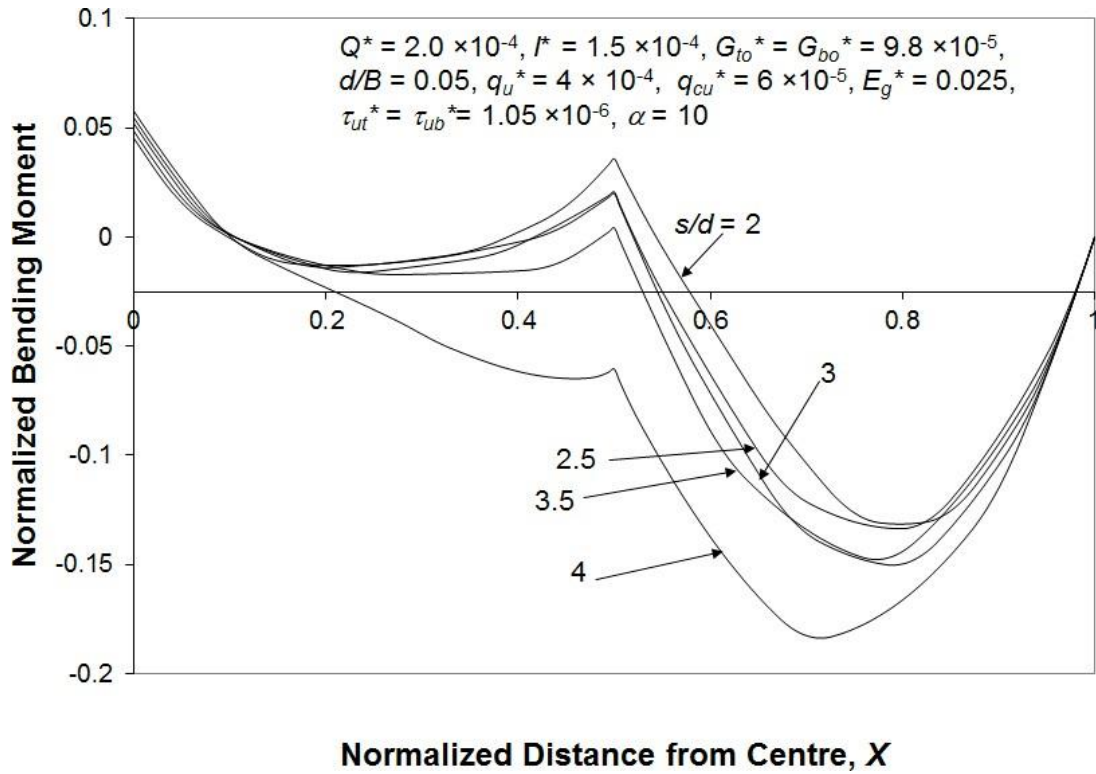


Figure 12 Variation of normalized bending moment in combined footing: effect of parameter, s/d

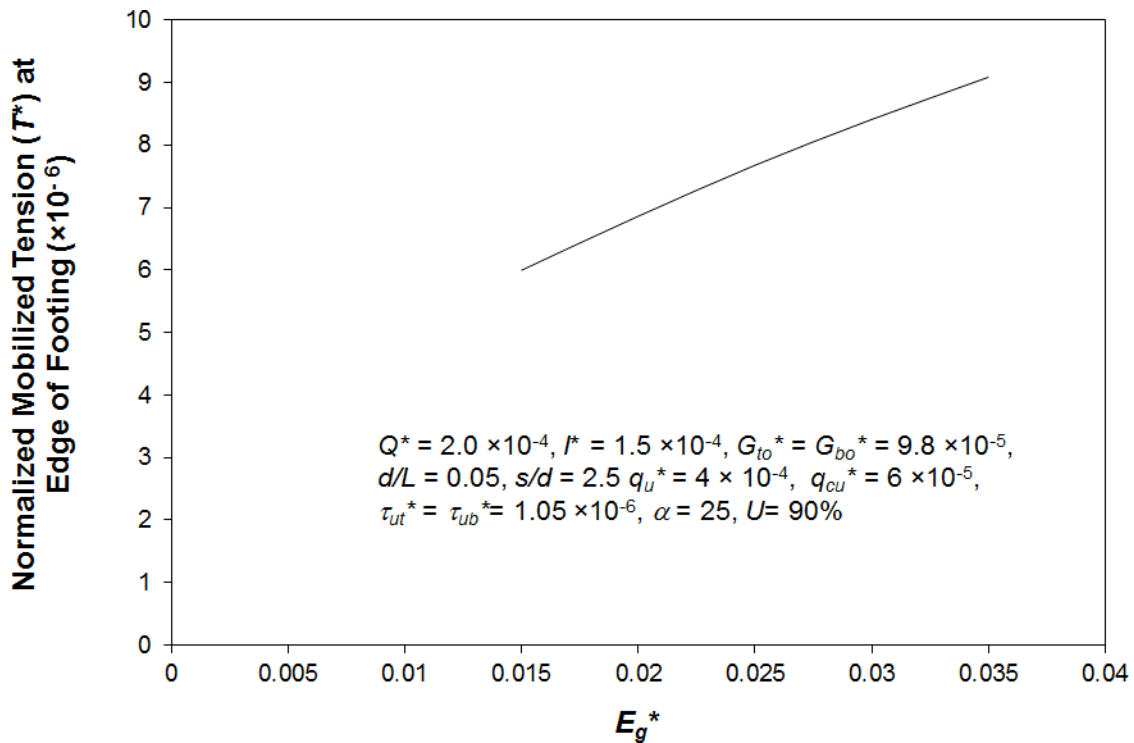


Figure 13 Variation of maximum normalized tension mobilized in geosynthetic: effect of tensile stiffness of geosynthetic

3.7 Influence of ultimate bearing resistance of foundation soil (q_u^*) and stone columns (q_{cu}^*)

An increase in deflection of the footing is expected due to reduction in the parameters q_u^* and q_{cu}^* . The same has been observed during the analysis and has been presented in Figs. 14 and 15. A reduction of about 54% and 62% has been observed in maximum normalized deflection of the footing corresponding to a respective reduction in q_u^* from 6×10^{-4} to 2×10^{-4} and in q_{cu}^* from 8×10^{-5} to 5×10^{-5} . The tension mobilized in geosynthetic layer has also been significantly affected by any variation in these two

parameters, q_u^* and q_{cu}^* .

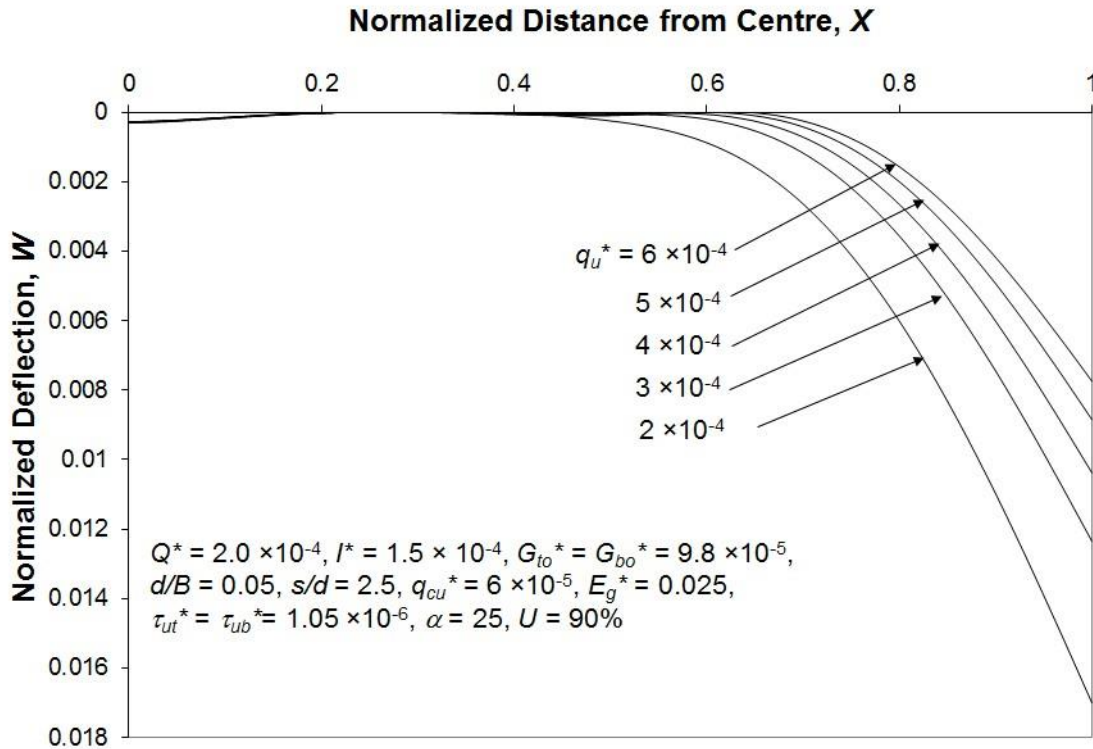


Figure 14 Variation of normalized deflection of combined footing: effect of ultimate bearing resistance of foundation soil (q_u^*)

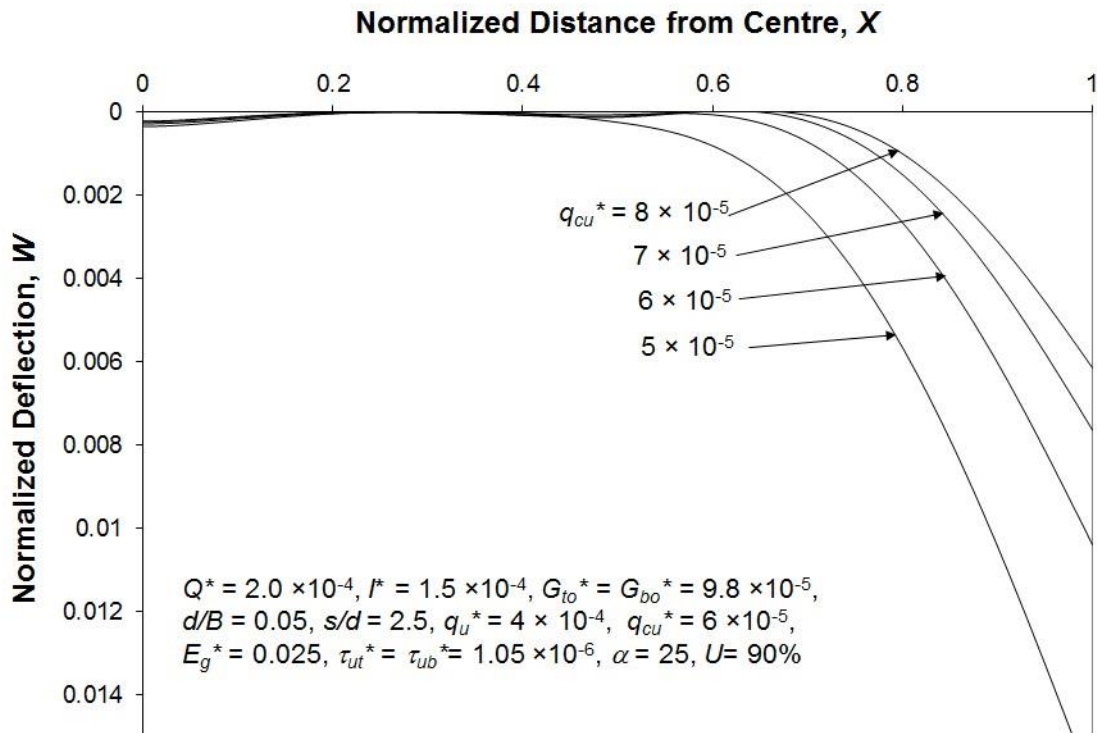


Figure 15 Variation of normalized deflection of combined footing: effect of ultimate bearing resistance of stone columns (q_{cu}^*)

3.8 Influence of degree of consolidation (U)

It is well known that deflection increases with increase in degree of consolidation. This effect has been quantified with respect to the present soil-footing system. It can be observed from Fig. 16 that for the values of input parameters considered in the analysis, the maximum deflection increases by about 114%

as degree of consolidation increases from 40% to 100%. The corresponding sharp increase of 248% has been observed in maximum normalized tension mobilized in the geosynthetic layer and this variation has been depicted in Fig. 17.

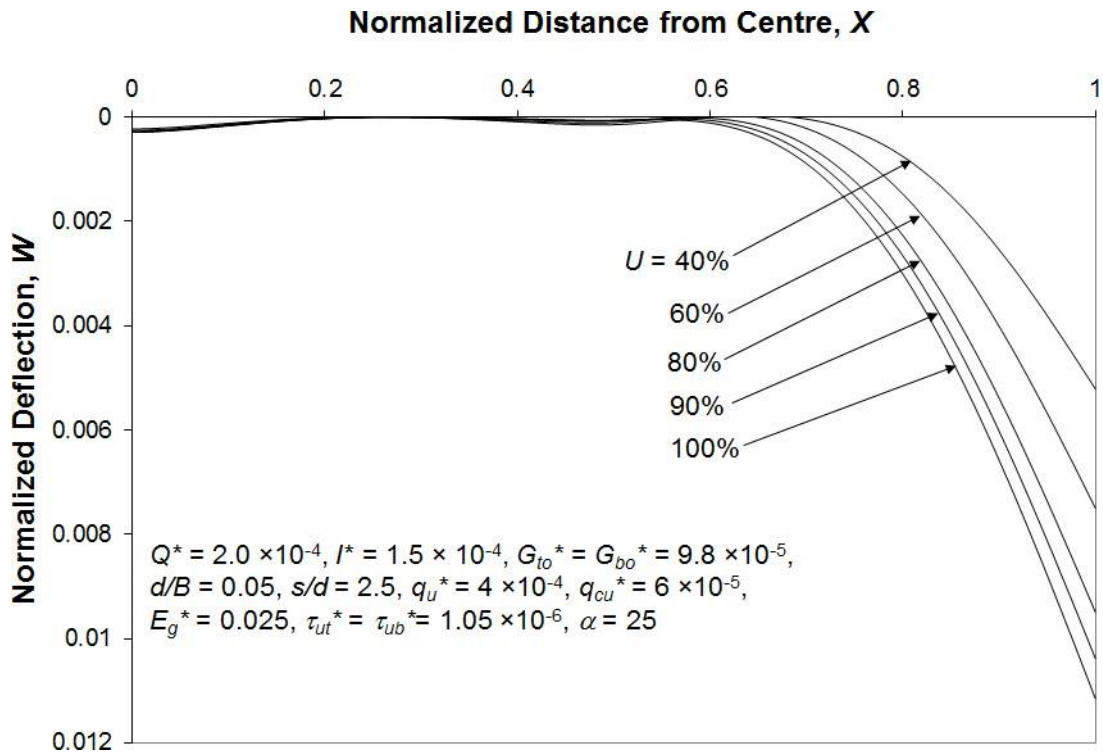


Figure 16 Variation of normalized deflection of combined footing: effect of degree of consolidation (U)

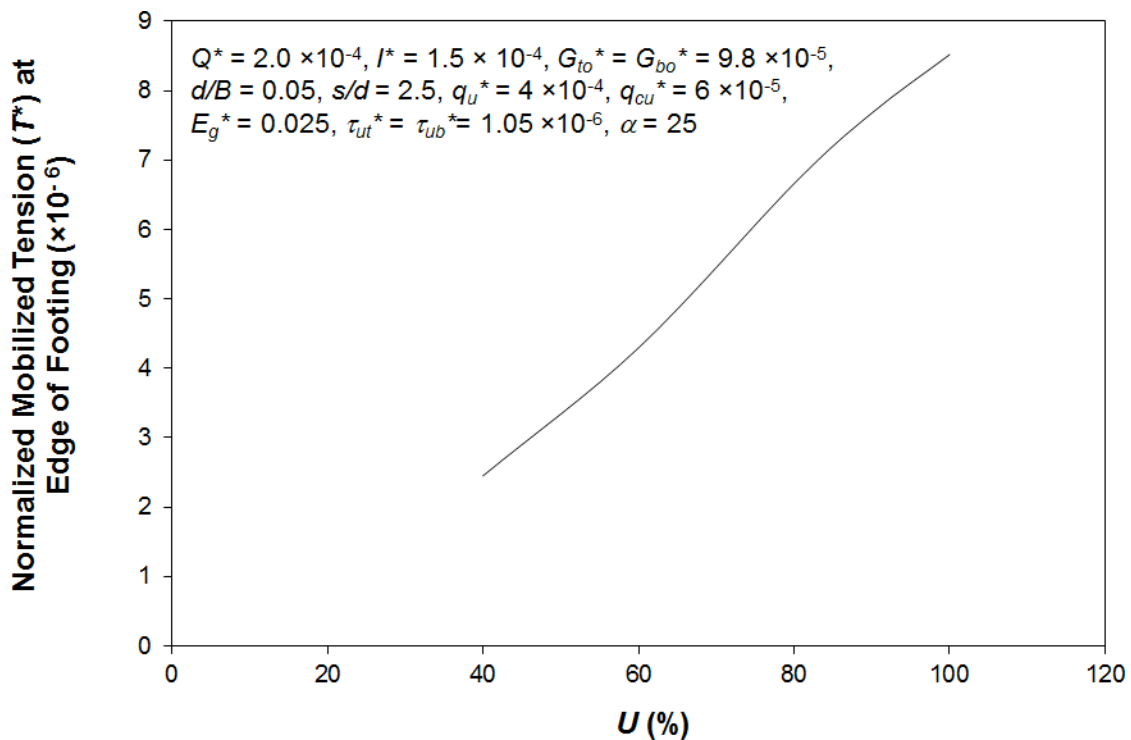


Figure 17 Variation of maximum normalized tension mobilized in geosynthetic: effect of degree of consolidation (U)

4.0 CONCLUDING REMARKS

The proposed model represented the behavior of combined footings resting on extensible geosynthetic-stone column reinforced earth beds. Nonlinear behavior of foundation soil, granular fill on top of

geosynthetic layer and stone columns have successfully been incorporated in the analysis. Results from the present study were found to be in good agreement with those existing in literature. The response of combined footing was found to be almost independent of type of geosynthetic (whether extensible or inextensible). However, response of geosynthetic in terms of tension mobilized was found to be significantly affected by type of geosynthetic. Values of tension mobilized in geosynthetic layer reduces to a large extent as the type of geosynthetic changes from inextensible to extensible. The influence of parameters like applied loads, flexural rigidity of footing, spacing and diameter of stone columns, ultimate bearing resistance of foundation soil and stone columns, tensile stiffness of geosynthetic layer and degree of consolidation have been quantified with the help of detailed parametric study for physically possible input parameters. Non-dimensional ready to use charts have been developed for response of footings in terms of its deflection and the bending moment and for response of geosynthetic in terms of tension mobilized in the geosynthetic layer. The footing can be designed as against settlement criteria employing these charts and its section modulus can be chosen accordingly. Further, appropriate selection of geosynthetics can be made with respect to its tensile stiffness.

REFERENCES

- [1] Balaam, N.P. & Booker, J.R. (1981). Analysis of Rigid Rafts Supported by Granular Piles. *International Journal for Numerical and Analytical Methods in Geomechanics*. 5: 379-403.
- [2] Alamgir, M., Miura, N., Poorooshasb, H. B. & Madhav, M. R. (1996). Deformation Analysis of Soft Ground Reinforced by Columnar Inclusions. *Computers and Geotechnics*. 18 (4): 267-290.
- [3] Shahu, J. T., Madhav, M. R. & Hayashi, S. (2000). Analysis of Soft Ground-Granular Pile-Granular Mat System. *Computers and Geotechnics*. 27 (1): 45-62.
- [4] Madhav, M. R. & Poorooshasb, H. B. (1988). A New Model for Geosynthetic Reinforced Soil. *Computers and Geotechnics*. 6 (4): 277-290.
- [5] Ghosh, C. & Madhav, M. R. (1994). Settlement Response of a Reinforced Shallow Earth Bed. *Geotextiles and Geomembranes*, 13: 643-656.
- [6] Shukla, S. K. & Chandra, S. (1994). A Generalized Mechanical Model for Geosynthetic-Reinforced Foundation Soil. *Geotextiles and Geomembranes*. 13: 813-825.
- [7] Yin, J. H. (1997). A Nonlinear Model of Geosynthetic-Reinforced Granular Fill over Soft Soil. *Geosynthetics International*. 4 (5): 523-537.
- [8] Maheshwari, P., Basudhar, P. K. & Chandra, S. (2004). Analysis of Beams on Reinforced Granular Beds. *Geosynthetics International*. 11 (6): 470-480.
- [9] Deb, K., Sivakugan, N., Chandra, S. & Basudhar, P. K. (2007). Generalized Model for Geosynthetic-Reinforced Granular Fill-Soft Soil with Stone Columns. *International Journal of Geomechanics, ASCE*. 7 (4): 266-276.
- [10] Deb, K., Chandra, S. & Basudhar, P. K. (2010). Analysis of Extensible Geosynthetics and Stone Column-Reinforced Soil. *Ground Improvement*. 163 (4): 231 – 236.
- [11] Maheshwari, P. & Khatri, S. (2012). Generalized Model for Footings on Geosynthetic – Reinforced Granular Fill – Stone Column Improved Soft Soil System. *International Journal of Geotechnical Engineering*. 6 (4): 403-414.
- [12] Zhou, W.-H., Zhao, L.-S. & Li, X.-B. (2014). Analytical Study for Geosynthetic Reinforced Embankment on Elastic Foundation. *Geotechnical Special Publication 238, Ground Improvement and Geosynthetics, ASCE*, 444-451.
- [13] Rajesh, S., Choudhary, K. & Chandra, S. (2015). A Generalized Model for Geosynthetic Reinforced Railway Tracks Resting on soft Clays. *International Journal of Numerical and Analytical Methods in Geomechanics*. 39: 310-326.
- [14] Zhao, L.-S., Zhou, W.-H., Fatahi, B., Li, X.-B. & Yuen, K.-V. (2016) A Dual Beam Model for Geosynthetic-Reinforced Granular Fill on an Elastic Foundation. *Applied Mathematical Modelling*. 40: 9254-9268.
- [15] Som, N. N. & Das, S. C. (2003). Theory and Practice of Foundation Design, Prentice – Hall of India Private Limited, New Delhi.
- [16] Bowles, J. E. (1996). Foundation Analysis and Design. 5th Edition, McGraw-Hill Book Co., Singapore.
- [17] Das, B. M. (1999), Principles of Foundation Engineering. 4th Edition, PWS Publishing, USA.
- [18] Desai, C. S. & Abel, J. F. (1987). Introduction to the Finite Element Method: A Numerical Method for Engineering Analysis, CBS Publishers and Distributors, India.

CHAPTER 13

ASSESSMENT OF SOIL EROSION BY SIMULATING RAINFALL ON AN EQUATORIAL ORGANIC SOIL

Johari, A.H.¹, Law, P.L.¹, Taib, S.N.L.¹ and Yong, L.K.¹

Abstract

Soil erosion occurs on construction sites partly due to site clearing that exposes the land to the erosive power of rainfall. A proposed construction project requires the submission of an Environmental Impact Assessment (EIA) to assess the impact of the project on the environment. Assessment of soil erosion is included in the EIA, but the equation to estimate soil erosion known as the Universal Soil Loss Equation (USLE) is only applicable to a soil containing up to four percent organic matter. This limitation of USLE requires an alternative that can predict soil erosion on an organic soil. This study attempts to assess erosion that occurs on an organic soil by simulated rainfall. Field soil samples were reconstructed into three shapes and exposed to simulated rainfall. Results indicate that the amount of organic soil loss decreases with increasing duration of rainfall. Particle size distribution shows that particles with sizes finer than coarse sand (1.7 mm) remained on the slopes. Equations were developed from the graphs of soil loss versus duration of simulated rainfall to estimate soil loss occurring on slopes covered by an organic soil. The outcome of this study can be a precursor to developing an equation to estimate soil erodibility of a slope overlain by an organic soil.

Keywords: Soil erosion, organic soil, simulated rainfall, sediment yield.

1.0 INTRODUCTION

Road construction projects are developing in the country as an infrastructure to connect different places and to spur economic growth. Studies have been conducted on soil erosion occurring on construction sites, such as on highway embankments [1], roadside slopes [2] and soil deposits [3]. Soil erosion occurs on construction sites due to site clearing that exposes the land surface to erosion by rainfall and human activities.

An assessment of soil erosion on a proposed construction project is essential as it is included in the Environmental Impact Assessment (EIA), a legal document that is compulsory to be submitted for approval of the intended project. The provided equation to estimate soil erosion (USLE) is limited to land where the soil has a maximum organic matter content of four percent [4]. An assessment of soil erosion on a construction site with the soil containing more than four percent of organic matter such as an organic soil or peat would bring about errors. Therefore, an equation to estimate soil erosion on an organic soil should be developed. The aim of this study is to investigate the extent of soil erosion occurring on organic soil by simulating rainfall at a laboratory in Universiti Malaysia Sarawak, Malaysia. The scope of this study includes determining the characteristics of collected soil samples, conducting simulated rainfalls on three shapes of soil slopes, analysing the soil samples for particle size distribution, and analysing runoff samples for sediment yield. The assessment of soil erosion conducted on an equatorial organic soil would bring about an understanding of erosion that is occurring on a land that comprises an organic soil. Furthermore, relevant authorities and engineering consultants would be able to assess soil erosion on an organic soil with more accuracy.

¹Department of Civil Engineering, Universiti Malaysia Sarawak, 93000, Kota Samarahan, Sarawak, Malaysia.

Many researchers have designed and constructed different types of rainfall simulators for various objectives such as erosion, infiltration and sediment transport [5]–[7]. Rainfall simulators have several advantages over natural rainfall as the rainfall characteristics can be controlled and repeated at a suitable time [8]. However, rainfall simulators have other shortfalls such as difficulty in reproducing rainfall intensity fluctuations, distribution of drop sizes, and varied values of kinetic energy of raindrops. Without rainfall simulation, the study of soil erosion requires high temporal resolution and long-term rainfall records to calculate rainfall intensity and kinetic energy, which can be unavailable for some locations [9].

In natural conditions, the state of Sarawak encounters over 4000 mm of rainfall per year and rainfall can be expected on almost every day, particularly during the rainy season [10]. An increasing amount of rainfall could contribute to a higher index of rainfall erosivity and consequently higher soil erosion. The characteristics of soil samples and sediment yield can help determine the factors of rainfall erosivity and soil erodibility embedded in the Revised Soil Loss Equation (RUSLE). RUSLE was developed to predict top soil erosion rate from agricultural areas or plantations located in temperate regions with low rainfall (1,000 mm/year) as compared to an equatorial region with more than 4,000 mm/year such as Sarawak, where more than 25% of the area is covered with organic soil and peat [10], [11]. The different climate where the RUSLE was developed and its inability to determine sediment yield of an organic soil could bring about deviations in estimating soil erosion rate for an organic soil, particularly in an equatorial region like Sarawak. The closest estimation method so far was developed by [12], which is suitable for mineral soils and on slope areas in Peninsular Malaysia. If successful, the outcome of this study would lead to a more cost-effective, reduced operational and maintenance works, and more accurate prediction of soil loss generated annually.

2.0 MATERIALS AND METHODS

2.1 Structure of Simulator

The rainfall simulator is a steel frame structure with dimensions of 0.64 m x 1.38 m at the base, 0.64 m x 1.38 m at the top and 1.0 m in height. The structure has a protruding triangle to support the sprinkler and is built with an adjustable steel angle of 30 mm x 30 mm x 5 mm. The water tank, pumping unit, and sprinkler were temporarily located at a height of approximately 10.36 meters on the 2nd floor of Chemical Engineering laboratory building in Universiti Malaysia Sarawak, Kota Samarahan, Malaysia.

The top of the main frame consists of an attached triangular structure to support the connecting hose and sprinkler. The sprinkler is 1.5 m in height from its base. The sprinkler is exposed to its surroundings to imitate natural rainfall. The source of water is a tap 25 m from the location of simulation. A submersible pumping unit is used to supply water to the sprinkler. The flow capacity of the pumping unit is a maximum of 13 m³ per hour. After calibration, the water pump was measured to be flowing at a rate of 0.436 m³/h. Figure 3 shows the overall setting and where the rainfall simulator was placed.



Figure 1 Rainfall simulator and water tanks placed on the 2nd floor of a building in Universiti Malaysia Sarawak.

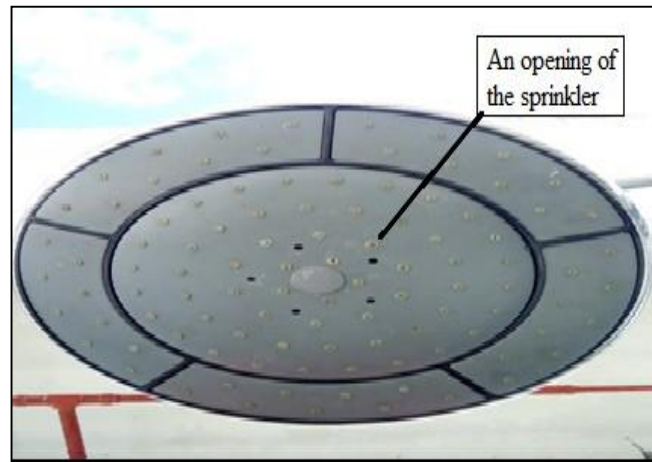


Figure 1 Nozzle openings are uniformly spaced.



Figure 2 Set-up of rainfall simulator.

2.2 Soil Slopes

The soil used for this study was taken from Sri Aman, Sarawak (coordinate: $1^{\circ}12'13''$ N, $111^{\circ}32'15''$ E), where the soil is visually classified as an organic soil. The soil sample weighed approximately 160 kg and was a disturbed sample. The soil was analysed for its physical properties. The approximate location of the soil sample is shown in Figure 4.

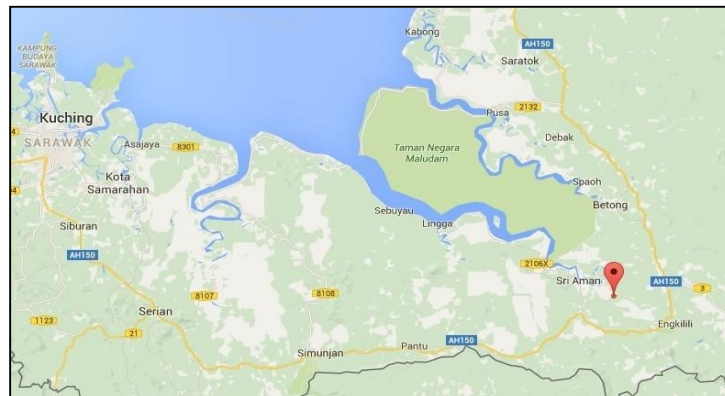


Figure 3 Soil sample location. (Accessed 10th April 2016, <http://maps.google.com>).

There were three simulated rainfalls with different types of slopes; cone, pyramid, and plateau. The shape of slope was varied to facilitate sampling of soil during rainfall and to replicate real berm shapes. All slopes had a similar steepness of 45° . As shown in Table 1, the cone-shaped slope was 1 m in diameter and 0.5 m in height. The loosely packed pyramid measured as 1 m by 1 m for the base and 0.5 m in height. The third slope was plateau-shaped with 1 m by 1 m at the base and 0.5 m in height. The flat surface at the top was 1 m in length by 60 mm in width.

Table 1 Characteristics of the studied soil.

Plot shape	Plot width (m)	Plot length (m)	Plot height (m)	Slope (degrees)
Cone	1 (diameter)	-	0.5	45
Pyramid	1	1	0.5	45
Plateau	1 (base), 0.06 (top)	1 (base, top)	0.5	45

2.3 Operation of Rainfall Simulator

The rainfall simulator was run for 30 minutes.

2.4 Collection of Soil Samples

For each of the soil slopes, soil samples were collected at five selected points, beginning at the toe of slope and up the slope at an interval of 32 mm. The weight of samples ranged from 50 g to 100 g. One sample was collected at each point. Soil samples were collected after 15 and 30 minutes of simulation. Soil samples were taken at two times to compare the amount and particle sizes of soil being eroded by the rainfall.

2.5 Analysis of Runoff

Runoff was collected at intervals of six minutes for 30 minutes. The collected volume for each of the

runoff samples was a minimum of 1 liter. A 1-liter volume is required to determine total suspended solids using standard method. The runoff samples were oven dried for 24 hours and then weighed to yield the value of Total Suspended Solids.

2.6 Analysis of Soil Samples

According to Malaysian Soil Classification System for Engineering Purposes and Field Identification, soil that contains 3% to 20% organic matter is termed slightly organic soil, 20% to 75% is termed organic soil and organic content more than 75% is termed peat. For this study, there were several physical characteristics to be determined; field density, organic content, specific gravity, particle size distribution,

and permeability. All procedures were conducted according to British Standard BS8110:1995.

Particle size distribution was analysed to study the composition of the eroded soil. Total suspended solids was analysed to study the amount of soil being eroded. An empirical equation was generated for every rainfall simulation to provide an estimate of sediment yield.

3.0 RESULTS AND ANALYSIS

3.1 Physical Properties of Soil Samples

The physical properties of the soil samples are presented in Table 2. The average moisture content of the soil sample was 605.33%. The average organic content was 88.25%. Field density of the samples taken on site was 0.23 Mg/m³. The average value of hydraulic conductivity was 2.83 x 10⁻⁴ cm/s. From sieve analysis, the mineral component of the soil samples had average values of 47.145% coarse sand, 41.560% very fine sand, 4.792% silt, and 3.612% clay.

Table 2 Physical properties of soil samples

Physical properties	Average value
Moisture content (%)	605.33
Organic content (%)	88.25
Field density (Mg/m ³)	0.379
Specific gravity	0.223
Hydraulic conductivity (cm/s)	2.83 x 10 ⁻⁴

Figure 5 presents the particle size distribution of soil samples collected on 5 points of the cone-shaped slope after 15 minutes. From the graph, most of the grains are retained on sieve size of 150 µm with a range of 38.45% to 59.82%, and on sieve size of 1.7 mm with a range of 30.59% to 55.24%. Figure 6 presents particle size distribution for Samples 6-10 collected after 30 minutes. Most of the grains with an average of 47.44% were retained on sieve size of 1.7 mm. Generally, most of the particles smaller than 1.7 mm were retained on the slopes. According to British Standard Institute, soil particles finer than 10 mm are considered as gravel. Soil particles that pass through a 1.7mm sieve are classified as coarse and medium coarse sand. Soils finer than 150 µm are categorised as fine sand, and soils that pass through a 63 µm sieve are considered as clay [13], [14].

Figure 7 displays the particle size distribution of soil samples for the pyramid-shaped slope with Samples 11-15. The samples were collected after 15 minutes of rainfall simulation. As shown in the graph, the 1.7mm sieve retained the highest percentage of the soil sample, with an average content of 53.45%. Figure 8 shows the particle size distribution of Samples 16-20. The 1.7mm sieve retained the highest percentage of grains, with an average of 58.18%. An average of 32.35% of the samples were retained on sieve size 150 µm. Figures 9 and 10 describe the particle size distribution the plateau- shaped slope, Samples 21-30. From Figure 9, an average 49.67% of the samples (Samples 21, 22, 23, and 25) were retained on a

sieve size of 150 μm , and an average of 37.63% of the samples retained on sieve size 1.7 mm. Figure 10 shows sieve size 1.7 mm retained most of the samples with an average of 43.88%. Sieve size of 150 μm held 43.56% of the grains. Different trends were collected from the plateau-shaped slope, where Sample 1 and 6 have the most soil retained on sieve sizes of 150 μm and pan (smaller than 63 μm). These different results may be due to smaller grains that have sufficient time to be displaced descending the slope to the edge of the tray.

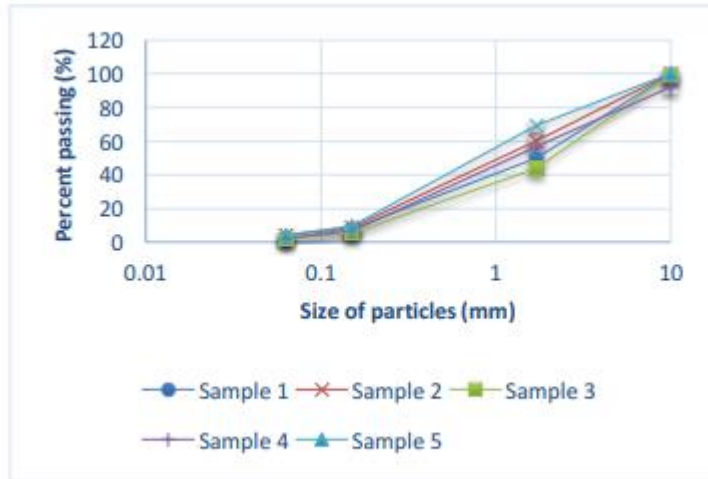


Figure 5 Particle size distribution of eroded soil after 15 minutes of rainfall simulation on cone-shaped slope.

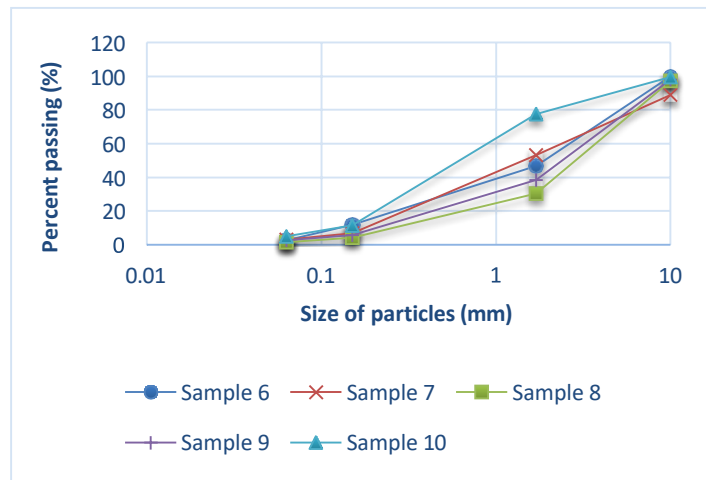


Figure 6 Particle size distribution of eroded soil after 30 minutes of rainfall simulation on cone-shaped slope.

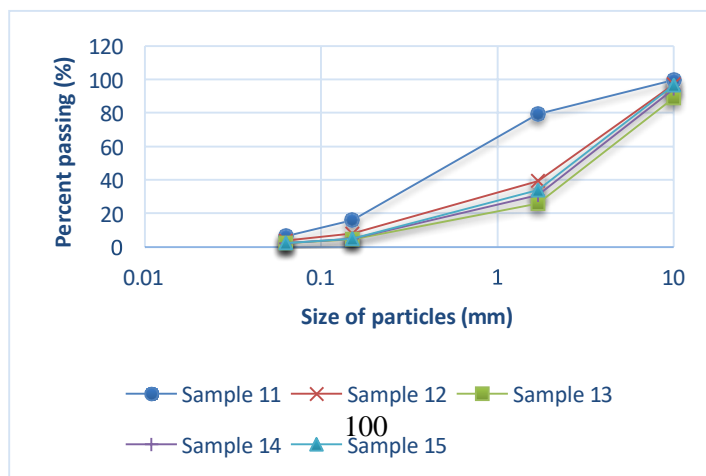


Figure 7 Particle size distribution for eroded soil after 15 minutes of rainfall simulation on pyramid-shaped slope.

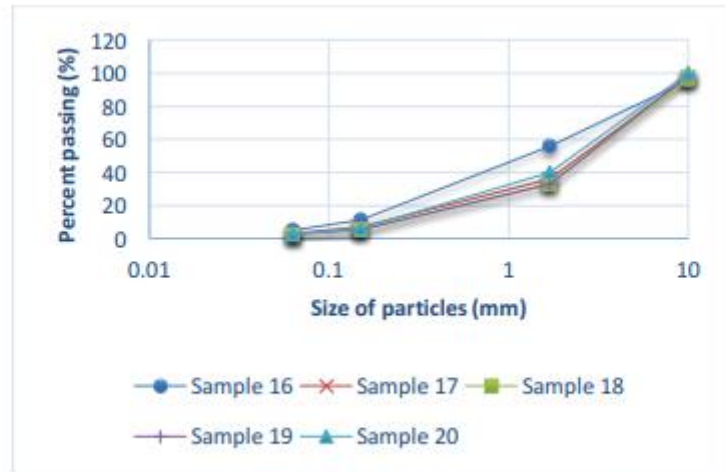


Figure 8 Particle size distribution for eroded soil after 30 minutes of rainfall simulation on pyramid-shaped slope.

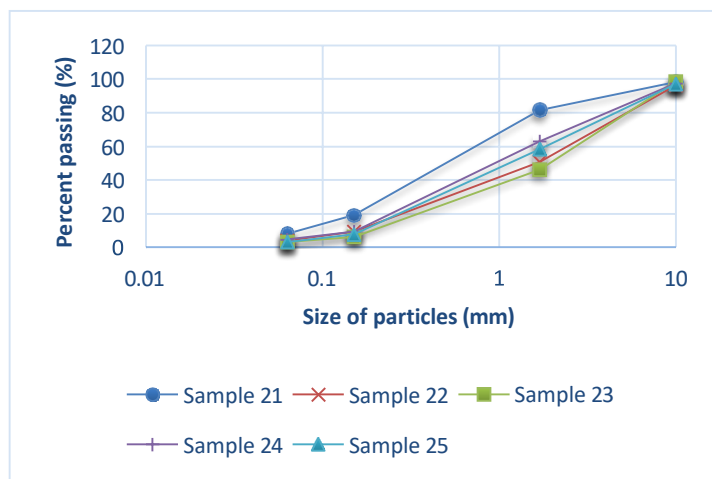


Figure 9 Particle size distribution of eroded soil after 15 minutes of rainfall simulation on plateau-shaped slope.

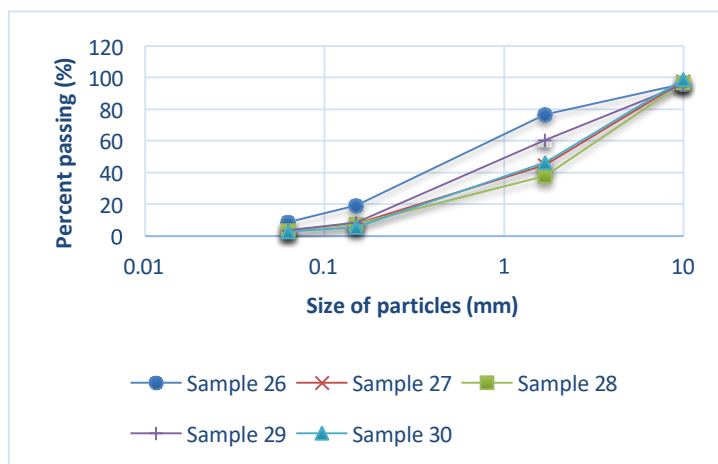


Figure 10 Particle size distribution of eroded soil after 30 minutes of rainfall simulation plateau-shaped slope.

3.2 Determination of Sediment Yield

To determine sediment yield, runoff was collected at 6 minute intervals after simulated rainfall had started. The runoff in the basin was stirred and kept in a 1.5-L bottle. A 1-liter volume of runoff was dried for 24 hours. The sediment in the dried runoff was weighed to measure sediment concentration. Sediment yield was determined by multiplying the sediment concentration with total estimated volume of runoff.

Table 3 shows sediment yield for one minute of simulated rainfall. The sediment yield was extrapolated from the time interval of when the runoff sample was taken and then multiplied by 6 minutes. Figure 11 is the graphical representation of sediment yield of the cone-shaped soil slope. Figure 11 also shows linear correlation of sediment yield in $\text{ton}\cdot\text{ha}^{-1}\cdot(6 \text{ minutes})^{-1}$ by curve fitting using Microsoft Excel. The coefficient of determination (R^2) of the linear equation shows a ratio of 0.5144. For the duration of 30 minutes of simulated rainfall, total sediment yield generated from soil erosion for cone-shaped soil slope was 3.58 tons per ha. Table 4 presents the sediment yield on the pyramid-shaped slope for 30 minutes. Total sediment yield for the simulated rainfall is 15.81 tons per ha. Figure 12 shows the linear equation to determine sediment yield. The equation indicates a good correlation with R^2 of 0.6113.

Table 5 describes sediment yield on the plateau-shaped soil slope, whereas Figure 13 displays the linear relationship of sediment yield over the duration of simulated rainfall. The graph shows that sediment yield is predicted to be reduced over duration of a rainfall event. The coefficient of determination indicates a good ratio of R^2 of 0.7517. Total estimated sediment yield for the simulated rainfall was 4.80 tons per ha. The equations generated from the graphs of sediment yield versus duration in Figures 11-13 are summarised in Table 6. The equations are required to estimate sediment yield occurring on slopes with similar characteristics and rainfall patterns.

Table 3 Correlation of sediment yield and duration of simulated rainfall.

Duration (minutes)	6	12	18	24	30
Total suspended solids ($\text{g}/\text{L}/\text{m}^2$)	7.00	6.38	3.07	5.00	4.00
Sediment yield ($\text{g}/\text{ha}/\text{min}$)	1.64×10^5	1.49×10^5	7.20×10^4	1.17×10^5	9.38×10^4
Sediment yield ($\text{ton}/\text{ha}/\text{min}$)	0.164	0.149	0.072	0.117	0.094

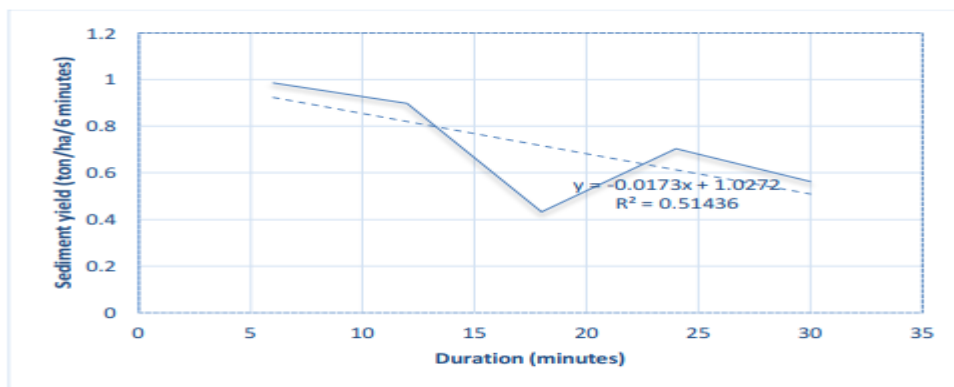


Figure 11 Extent of sediment yield on cone-shaped slope against duration and its regression equation.

Table 4 Sediment yield against duration of simulated rainfall on pyramid-shaped slope.

Duration (minutes)	6	12	18	24	30
Total suspended solids (g/L/m ²)	50.42	24.00	8.00	18.00	12.00
Sediment yield (g/ha/min)	1.18×10^6	5.62×10^5	1.87×10^5	4.22×10^5	2.81×10^5
Sediment yield (ton/ha/min)	1.182	0.563	0.187	0.422	0.281

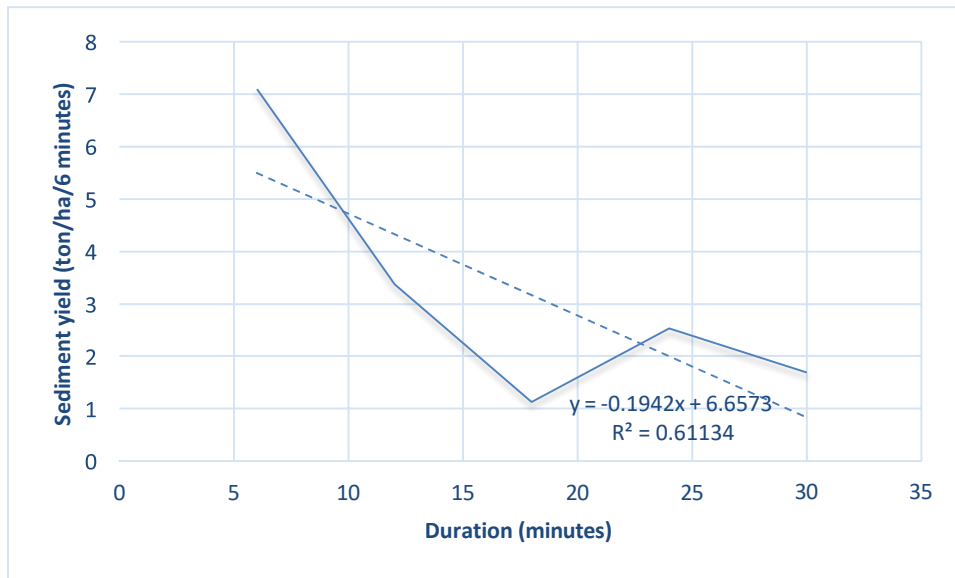


Figure 12 Progression of sediment yield on pyramid-shaped slope against duration of simulated rainfall.

Table 5 Sediment yield against duration of simulated rainfall on plateau-shaped slope.

Duration (minutes)	6	12	18	24	30
Total suspended solids (g/L/m ²)	8.14	7.28	8.14	6.00	4.56
Sediment yield (g/ha/min)	1.91×10^5	1.71×10^5	1.91×10^5	1.41×10^4	1.07×10^5
Sediment yield (ton/ha/min)	0.191	0.171	0.191	0.141	0.107

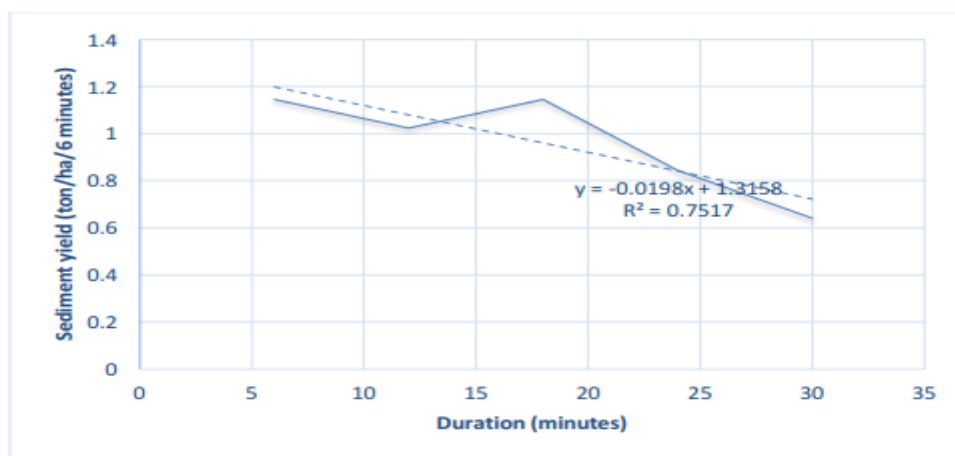


Figure 13 Correlation of sediment yield on plateau-shaped slope and duration of simulated rainfall.

Table 6 Summary of equations generated from the correlations of sediment yield and duration of simulated rainfall.

Hill slope	Soil loss rate	R ²
Cone	$y = -0.0173x + 1.0272$	0.5144
Pyramid	$y = -0.1942x + 6.6573$	0.6113
Plateau	$y = -0.0198x + 1.3158$	0.7517

4.0 CONCLUSIONS

Results have shown that soil loss decreases with increasing duration of simulated rainfall. Sediment yield of cone-shaped slope from simulated rainfall was estimated at 3.58 tons per hectare. The estimated sediment yield of pyramid-shaped slope and plateau-shaped slope were 15.81 tons per hectare and 4.80 tons per hectare respectively. Particles with sizes of less than 1.7 mm were mostly deposited on the toe of slopes. This may be due to random arrangement of the soil particles in the soil plot. The shapes of the slopes (cone, pyramid and plateau) appeared to be indistinctive upon completion of the simulated rainfalls. Equations were generated from the correlations between sediment yield and duration of simulated rainfalls to estimate sediment yield for slopes containing an organic soil. The outcome of this study can serve as a preliminary investigation to generate a new equation to estimate soil erodibility of an equatorial organic soil, particularly in Sarawak.

REFERENCES

- [1] R. A. Persyn, T. D. Glanville, T. L. Richard, J. M. Laflen, and P. M. Dixon, "Environmental effects of applying composted organics to new highway embankments: Part 1. Interrill runoff and erosion," *Trans. ASAE*, vol. 47, no. 2, p. 7, 2004.
- [2] X. Z. Xu, H. W. Zhang, G. Q. Wang, S. C. Chen, and W. Q. Dang, "An experimental method to verify soil conservation by check dams on the Loess Plateau, China," *Environ. Monit. Assess.*, vol. 159, no. 1–4, pp. 293–309, 2009.
- [3] J. Dong, K. Zhang, and Z. Guo, "Runoff and soil erosion from highway construction spoil deposits: A rainfall simulation study," *Transp. Res. Part D Transp. Environ.*, vol. 17, no. 1, pp. 8–14, 2012.
- [4] W. H. Wischmeier and D. D. Smith, *Predicting rainfall erosion losses - A Guide to Conservation Planning*, no. 537. 1978.
- [5] G. S. Fifield, *Field Manual on Sediment and Erosion Control Best Management Practices for Contractors and Inspectors*. Santa Barbara, California, USA: Forester Press, 2001.
- [6] L. Ooshaksaraie, N. E. A. Basri, A. A. Bakar, and K. N. A. Maulud, "Erosion and sediment control plans to minimize impacts of housing construction activities on water resources in Malaysia," *Eur. J. Sci. Res.*, vol. 33, no. 3, pp. 461–470, 2009.
- [7] I. A. R. Al-Ani, L. Mohd Sidek, M. N. Mohd Desa, and N. E.A.B., "Knowledge Based Expert System for Minimising Stormwater Erosion and Sedimentation in Malaysian Construction Sites," in *Proceeding of the International Conference on Advanced Science, Engineering and Information Technology*, 2011.
- [8] S. Niu, X. Jia, J. Sang, X. Liu, C. Lu, and Y. Liu, "Distributions of Raindrop Sizes and Fall Velocities in a Semiarid Plateau Climate: Convective versus Stratiform Rains," *J. Appl. Meteorol. Climatol.*, vol. 49, no. Rotstayn 1997, pp. 632–645, 2010.
- [9] A. Shamshad, M. N. Azhari, M. H. Isa, W. M. A. W. Hussin, and B. P. Parida, "Development of an appropriate procedure for estimation of RUSLE EI30 index and preparation of erosivity maps for Pulau Penang in Peninsular Malaysia," *Catena*, vol. 72, no. 3, pp. 423–432, 2008.
- [10] Malaysian Meteorological Department, "General Climate of Malaysia," 2016. [Online]. Available: www.met.gov.my.
- [11] M. Mohamed, E. Padmanabhan, B. L. H. Mei, and W. B. Siong, "The Peat Soils of Sarawak," 2002.
- [12] K. H. Tew, *Production of Malaysian soil erodibility nomograph in relation to soil erosion issues*. Subang Jaya, Selangor: VT Soil Erosion Research and Consultancy, 1999.
- [13] British Standard Institution, "British Standard Methods of Test for Soils for Civil Engineering Purposes BS1377-2," *Br. Stand.*, p. 72, 1990.
- [14] M. F. Yusof, R. Abdullah, H. M. Azamathulla, N. A. Zakaria, and A. A. Ghani, "Modified Soil Erodibility Factor, K for Peninsular Malaysia Soil Series," *3rd Int. Conf. Manag. Rivers 21st Century Sustain. Solut. Glob. Cris. Flooding, Pollut. Water Scarcity*, pp. 799–808, 2011.

CHAPTER 14

COMPARISON OF THE BEHAVIOR OF FIBER AND MESH REINFORCED SOILS

Y. C. Fung¹ and Shenbaga. R. Kaniraj¹

Abstract

Soft soil does not have good soil properties and is not suitable for constructing pavement structures as shear strength is required to resist the shear stress developed by traffic loading. To increase shear strength in this study, lime is used as the soil stabilizing agent and fiber and mesh are used as the soil reinforcement materials. The proper amount of lime added to soil will increase the shear strength as the lime-treated soil will decrease moisture susceptibility and migration. Shear strength of the lime-treated soil can be further improved by adding reinforcement materials such as fiber and mesh. The reinforcement materials will interlock with groups of particles and provide tensile strength to the soil matrix. The type of soil used in this study is high plasticity elastic silt with sand which is classified using the Unified Soil Classification System (USCS). Quicklime (calcium oxide) is used in this study at the minimum amount required for stabilizing the soil, which is 9%. The amount of fiber and mesh added to the soil sample is 0.5% of the dry weight of the soil used. Cylindrical samples were prepared with a moisture content of 22% (OMC) for untreated soil and 21% (OMC) for lime-treated soil samples. The lime-treated soil samples were cured for 7, 14, 28, 56, 90 and 120 days. Unconfined compression tests were conducted to determine unconfined compressive strength (UCS) and stress-strain characteristics. The unconfined compressive strength of the lime-treated samples increased as curing period increased but the failure strain decreased. The UCS and failure strain for reinforced lime-treated soil samples are higher than the unreinforced lime-treated soil samples.

Keywords: Soil stabilization, soil reinforcement, lime, fiber, mesh.

1.0 INTRODUCTION

Sarawak, especially the Kuching Division, is developing rapidly. Many buildings, roads and other infrastructure need to be constructed. Sarawak's lands are composed of soft soil. Soil reinforcement or soil stabilization must be done before infrastructure can be built. Discovering new and more efficient soil stabilization and soil reinforcement methods are crucial to overcome these soft soil issues.

Good soil properties such as high shear strength, high stiffness modulus and high durability are essential for road pavement construction. Soil stabilization is a technique introduced with the aim of improving the physical and chemical characteristics of soil so that the soil is able to meet the requirements of specific engineering projects [1]. Cement, lime and mineral additives such as fly ash, silica fume, and rice husk ash are added to the soil to stabilize it [2]. Fiber and some natural materials such as oil palm empty fruits bunch are commonly used as soil reinforcement materials [3].

This study compares the behavior of untreated soil, stabilized soil, and fiber and mesh reinforced soil. Unconfined compression test is conducted on (a) untreated, (b) lime treated, (c) fiber reinforced lime treated, (d) mesh reinforced, (e) fiber reinforced lime treated soil and (f) mesh reinforced lime treated soil samples to investigate the effectiveness of fiber and mesh reinforcement on treated and untreated soils. The lime treated soil samples were cured for 7, 14, 28, 56, 90 and 120 days before unconfined compression test were carried out.

2.0 MATERIALS

The materials used in this research were high plasticity elastic silt with sand (MH) soil, Calcium Oxide (quicklime), fiber and mesh. The soil used in this study was collected at the road side of Kuching-Kota

¹ Department of Mechanical and Manufacturing, Universiti Malaysia Sarawak, 93000, Kota Samarahan, Sarawak, Malaysia

Samarahan Expressway at 1°28'58.2"N 110°24'45.0"E. The Calcium Oxide (quicklime) was manufactured by SIGMA-ALDRICH. The fiber element used in this study is cut from an insect net. The length of the fiber is 7mm with diameter of 1mm. The mesh element used in this study is also cut from the same insect net as the fiber. The mesh was cut into a diamond shape 7mm to each side, with 2mm x 2mm openings.

3.0 EXPERIMENTAL PROCEDURES

3.1 Mix proportion and curing period

The fiber reinforced soil sample contained 0.5% fiber, the mesh reinforced soil sample contained 0.5% mesh and the lime treated soil sample contained 9% lime. The initial consumption of lime test is very important for determination of the amount of lime required for soil stabilization. The initial consumption of lime, which is the amount of lime consumed in the initial ion exchange reaction, is the minimum lime content required for the soil sample to achieve a permanent gain in strength [4]. Soil samples were mixed with 5% to 14% lime and tested for pH value. The samples recording p values in the range of . to . at C with the least percentage of lime content were selected as the initial consumption of lime. The lime treated soil samples were cured for 7, 14, 28, 56, 90 and 120 days before unconfined compression tests were carried out.

4.0 TEST CONDUCTED

Unconfined compression test was done to determine the shear parameters of cohesive soil. This test is carried out on a cylindrical specimen. The height of the specimen must be twice the diameters of the specimen. Specimens of 35 mm in diameter and 70 mm in height were used. The test was done by referring to BS 1377: Part 7: 1990 [5].

5.0 RESULTS AND ANALYSIS

4.1 Unconfined compressive strength

The unconfined compression strength (UCS) test is a type of unconsolidated-undrained triaxial test in which the confining pressure is equal to 0 kPa. This test was done on untreated samples, treated samples, reinforced and unreinforced samples by referring to BS 1377: Part 7: 1990 [5].

The average UCS strength and failure strength of untreated soil samples were 81.68 kN/m² and 4.19% respectively. For fiber reinforced untreated soil samples, the average UCS and average failure strain were 107.26 kPa and 5.87% respectively. For mesh reinforced untreated soil samples, the average UCS and average failure strain were 105.81 kPa and 5.24% respectively. For lime treated soil, fiber reinforced lime treated soil and mesh reinforced lime treated soil samples, the UCS increased as the curing period increased, whereas the average failure strain decreased as the curing period increased. The average UCS for lime treated soil samples was higher compared to untreated soil samples. The average UCS and failure strain of reinforced lime treated soil samples were higher compared to lime treated soil samples. Hence, lime was able to increase the UCS of the soil sample but reduce the failure strain as curing period increased. Fiber and mesh reinforcement are able to increase the UCS and untreated and lime treated soil samples. Figures 1-6 show the result of variation of axial stress (kPa) against axial strain for untreated, fiber reinforced, mesh reinforced, lime treated, lime treated fiber reinforced and lime treated mesh reinforced soil specimens.

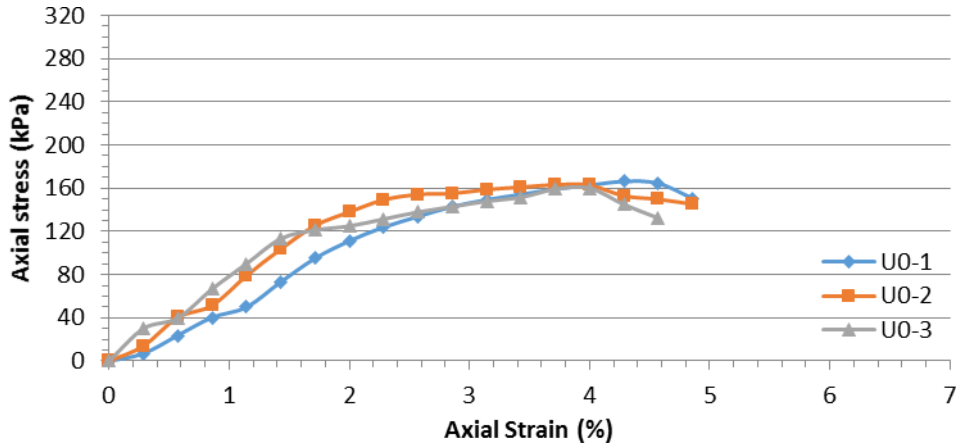


Figure 1 Variation of axial stress (kPa) against axial strain for untreated soil specimens

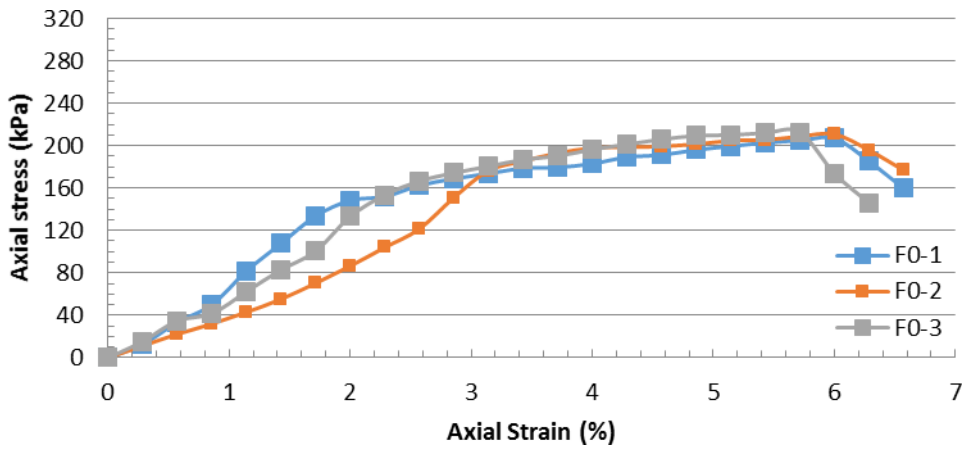


Figure 2 Variation of axial stress (kPa) against axial strain for fiber reinforced soil specimens

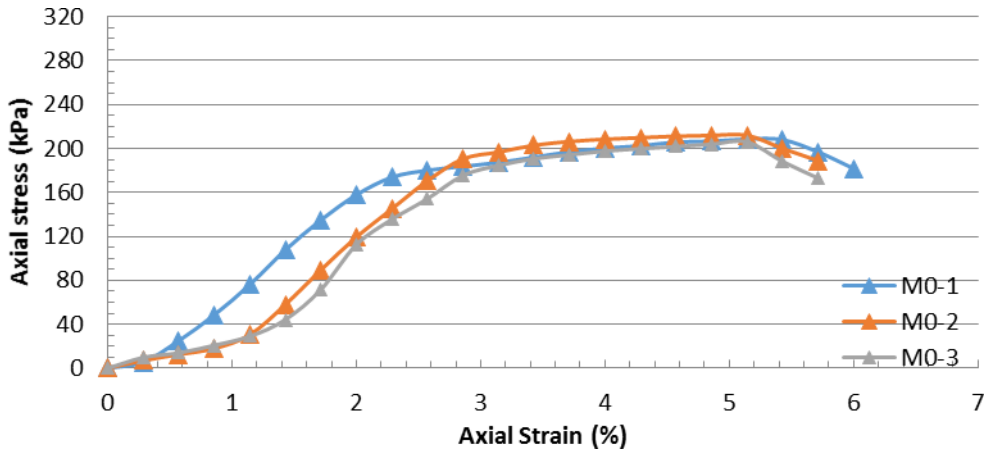


Figure 3 Variation of axial stress (kPa) against axial strain for mesh reinforced soil specimens

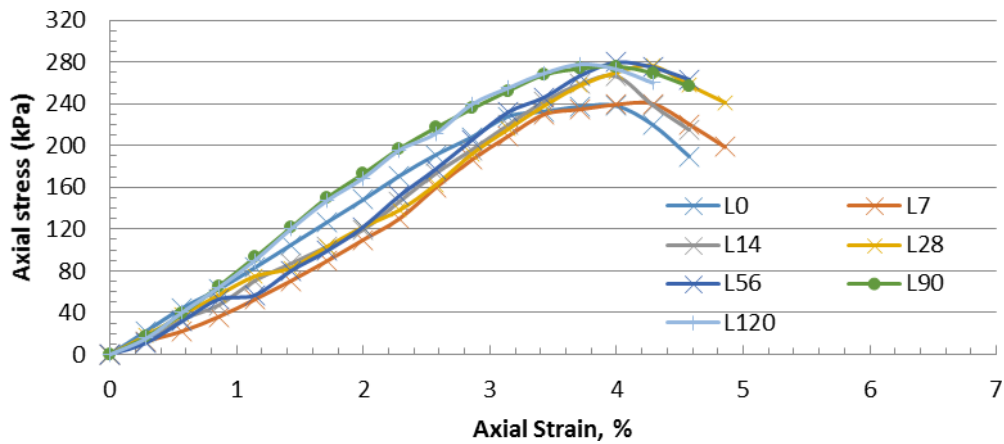


Figure 4 Variation of axial stress (kPa) against axial strain for lime treated soil specimens at different curing periods

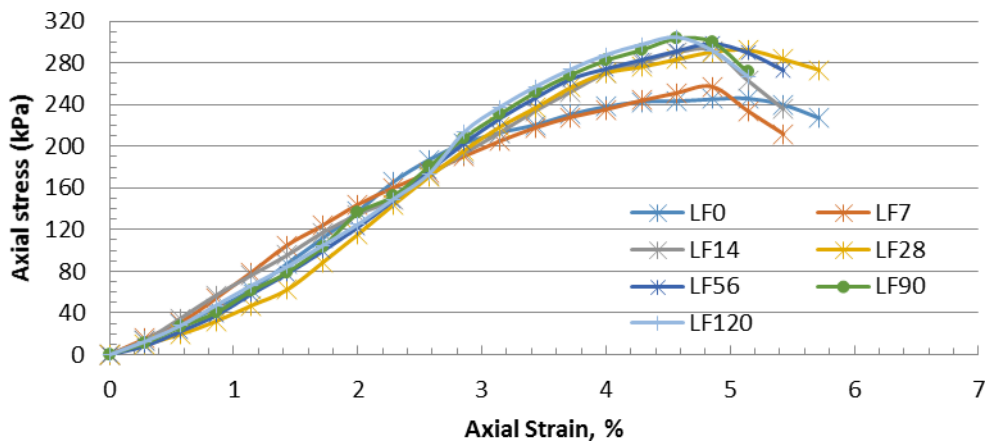


Figure 5 Variation of axial stress (kPa) against axial strain for fiber reinforced lime treated soil specimens at different curing periods

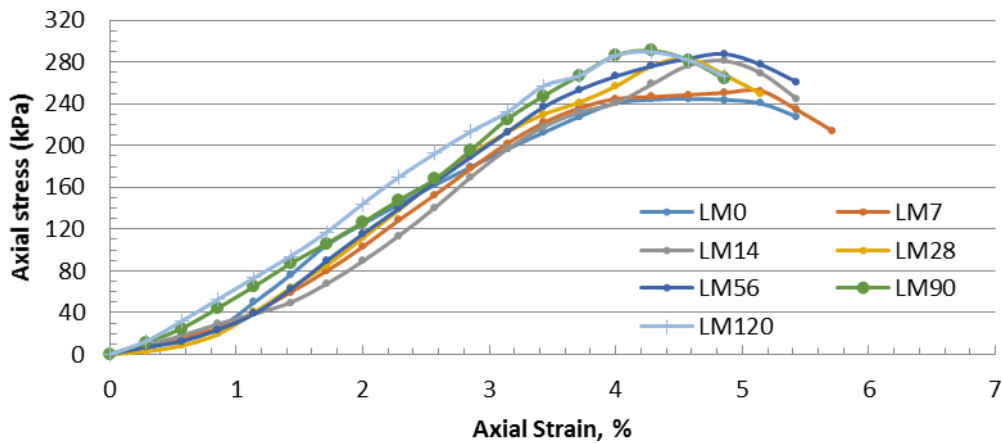


Figure 6 Variation of axial stress (kPa) against axial strain for mesh reinforced lime treated soil specimens at different curing periods

The unconfined compressive strength of fiber reinforced lime treated soil samples are the highest, followed by mesh reinforced lime treated soil samples and lime treated soil samples. This shows that fiber reinforcement is more effective compared to mesh reinforcement for this particular case. The results also show that the increment in unconfined compressive strength is less significant (less than 5%) after a 28 day curing period. Figure 7 shows the variation of unconfined compressive strength against different curing periods for lime treated, fiber reinforced lime treated and mesh reinforced lime treated samples.

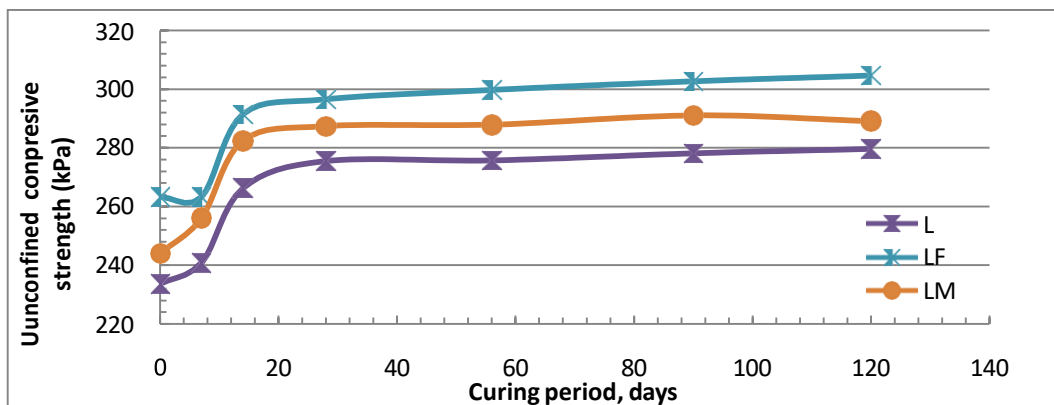


Figure 7 Variation of unconfined compressive strength against curing period for lime treated, fiber reinforced lime treated and mesh reinforced lime treated samples

4.2 Scanning Electron Micrograph

Scanning electron micrography was done on untreated soil samples and, after 90 days of curing, on lime treated soil samples, fiber reinforced lime treated soil samples and mesh reinforced lime treated soil samples. Figure 8 to Figure 11 shows the scanning electron micrography mentioned. All the scanning electron micrography were enlarged by 500 times.

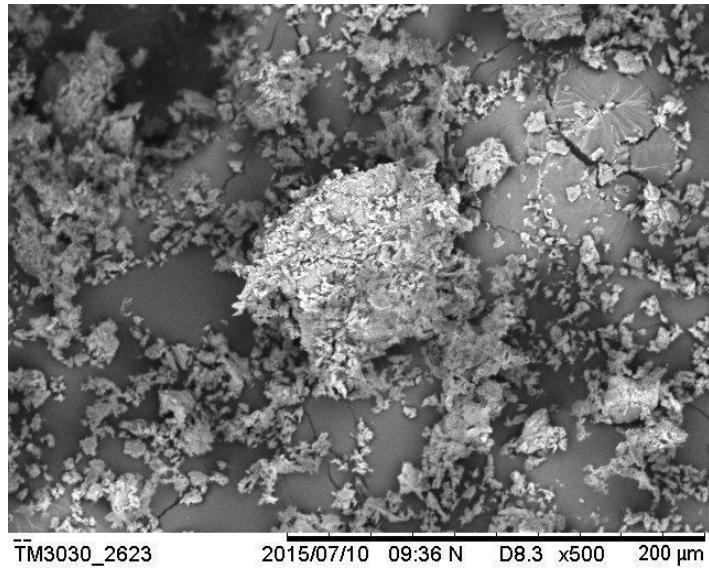


Figure 8 SEM image of untreated soil sample

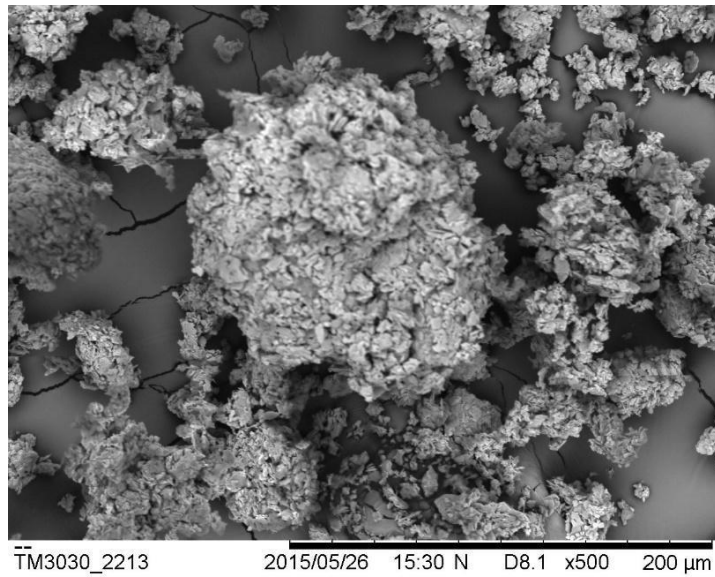


Figure 9 SEM image of lime treated soil sample

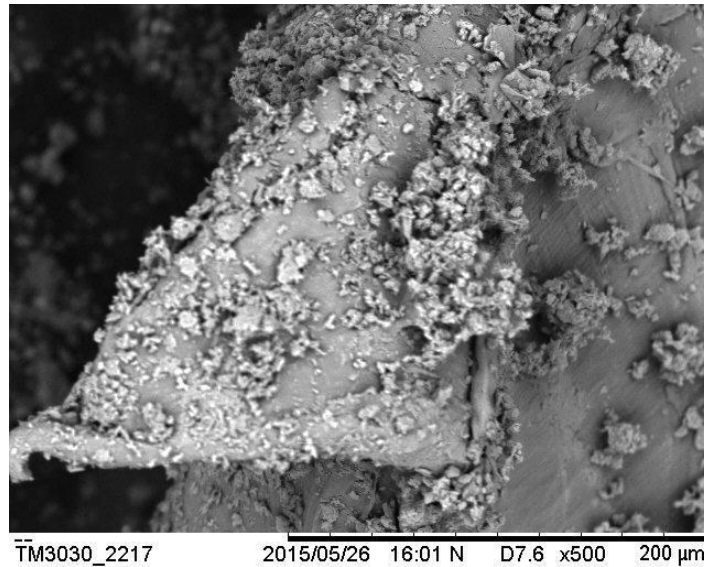


Figure 10 SEM image of fiber reinforced lime treated soil sample

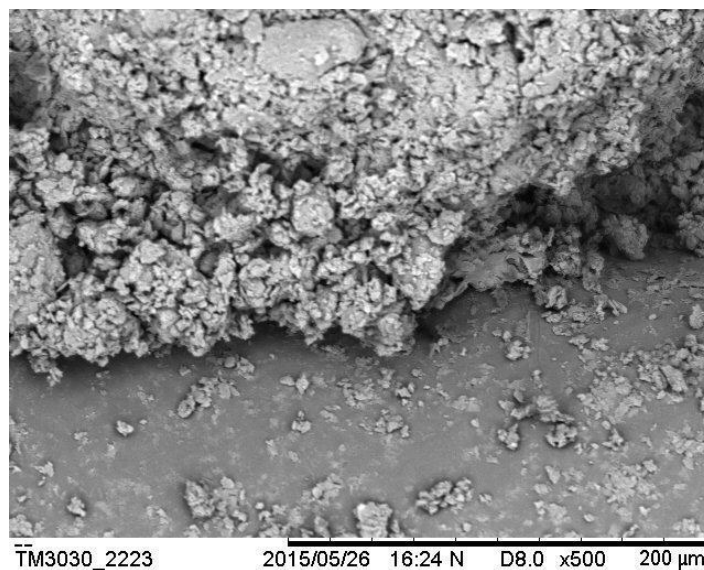


Figure 11 SEM image of mesh reinforced lime treated soil sample

5.0 CONCLUSION

The soil sample used in this study is classified as high plasticity elastic silt with sand (MH) using the Unified Soil Classification System (USCS), with organic content of 0.95%. The specific gravity of the soil is 2.58. The optimum moisture content and maximum dry density of the untreated soil sample are 21% and 1680 kN/m³ respectively. The optimum moisture content and maximum dry density of the lime treated soil sample are 22% and 1560 kN/m³ respectively. The unconfined compressive strength of the soil sample increased as curing period increased, but the failure strain of the soil sample decreased as the curing period increased. The pozzolanic reaction that happens during the curing period contributes to the development of strength of the soil sample but the ductility of the treated sample reduced due to moisture loss. Adding fiber and mesh was able to increase the strength and the failure strain as the fiber and mesh was able to interlock with groups of particles and provide tensile force to the soil matrix. The increment of unconfined compressive strength of lime treated soil samples after 28 days of curing period are less significant, at less than 5%.

REFERENCES

- [1] Kolas, S., Kasselouri-Rigopoulou, V., & Karahalios, A. (2005). Stabilization of clayey soils with high calcium fly ash and cement. *Cement Concrete Composite*, 27, 301–313.
- [2] Sharma, N.K., Swain, S. K., Sahoo, & U.C. (2012). Stabilization of a clayey soil with fly ash and lime: a micro level investigation. *GeotechGeolEng*, 30, 1197–1205.
- [3] Ahmad, F., Bateni, F., & Azmi, M. (2009). Performance evaluation of silty sand reinforced with fibres. *Geotextiles and Geomembranes*, 28, 93-99.
- [4] British Standard Institution. (1990). BS 1924, *Stabilised Materials for Civil Engineering Purposes*. London, UK: British Standard Institution.
- [5] British Standard Institution. (1990). BS 1377, *Methods of Test for Soils*. London, UK: British Standard Institution.

CHAPTER 15

UPLIFT CAPACITY OF SINGLE AND GROUP OF GRANULAR ANCHOR PILE SYSTEM

Pradeep Kumar¹, Mohit Kumar², V. K. Chandaluri³ and V. A. Sawant⁴

Abstract

In view of increased development in the infrastructure across the world, now it becomes necessary to go for the marginal sites having weak soil for foundation. Foundations are normally designed to transfer compressive and uplift forces safely to the subsoil, wherein piles provide an appropriate solution. But the option of pile foundation is quite expensive. Before going for pile foundation, the feasibility of other alternatives must be accessed thoroughly. If it is possible to adopt some suitable ground improvement technique for enhancement of foundation strength, then it should be considered. In the present study, Granular Anchor Pile System is proposed to with stand uplift forces. The present paper, based on a field study, briefly discusses the basic principles associated with the granular pile. The analysis of field test data indicates that the proposed granular pile system is a viable means for ground improvement. It is found effective for improving varying soil conditions and capable of providing resistance to compressive forces in addition to the uplift resistance. Besides, this foundation technique has been found cost effective as compared to the concrete piles.

Keywords: Granular anchor pile, uplift capacity, anchor plate

1.0 INTRODUCTION

Keeping in view the emerging demand of infrastructure, utilization of the poor and marginal sites is unavoidable. Development of these sites with ground improvement techniques has become a subject of profound interest for geotechnical engineers. A variety of ground improvement methods are in practice these days. Various compaction techniques can be adopted for stabilization of loose cohesionless soils. For cohesive soils, consolidation by preloading, grouting, electro-osmosis, electrochemical hardening, stabilization through lime columns, are preferred ground improvement techniques. Ground improvement by various methods can be quantified by assessing the improved bearing capacity and reduced settlement of the treated ground. In real field situations one may come across situations like, limited area for foundation due to presence of existing structures, or where piling may not be adopted due risks of settlement from vibrations, excavations/ loss of ground. In such situations, granular piles can be used as an economical and effective alternative. Installing granular piles in soft cohesive soils and loose cohesionless deposits is an accepted and popular ground improvement technique [1]. Granular pile installation does not require heavy machinery or skilled labour like pile foundation. Gravel backfill is placed into the borehole in stages. In each stage, backfill is compacted by a steel hammer. Compaction displaces the filling material in radial outward direction resulting densification of surrounding soil. This has resulted in significant increase in load carrying capacity and reduction in settlement. Installation of granular piles is one of most preferred method of improving soft ground or loose sand deposits. Granular piles act as reinforcement in the subsoil. It improves drainage pattern and helps in dissipation of excess pore water pressure. Installation of granular pile results in densification of surrounding soil. This will improve bearing capacity, the rate of consolidation and the liquefaction resistance of the ground. In addition, total and differential settlements get reduced by 60-80%. In field, granular piles are installed with the help of vibro-processes or through rammed stone columns technique.

¹Central Building Research Institute Roorkee, Roorkee 247667, India

^{2,3,4} Department of Civil Engineering, Indian Institute of Technology Roorkee, Roorkee 247667, India
Email: sawntfce@iitr.ac.in

Structures like transmission towers or foundations on expansive soil are subjected to uplift forces. In such case, conventional approach is to adopt under-reamed pile foundation. But in the present study, normal granular pile technique with little modification is suggested to counter the uplift force. 'Granular Anchor Pile (GAP)' is the modified form of granular pile. It may be defined as the enhanced granular pile which is reinforced with anchor plate and anchor rod. An anchor plate is a circular steel plate embedded into a concrete pedestal at the bottom of predrilled hole. It is connected to a steel anchor rod which may protrude above pile head (*Figure 1*).

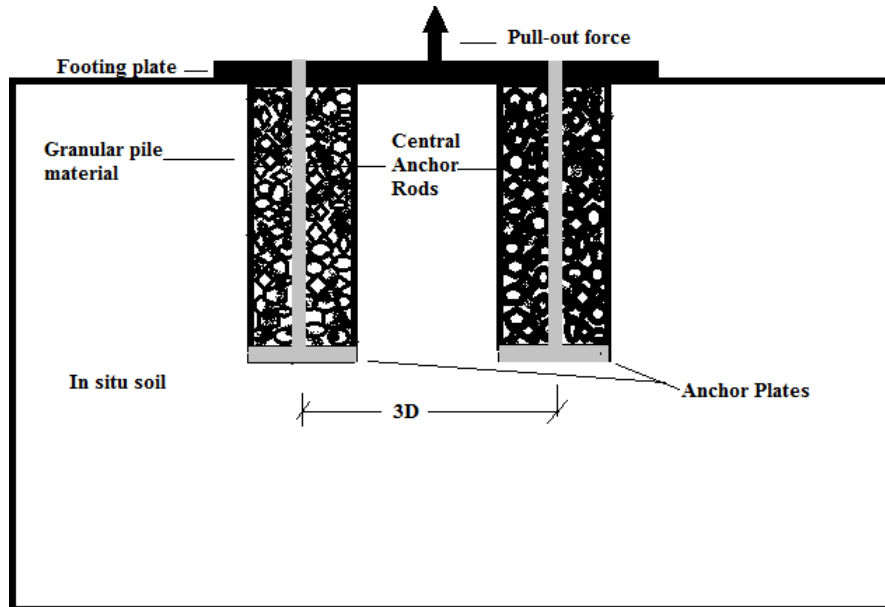


Figure 1 Concept of the granular anchor pile (GAP) foundation system

Few studies have been reported on granular anchored pile to resist uplift forces [1-5]. Kumar and Ranjan [6] have reported the field study of GAP system. Phanikumar et al. [7] reported laboratory investigations on a limited scale for heave control of expansive soils. Ibrahim et al. [8] conducted laboratory tests in addition to a series of numerical modelling using PLAXIS software to study the behavior of GAPF system in expansive soil. Study revealed that the heave can be reduced with increasing length and diameter of GAP. Johnson and Sandeep [9] conducted laboratory tests to study the effect of relative density of fill material and granular pile diameter on the pull capacity of the GAP. The pull-out capacity of the GAP observed to increase with relative density of the granular material and diameter of the GAP. Krishna and Murty [10] discovered that the GAPs exhibit promising pullout capacity even under fully wet condition compared to conventional concrete piles. Phanikumar [11] studied the influence of geogrid reinforcement on uplift capacity of GAP in expansive clay beds. The pullout capacity of the GAP increased with increasing number of geogrid layers, decreasing spacing between them, and with decreasing distance between anchor plate and bottom geogrid.

The uplift capacity can be accurately predicted only when reliable estimation of the in situ properties of the ground and of the granular pile material is possible. A method for determination of the same is presented here. Present study reports the field investigation of GAP at two sites. Estimation of uplift capacity from limit equilibrium approach is also discussed. The predicted capacities from limit equilibrium approach are in good agreement with measured uplift capacity of GAP in the field.

2.0 METHODOLOGY

Two sites are selected for conducting field investigations. They are designated as Site-1 and Site-2. The detailed subsoil investigations in the field have been carried out at the selected sites. Then necessary laboratory investigations are carried out on disturbed/undisturbed samples collected from field for measurement of essential soil properties. Testing program included advancement of borehole

supplemented with standard penetration tests (SPT) at regular intervals, dynamic cone penetration tests (DCPT) and static cone penetration tests (SCPT). Further, the undisturbed and disturbed soil samples were collected from appropriate locations for laboratory investigations. Basic classification tests were carried out on undisturbed samples.

2.0 SITE-1

The water table during the testing period was 6.2 m below ground. Study of bore log at site indicate the presence of poorly graded sand (SP) starting from the surface to 4 m depth. It is underlain by 1 m thick inorganic silt (ML). Again soil between 5 m to 8 m depth was found to be poorly graded sand (SP). Further extension of borehole beyond 8 m depth indicated the presence of this silty soil (ML). Observed SPT N values at different depths are tabulated in Table 1. Similarly static cone resistance values were recorded as 3600 kPa and 3200 kPa at 2 m and 3 m depth, respectively. But the values decreased to 2200 kPa and 1000 kPa at 4 m and 6 m depth, respectively. Beyond this depth it was again observed increasing. The grain size analysis marked the presence of fine to medium sand between 82 to 97 % with 10 to 12 % of silt contents with almost no clay. However, a thin layer of 10 % clay content was observed as exception.

Table 1 SPT value and angle of internal friction along depth at site-1

Depth (m)	SPT (N)	Angle of friction
0.75	6	28°
3	6	28°
5	11	29°
6	12	29°
7	14	30°
8.5	9	29°

2.1 SITE-2

As per the bore-log, the subsoil at the site reported an upper clay layer of intermediate plasticity (CI) starting from the ground surface to 3 m depth. It is followed by clay of low plasticity (CL) between 3 m to 6 m depth. Between 6 m to 10 m depth again clay of intermediate plasticity (CI) was observed. Thus, the subsoil in general consists of soft cohesive-soil deposit ranging from CL to CI. Observed SPT N values at different depths are tabulated in Table 2. The grain size analysis of samples collected from different depths was carried out using Digital Particle Size Analyzer. It indicated the presence of silt and clay. The percentages of silts varied from 95% to 52%. Triaxial tests have been conducted on undisturbed samples of cohesive soils.

Table 2 Soil properties along depth at site-2

Depth (m)	SPT (N)	Liquid limit	Plastic limit	Cohesion kPa	Angle of friction
0.75	4				
1.5	7	43	22	50	15°
3	10	43	24		
4.5	9	29	17	50	10°
6	14	27	16		
7.5	13	37	19	50	15°
9.5	16	20	NP		

(NP- Non-plastic)

2.2 PROCEDURE FOR CONSTRUCTION OF GAP AND LOAD APPLICATION IN THE FIELD

Initially, borehole of desired depth in the ground is drilled using a manually operated spiral auger. Then, cement concrete mixture (1:2:4) is poured at its bottom through a tremie pipe. Then a prefabricated anchor plate with anchor rod is lowered and positioned at the bottom. Another layer of 150 mm thick concrete is poured over anchor plate. Borehole is then left for seven days for initial setting of concrete. Then granular pile is installed with stone aggregate sand mixture in predetermined layers. Each layer was given uniform amount of compaction energy throughout the investigations.

After the test bed is ready, the other end of MS anchor rod is connected to the loading jack with the help of specially designed and fabricated attachment provided at its top to transfer the uplift force to the GAP system. The pullout force is then applied through the remote controlled hydraulic pump and jack placed at the loading/top girder of the MS frame. Pullout force is applied in increments. The exact load increment is measured through a load cell. The upward movement of GAP is measured with the help of two dial gauges. The uplift movements corresponding to each incremental uplift force were recorded till the soil fails in bulging.

In this study, the uplift capacity of single GAP and group of GAP system (both 2 GAP and 4 GAP system) is determined. In case of group piles, center to centre spacing of 3 times pile diameter is considered in the present study. The diameter of GAP is considered as 0.3 m. But to examine the effect of diameter, two cases with 0.35 m diameter are also considered. To study the effect of Length to Diameter on uplift capacity of single GAP, four different L/D ratios are considered in the field study. For the case of group GAP, L/D ratio is taken as 20.

3.0 LIMIT EQUILIBRIUM APPROACH

Bottom portion of GAP equal to critical height H_c is considered to bulge due to uniform lateral stress σ_r in subsoil due to gradual increase in uplift stress q and consequently σ_r in pile body (*Figure 2*). Cylindrical zone around the bulged pile having a radius R_u will undergo a state of plastic equilibrium. Beyond this zone of plastic equilibrium of radius R_p , soil is considered to be in elastic state. Ultimate uplift force applied at pile top is considered to be resisted by weight of GAP and force required to provide to restraint against bulging of GAP. Unit friction along the GAP shaft is not considered as there is no enough relative movement between GAP and surrounding soil. Ratio of radius of plastic zone and cylindrical cavity (R_p/R_u), reduced rigidity index I_{rr} and lateral limiting stress σ_{rL} are parameters controlling uplift capacity.

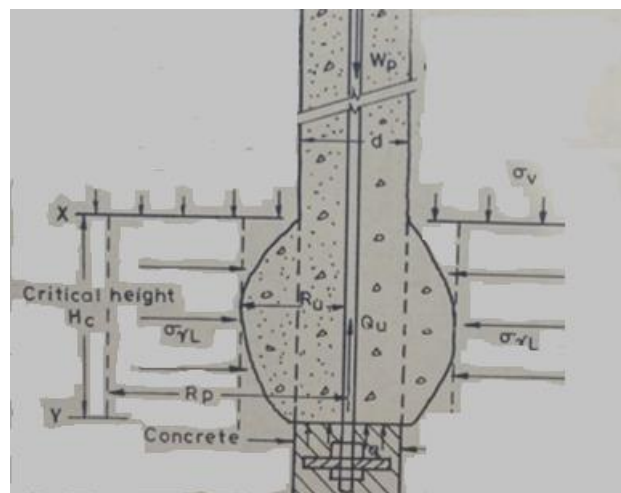


Figure 2 Bulging at bottom of GAP [12]

Ultimate uplift capacity Q_u is calculated using following steps:

1. Effective normal stress σ_v at bulging

Assuming H_c equal to five times diameter of pile,

$$\sigma_v = \gamma \times z = \gamma \times (L - 5D) \quad (1)$$

2. Effective mean normal stress σ_m

$$\sigma_m = \left(\frac{1 + 2K_0}{3} \right) \sigma_v \quad \text{where } K_0 = 1 - \sin(1.2\phi) \quad (2)$$

3. Elastic soil modulus is obtained from

$$E_s = 2q_c (1 + R_D^2) \quad (3)$$

In which, q_c is static cone penetration resistance and R_D is relative density of soil.
Corrected Modulus

$$E_{cor} = E_s \left(\frac{\sigma_v}{100} \right)^{0.5} \quad (4)$$

4. Rigidity Index I_r

$$I_r = \left(\frac{0.5E_{cor} / (1 + \mu)}{c + \sigma_m \tan \phi} \right) \quad (5)$$

Reduced Rigidity Index I_{rr}

$$I_{rr} = \left(\frac{I_r}{1 + I_r \varepsilon_v} \right) \quad \text{where } \varepsilon_v = \frac{\sigma_m}{K_{bulk}} \quad (6)$$

Dimensionless cavity expansion factors F_q and F_c

$$F_q = (1 + \sin \phi) (I_{rr} \sec \phi)^{\sin \phi / (1 + \sin \phi)}$$

$$F_c = (F_q - 1) \cot \phi \quad (7)$$

$$F_c = 1 + \ln(I_{rr}) \quad \text{for } \phi = 0$$

5. Lateral limiting stress σ_{rl} are

$$\sigma_{rl} = F_c c_u + F_q \sigma_m \quad (8)$$

6. Ultimate resistance in bulging q_{ub}

$$q_{ub} = K_p \sigma_{rl} = \frac{1 + \sin \phi_p}{1 - \sin \phi_p} \times \sigma_{rl} \quad (9)$$

7. Resistance in bulging Q_b

$$Q_b = q_{ub} A_p \quad (10)$$

8. Weight of GAP

$$W_p = \gamma_p A_p L \quad (11)$$

9. Ultimate uplift capacity Q_u

$$Q_u = Q_b + W_p \quad (12)$$

4.0 RESULTS AND ANALYSIS

The pullout capacities were obtained from the pullout force versus displacement curves by intersecting tangent methods. Values of pullout capacities are listed in *Table 3* and *4*. Values of pullout capacities are observed to be increasing with the increase in L/D ratio. This increase is observed to be marginal beyond L/D equal to 13.3. There is a particular length of pile beyond which further increase in length will not have significant effect on the pullout capacity. In the present study this length may be considered corresponding to L/D ratio of about 13.3. For groups of GAP systems, the pullout capacities were found almost equal to the value of a single GAP system multiplied by the number of GAP systems.

Table 3 Ultimate Uplift capacity at site-1

Type of GAP	L/D	S/D	Ultimate Uplift capacity (kN)	
			Field Test	Analytical
Single	6.66	-	45	27.4
Single	10.0	-	70	54.1
Single	13.3	-	75	67.7
Single	20.0	-	80	78.8
2 GAP	20.0	3	170	157.6
4 GAP	20.0	3	310	315.2

GAP- Granular Anchor Pile, 2 GAP- Group of 2 GAP, 4 GAP- Group of 4 GAP,
 S/D - c/c pile spacing to diameter ratio in group pile

Table 4 Ultimate Uplift capacity at site-2

Type of GAP	L/D	D (m)	S/D	Ultimate Uplift capacity (kN)	
				Field Test	Analytical
Single	6.66	0.3	-	35	44.0
Single	13.3	0.3	-	45	48.9
Single	20.0	0.3	-	47	54.4
2 GAP	13.3	0.3	3	80	97.8
2 GAP	20.0	0.3	3	90	108.8
2 GAP	20.0	0.35	3	200	154.8
3 GAP	13.3	0.3	3	120	146.7
3 GAP	20.0	0.3	3	140	163.2
3 GAP	20.0	0.35	3	220	222.2
6 GAP	13.3	0.3	3	260	293.4
6 GAP	20	0.3	3	300	326.4

Analytical estimation of pull out capacity is also given in the same tables for comparison. The pull out capacity of group of GAP is estimated by multiplying number of piles with capacity of single GAP. It forces group efficiency equal to one. Assuming densification of soil taking place in the installation and pile spacing greater than or equal to 3 times diameter, this assumption is justifiable. The comparison of field and analytical result indicates average error of 15% with field results. Difference is more for lower values of L/D ratio. With increase in of L/D ratio good agreement is observed between field and analytical approaches. Various parameters that are observed to influence the ultimate pullout capacity of the GAP system in the present study were length, diameter, spacing, number of GAP and the soil characteristics.

5.0 PERFORMANCE STUDY

Granular anchor pile (GAP) are mainly designed focusing its ability to resist uplift forces. In the present study, the performance of GAP and pile of same length and diameter are compared from economic considerations and their ultimate capacities. In the economic comparison, it is assumed that cost of installation of GAP and concrete pile is nearly same. Hence, only material costs are compared. Material costs are evaluated for four L/D considered in the study. Their material cost is reported in *Table 5* along with percentage difference. It can be observed that material cost is nearly increased by 100% for concrete piles. Difference is increasing with L/D ratio. Similarly, uplift capacity of concrete pile in same ground conditions are evaluated for four L/D considered in the study. The uplift capacity of GAP and pile are compared in *Table 5*. For smaller L/D ratio capacity of pile is 77 % less as compared to GAP. However, with increase in length, difference in capacity is reducing. For L/D ratio of 20, capacities are almost equal. This fact again underlines the importance of optimum L/D ratio of GAP.

Table 5 Ultimate Uplift capacity at site-1 for 300mm diameter GAP

No.	L/d	Material cost of GAP (INR)	Material cost of concrete pile (INR)	% difference	Ultimate Uplift capacity of GAP(kN)		Concrete Pile Strength (kN)
					Field Test	Analytical	
1	6.66	836.80	1653.25	97.57	45	27.4	9.92
2	10.0	1096.64	2248.58	105.04	70	54.1	20.19
3	13.3	1356.48	2843.91	109.65	75	67.7	34.39
4	20.0	1876.16	4034.57	115.04	80	78.8	74.02

6.0 CONCLUSIONS

The analysis of field test data indicate that the GAP system is an effective foundation system for structure subjected to uplift loads. Various parameters that are observed to influence the ultimate pullout capacity of the GAP system in the present study were length, diameter, spacing, number of GAP and the soil characteristics. Based on the study following conclusions are made:

1. Pullout capacities are observed to be increasing with the increase in L/D ratio up to an optimum value for L/D ratio.
2. For groups of GAP systems, the pullout capacities were found almost equal to the value of a single GAP system multiplied by the number of GAP systems.
3. The comparison of field and analytical result indicates average error of 15% with field results. Difference is more for lower values of L/D ratio. With increase in of L/D ratio good agreement is observed between field and analytical approaches.
4. From economic considerations, the material cost of GAP is nearly half of the concrete pile of same dimension. Hence it can be considered as an alternative option to pile foundation where site is not prone to earthquake hazard.
5. Comparison of uplift capacities indicated that GAP is more effective than pile at smaller L/D ratio.

REFERENCES

- [1] Kumar, P. (2002). Granular Anchor Pile System under Axial Pullout Loads, *Ph.D, Thesis*, I.I.T, Roorkee.
- [2] Phanikumar, B.R. (1997), A Study of Swelling Characteristics of Granular Pile Anchor Foundation System in Expansive Soils". *Ph.D. Thesis*, JNTU, Kakinada
- [3] Ranjan, G. and Kumar, P. (2000), Behaviour of Granular Piles under Compressive and Tensile Loads, *Geotechnical Engineering, J. of SEAGS*, 31(3) : 209-214.
- [4] Madhav, M.R and Vidyaranya, B. (2005), Analysis and Displacements of Granular Anchor Piles, *International Conference on Soil-Structure Interaction*, St. Petersburg.
- [5] Kranthikumar, A, Sawant, V. A., Pradeep Kumar and Shukla, S K, (2017), Numerical and Experimental Investigations of Granular Anchor Piles in Loose Sandy Soil Subjected to Uplift Loading, *International Journal of Geomechanics*, ASCE, 17(2): 04016059, 1-10
- [6] Kumar, P. and Ranjan, G. 1999. Granular Pile System for Uplifting Loads A Case Study. *Int. Conf. on Offshore and Near shore Geotechnical Engineering, GEOSHORE, Mumbai*, pp.427-432.
- [7] Phanikumar, B.R., Sharma, R.S., Srirama Rao, A. and Madhav, M.R. 2004. Granular Pile Anchor Foundation System for Improving the Engineering Behaviour of Expansive Clay Beds. *Geotech. Testing J., ASTM*, 27(3):1-9.
- [8] Ibrahim, S. F., Aljorany, A. N., & Aladly, A. I. (2014). Heave behavior of granular pile anchor-foundation (GPA-foundation) system in expansive soil. *J. Civil Eng. Urban*, 4(3), 213-222.
- [9] Johnson, N., & Sandeep, M. N. (2016). Ground Improvement Using Granular Pile Anchor Foundation. *Procedia Technology*, 24, 263-270.
- [10] Krishna, P. H., & Murty, V. R. (2016). Anchor Piled Footings—An Alternative Foundation Technique in Expansive Soils. *International Journal of Advanced Research in Engineering*, 2(2), 17-21.
- [11] Phanikumar, B. R. (2016). Influence of Geogrid Reinforcement on Pullout Response of Granular Pile-Anchors (GPAs) in Expansive Soils. *Indian Geotechnical Journal*, 46(4), 437-444.
- [12] Rao, B. G. (1982), Behaviour of Skirted Granular Piles, *Ph.D, Thesis*, University of Roorkee, Roorkee.

CHAPTER 16

REFINEMENT OF TOPOGRAPHICAL FACTOR FOR ESTIMATING SOIL LOSS AND SEDIMENT YIELD IN EQUATORIAL REGIONS

L. K. Yong¹, P. L. Law², S. N. L. Taib³, D. Y. S. Mah and A. H. Johari⁴

Abstract

This paper aims to improve the Topographical Factor for estimation soil loss and sediment yield in Equatorial region. In the Revised Universal Soil Loss Equation (RUSLE), Topographical factor (LS) is derived as soil loss amount related to gently-inclined plane surface of 72.6ft (22.13m) slope length and 9% slope gradient in United States of America (USA). The terrains in equatorial region (especially at construction sites) comprise of more cone-shaped and pyramid-shaped characterized with steeper slopes and shorter slope lengths as compared to agricultural lands in USA. Topographical Factors (T_T , T_C & T_P) in equatorial region were found as function of sediment yield (SY), surface runoff velocity (RV), and silt and clay compositions (SC). Triangular prism-shaped slope could be used as reference or indicator due to the shape is comparable or almost similar to that of the RUSLE's gently-inclined plane surface. Cone-shaped and pyramid-shaped showed approximately 80% and 77%, respectively similar to triangular prism-shaped. Therefore, the Topographical Factors for triangular prism-shaped, cone-shaped and pyramid-shaped landscapes in equatorial region: $T_T = 1.0 \times LS$ (Triangular Prism), $T_C = 0.8 \times LS$ (Cone) and $T_P = 0.77 \times LS$ (Pyramid).

Keywords: Topographical factors, slope length, slope steepness, equatorial.

1.0 INTRODUCTION

Topographical Factor (LS) in the Revised Universal Soil Loss Equation (RUSLE) can be defined as the soil loss ratio indicated by unit plot with slope length of 72.6ft (22.13m), 6ft (1.83m) width and slope gradient of 9% as shown in Figure 1 [1]. It is a combined index of the factors that could affect the soil loss amount which are slope length (L) and slope steepness (S). It is a measure of the capacity of overland flow/surface runoff to transport sediment/soil particles [2]. The LS is dimensionless, having LS values (RUSLE experimental values normalized to 72.6-ft slope length and 9% slope gradient) equal to or greater than zero [2]. The LS was developed by Wischmeier and Smith in 1958, together with other factors - rainfall erosivity (R), soil erodibility (K), cover management (C) and support practice (P) to form the Universal Soil Loss Equation (USLE) for soil loss prediction [1]. The USLE was later revised by Renard et al. in 1997 to become the Revised Universal Soil Loss Equation (RUSLE) for estimation of soil loss amount in agricultural areas [3].

The Revised Universal Soil Loss Equation (RUSLE) by Renard et al. (1997) can be considered as one of the best soil loss estimates for the agricultural sector in temperate regions as it is closely related to the amount of soil loss from agricultural lands [3,4]. The LS values in the RUSLE were evaluated from soil loss data on thirty-seven (37) agricultural/cultivated lands in the eastern USA where the terrain is composed of gently-inclined plane surfaces as illustrated in Figure 1 [1]. However, in equatorial regions,

^{1,2,3,4,5}Department of Civil Engineering, Universiti Malaysia Sarawak, 93000, Kota Samarahan, Sarawak, Malaysia

terrain (especially at construction sites) is characterized by steeper slopes and shorter slope lengths as compared to agricultural lands in the eastern USA. Since steeper and shorter hill slopes result in higher overland flows/surface runoffs as compared to RUSLE’s 37 experimental sites in the eastern USA, equatorial regions could experience more soil particles being washed downslope. Theoretically, the application of RUSLE’s LS in equatorial regions would grossly underestimate the soil loss rate and sediment yield.

This study aims to improve the Topographical Factors for different topographical shapes to estimate soil loss amount in equatorial regions; for instance, T_T for triangular prism-shaped, T_C for cone-shaped and T_P for pyramid-shaped. RUSLE’s LS considers gently-inclined plane surfaces only and does not consider T_C and T_P . RUSLE’s LS is generally applicable for four types of land, which are 1) rangeland and other consolidated soil conditions with cover (low ratio of rill to inter-rill erosion), 2) row-cropped agricultural and other moderately consolidated soil conditions with little-to-moderate cover (moderate ratio of rill to inter-rill erosion), 3) freshly prepared construction sites and other highly disturbed soil conditions with little or no cover (high ratio of rill to inter-rill erosion), and 4) thawing soils where most of the soil erosion is caused by surface flow (Table 1). Topographical factor (LS) was revised by Jones et al. (1996) with adopted U.S. Army Land Condition-Trend Analysis (LCTA) Data Gaps and thus proposed LS values (Table 1) for estimation of soil loss rate [5].

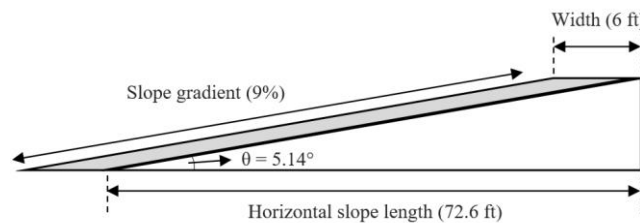


Figure 1: The unit plot shape of RUSLE

Table 1 LS values by previous researchers

No.	Typical Applications	LS Values (unitless)		
		Wischmeier & Smith (1958)	Renard et al. (1997)	Jones et al. (1996)
1.	Rangelands, pasture, other consolidated soils with cover		0.05 - 34.71	1.00
2.	Row-cropped agricultural and other moderately consolidated soil conditions with little to moderate cover	0.06 - 12.90	0.05 - 52.70	2.00
3.	Freshly prepared construction sites and other highly disturbed soil conditions with little or no cover		0.05 - 72.15	3.00
4.	Thawing soils where erosion is caused by surface flow		0.02 - 10.59	4.00

(Sources: Wischmeier & Smith, 1958; Renard et al., 1997; Jones et al., 1996)

In most soil erosion studies, soil loss amount is measured by sampling the sediment concentration of the runoff collected at the end of observation plots and then determining the LS values with reference to RUSLE’s unit plot (72.6-ft slope length and 9% slope gradient) [6]. LS values also can be determined by

using Digital Elevation Model (DEM), Open-Source C++ Program and Geographic Information System (GIS) which were developed based on topographical shapes (gently-inclined plane surfaces) in the eastern USA where slope length is 72.6 ft and slope gradient is 9% [7, 8, 9]. However, there are differences between soil loss and sediment yield. Soil loss can be defined as the movement of soil particles regardless of distance within an observation plot, while the amount of soil particles collected at the end of an observation plot is defined as sediment yield as illustrated in Figure 2 [10]. As the smaller soil particles such as silt and clay would be continually displaced during rainfall, soil loss cannot be measured due to the distance of moving soil particles and smaller sizes of soil particles cannot be observed. Sediment yield can be measured precisely (by measuring the concentration or total suspended solids of surface runoff) because the soil particles can be collected at the end of the observation plot.

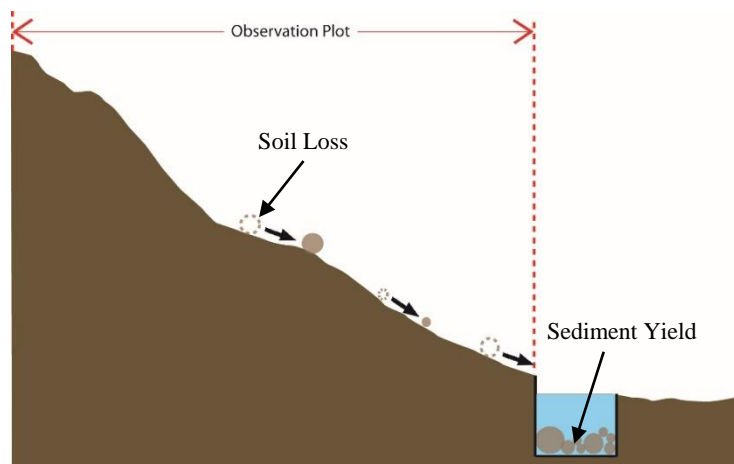


Figure 2 Soil loss and sediment yield

2.0 METHODOLOGY

2.1 SLOPE LENGTH FACTOR, L

Slope length is defined as the horizontal distance from the origin of overland flow to the point where deposition begins as shown in Figure 3 [2, 4]. The amount of soil loss and sediment yield increase with slope length [2, 4]. Slope length can be related to rill erosion due to surface runoff which is usually measured in less than 400-ft although longer slope lengths of up to 1000-ft are commonly found in United States of America (USA). Slope length can be measured on agricultural lands, while for steeper slopes (slope gradient more than 9%), slope lengths should be converted to horizontal distance for soil loss estimation by using the RUSLE [2, 4]. Slope lengths are commonly measured on contour maps, however slope lengths estimated from contour maps are usually too long [2, 4]. This is because most maps do not have the details to indicate all concentrated of runoff flow areas that accomplish RUSLE's defined slope length [2, 4].

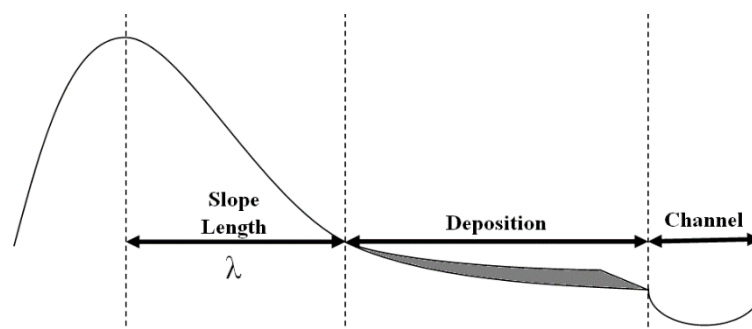


Figure 3 Slope profile defined in the RUSLE

The first equation published by Zingg (1940) for prediction of field soil loss which described the slope length factor is shown below [6, 11]:

$$L = a\lambda^m \quad (1)$$

where L is soil loss amount in mass per unit area per unit time, “λ” is the slope length in meters, “a” and “m” are empirical coefficients. Field studies at 37 agricultural sites in the eastern USA were carried out for soil loss data based on the slope profile illustrated in Figure 3 with slope lengths ranging from 30 to 300-ft and slope gradients ranging between 3 to 18% [1]. Average slope length and slope gradient for 37 agricultural sites are 72.6-ft (22.13-m) and 9%, respectively [1]. The slope length of 72.6-ft (22.13-m) was thus adopted/applied in the RUSLE to estimate soil loss as shown in Equations 2 and 3 [1]:

$$L = (\lambda/72.6)^m \text{ (unitless, } \lambda \text{ in feet)} \quad (2)$$

$$L = (\lambda/22.13)^m \text{ (unitless, } \lambda \text{ in meter)} \quad (3)$$

where:

λ = Horizontal slope length

m = A variable slope length exponent, unitless.

In the RUSLE, m is related to the ratio β of rill erosion to inter-rill erosion which is shown as a continuously increasing value as stated in the Equation 4.

$$m = \frac{\beta}{1+\beta} \quad (4)$$

where:

β = Sediment load contributed from rill erosion,

1 + β = Sediment load contributed from inter-rill erosion, and the value of β can be computed as shown in the following equation:

$$\beta = \frac{\text{SIN}\theta/0.0896}{3.0(\text{SIN}\theta)^{0.8}+0.56} \quad (5)$$

where:

θ = Slope angle in degree.

2.1.1 SLOPE LENGTH EXPONENT, m

Slope length exponent (m) is defined as the ratio of rill erosion to inter-rill/sheet erosion. Slope length factor (L) by several authors is dependent on the slope length exponent (m) as tabulated in Table 2. Rill erosion is affected by surface runoff, where higher amount of surface runoff would carry more soil particles in the rill. Inter-rill erosion happens due to the impact of falling raindrops, where larger raindrop size comprises of larger kinetic energy to detach the soil particles. Slope length affects rill and inter-rill/sheet erosion, where longer slope length could yield more severe rill and inter-rill/sheet erosion [4]. The effects of rill and inter-rill erosion have been evaluated separately by using uniform-gradient (0.2% to 60%) plots and thus classified the slope length exponent (m) values into low, moderate and high rill/inter-rill ratio [15]. The result of slope length exponent (m) was adopted in the RUSLE’s L-factor as shown in the Table 3.

Table 2 Slope-length exponents (m) by previous researchers

No.	Researchers	m Value		Remark
1.	Zingg, 1940 [11]	0.6		-
2.	Musgrave, 1947 [12]	0.3		-
3.	Wischmeier & Smith, 1958 [1]	<u>m value</u>	<u>Slope gradient</u>	Universal Soil Loss Equation (USLE)
		0.2	≤ 1%	
		0.3	1% to 3%	
		0.4	3.5% to 4.5%	
		0.5	≥ 5%	
4.	Moore & Burch, 1986 [13]	0.4		
5.	McCool et al., 1987 [14]	0.5		-
6.	Moore & Wilson, 1992 [2]	0.6		
7.	Renard et al., 1997 [4]	Table 3		Revised Universal Soil Loss Equation (RUSLE)
8.	Liu et al., 2000 [6]	0.44		Location at three sites on Loess Plateau of China.

Table 3 Slope-length exponents (m) in the RUSLE for range of slopes and rill/inter-rill erosion classes

Slope (%)	Rill/Inter-rill Ratio		
	Low	Moderate	High
0.2	0.02	0.04	0.07
0.5	0.04	0.08	0.16
1.0	0.08	0.15	0.26
2.0	0.14	0.24	0.39
3.0	0.18	0.31	0.47
4.0	0.22	0.36	0.53
5.0	0.25	0.40	0.57
6.0	0.28	0.43	0.60
8.0	0.32	0.48	0.65
10.0	0.35	0.52	0.68
12.0	0.37	0.55	0.71
14.0	0.40	0.57	0.72
16.0	0.41	0.59	0.74
20.0	0.44	0.61	0.76
25.0	0.47	0.64	0.78
30.0	0.49	0.66	0.79
40.0	0.52	0.68	0.81
50.0	0.54	0.70	0.82
60.0	0.55	0.71	0.83

(Sources: McCool et al., 1989; Renard et al., 1997)

2.2 SLOPE STEEPNESS FACTOR, S

Soil loss is strongly related to slope steepness that affects surface runoff velocity and infiltration rate. Surface runoff velocity is increasing with the gradient of slope, while the infiltration rate is decreasing [16, 17, 18]. Many classifications of slope steepness for soil and land surveys considered slope gradient of 30% as a starting point for “steep” slopes [19, 20, 21]. The data used to develop USLE and RUSLE

involved slopes only up to 18% [2, 4, 15, 21]. Table 4 shows the slope steepness factor (S) by previous researchers.

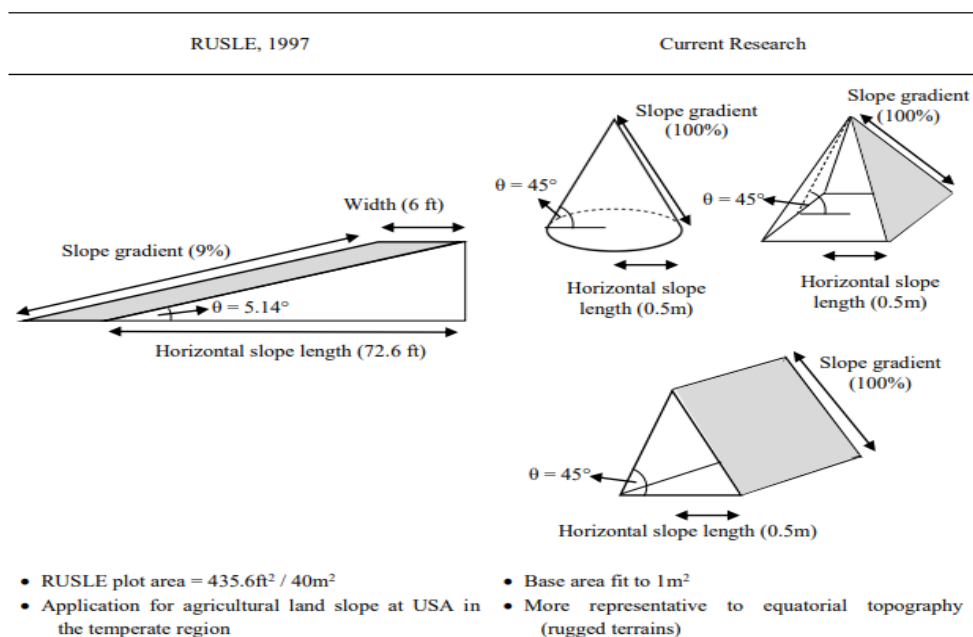
Table 4 Slope steepness factor (S value)

No.	Researchers	S value	Remark
1.	Wischmeier & Smith, 1978 [22]	$S = 65.41 \sin^2 \theta + 4.56 \sin \theta + 0.065$ $S = 10.8 \sin \theta + 0.03$ $S = 16.8 \sin \theta - 0.50$	Universal Soil Loss Equation (USLE) Slope gradient < 9% Slope gradient ≥ 9%
2.	McCool et al., 1987 [14]	$S = 3.0(\sin \theta)^{0.8} + 0.56$ $S = \left(\frac{\sin \theta}{0.0896}\right)^{0.6}$	Slope length < 15ft Water drains freely Thawing soils with slope gradient ≥ 9%
3.	Moore & Wilson, 1992 [2]	$S = \left(\frac{\sin \theta}{0.0896}\right)^{1.3}$	$0 < \theta \leq 90^\circ$
4.	Liu et al., 1994 [21]	$S = 21.91 \sin \theta - 0.96$	$0 < \theta \leq 90^\circ$
5.	Nearing, 1997 [23]	$S = -1.5 + \frac{17}{1 + e^{2.3-6.1 \sin \theta}}$	$0 < \theta \leq 90^\circ$

Most researchers normalized their results to 72.6-ft horizontal slope length and 9% slope gradient, developed by Wischmeier and Smith (1958) for agricultural lands in United States of America (USA); where the topographical shapes are “gently-inclined plane-surfaced” and characterized by relatively flat

and long slope length [4, 24, 25], while the terrains in equatorial regions especially at construction sites, comprise of comparatively more cone-shaped and pyramid-shaped topography characterized with steeper slopes and shorter slope lengths. Hence, higher rainfall intensity coupled with steeper and shorter hill slopes would result in higher surface runoff velocity (as compared to RUSLE’s 37 experimental sites in Eastern USA), could lead equatorial regions to experience more soil particles being washed down the slope. Table 5 compares the differences in topographical shapes between RUSLE and equatorial regions.

Table 5 RUSLE topographical shape vs equatorial



2.3 TOPOGRAPHICAL SHAPE MOULDS

Three topographical shapes (triangular prism, cone and pyramid) were developed to observe the surface runoff patterns, surface runoff velocity and amount of sediment yield. These topographical shapes were made by using fabricated moulds in accordance with Standard Proctor Test (SPT). The base area of the fabricated moulds were fixed to 1m² and divided into three compartments for the easement of soil filling and compaction. The method of soil compaction and number of blows were also in accordance with SPT. Triangular prism and pyramid moulds were fabricated by using 12-mm thick plywood, and the cone mould was made by using iron and aluminum because plywood could not make round shape. Table 6 shows the experimental moulds.

Table 6 Experimental moulds

Shape	Mould Design	Mounting Moulds
Triangular Prism	<p>Diagram of a triangular prism mould design. It shows a 3D view of a triangular prism with a 45-degree angle ($\theta = 45^\circ$) between the slope and the horizontal. The horizontal slope length is 0.5m. The slope gradient is 100%.</p>	<p>Photograph of the physical triangular prism moulds. It shows three wooden compartments of different sizes, each with a 45-degree slope, used for soil compaction.</p>
Cone	<p>Diagram of a cone mould design. It shows a 3D view of a cone with a 45-degree angle ($\theta = 45^\circ$) between the slope and the horizontal. The horizontal slope length is 0.5m. The slope gradient is 100%.</p>	<p>Photograph of the physical cone moulds. It shows two circular metal moulds of different sizes, one with a 45-degree slope, used for soil compaction.</p>
Pyramid	<p>Diagram of a pyramid mould design. It shows a 3D view of a pyramid with a 45-degree angle ($\theta = 45^\circ$) between the slope and the horizontal. The horizontal slope length is 0.5m. The slope gradient is 100%.</p>	<p>Photograph of the physical pyramid moulds. It shows three wooden compartments of different sizes, each with a 45-degree slope, used for soil compaction.</p>

2.4 SOIL SAMPLE PREPARATION

Two mineral soil samples were collected around Kuching, Sarawak: Sample Soil A was collected at a field near Santubong River and Sample Soil B was collected from a slope located at Kota Samarahan. Soil analysis for Grain Size Distribution and Standard Proctor Test (SPT) were carried out to obtain particle size distribution, soil composition, soil classification, optimum moisture content and maximum dry density. Two kilogram (2 kg) total mass of oven dried soil samples A and B were used for grain size

distribution analysis as shown in Figure 4. The soil samples were placed on woven wire mesh sieves (63µm-14mm) and separated into several sizes by using a sieve machine. All sieve pans were weighed before and after shaking; subsequently the percentage retained of each sieve was determined. Outcomes of grain size distribution and soil classification are shown in Figure 5 and Figure 6.



Figure 4 Soil samples

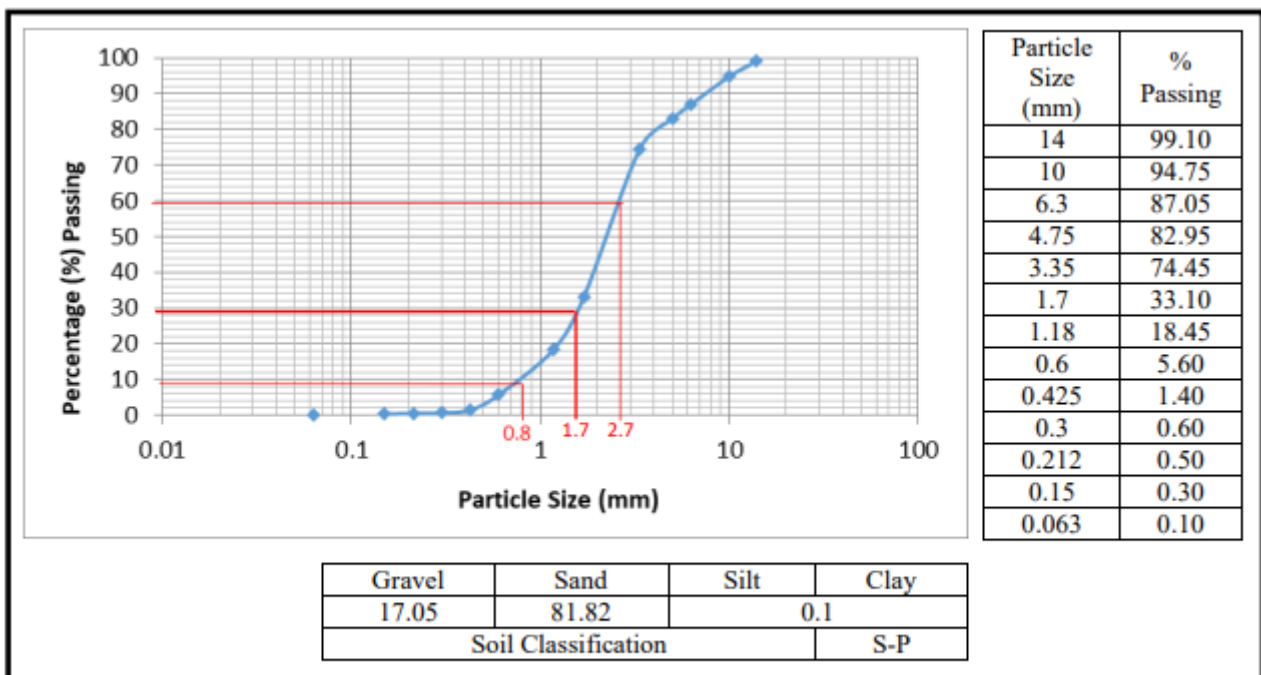


Figure 5 Grain size distribution of soil sample A

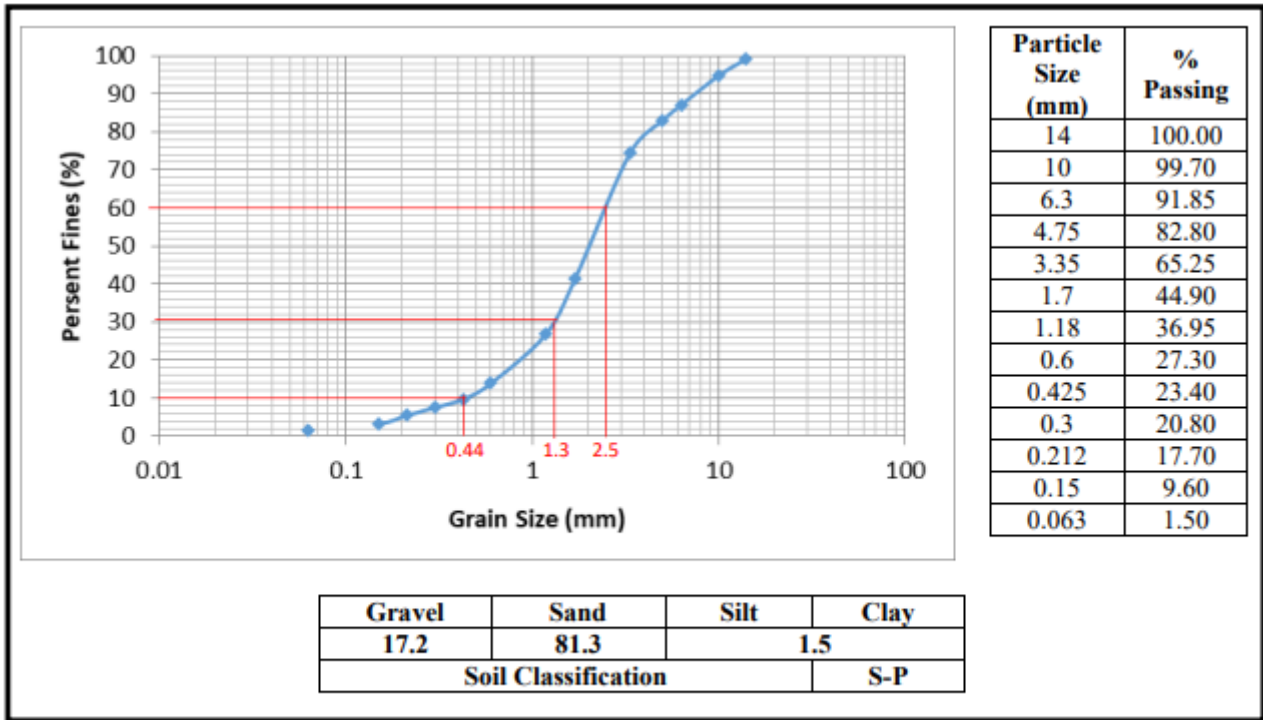


Figure 6 Grain size distribution of soil sample B

2.4 DEVELOPMENT OF TOPOGRAPHICAL FACTORS

In this research, topographical factors are a function of sediment yield (SY), surface runoff velocity (RV) and silt and clay compositions (SC). A rainfall simulator was fabricated to simulate equatorial “High-to-Extremely High” rainfall intensity of approximately 150mm/hr on triangular prism, cone and pyramid soil samples. Observations of sediment yield, surface runoff patterns coupled with surface runoff velocity and silt and clay compositions were carried out. Sediment yield can be defined as the amount of soil collected at the outflow end of an observation plot. The experimental soil samples were placed under simulated rainfall for 30 minutes with rainfall intensity of about 150mm/hr. The mass of soil samples would vary due to the huge amount of soil particles detached by raindrops and transported by surface runoff. The difference of soil sample mass (before and after rainfall simulation) is considered as sediment yield (SY).

Soil loss and sediment yield are strongly related to surface runoff velocity, whereby shorter slope length and steeper slope would result in higher surface runoff velocity that could transport more soil particles downslope. The surface runoff velocity on slope would increase with flow distance. Therefore the peak runoff velocity always occurs downslope; locations a, b, c, d and e on slopes were selected to compute the surface runoff velocity (RV). Surface runoff from each soil sample was collected in a sediment basin for the 30-minute rainfall simulation. The surface runoff velocity (RV) on slope at locations “a” to “e” can be determined by correlating the flow rate equation ($Q=AV$) and kinematic equation ($V^2=2gh$) as following equations:

$$RV = Q/A \tag{6}$$

$$RV = \sqrt{2gh} \tag{7}$$

where

RV = Surface runoff velocity, m/s

Q = Total volume of surface runoff, m³/s

A = Cross-sectional area of soil sample where surface runoff flows through ($A=L_n \times h$), m²

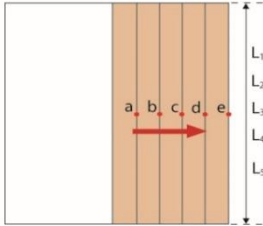
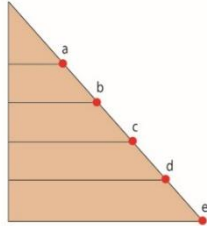
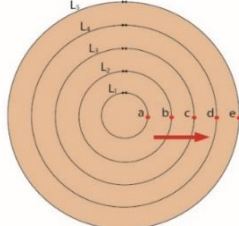
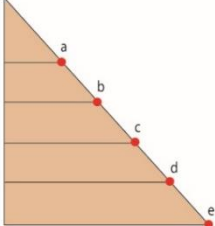
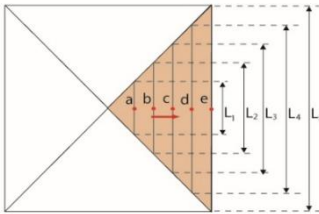
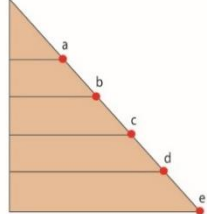
g = Gravitational constant, 9.81 m²/s

h = Height of surface runoff on slope, m

To determine the height of surface runoff on slope (h), equations (6) and (7) can be integrated and become equation (8). The length of cross-sectional area (L_n) of each topographical shape is shown in Table 7.

$$h^3 = \frac{Q^2}{2gL_n^2} \quad (n=1,2,3,4,5) \quad (8)$$

Table 7 Surface runoff pattern of triangular-, cone- and pyramid-shaped

Shape	Top View	Side View
Triangular Prism		
Cone		
Pyramid		

Note:  Flow Direction

Surface runoff velocity would carry small soil particles such as silt and clay from higher ground to downslope. However, the soil particles are transported from upslope to downslope whilst the compositions of surface soil would be continually changing; the smallest soil particles would be detached, followed by smaller particles that would be washed downslope. In this study, a small amount of soil samples at locations S1 to S5 (Figure 7) on slope were taken after 15- and 30-minute simulated rainfall events. The soil samples were placed into small containers and oven-dried for 24 hours, subsequently sieved passing through 63µm-opening sieve (silt & clay sizes <63 µm). Thus, the percentage of silt and clay compositions (SC) can be determined.

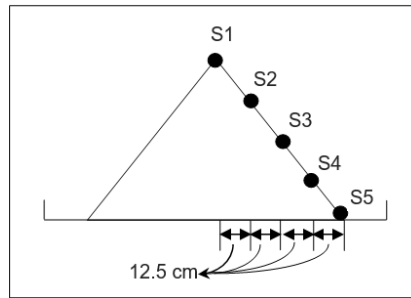


Figure 7 Locations S1 to S5 on soil sample slope



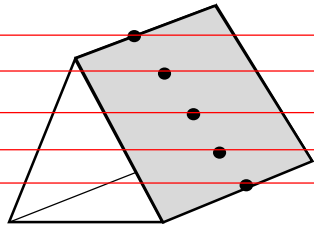
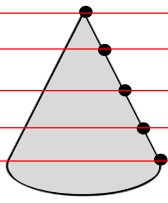
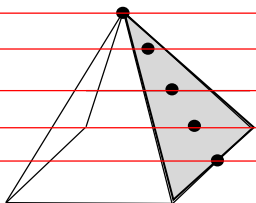
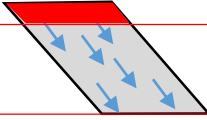
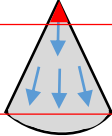
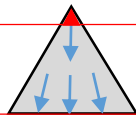
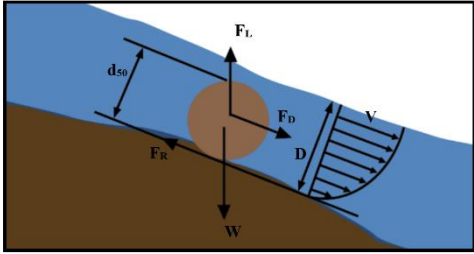
Figure 8 Soil samples collected at locations S1 to S5

In this study, topographical factors (T_T , T_C & T_P) were developed by correlating sediment yield (SY), surface runoff velocity (RV), and silt and clay compositions (SC). These sub-factors have their individual weightages, and those weightages were determined by comparing the percentage differences (%) of cone versus triangular prism and pyramid versus triangular prism. The topographical factor (T) can be expressed as in Equation 9. Table 7 shows the LS -factor in equatorial regions and its correlation to sediment yield, surface runoff velocity and soil compositions.

$$T = [a(SY) + b(RV) + c(SC)] \times LS \quad (9)$$

where,
 a, b, c = weightage, unitless

Table 7 LS-factor correlated with sediment yield (SY), surface runoff velocity (RV) and silt and clay compositions (SC)

	Triangular Prism	Cone	Pyramid
Locations S1 to S5 (Soil samples taken for determination of soil compositions after simulated rainfall events)			
			
	<ul style="list-style-type: none"> • Uniform top area, highest surface runoff velocity among three shapes. • Most rill erosion among three shapes. 	<ul style="list-style-type: none"> • Tapered top area small, surface runoff velocity lower. • Fewer rills would be formed. 	<ul style="list-style-type: none"> • Rapidly tapered top area among three shapes, lowest surface runoff velocity. • Fewer rills would be formed.
Surface Runoff			
	<ul style="list-style-type: none"> • Forces acting on soil particles when surface runoff occurs including lifting force (F_L), drag force due to the velocity of runoff (F_D), resistance force (F_R), and weight due to the gravity force (W). When a critical velocity (V) is exceeded due to the increasing depth of surface runoff (D), the soil particle (depending on particle size) would re-suspend to a new position [26]. 		
Topographical factor (LS)	$T_T = 1.0 (LS)^*$	$T_C = < 1.0 (LS)^*$	$T_P = < 1.0 (LS)^*$
	<p>(LS)* as the function of sediment yield, surface runoff velocity and silt & clay compositions</p> <p>= $a(SY) + b(RV) + c(SC)$, where a, b & c represent the weightage of soil loss contribution</p>		

2.6 SLOPE LENGTH EXPONENT, m VALUE

Slope length exponent, m, represents the ratio of rill to inter-rill erosion which is used for determination of slope length (L) in the RUSLE [2, 15]. However, m in the RUSLE considers slope only up to 60%,

while missing values of higher slope gradient (>60%) probably due to a lack of soil loss data. In this research, m values were extended to slope gradient 100% in this research by extrapolation as shown in

Table 8. RUSLE’s LS values for construction and other highly disturbed soil conditions are adopted in this research as shown in Table 9.

Table 8: Slope-length exponents (m) for range of slopes and rill/inter-rill erosion classes up to slope gradient 100%

Slope (%)	Rill/Interrill Ratio (m)		
	Low	Moderate	High
0.2	0.02	0.04	0.07
0.5	0.04	0.08	0.16
1.0	0.08	0.15	0.26
2.0	0.14	0.24	0.39
3.0	0.18	0.31	0.47
4.0	0.22	0.36	0.53
5.0	0.25	0.40	0.57
6.0	0.28	0.43	0.60
8.0	0.32	0.48	0.65
10.0	0.35	0.52	0.68
12.0	0.37	0.55	0.71
14.0	0.40	0.57	0.72
16.0	0.41	0.59	0.74
20.0	0.44	0.61	0.76
25.0	0.47	0.64	0.78
30.0	0.49	0.66	0.79
40.0	0.52	0.68	0.81
50.0	0.54	0.70	0.82
60.0	0.55	0.71	0.83
70.0	0.56*	0.72*	0.84*
80.0	0.57*	0.73*	0.85*
90.0	0.58*	0.74*	0.86*
100.0	0.59*	0.75*	0.87*

(Sources: McCool et al., 1989; Renard et al., 1997)

Note: * is the m value by extrapolation.

Table 9 RUSLE LS values for construction and other highly disturbed soil conditions

Slope gradient (%)	Horizontal Slope Length (ft)																
	<3	6	9	12	15	25	50	75	100	150	200	250	300	400	600	800	1000
0.2	0.05	0.05	0.05	0.05	0.05	0.05	0.05	0.05	0.05	0.05	0.06	0.06	0.06	0.06	0.06	0.06	0.06
0.5	0.07	0.07	0.07	0.07	0.07	0.07	0.08	0.08	0.09	0.09	0.10	0.10	0.10	0.11	0.12	0.12	0.13
1	0.09	0.09	0.09	0.09	0.09	0.10	0.13	0.14	0.15	0.17	0.18	0.19	0.20	0.22	0.24	0.26	0.27
2	0.13	0.13	0.13	0.13	0.13	0.16	0.21	0.25	0.28	0.33	0.37	0.40	0.43	0.48	0.56	0.63	0.69
3	0.17	0.17	0.17	0.17	0.17	0.21	0.30	0.36	0.41	0.50	0.57	0.64	0.69	0.80	0.96	1.10	1.23
4	0.20	0.20	0.20	0.20	0.20	0.26	0.38	0.47	0.55	0.68	0.79	0.89	0.98	1.14	1.42	1.65	1.86
5	0.23	0.23	0.23	0.23	0.23	0.31	0.46	0.58	0.68	0.86	1.02	1.16	1.28	1.51	1.91	2.25	2.55
6	0.26	0.26	0.26	0.26	0.26	0.36	0.54	0.69	0.82	1.05	1.25	1.43	1.60	1.90	2.43	2.89	3.30
8	0.32	0.32	0.32	0.32	0.32	0.45	0.70	0.91	1.10	1.43	1.72	1.99	2.24	2.70	3.52	4.24	4.91
10	0.35	0.37	0.38	0.39	0.40	0.57	0.91	1.20	1.46	1.92	2.34	2.72	3.09	3.75	4.95	6.03	7.02
12	0.36	0.41	0.45	0.47	0.49	0.71	1.15	1.54	1.88	2.51	3.07	3.60	4.09	5.01	6.67	8.17	9.57
14	0.38	0.45	0.51	0.55	0.58	0.85	1.40	1.87	2.31	3.09	3.81	4.48	5.11	6.30	8.45	10.40	12.23
16	0.39	0.49	0.56	0.62	0.67	0.98	1.64	2.21	2.73	3.68	4.56	5.37	6.15	7.60	10.26	12.69	14.96
20	0.41	0.56	0.67	0.76	0.84	1.24	2.10	2.86	3.57	4.85	6.04	7.16	8.23	10.24	13.94	17.35	20.57
25	0.45	0.64	0.80	0.93	1.04	1.56	2.67	3.67	4.59	6.30	7.88	9.38	10.81	13.53	18.57	23.24	27.66
30	0.48	0.72	0.91	1.08	1.24	1.86	3.22	4.44	5.58	7.70	9.67	11.55	13.35	16.77	23.14	29.07	34.71
40	0.53	0.85	1.13	1.37	1.59	2.41	4.24	5.89	7.44	10.35	13.07	15.67	18.17	22.95	31.89	40.29	48.29
50	0.58	0.97	1.31	1.62	1.91	2.91	5.16	7.20	9.13	12.75	16.16	19.42	22.57	28.60	39.95	50.63	60.84
60	0.63	1.07	1.47	1.84	2.19	3.36	5.97	8.37	10.63	14.89	18.92	22.78	26.51	33.67	47.18	59.93	72.15

3.0 RESULT AND DISCUSSION

3.1 SEDIMENT YIELD

Soil erosion can be defined as the movement of soil particle regardless of distance. The experimental topographical factors (T_T , T_C & T_P) are functions of sediment yield (SY), surface runoff velocity (RV) and percentage of silt and clay content (SC). Measurements of sediment yield, amount of rainwater for 30-minute rainfall simulation on soil sample, and the characteristics or compositions of silt and clay on slope after a rainfall event were carried out. Table 10 shows the recorded values of sediment yield after each simulated rainfall event.

Table 10 Experimental sediment yield of triangular-prism, cone and pyramid shapes

Shape	Triangular Prism		Cone		Pyramid	
	Sample A	Sample B	Sample A	Sample B	Sample A	Sample B
Soil Sample						
Weight Before (kg)	352.6	363.8	159.4	163.5	227.2	236.8
Weight After (kg)	345.5	356.2	155.8	159.7	223.0	232.2
Sediment Yield (kg/m ²)	7.1	7.6	3.6	3.8	4.2	4.6
Average Sediment Yield (kg/m ²)	7.4		3.7		4.4	

In Table 10, it is found that the triangular prism soil samples have the highest sediment yield with 7.1 kg/m² for sample A and 7.6 kg/m² for sample B with an average of 7.4 kg/m². The cone soil samples recorded the lowest sediment yield; 3.6 kg/m² for sample A and 3.8 kg/m² for sample B with an average sediment yield of about 3.7 kg/m². It is shown that the cone soil samples yielded approximately 50% lower than triangular prism. The pyramid sample A and sample B recorded sediment yield values of 4.2 and 4.6 kg/m², respectively, and an average sediment yield of about 4.4 kg/m² which is 40.5% lower than the triangular prism soil samples.

3.2 SURFACE RUNOFF VELOCITY

Sediment yield is strongly related to surface runoff velocity, whereby higher surface runoff velocity could transport more soil particles downslope, and hence more soil particles can be collected at the end of the experimental plot. The surface runoff patterns for triangular prism, cone and pyramid are illustrated in Table 11. Table 12 and Figure 7 show the summary of calculated velocities at locations “a” to “e” on the three soil sample shapes.

Table 12: Surface runoff velocities at locations a-e on soil sample shapes

Location	Surface Runoff Velocity, RV (cm/s)		
	Triangular Prism	Cone	Pyramid
a	4.17	3.59	3.37
b	5.26	4.52	4.25
c	6.02	5.17	4.87
d	6.62	5.69	5.35
e	7.13	6.14	5.78

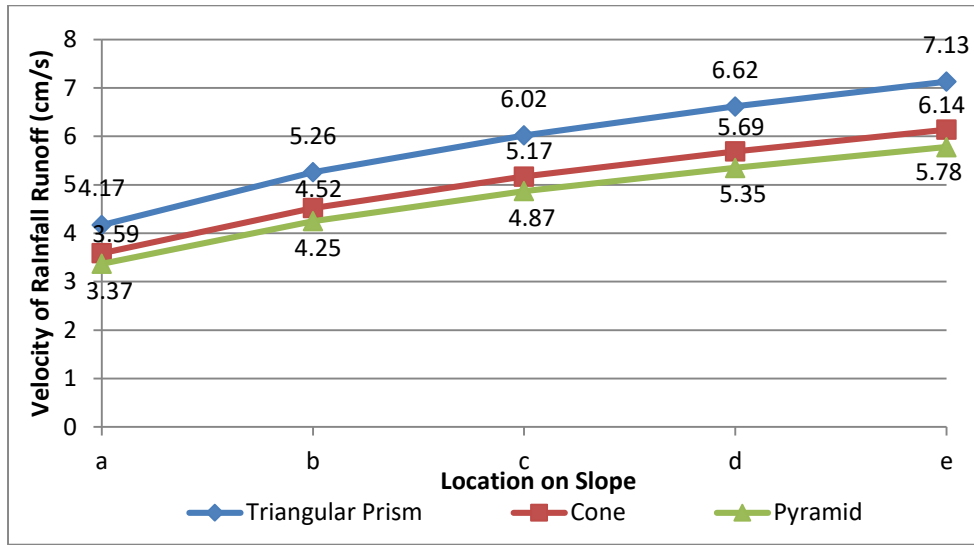


Figure 7 Surface runoff velocities at locations a-e for triangular prism, cone and pyramid soil sample shapes

In Table 12, the triangular prism soil sample shows the highest surface runoff velocity (RV) among the three shapes at 4.17, 5.26, 6.02, 6.62 and 7.13 cm/s at locations a, b, c, d and e, respectively. The cone RV values measured 3.59, 4.52, 5.17, 5.69 and 6.14 cm/s at locations “a” to “e”, respectively. The pyramid RV values recorded 3.37, 4.25, 4.87, 5.35 and 5.78 cm/s at location “a” to “e”, respectively, indicating the lowest values recorded among the three shapes. The triangular prism-shaped slope could be used as the reference or as an indicator since the characteristics of slope surface is similar to that of the plane slope surface of the RUSLE. Table 13 compares the dissimilarity in surface runoff velocity (RV) at locations “a” to “e” among the three shapes. The average cone RV value of 14.01% lower and pyramid RV value of 19.12% lower were recorded as compared to the observed values of the triangular prism samples.

Table 13 Percentage comparison of surface runoff velocity (RV) at locations “a” to “e”

Location	Triangular Prism (RUSLE) (cm/s)	Cone (cm/s)	Cone % Lower than Triangular Prim (RUSLE)
a	4.17	3.59	13.91 %
b	5.26	4.52	14.07 %
c	6.02	5.17	14.12 %
d	6.62	5.69	14.05 %
e	7.13	6.14	13.88 %
		Average	14.01 %
Location	Triangular Prism (RUSLE) (cm/s)	Pyramid (cm/s)	Pyramid % Lower than Triangular Prim (RUSLE)
a	4.17	3.37	19.18 %
b	5.26	4.25	19.20 %
c	6.02	4.87	19.10 %
d	6.62	5.35	19.18 %
e	7.13	5.78	18.93 %
		Average	18.93 %

3.3 SILT AND CLAY COMPOSITIONS

Small particles such as silt and clay have been transported downslope by surface runoff. The composition of surface soil would be continually changing during rainfall since the smaller particles (silt and clay) were displaced continuously. Small amount of soil samples were taken to test the percentage of silt and clay at locations S1 to S5 after 15-minute and 30-minute rainfall simulation. The results of silt and clay percentages for sample A and sample B are shown in Table 14 and Table 15.

Table 14 Comparison of silt & clay of cone-shaped vs triangular prism-shaped

Location	Percentage of Silt and Clay at 15-min Rainfall Simulation					
	Triangular Prism		Cone		% higher or lower	
	Sample A	Sample B	Sample A	Sample B	Sample A	Sample B
S1	11.4%	40.7%	17.8%	52.7%	6.4%	12.0%
S2	12.4%	54.8%	15.8%	47.8%	3.4%	7.0%
S3	13.0%	53.3%	19.1%	48.9%	6.1%	4.4%
S4	14.6%	49.2%	16.6%	50.2%	2.0%	1.0%
S5	15.1%	46.5%	15.4%	59.6%	0.3%	13.1%
				Average	3.6%	7.5%
						5.6%
Location	Percentage of Silt and Clay at 30-min Rainfall Simulation					
	Triangular Prism		Cone		% higher or lower	
	Sample A	Sample B	Sample A	Sample B	Sample A	Sample B
S1	10.2%	27.9%	14.6%	29.9%	4.4%	2.0%
S2	10.8%	54.0%	12.7%	41.3%	1.9%	12.7%
S3	12.6%	42.8%	16.0%	50.5%	3.4%	7.7%
S4	14.3%	49.4%	16.4%	53.6%	2.1%	4.2%
S5	13.7%	44.2%	13.8%	48.6%	0.1%	4.4%
				Average	2.4%	6.2%
						4.3%

Table 15 Comparison of silt & clay of pyramid-shaped vs triangular prism-shaped

Location	Percentage of Silt and Clay at 15-min Rainfall Simulation					
	Triangular Prism		Pyramid		% higher or lower	
	Sample A	Sample B	Sample A	Sample B	Sample A	Sample B
S1	11.4	40.7	11.9	30.7	4.4%	10.0%
S2	12.4	54.8	9.8	30.9	21.0%	23.9%
S3	13.0	53.3	14.5	48.2	11.5%	5.1%
S4	14.6	49.2	10.7	44.0	26.7%	5.2%
S5	15.1	46.5	7.5	37.3	50.3%	9.2%
				Average	22.8%	10.7%
						16.8%
Location	Percentage of Silt and Clay at 30-min Rainfall Simulation					
	Triangular Prism		Pyramid		% higher or lower	
	Sample A	Sample B	Sample A	Sample B	Sample A	Sample B
S1	10.2	27.9	9.8	25.5	3.9%	2.4%
S2	10.8	54.0	12.6	30.8	16.7%	23.2%
S3	12.6	42.8	12.1	29.6	4.0%	13.2%
S4	14.3	49.4	11.9	33.1	16.8%	16.3%
S5	13.7	44.2	6.4	43.6	53.3%	0.6%
				Average	18.9%	11.1%
						15.0%

Table 14 shows the composition of silt and clay (sample A and sample B) at the slope surface for the cone and triangular prism samples after 15-minute and 30-minute simulated rainfall events. The compositions of silt and clay on the slope of soil samples at locations S1 to S5 show inconsistency for both sample A and sample B. The composition of silt and clay particles for sample A and sample B for 15-minute rainfall event recorded 3.6% and 7.5%, respectively. For 30-minute rainfall simulation, the silt and clay recorded 2.4% and 6.2% for sample A and sample B, respectively. Hence, the average silt and clay compositions on slopes of cone and triangular prism shapes is 5.0%.

In Table 15, an inconsistency in the composition of silt and clay at locations S1 to S5 was noticed. The average silt and clay percentages for sample A and sample B were 22.8% and 10.7% respectively for the 15-minute simulated rainfall event. For the 30-minute simulation, the average compositions of silt and clay were approximately 18.9% and 11.1% for sample A and sample B, respectively. Hence, the average silt and clay composition on the slopes of pyramid and triangular prism shapes is 15.9%.

3.4 TOPOGRAPHICAL FACTOR AS FUNCTION OF SEDIMENT YIELD, RUNOFF VELOCITY AND SILT/CLAY COMPOSITION

In this study, the triangular prism slope can be used as the reference or as an indicator since the characteristics are similar to the plane slope surface of the RUSLE. The cone and pyramid shapes are compared by the degree of similarity or dissimilarity to the triangular prism (Table 16). Table 17 shows the normalized topographical factors or weightages for determination of coefficient of LS-factor in Equation 10.

Table 16 Difference and similarity of cone- and pyramid-shaped as compared to triangular prism-shaped

Cone-shaped	% Difference	% Similarity
Sediment Yield (SY)	50.0%	50.0%
Surface Runoff Velocity (RV)	14.0%	86.0%
% Silt & Clay (SC)	5.0%	95.0%

Pyramid-shaped	% Difference	% Similarity
Sediment Yield (SY)	40.5%	59.5%
Surface Runoff Velocity (RV)	19.1%	80.9%
% Silt & Clay (SC)	15.9%	84.1%

Table 17 Normalization of topographical factors

No.	Cone-shaped	Pyramid-shaped
1.	$\frac{(0.2)(0.50) + (0.5)(0.86) + (0.3)(0.95)}{0.815}$	$\frac{(0.2)(0.60) + (0.5)(0.81) + (0.3)(0.84)}{0.777}$
2.	$\frac{(0.25)(0.50) + (0.5)(0.86) + (0.25)(0.95)}{0.793}$	$\frac{(0.25)(0.60) + (0.5)(0.81) + (0.25)(0.84)}{0.765}$
3.	$\frac{(0.2)(0.50) + (0.6)(0.86) + (0.2)(0.95)}{0.806}$	$\frac{(0.2)(0.60) + (0.6)(0.81) + (0.2)(0.84)}{0.774}$
Average	0.80	0.77

In Table 16, the sediment yield of cone and pyramid shapes are 50% and 59.5% respectively, similar to the triangular prism; SY values are 0.5 and 0.6 respectively. The surface runoff velocities are 86% and 80.9%, for cone and pyramid respectively, similar to triangular prism; RV values are 0.86 and 0.81 for cone and pyramid respectively. The degree of similarity of silt and clay compositions of cone and pyramid was 95% and 84.1% respectively compared to triangular prism. In Table 17, the average coefficient is 0.8 for cone and 0.77 for pyramid. Therefore, topographical factors can be written as:

$$T_T = 1.0 \times LS \quad (\text{for triangular prism-shaped terrain}) \quad (11)$$

$$T_C = 0.8 \times LS \quad (\text{for cone-shaped terrain}) \quad (12)$$

$$T_P = 0.77 \times LS \quad (\text{for pyramid-shaped terrain}) \quad (13)$$

Table 18, Table 19 and Table 20 show the normalized Equatorial Topographical Factor for the three terrain shapes.

Table 18 Normalized topographical factor for triangular prism-shaped terrain (T_T)

Slope gradient (%)	Horizontal Slope Length (ft)																
	<3	6	9	12	15	25	50	75	100	150	200	250	300	400	600	800	1000
0.2	0.05	0.05	0.05	0.05	0.05	0.05	0.05	0.05	0.05	0.05	0.06	0.06	0.06	0.06	0.06	0.06	0.06
0.5	0.07	0.07	0.07	0.07	0.07	0.07	0.08	0.08	0.09	0.09	0.10	0.10	0.10	0.11	0.12	0.12	0.13
1	0.09	0.09	0.09	0.09	0.09	0.10	0.13	0.14	0.15	0.17	0.18	0.19	0.20	0.22	0.24	0.26	0.27
2	0.13	0.13	0.13	0.13	0.13	0.16	0.21	0.25	0.28	0.33	0.37	0.40	0.43	0.48	0.56	0.63	0.69
3	0.17	0.17	0.17	0.17	0.17	0.21	0.30	0.36	0.41	0.50	0.57	0.64	0.69	0.80	0.96	1.10	1.23
4	0.20	0.20	0.20	0.20	0.20	0.26	0.38	0.47	0.55	0.68	0.79	0.89	0.98	1.14	1.42	1.65	1.86
5	0.23	0.23	0.23	0.23	0.23	0.31	0.46	0.58	0.68	0.86	1.02	1.16	1.28	1.51	1.91	2.25	2.55
6	0.26	0.26	0.26	0.26	0.26	0.36	0.54	0.69	0.82	1.05	1.25	1.43	1.60	1.90	2.43	2.89	3.30
8	0.32	0.32	0.32	0.32	0.32	0.45	0.70	0.91	1.10	1.43	1.72	1.99	2.24	2.70	3.52	4.24	4.91
10	0.35	0.37	0.38	0.39	0.40	0.57	0.91	1.20	1.46	1.92	2.34	2.72	3.09	3.75	4.95	6.03	7.02
12	0.36	0.41	0.45	0.47	0.49	0.71	1.15	1.54	1.88	2.51	3.07	3.60	4.09	5.01	6.67	8.17	9.57
14	0.38	0.45	0.51	0.55	0.58	0.85	1.40	1.87	2.31	3.09	3.81	4.48	5.11	6.30	8.45	10.40	12.23
16	0.39	0.49	0.56	0.62	0.67	0.98	1.64	2.21	2.73	3.68	4.56	5.37	6.15	7.60	10.26	12.69	14.96
20	0.41	0.56	0.67	0.76	0.84	1.24	2.10	2.86	3.57	4.85	6.04	7.16	8.23	10.24	13.94	17.35	20.57
25	0.45	0.64	0.80	0.93	1.04	1.56	2.67	3.67	4.59	6.30	7.88	9.38	10.81	13.53	18.57	23.24	27.66
30	0.48	0.72	0.91	1.08	1.24	1.86	3.22	4.44	5.58	7.70	9.67	11.55	13.35	16.77	23.14	29.07	34.71
40	0.53	0.85	1.13	1.37	1.59	2.41	4.24	5.89	7.44	10.35	13.07	15.67	18.17	22.95	31.89	40.29	48.29
50	0.58	0.97	1.31	1.62	1.91	2.91	5.16	7.20	9.13	12.75	16.16	19.42	22.57	28.60	39.95	50.63	60.84
60	0.63	1.07	1.47	1.84	2.19	3.36	5.97	8.37	10.63	14.89	18.92	22.78	26.51	33.67	47.18	59.93	72.15
70	0.63	1.12	1.58	2.01	2.43	3.73	6.68	9.39	11.95	16.80	21.40	25.81	30.08	38.30	53.84	68.56	82.69
80	0.67	1.20	1.69	2.16	2.62	4.04	7.28	10.28	13.12	18.52	23.65	28.59	33.38	42.63	60.17	76.84	92.89
90	0.69	1.26	1.78	2.28	2.77	4.29	7.79	11.04	14.14	20.04	25.67	31.10	36.38	46.59	66.03	84.57	102.46
100	0.71	1.30	1.85	2.38	2.89	4.50	8.23	11.71	15.03	21.39	27.48	33.37	39.10	50.22	71.46	91.79	111.45

Table 19 Normalized topographical factor for cone-shaped terrain (T_C)

Slope gradient (%)	Horizontal Slope Length (ft)																
	<3	6	9	12	15	25	50	75	100	150	200	250	300	400	600	800	1000
0.2	0.04	0.04	0.04	0.04	0.04	0.04	0.04	0.04	0.04	0.04	0.05	0.05	0.05	0.05	0.05	0.05	0.05
0.5	0.06	0.06	0.06	0.06	0.06	0.06	0.06	0.06	0.07	0.07	0.08	0.08	0.08	0.09	0.10	0.10	0.10
1	0.07	0.07	0.07	0.07	0.07	0.07	0.08	0.10	0.11	0.12	0.14	0.14	0.15	0.16	0.18	0.21	0.22
2	0.10	0.10	0.10	0.10	0.10	0.13	0.17	0.20	0.22	0.26	0.30	0.32	0.34	0.38	0.45	0.50	0.55
3	0.14	0.14	0.14	0.14	0.14	0.17	0.24	0.29	0.33	0.40	0.46	0.51	0.55	0.64	0.77	0.88	0.98
4	0.16	0.16	0.16	0.16	0.16	0.21	0.30	0.38	0.44	0.54	0.63	0.71	0.78	0.91	1.14	1.32	1.49
5	0.18	0.18	0.18	0.18	0.18	0.25	0.37	0.46	0.54	0.69	0.82	0.93	1.02	1.21	1.53	1.80	2.04
6	0.21	0.21	0.21	0.21	0.21	0.29	0.43	0.55	0.66	0.84	1.00	1.14	1.28	1.52	1.94	2.31	2.64
8	0.26	0.26	0.26	0.26	0.26	0.36	0.56	0.73	0.88	1.14	1.38	1.59	1.79	2.16	2.82	3.39	3.93
10	0.28	0.30	0.30	0.31	0.32	0.46	0.73	0.96	1.17	1.54	1.87	2.18	2.47	3.00	3.96	4.82	5.62
12	0.29	0.33	0.36	0.38	0.39	0.57	0.92	1.23	1.50	2.01	2.46	2.88	3.27	4.01	5.34	6.54	7.66
14	0.30	0.36	0.41	0.44	0.46	0.68	1.12	1.50	1.85	2.47	3.05	3.58	4.09	5.04	6.76	8.32	9.78
16	0.31	0.39	0.45	0.50	0.54	0.78	1.31	1.77	2.18	2.94	3.65	4.30	4.92	6.08	8.21	10.15	11.97
20	0.33	0.45	0.54	0.61	0.67	0.99	1.68	2.29	2.86	3.88	4.83	5.73	6.58	8.19	11.15	13.88	16.46

25	0.36	0.51	0.64	0.74	0.83	1.25	2.14	2.94	3.67	5.04	6.30	7.50	8.65	10.82	14.86	18.59	22.13
30	0.38	0.58	0.73	0.86	0.99	1.49	2.58	3.55	4.46	6.16	7.74	9.24	10.68	13.42	18.51	23.26	27.77
40	0.42	0.68	0.90	1.10	1.27	1.93	3.39	4.71	5.95	8.28	10.46	12.54	14.54	18.36	25.51	32.23	38.63
50	0.46	0.78	1.05	1.30	1.53	2.33	4.13	5.76	7.30	10.20	12.93	15.54	18.06	22.88	31.96	40.50	48.67
60	0.50	0.86	1.18	1.47	1.75	2.69	4.78	6.70	8.50	11.91	15.14	18.22	21.21	26.94	37.74	47.94	57.72
70	0.50	0.90	1.27	1.61	1.94	2.98	5.34	7.51	9.56	13.44	17.12	20.65	24.06	30.64	43.07	54.85	66.16
80	0.53	0.96	1.36	1.73	2.09	3.23	5.82	8.22	10.50	14.82	18.92	22.87	26.71	34.11	48.14	61.48	74.32
90	0.55	1.01	1.43	1.83	2.21	3.43	6.23	8.83	11.31	16.04	20.54	24.88	29.11	37.28	52.83	67.66	81.97
100	0.57	1.04	1.48	1.90	2.31	3.60	6.58	9.36	12.03	17.12	21.98	26.69	31.28	40.18	57.17	73.43	89.16

Table 20 Normalized topographical factor for pyramid-shaped terrain (T_p)

Slope gradient (%)	Horizontal Slope Length (ft)																
	<3	6	9	12	15	25	50	75	100	150	200	250	300	400	600	800	1000
0.2	0.04	0.04	0.04	0.04	0.04	0.04	0.04	0.04	0.04	0.04	0.05	0.05	0.05	0.05	0.05	0.05	0.05
0.5	0.05	0.05	0.05	0.05	0.05	0.05	0.06	0.06	0.07	0.07	0.08	0.08	0.08	0.08	0.09	0.09	0.10
1	0.07	0.07	0.07	0.07	0.07	0.08	0.10	0.11	0.12	0.13	0.14	0.15	0.15	0.17	0.18	0.20	0.21
2	0.10	0.10	0.10	0.10	0.10	0.12	0.16	0.19	0.22	0.25	0.28	0.31	0.33	0.37	0.43	0.49	0.53
3	0.13	0.13	0.13	0.13	0.13	0.16	0.23	0.28	0.32	0.39	0.44	0.49	0.53	0.62	0.74	0.85	0.95
4	0.15	0.15	0.15	0.15	0.15	0.20	0.29	0.36	0.42	0.52	0.61	0.69	0.75	0.88	1.09	1.27	1.43
5	0.18	0.18	0.18	0.18	0.18	0.24	0.35	0.45	0.52	0.66	0.79	0.89	0.99	1.16	1.47	1.73	1.96
6	0.20	0.20	0.20	0.20	0.20	0.28	0.42	0.53	0.63	0.81	0.96	1.10	1.23	1.46	1.87	2.23	2.54
8	0.25	0.25	0.25	0.25	0.25	0.35	0.54	0.70	0.85	1.10	1.32	1.53	1.72	2.08	2.71	3.26	3.78
10	0.27	0.28	0.29	0.30	0.31	0.44	0.70	0.92	1.12	1.48	1.80	2.09	2.38	2.89	3.81	4.64	5.41
12	0.28	0.32	0.35	0.36	0.38	0.55	0.89	1.19	1.45	1.93	2.36	2.77	3.15	3.86	5.14	6.29	7.37
14	0.29	0.35	0.39	0.42	0.45	0.65	1.08	1.44	1.78	2.38	2.93	3.45	3.93	4.85	6.51	8.01	9.42
16	0.30	0.38	0.43	0.48	0.52	0.75	1.26	1.70	2.10	2.83	3.51	4.13	4.74	5.85	7.90	9.77	11.52
20	0.32	0.43	0.52	0.59	0.65	0.95	1.62	2.20	2.75	3.73	4.65	5.51	6.34	7.88	10.73	13.36	15.84
25	0.35	0.49	0.62	0.72	0.80	1.20	2.06	2.83	3.53	4.85	6.07	7.22	8.32	10.42	14.30	17.89	21.30
30	0.37	0.55	0.70	0.83	0.95	1.43	2.48	3.42	4.30	5.93	7.45	8.89	10.28	12.91	17.82	22.38	26.73
40	0.41	0.65	0.87	1.05	1.22	1.86	3.26	4.54	5.73	7.97	10.06	12.07	13.99	17.67	24.56	31.02	37.18
50	0.45	0.75	1.01	1.25	1.47	2.24	3.97	5.54	7.03	9.82	12.44	14.95	17.38	22.02	30.76	38.99	46.85
60	0.49	0.82	1.13	1.42	1.69	2.59	4.60	6.44	8.19	11.47	14.57	17.54	20.41	25.93	36.33	46.15	55.56
70	0.48	0.87	1.22	1.55	1.87	2.87	5.14	7.23	9.20	12.94	16.48	19.87	23.16	29.49	41.46	52.79	63.67
80	0.51	0.92	1.30	1.67	2.01	3.11	5.61	7.91	10.10	14.26	18.21	22.02	25.71	32.83	46.33	59.17	71.53
90	0.53	0.97	1.37	1.76	2.13	3.31	6.00	8.50	10.89	15.43	19.77	23.95	28.01	35.88	50.85	65.12	78.89
100	0.55	1.00	1.42	1.83	2.22	3.47	6.33	9.01	11.58	16.47	21.16	25.69	30.11	38.67	55.03	70.68	85.82

4.0 CONCLUSION

In conclusion, topographical factors (T_T, T_C & T_P) in equatorial regions were found as functions of sediment yield (SY), surface runoff velocity (RV) and silt and clay compositions (SC). The triangular prism shape was used as an indicator for cone and pyramid shapes due to the similar shape to RUSLE's plot which is an inclined plane surface. Cone showed 50% similarity of sediment yield, 86% of surface runoff velocity and 95% of silt and clay compositions compared to triangular prism. The similarity of sediment yield, surface runoff velocity and silt and clay compositions were 59.5%, 80.9% and 84.1% respectively compared to triangular prism. Therefore, this research experimentally developed the topographical factors for triangular prism-shaped, cone-shaped and pyramid-shaped landscapes: T_T = 1.0 × LS (Triangular Prism), T_C = 0.8 × LS (Cone) and T_P = 0.77 × LS (Pyramid). These Topographical Factors (T_T, T_C & T_P) can be used to replace the RUSLE's and MUSLE's LS to estimate the soil loss and sediment yield in equatorial regions.

REFERENCES

- [1] Wischmeier, W.H., & Smith, D.D. (1958). Rainfall Energy and Its Relationship to Soil Loss. *Transaction American Geophysical Union*, 39(2): 285-291.
- [2] Moore, I.D., & Wilson, J.P. (1992). Length-slope Factors for the Revised Universal Soil Loss Equation: Simplified Method of Estimation. *Journal of Soil and Water Conservation*, 47(5): 423-428.
- [3] El-Hassanin, A.S., Labib, T.M. and Gaber, E.I. (1993). Effect of Vegetation Cover and Landscape on Runoff and Soil Losses from Watersheds of Burundi. *Agricultural Ecosystems and Environment*. 43, 301-308.
- [4] Renard, K.G., Foster, G.R., Weesies, G.A., McCool, D.K. and Yoder, D.C. (1997). *Predicting Soil Erosion by Water: A Guide to Conservation Planning with the Revised Universal Soil Loss Equation*. U.S. Department of Agriculture, Agriculture Handbook 703, pp.384.
- [5] Jones, D.S., Kowalski, D.G., & Shaw, R.B. (1996). Calculating Revised Universal Soil Loss Equation (RUSLE) Estimates on Department of Defense Lands: A Review of RUSLE Factors and U.S. Army Land Condition-Trend Analysis (LCTA) Data Gaps.
- [6] Liu, B.Y., Nearing, M.A., Shi, P.J., & Jia, Z.W. (2000). Slope Length Effects on Soil Loss for Steep Slopes. *Soil Science Society of America Journal*, 64: 1759-1763.
- [7] Desmet, P.J.J., and Govers, G. (1996). A GIS-procedure for automatically calculating the USLE LS-factor on topographically complex landscape units. *Journal of Soil and Water Conservation*, 51(5), 427-433.
- [8] Mukherjee, S., Joshi, P.K., Mukherjee, S., Ghosh, A., Garg, R.D. & Mukhopadhyay, A. (2014). Evaluation of vertical accuracy of open source Digital Elevation Model (DEM). *International Journal of Applied Earth Observation and Geoinformation*, 21:205–217.
- [9] Panagos, P., Borrelli, P. and Meusburger, K. (2015). A New European Slope Length and Steepness Factor (LS-Factor) for Modeling Soil Erosion by water. *Geosciences* 5, 117-126.
- [10] Lal, R. (1994). Global Soil Erosion by Water and Carbon Dynamics. In Lal, R., Kimble, J.M., Levine, E. & Stewart, B.A. (Eds). *Soils and Global Change*. CRC/Lewis Boca Raton, FL: 131-41.
- [11] Zingg, A.W. (1940). Degree and Length of Land Slope as It Affects Soil Loss in Runoff. *Agricultural Engineering*, 21(2):59-64.
- [12] Musgrave, G.W. (1947). The Quantitative Evaluation of Factors in Water Erosion - A First Approximation. *Journal of Soil and Water Conservation*, 2: 133-138.
- [13] Moore, I. and Burch, G. (1986) Physical basis of the length-slope factor in the Universal Soil Loss Equation. *Soil Science of America Journal*, 50: 1294 – 1298.
- [14] McCool, D.K., Brown, L.C., Foster, G.R., Mutchler, C.K., and Meyer L.D. (1987). Revised Slope Steepness factor for the Universal Soil Loss Equation. *Transaction of the America Society of Agricultural Engineers*, 30:1387-1396.
- [15] McCool, D.K., Brown, L.C., Foster, G.R., Mutchler, C.K., & Meyer L.D. (1989). Revised Slope factor for the Universal Soil Loss Equation. *Transaction of the America Society of Agricultural Engineers*, 32:1571-1576.
- [16] Sharma, K., Singh, H., & Pareek, O. (1983). Rainwater Infiltration into a Bare Loamy Sand. *Hydrological Science Journal*, 28: 417-424.
- [17] Luk, S.H., Cai, Q., & Wang, G.P. (1993). Effects of Surface Crusting and Slope Gradient on Soil and Water Losses in the Illy Loess Egon, North China. *Catena*, 24: 29-45.
- [18] Fox, D.M., Bryan, R.B., & Price, A.G. (1997). The Influence of Slope Angle on Final Infiltration Rate for Interrill Conditions. *Geoderma*, 80: 181-194.
- [19] McDonald, R.C., Isbell, J.G., Speight, J.G., Walker, J., & Hopkins, M.S. (1984). Australian Soil and Land Survey. Field Handbook. Melbourne, Australia: Inkata Press.
- [20] Liu, B.Y., & Tang, K.L. (1987). Slope Gradient Classification and Distribution of the Slope Gradient of Wangdog Watershed. (In Chinese). *Bulletin Soil Water Conservation*, 7(3): 59-64.
- [21] Liu, B.Y., Nearing, M.A., and Risse, L.M. (1994). Slope Gradient Effects on soil loss for steep slopes. *Transaction of the America Society of Agricultural Engineers*, 37:1835-1840.
- [22] Wischmeier, W.H. and Smith, D.D. (1978). Predicting Rainfall Erosion Losses – A Guide to Conservation Planning. U.S. Department of Agriculture, Agriculture Handbook No.537. Washington, DC, USA.
- [23] Nearing, M.A. (1997). A Single, Continuous Function for Slope Steepness Influence on Soil Loss. *Soil Science Society of America Journal*, 61:917-919.
- [24] Wischmeier, W.H. (1959). A Rainfall Erosion Index for a Universal Soil-loss Equation. *Soil Science Society of America Journal*, 23(3): 246-249.
- [25] Roux, L.J.S., & Roos, Z.N. (1991). The Effect of Rainfall Factors and Antecedent Soil Moisture on Soil Loss on a Low-angled Slope in a Semi-arid Climate. *Water SA WASADV*, 17(3): 167-172.
- [26] Tippayawong, N., & Preechawuttipong, I. (2011). Analysis of Microparticle Resuspension in Turbulent Flows with Horizontally Vibrating Surface. *Australian Journal of Basic and Applied Sciences*, 5(7): 356-363.

CHAPTER 17

EFFECT OF WALL INCLINATION ON DYNAMIC ACTIVE THRUST FOR COHESIVE SOIL BACKFILL

A. Gupta¹, V. Yadav², V. A. Sawant³ and R. Agarwal⁴

Abstract

Design of retaining walls under seismic conditions is based on the calculation of seismic earth pressure behind the wall. To calculate the seismic active earth pressure behind the vertical retaining wall, many researchers report analytical solutions using the pseudo-static approach for both cohesionless and cohesive soil backfill. Design charts have been presented for the calculation of seismic active earth pressure behind vertical retaining walls in the non-dimensional form. For inclined retaining walls, the analytical solutions for the calculation of seismic active earth pressure as well as the design charts (in non-dimensional form) have been reported in few studies for $c-\phi$ soil backfill. One analytical solution for the calculation of seismic active earth pressure behind inclined retaining walls by Shukla (2015) is used in the present study to obtain the design charts in non-dimensional form. Different field parameters related with wall geometry, seismic loadings, tension cracks, soil backfill properties, surcharge and wall friction are used in the present analysis. The present study has quantified the effect of negative and positive wall inclination as well as the effect of soil cohesion (c), angle of shearing resistance (ϕ), surcharge loading (q) and the horizontal and vertical seismic coefficient (k_h and k_v) on seismic active earth pressure with the help of design charts for $c-\phi$ soil backfill. The design charts presented here in non-dimensional form are simple to use and can be implemented by field engineers for design of inclined retaining walls under seismic conditions. The active earth pressure coefficients for cohesionless soil backfill achieved from the present study are validated with studies reported in the literature.

Keywords: Inclined retaining wall, pseudo-static approach, cohesion, surcharge, seismic active earth pressure, wall inclination

1.0 INTRODUCTION

In the field under seismic conditions, seismic active earth pressure behind retaining walls can be calculated using explicit generalized expressions. The available generalized solutions take lots of time and effort and have a chance of error in the calculation of seismic active earth pressure. The pseudo-static approach was introduced to determine the seismic active earth pressure behind retaining walls by Okabe [1] and Mononobe and Matsuo [2], called the Mononobe and Okabe method. The soil backfill was assumed as cohesionless in their study. But in real field situations, the design of retaining walls encounters $c-\phi$ soil backfills for which the Mononobe-Okabe method cannot be used. A simple expression has been reported by Shukla et al. [3] for calculating the dynamic active thrust behind the vertical retaining wall with $c-\phi$ soil backfill, but wall friction and soil-wall adhesion were not considered in this study. Kim et al. [4] reported the calculations of total dynamic active thrust behind the retaining wall in terms of the inclination of failure plane by the hit and trial method. Due to the hit and trial method this study has limited application in real design practices. Using the pseudo-static approach, the effect of wall friction and soil-wall adhesion were incorporated in the analytical expressions presented by Shukla and Bathurst [5]. For sloping soil backfill, Shukla [6] obtained analytical expressions to calculate the seismic active earth pressure. Shukla [7] further extended the generalized explicit solution to calculate the dynamic active thrust behind the inclined retaining wall incorporating the sloping soil backfill.

^{1,3}Department of Civil Engineering, Indian Institute of Technology Roorkee, 247667, Roorkee, Uttarakhand, India

^{2,4}Department of Civil Engineering KNIT Sultanpur, 228001, Sultanpur, Uttar Pradesh, India

Email: sawntfce@iitr.ac.in

The expressions were associated the effect of wall inclination as well as the effect of soil cohesion, angle of shearing resistance, soil-wall adhesion, tension cracks, surcharge loading and the horizontal and vertical seismic coefficient. An expression for the critical inclination of failure plane (α_{cri}) was also presented in this study. Using the generalized expression by Shukla [7], the design charts for calculating the dynamic active thrust were developed by Gupta et al.

[8] showing the effect of surcharge loading only. The present study has obtained the design charts for calculating the seismic active earth pressure considering the effect of wall inclination on the dynamic active thrust. The design charts reduce effort in calculation of seismic active earth pressure behind inclined retaining walls, and are very helpful for field engineers in the analysis of inclined retaining walls.

2.0 ANALYTICAL DERIVATION

Figure 1 shows a retaining wall A_1A_2 . The height of wall H supports cohesive soil backfill with cohesion (c) and angle of shearing resistance (ϕ). An active trial failure wedge ($A_1A_2A_3$) is of weight W . The back face of the retaining wall is inclined at β with the horizontal. A_2A_3 is the assumed failure plane, passing through the bottom of the wall. A_2A_3 makes an angle α with the horizontal. The seismic inertial forces are k_hW and k_vW in the horizontal and vertical direction. k_h and k_v are the seismic horizontal and vertical seismic coefficient. A surcharge q per unit surface area is at the top of the sloping backfill. k_hqB and k_vqB are the seismic loads due to surcharge along the horizontal and vertical directions. The length of A_1A_3 is taken as B .

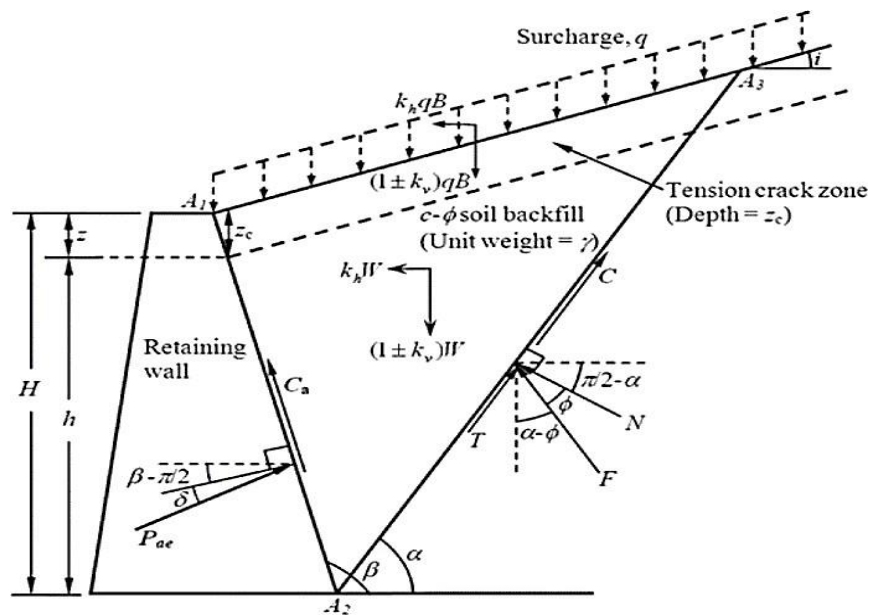


Figure 1 Forces in a trial failure wedge of an inclined retaining wall for $c-\phi$ soil backfill in active state (after Shukla [7])

The depth of tension crack is z_c from the top of the sloping soil backfill. The height of wall H is taken as the sum of z and h . On the failure plane, the frictional force is T and normal force is N . The force F is the resultant force of T and N . C_a is the total adhesive force mobilized along the soil-wall interface. Wall friction angle is δ and total cohesive force is shown by C . An angle i is made by the sloping backfill (A_1A_3) with horizontal.

Now, using the force equilibrium in the horizontal and vertical direction, the following equations can be obtained as:

$$P_{ae} \cos(\beta + \delta) + (1 \pm k_v)(W + qB) - F \cos(\alpha - \phi) - \frac{\bar{c} H \sin(\beta - i) \sin \alpha}{\sin \beta \sin(\alpha - i)} a_f \bar{c} H = 0 \quad (1)$$

$$P_{ae} \sin(\beta + \delta) - k_h(W + qB) - F \sin(\alpha - \phi) + \frac{\bar{c} H \sin(\beta - i) \cos \alpha}{\sin \beta \sin(\alpha - i)} a_f \bar{c} H \cot \beta = 0 \quad (2)$$

Eliminating F from equations (1) and (2) and further simplifying, P_{ae} can be expressed as:

$$P_{ae} = \frac{1}{2} \left(\frac{a_1 \tan^2 \alpha - b_1 \tan \alpha + c_1}{a_2 \tan^2 \alpha - b_2 \tan \alpha + c_2} \right) \gamma H^2 \quad (3)$$

Here, a_1, b_1, c_1 and a_2, b_2, c_2 are the non-dimensional constants defined as follows:

$$\begin{aligned} a_1 &= m_1 \cos \beta \cos(\theta - \phi) + m_2 \cos i \sin(\beta + \phi) + m_3 & a_2 &= \cos i \cos(\beta + \delta + \phi) \\ b_1 &= m_1 \sin(\beta - \theta + \phi) + m_2 \cos(i + \beta + \phi) & b_2 &= \sin(\beta + \delta + \phi + i) \\ c_1 &= m_3 - m_1 \sin \beta \sin(\phi - \theta) - m_2 \sin i \cos(\beta + \phi) & c_2 &= \sin i \sin(\beta + \delta + \phi) \\ m_1 &= \left(\frac{1 \pm k_v}{\cos \theta} \right) \left[\frac{2q}{\gamma H} + \frac{\sin(\beta - i)}{\sin \beta} \right] \operatorname{cosec} \beta & m_2 &= a_f \left(\frac{2c}{\gamma H} \right) \left(1 - \frac{z_c}{2H} \right) \operatorname{cosec} \beta \\ m_3 &= \left(\frac{2c}{\gamma H} \right) \left(1 - \frac{z_c}{2H} \right) \sin(\beta - i) \cos \phi \operatorname{cosec} \beta & \theta &= \tan^{-1} \left(\frac{k_h}{1 \pm k_v} \right) \\ z_c &= \left(\frac{2c}{\gamma} \right) \tan \left(45^\circ + \frac{\phi}{2} \right) & \bar{c} &= \left(1 - \frac{z_c}{2H} \right) c \end{aligned}$$

For optimization, the following condition must be satisfied for the value of dynamic active pressure P_{ae} .

$$\frac{\partial P_{ae}}{\partial \alpha} = 0 \quad \text{or} \quad \frac{\partial P_{ae}}{\partial \tan \alpha} = 0 \quad (4)$$

$$(a_2 b_1 - a_1 b_2) \tan^2 \alpha - 2(a_2 c_1 - a_1 c_2) \tan \alpha + (b_2 c_1 - b_1 c_2) = 0 \quad (5)$$

Equation (5) is solved for $\tan \alpha$ to get the critical inclination of failure plane, $\alpha = \alpha_c$ as:

$$\alpha_{cri} = \tan^{-1} \left[\frac{(a_2 c_1 - a_1 c_2) \pm \sqrt{(a_2 c_1 - a_1 c_2)^2 - (a_2 b_1 - a_1 b_2)(b_2 c_1 - b_1 c_2)}}{(a_2 b_1 - a_1 b_2)} \right] \quad (6)$$

On substituting $\alpha = \alpha_{cri}$ into equation (3), P_{ae} is obtained as:

$$P_{ae} = \frac{1}{2} \left(\frac{a_1 \tan^2 \alpha_{cri} - b_1 \tan \alpha_{cri} + c_1}{a_2 \tan^2 \alpha_{cri} - b_2 \tan \alpha_{cri} + c_2} \right) \gamma H^2 \quad (7)$$

Or

$$K_{ae} = P_{ae}^* = \frac{P_{ae}}{0.5 \gamma H^2} = \left(\frac{a_1 \tan^2 \alpha_{cri} - b_1 \tan \alpha_{cri} + c_1}{a_2 \tan^2 \alpha_{cri} - b_2 \tan \alpha_{cri} + c_2} \right) \gamma H^2 \quad (8)$$

Where K_{ae} is the coefficient of seismic active earth pressure.

3.0 RESULTS AND DISCUSSION

According to the generalized analytical expression shown in equation (8), design charts can be presented to calculate total active earth pressure on retaining walls for different wall inclinations taken as -15° , 0° and 15° with vertical ($\beta = 75^\circ$, 90° and 105°). c^* and q^* are as non-dimensional cohesion and non-dimensional surcharge defined in equation (9). We also consider the k_v is positive for the upward direction.

$$c^* = \frac{c}{\gamma H} \quad \text{and} \quad q^* = \frac{q}{\gamma H} \quad (9)$$

The design charts obtained from the present study are shown in Figures 2, 3, 4, and 5. Figures 2 and 3 present the design charts for calculating the seismic active earth pressure from $c-\phi$ soil backfill for the negative wall inclination as $\beta = 75^\circ$ and 90° respectively for surcharge loading $q^* = 0.2$. Figures 4 and 5 are showing the design charts for the positive wall inclination $\beta = 105^\circ$ for surcharge loading $q^* = 0$ and 0.2 . Effect of surcharge is also showing in Figures 4 and 5. Variations of parameters considered are stated in Table 1.

Table 1 Variation of parameters considered in the present study

Description	Values are taken
Unit weight of soil backfill (γ)	18 kN/m ³
The height of retaining wall (H)	10 m
Non-dimensional soil cohesion (c^*)	0.0, 0.05, 0.1 and 0.2
Soil friction angle (ϕ)	5° , 10° , 15° , 20° , 25° , 30° , 35° , 40° , 45° and 50°
Non-dimensional surcharge (q^*)	0.0 and 0.2
Wall inclination with vertical (β)	-15° , 0° and 15°
Wall friction angle (δ)	0.5ϕ
Coefficient of horizontal seismic acceleration (k_h)	0.0, 0.1, 0.2, 0.3 and 0.4
Coefficient of vertical seismic acceleration (k_v)	0.0, $0.25 k_h$, $0.5 k_h$ and $1.0 k_h$

3.1 EFFECT OF WALL INCLINATION DUE TO c AND ϕ OF SOIL ON K_{ae}

Figures 2, 3, 4, and 5 show that the calculated value of K_{ae} reduces with increase in c and ϕ of soil backfill. For example, at $\phi = 20^\circ$ and $c^* = 0.1$, wall inclination angle β increases from (75° to 90°) and (75° to 105°), the value of K_{ae} increases about 69.8 and 159.5%. Yet, the successive percentage increment is reducing with respect to increase of inclination angle of back slope of retaining wall. The effect of the increment of ϕ for the same values of soil cohesion can be noticed from Figures 2 to 5. On increasing the value of ϕ with constant variation of cohesion of soil, the reduction in the value of K_{ae} is clearly observed. For example at $c^* = 0$ and $k_h = 0$ on increasing ϕ from 30° to 40° K_{ae} decreases by 45.1, 33.8 and 23.1% for different wall inclination as 75° , 90° and 105° respectively. The example is showing the reduction in K_{ae} when wall inclination moves from its negative to its positive value. The effect of increment of c value for the same values of ϕ can also be quantified from Figures 2 to 5. For example at $\phi = 30^\circ$ and $k_h = 0$ when on increasing c^* from 0 to 0.1 the K_{ae} decreases by 67.6, 77.6 and 24.2% when the wall inclination angle changes from 75° , 90° and 105° respectively. From the example the small increment of active earth pressure on moving β from 75° to 90° and a large reduction in active earth pressure for β changes from 90° to 105° can be noticed.

3.2 EFFECT OF WALL INCLINATION DUE TO k_h ON K_{ae}

The effect of k_h on K_{ae} can be also quantified from Figures 2 to 5. It can be observed that the value of K_{ae} increases considerably when the value of k_h increases. On taking $\phi = 20^\circ$, $c^* = 0.1$, $\beta = 75^\circ$ and $q^* = 0.2$, the value of K_{ae} increases by about 46.2, 103.3, 177.6 and 286.3%, when k_h value increases from 0.0 to 0.1, 0.2, 0.3 and 0.4 respectively. For the respective increment of k_h the value of K_{ae} increases by about 26.2, 59.1, 102.6 and 168.3% (for vertical wall) and the percent increase in K_{ae} is 18.3, 41.8, 74.3 and 126.2 (for $\beta = 105^\circ$). When k_h increases from 0.0 to 0.1, 0.1 to 0.2, 0.2 to 0.3 and 0.3 to 0.4, the percentage increase in the K_{ae} is about 46.2, 39.1, 36.6 and 39.2% ($\beta = 75^\circ$) for $\phi = 20^\circ$, $c^* = 0.1$, and $q^* = 0.2$. The percentage increase in K_{ae} for the respective increment in k_h is 26.2, 25.9, 27.4 and 32.4 (for $\beta = 90^\circ$) and 18.3, 19.9, 22.9 and 29.7 (for $\beta = 105^\circ$). The value of K_{ae} increases for the same horizontal seismic coefficient in all three inclination angles ($\beta = 75^\circ$, 90° and 105°) of retaining wall. While the successive percentage increment in K_{ae} reduces with respect to increase in wall inclination angle. From this we can easily say that the percentage increment is reducing with wall inclination angle.

3.3 EFFECT OF WALL INCLINATION DUE TO k_v ON K_{ae}

The effect of k_v on K_{ae} can be also quantified from Figures 2 to 5. It can be observed that the value of the K_{ae} increases marginally when the value of k_v increases. For example at $\beta = 75^\circ$, $\phi = 30^\circ$, $c^* = 0.0$, $q^* = 0.2$ and $k_h = 0.1$, on increasing the k_v from 0 to $0.25k_h$, $0.25k_h$ to $0.5 k_h$ and $0.5 k_h$ to k_h the respective values of K_{ae} decrease by 1.86, 1.88 and 3.83% respectively. On increasing the value of k_h from 0.1 to 0.3 for the respective increment of k_v , the increase in K_{ae} is 1.41, 0.82 and 1.93%. For the vertical wall at $\phi = 30^\circ$, $c^* = 0.0$, $q^* = 0.2$ and $k_h = 0.1$, on increasing k_v from 0 to $0.25k_h$, $0.25k_h$ to $0.5 k_h$ and $0.5 k_h$ to k_h , K_{ae} decreases by 2.0, 2.03 and 4.13% respectively. The respective percentage increase in K_{ae} is 2.1, 2.5 and 4.31 for $\beta = 105^\circ$. From the example, it is clearly observed that for all wall inclination ($\beta = 75^\circ$, 90° and 105°) of retaining wall, the value of K_{ae} is reducing but the rate of reduction is very marginal.

3.4 EFFECT OF SURCHARGE ON K_{ae}

The effect of surcharge on the value of K_{ae} can be clearly noticed from Figures 4 and 5. From the developed design charts, it can be determined that the increment of surcharge affects the considerable increase on K_{ae} . For example, on increasing the value of k_h from 0.0 to 0.4 at $\beta = 105^\circ$, $\phi = 30^\circ$, and $c^* = 0.0$, when q^* increases from 0 to 0.2, an increment is of 40% in K_{ae}

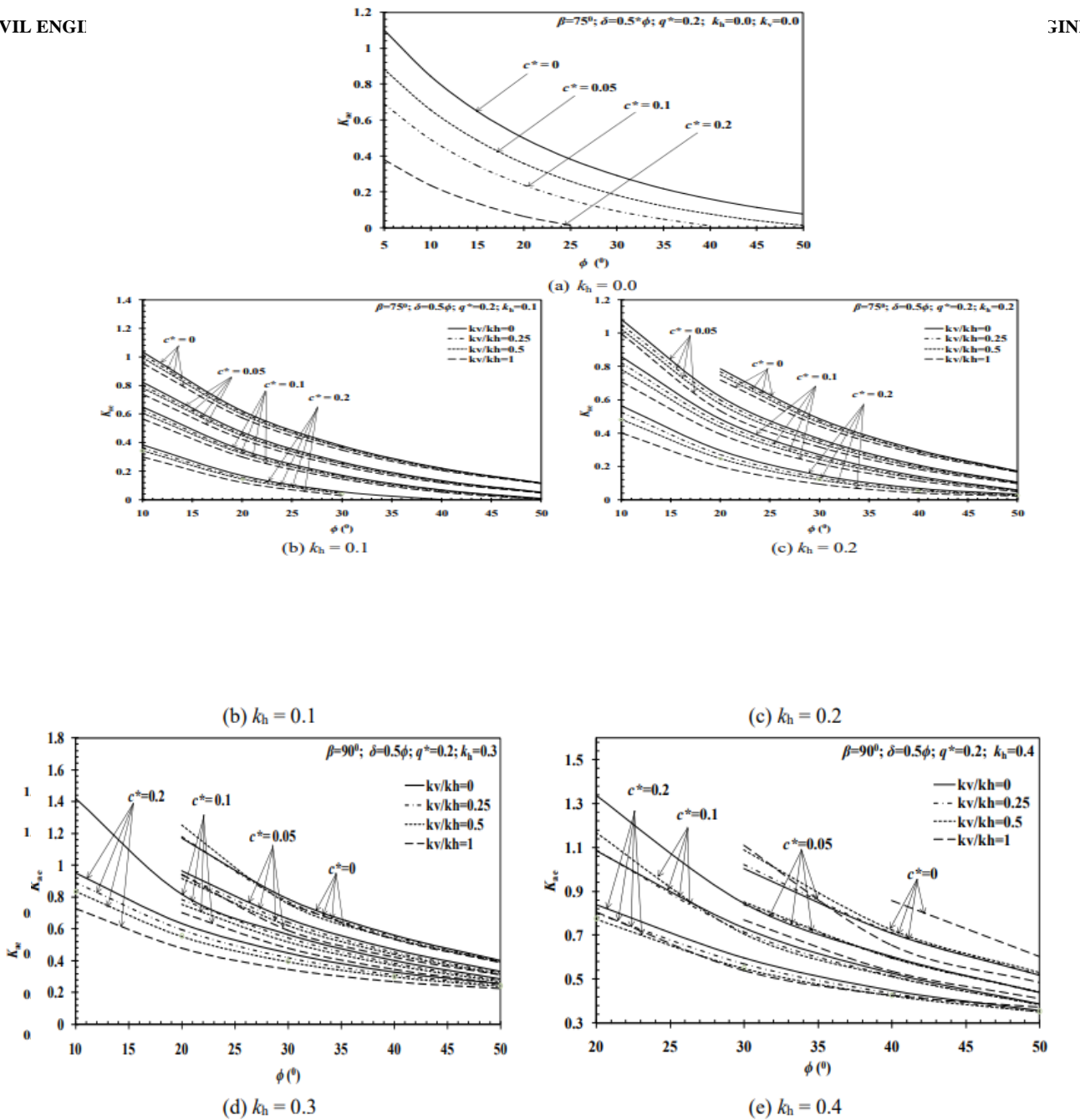
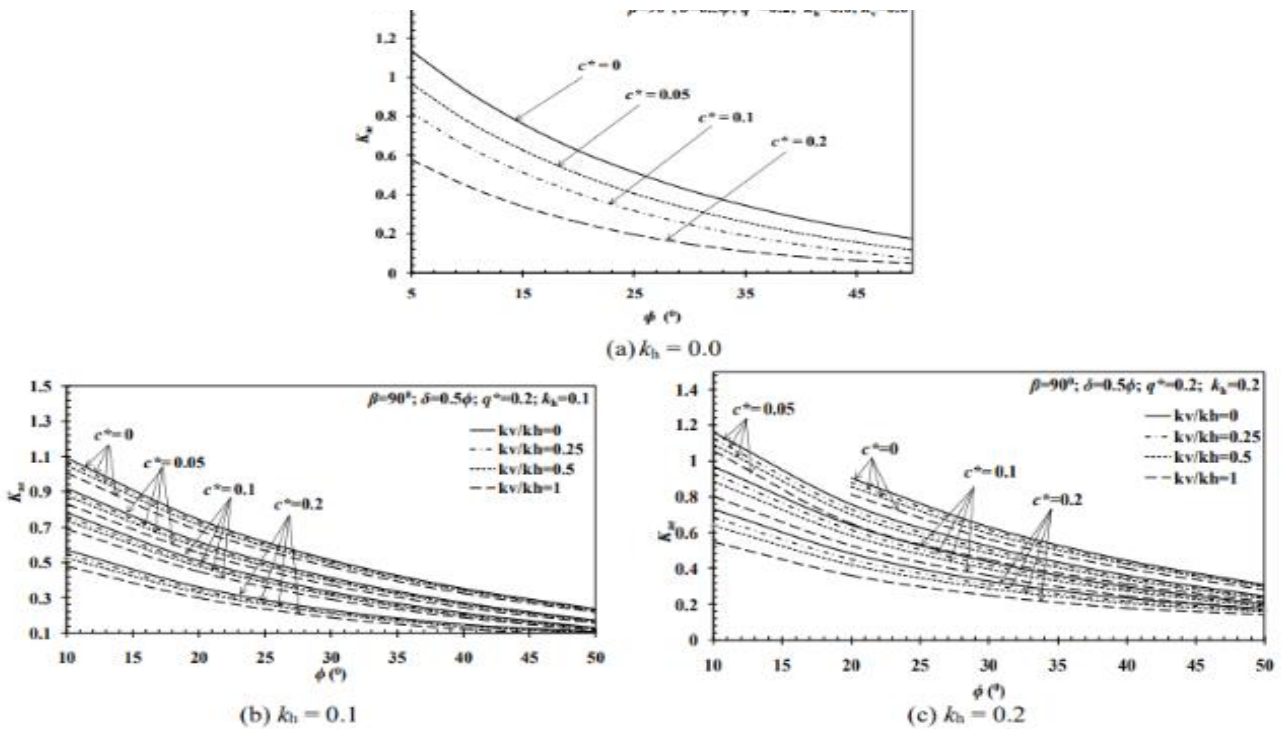
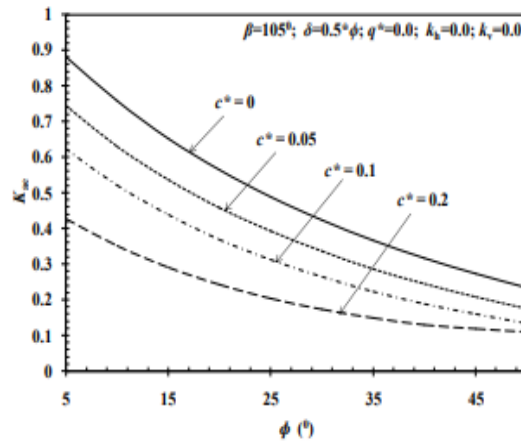
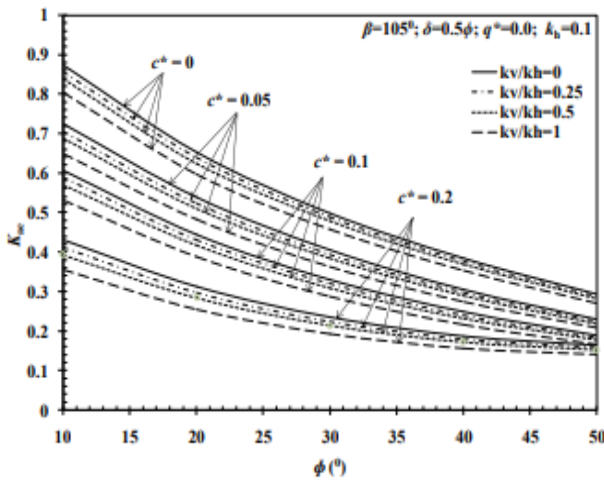


Figure 3 Design charts for K_{ac} for different values of k_h , k_v and c^* for vertical wall with surcharge loading $q^* = 0.2$

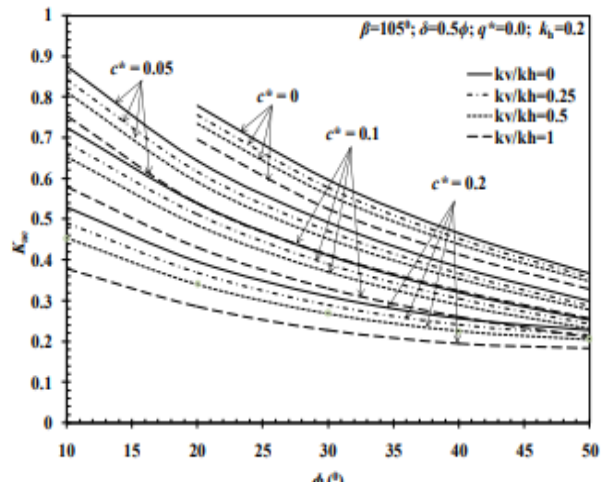




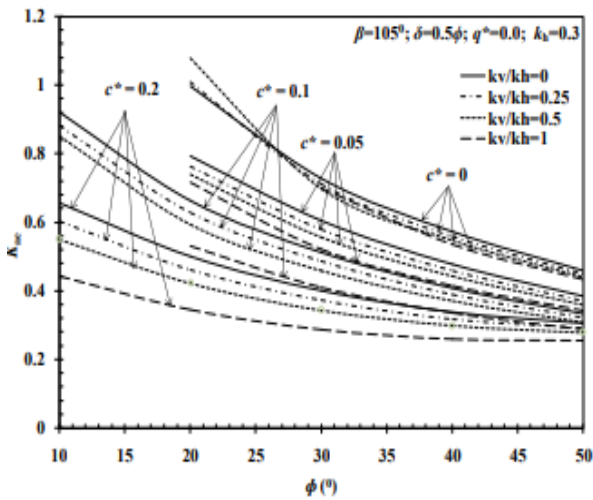
(a) $k_h = 0.0$



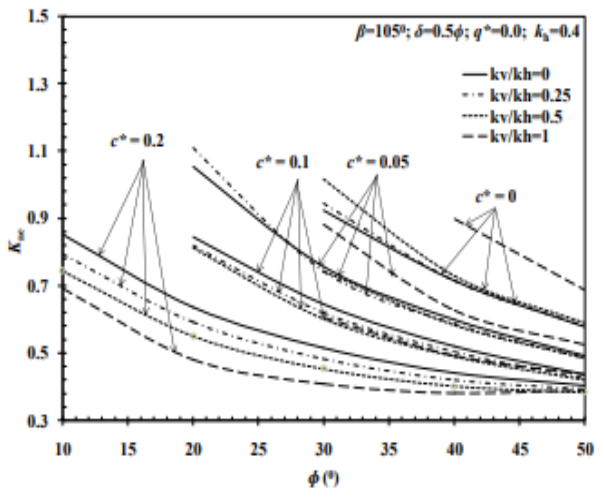
(b) $k_h = 0.1$



(c) $k_h = 0.2$



(d) $k_h = 0.3$



(e) $k_h = 0.4$

Figure 4 Design charts for K_{ae} for different values of k_h , k_v and c^* for wall with $\beta = 105^\circ$ without surcharge

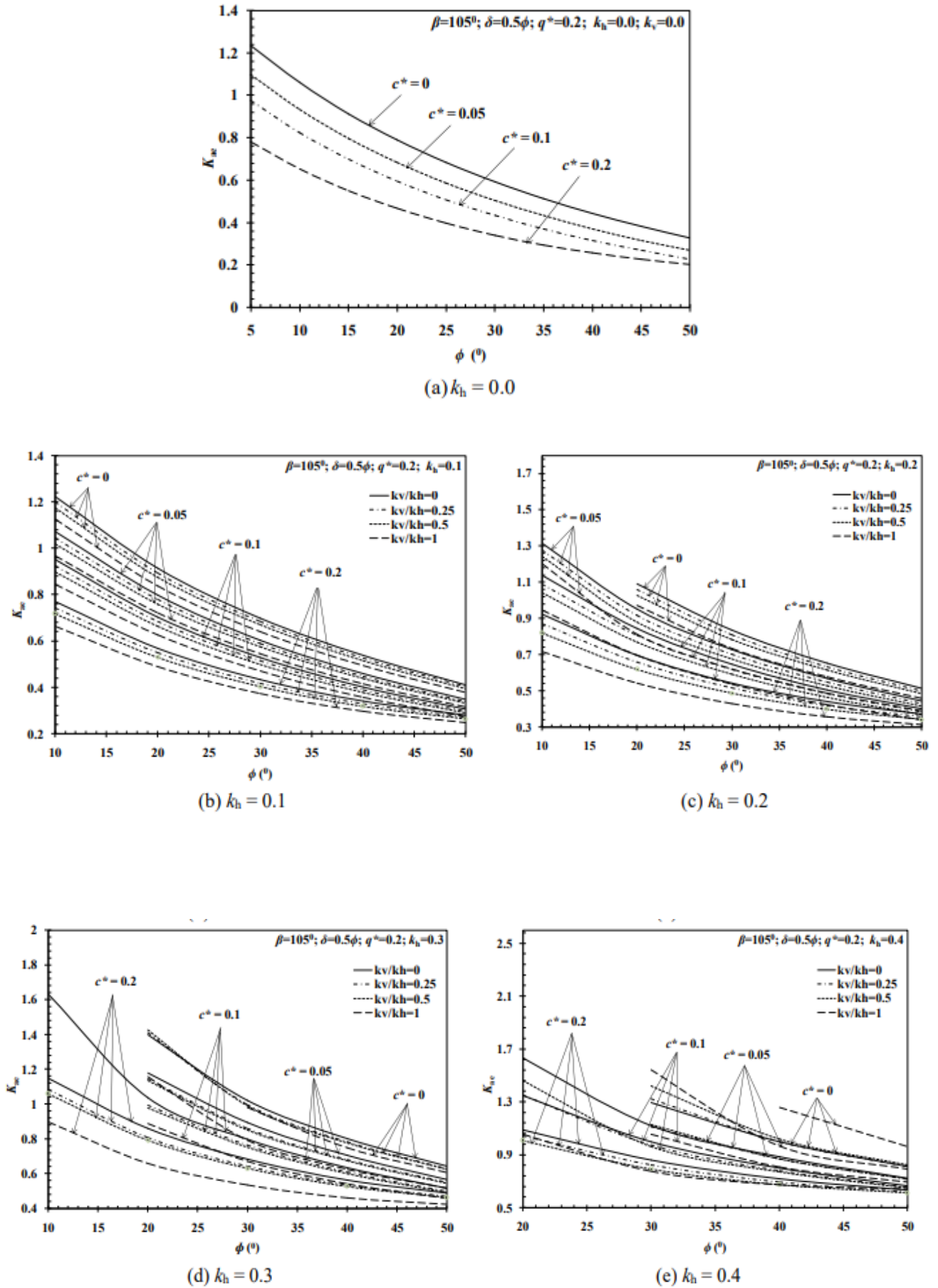


Figure 5 Design charts for K_{oe} for different values of k_h , k_v and c^* for wall with $\beta = 105^\circ$ and surcharge loading $q^* = 0.2$

3.5 VALIDATION OF PRESENT WORK

The coefficient of seismic active earth pressure K_{ae} is compared with Mononobe and Okabe, Cheng [9], and Ghanbari and Ahmadabadi [10] in Table 2. For the given set of parameters, the values of K_{ae} show a good agreement.

Table 2 Comparison of results for calculation of active earth pressure coefficient ($i = 0^\circ$; $k_v = 0$; $c = 0$; $\delta = (2/3)\phi$ and $\beta = 90^\circ$)

ϕ ($^\circ$)	Mononobe and Okabe	Cheng [8]	Ghanbari and Ahmadabadi [9]		Present Study
			Based on Limit Equilibrium Method	Based on Horizontal Slice Method	
$k_h = 0.0$					
20	0.438	0.426	0.438	0.440	0.438
25	0.361	0.346	0.361	0.362	0.361
30	0.297	0.279	0.297	0.299	0.297
$k_h = 0.05$					
20	0.479	0.456	0.478	0.479	0.478
25	0.397	0.380	0.397	0.398	0.397
30	0.330	0.330	0.330	0.330	0.310
$k_h = 0.1$					
20	0.525	0.511	0.526	0.526	0.525
25	0.438	0.419	0.438	0.438	0.438
30	0.366	0.344	0.366	0.366	0.366
$k_h = 0.2$					
20	0.647	0.629	0.647	0.645	0.647
25	0.539	0.516	0.539	0.539	0.539
30	0.454	0.426	0.454	0.453	0.454

4.0 CONCLUSIONS

In the present work, design charts are developed to calculate the total active thrust from c - ϕ soil backfill for three different wall inclination angles from -15° to 15° (as $\beta = 75^\circ$, $\beta = 90^\circ$ and $\beta = 105^\circ$). The following points can be summarized:

1. The active earth pressure coefficient (K_{ae}) reduces with respect to increase in angle of shearing resistance of soil backfills and increase in cohesion (c), and irrespective of non-dimensional surcharge loading on backfills.
2. The value of K_{ae} increases marginally for negative value of wall inclination and reduces considerably for positive value of wall inclination.
3. The value of K_{ae} increases with increase in horizontal seismic coefficient (k_h), yet the percentage increment is marginally reduced with respect to the increment of k_h with the increase in wall inclination angle.
4. There is considerable increment in K_{ae} as wall inclination angle (β) increases from 75° to 105° , while percentage increment substantially reduces as the increment in the value of horizontal seismic coefficient (k_h) increases.
5. The value of K_{ae} increases marginally with increase in k_v . The rate of percentage increase is also very slow.

REFERENCES

- [1] Okabe, S. (1926). General theory of earth pressure and seismic stability of retaining wall and dam. *Journal of the Japan Society of Civil Engineers*. 10(6): 1277-1323.
- [2] Mononobe, N. & Matsuo, H. (1929). On the determination of earth pressure during earthquakes. In the Proceedings of the World Engineering Congress, Tokyo, Japan. 9: 179-187.
- [3] Shukla, S. K., Gupta, S. K. & Sivakugan, N. (2009). Active earth pressure on retaining wall for $c-\phi$ soil backfill under seismic loading condition. *Journal of Geotechnical and Geoenvironmental Engineering*, ASCE. 135(5): 690- 696.
- [4] Kim, W. C., Park, D. & Kim, B. (2010). Development of a generalised formula for dynamic active earth thrust. *Geotechnique*. 60(9): 721-727.
- [5] Shukla, S. K. & Bathurst, R. J. (2012). An analytical expression for the dynamic active thrust from $c-\phi$ soil backfill on retaining walls with wall friction and adhesion. *Geomechanics and Engineering: An International Journal*. 4(3): 209-218.
- [6] Shukla, S. K. (2013). Seismic active earth pressure from sloping $c-\phi$ soil backfills. *Indian Geotechnical Journal*, 43(3): 274-279.
- [7] Shukla, S. K. (2015). Generalized analytical expression for dynamic active thrust from $c-\phi$ soil backfills. *International Journal of Geotechnical Engineering*. 9(4): 416-421.
- [8] Gupta, A., Chandaluri, V. K., Sawant, V. A. & Shukla, S. K. (2018). Development of design charts for the dynamic active thrust from $c-\phi$ soil backfills. *Soil Dynamics and Earthquake Geotechnical Engineering*. (IGC 2016 Volume 3). Springer, Singapore.111-122. doi: <https://doi.org/10.1007/978-981-13-0562-7>.
- [9] Cheng, Y. M. (2003). Seismic lateral earth pressure coefficients for $c-\phi$ soils by slip line method. *Computers and Geotechnics*. 30(18): 661-670.
- [10] Ghanbari, A. & Ahmadabadi, M. (2010). Active earth pressure on inclined retaining walls in slice and pseudo-static conditions. *International Journal of Civil Engineering*. 8(2): 159-173.

4.0 CONCLUSIONS

In the present work, design charts are developed to calculate the total active thrust from $c-\phi$ soil backfill for three different wall inclination angles from -15° to 15° (as $\beta = 75^\circ$, $\beta = 90^\circ$ and $\beta = 105^\circ$). The following points can be summarized:

6. The active earth pressure coefficient (K_{ae}) reduces with respect to increase in angle of shearing resistance of soil backfills and increase in cohesion (c), and irrespective of non-dimensional surcharge loading on backfills.
7. The value of K_{ae} increases marginally for negative value of wall inclination and reduces considerably for positive value of wall inclination.
8. The value of K_{ae} increases with increase in horizontal seismic coefficient (k_h), yet the percentage increment is marginally reduced with respect to the increment of k_h with the increase in wall inclination angle.
9. There is considerable increment in K_{ae} as wall inclination angle (β) increases from 75° to 105° , while percentage increment substantially reduces as the increment in the value of horizontal seismic coefficient (k_h) increases.
10. The value of K_{ae} increases marginally with increase in k_v . The rate of percentage increase is also very slow.

REFERENCES

- [11] Okabe, S. (1926). General theory of earth pressure and seismic stability of retaining wall and dam. *Journal of the Japan Society of Civil Engineers*. 10(6): 1277-1323.
- [12] Mononobe, N. & Matsuo, H. (1929). On the determination of earth pressure during earthquakes. In the Proceedings of the World Engineering Congress, Tokyo, Japan. 9: 179-187.
- [13] Shukla, S. K., Gupta, S. K. & Sivakugan, N. (2009). Active earth pressure on retaining wall for $c-\phi$ soil backfill under seismic loading condition. *Journal of Geotechnical and Geoenvironmental Engineering*, ASCE. 135(5): 690- 696.
- [14] Kim, W. C., Park, D. & Kim, B. (2010). Development of a generalised formula for dynamic active earth thrust. *Geotechnique*. 60(9): 721-727.
- [15] Shukla, S. K. & Bathurst, R. J. (2012). An analytical expression for the dynamic active thrust from $c-\phi$ soil backfill on retaining walls with wall friction and adhesion. *Geomechanics and Engineering: An International Journal*. 4(3): 209-218.
- [16] Shukla, S. K. (2013). Seismic active earth pressure from sloping $c-\phi$ soil backfills. *Indian Geotechnical Journal*, 43(3): 274-279.
- [17] Shukla, S. K. (2015). Generalized analytical expression for dynamic active thrust from $c-\phi$ soil backfills. *International Journal of Geotechnical Engineering*. 9(4): 416-421.
- [18] Gupta, A., Chandaluri, V. K., Sawant, V. A. & Shukla, S. K. (2018). Development of design charts for the dynamic active thrust from $c-\phi$ soil backfills. *Soil Dynamics and Earthquake Geotechnical Engineering*. (IGC 2016 Volume 3). Springer, Singapore. 111-122. doi: <https://doi.org/10.1007/978-981-13-0562-7>.
- [19] Cheng, Y. M. (2003). Seismic lateral earth pressure coefficients for $c-\phi$ soils by slip line method. *Computers and Geotechnics*. 30(18): 661-670.
- [20] Ghanbari, A. & Ahmadabadi, M. (2010). Active earth pressure on inclined retaining walls in slice and pseudo-static conditions. *International Journal of Civil Engineering*. 8(2): 159-173.

CHAPTER 18

PREDICTION OF CALIFORNIA BEARING RATIO OF FINE- GRAINED SOIL STABILIZED WITH ADMIXTURES USING SOFT COMPUTING SYSTEMS

Islam M. Rafizul¹ and Animesh Chandra Roy¹

Abstract

The main focus of this study was to predict California bearing ratio (CBR) of stabilized soils with quarry dust (QD) and lime as well as rice husk ash (RHA) and lime. In the laboratory, stabilized soils were prepared at varying mixing proportions of QD as 0, 10, 20, 30, 40 and 50%; lime of 2, 4 and 6% with varying curing periods of 0, 7 and 28 days. Moreover, admixtures of RHA with 0, 4, 8, 12 and 16%; lime of 0, 3, 4 and 5% was used to stabilize soil with RHA and lime. In this study, soft computing systems like SLR, MLR, ANN and SVM were implemented for the prediction of CBR of stabilized soils. The result of ANN reveals QD, lime and OMC were the best independent variables for the stabilization of soil with QD, while, RHA, lime, CP, OMC and MDD for the stabilization of soil with RHA. In addition, SVM proved QD and lime as well as RHA, lime, CP, OMC and MDD were the best independent variables for the stabilization of soil with QD and RHA, respectively. The optimum content of QD was found 40% and lime 4% at varying curing periods to get better CBR of stabilized soil with QD and lime. Moreover, the optimum content of RHA was also found 12% and lime 4% at varying curing periods to get better CBR of stabilized soil with RHA and lime. The observed CBR and selected independent variables can be expressed by a series of developed equations with reasonable degree of accuracy and judgment from SLR and MLR analysis. The model ANN showed comparatively better values of CBR with satisfactory limits of prediction parameters (RMSE, OR, R² and MAE) as compared to SLR, MLR and SVM. Therefore, model ANN can be considered as best fitted for the prediction of CBR of stabilized soils. Finally, it might be concluded that the selected optimum content of admixtures and newly developed techniques of soft computing systems will further be used of other researchers to stabilize soil easily and then predict CBR of stabilized soils.

Keywords: Soil, Admixtures, CBR, Regression Analysis, ANN, SVM

1.0 INTRODUCTION

The strength of an underlying soil to be used as a subgrade of highway and foundation is assessed from its California Bearing Ratio (CBR) value [1]. Moreover, geotechnical engineer needs to ensure bearing capacity of underlying soil for the subgrade of highway and the design of foundation for civil infrastructures. If the value of CBR in soil is low, the thickness of pavement is high, which will result in high cost of construction and vice-versa. To increase the CBR value of soil, soil improvement or stabilized techniques may be applied to existing soft soil. Soil stabilization may be defined as any process by which a soil material is improved and made more stable resulting in improved bearing capacity, increase in soil strength and durability under adverse moisture and stress conditions [2]. The CBR of stabilized soil depends on different factors like percentage of admixtures, curing period, curing temperature, compaction properties of soil, Atterberg's limit of soil, particle sizes of soil, etc. The test of CBR is not only expensive but also time consuming. There are different techniques for improving CBR of soil, one being stabilization using different admixtures like cement, lime, fly ash, rich husk ash (RHA), gypsum, baggage ash, quarry dust (QD), geotextile, etc. The successful stabilization of soils has to depend on the proper selection of admixtures and amount of admixtures added [3]. In this study, to stabilize soil, the admixtures such QD, lime and RHA at varying percentages were used.

¹Department of Civil Engineering, Khulna University of Engineering & Technology, Khulna-9203, Bangladesh
Email:imrafizul@yahoo.com

The QD is a byproduct of the crushing process which is a concentrated material to use as aggregates for concreting purpose, especially as fine aggregates [4,5]. The lime is a calcium-containing inorganic mineral in which oxides, and hydroxides predominate. The lime usually used for the stabilization of soil is commercially available quick lime. RHA is a by-product from the burning of rice husk. In the literature various researchers in civil engineering field are used softcomputing systems such as artificial neural network (ANN), support vector machine (SVM), simple linear regression (SLR) and multiple linear regressions (MLR) for the prediction of CBR of stabilized soils [6]. CBR of soil has been predicted using ANN by a number of researchers [6]. ANN is an effective tool for analyzing and predicting of CBR stabilized soil. ANNs are a form of artificial intelligence and mimics the nervous system of the human brain [7]. The coefficient of regression (R^2), mean square error (MSE) and over fitting ratio (OR) is mostly used for evaluating the performance of ANN models. The root means square error (RMSE) indicates the accuracy of approximation as overall, without indicating the individual data points [7,8]. The OR is defined as the ratio of Root mean square error (RMSE) for testing and training data and its value close to 1.0 shows good generalization of the ANN model [9, 10,11]. In addition, SVM has also been applied for the prediction and analysis of geotechnical parameters of stabilized soils. SVM has been also applied for prediction of settlement of foundations on cohesionless soil, swelling pressure of expansive soil and compaction behavior of stabilized soil [12,13,14].

In this study, the soft computing systems such as simple linear regression (SLR) and multiple linear regressions (MLR) were performed to establish relationship between CBR and other independent variables of SLR and MLR techniques. In addition, the algorithms of Levenberg-Marquardt neural network (LMNN), Bayesian regularization neural network (BRNN) and scaled conjugate gradient neural network (SCGNN) of ANN's back propagation was performed for the prediction of CBR of stabilized soils. The SVM with different kernel functions like support vector machine-linear (SVM-L), support vector machine-quadratic (SVM-Q) and support vector machine-cubic (SVM-C) was performed to select a best fitted model of SVM. The coefficient of regression (R^2), root mean square error (RMSE) and mean absolute error (MAE) is mostly used for evaluating the performance of SVM models. The aim of this study is to analyze CBR of fine-grained soil stabilized with different admixtures, to predict CBR of stabilized soil using soft computing systems and to check the accuracy of the observed and predicted CBR of stabilized soil from soft computing systems. In this study, the selected optimum content of admixtures and newly developed techniques of soft computing systems will further be used of other researchers to stabilize soil easily and then predict CBR of stabilized soils.

2.0 METHODOLOGY

In this study, for the prediction of CBR of stabilized soils, the soft computing systems like SLR, MLR, ANN and SVM with different kernel functions were performed. The overall methodology of this study is described in the following articles.

2.0 COLLECTION OF SOIL SAMPLE

In the laboratory, for the preparation stabilized soils, disturbed soil samples were collected at a depth of 5 feet from the existing ground surface from KUET campus, Bangladesh. Proper care was taken to remove any loose soil during sampling of soil sample.

2.1 LABORATORY INVESTIGATIONS

In the laboratory, the physical and index properties of soil sample were measured through ASTM standard test methods. The laboratory results of soil samples with ASTM testing standards are provided in Table 1. Besides, in the laboratory, specific gravity, OMC, MDD, gravel, sand, silt and was found 2.65, 10.02%, 19.8kN/m³, 0.38%, 86.02%, 9.03% and 4.57%, respectively, of QS.

Table 1: Physical properties of soil used in this study

Soil parameters	Unit	Value	Analytical method
Specific Gravity	--	2.70%	ASTM D 854
Initial Moisture Content	--	26%	ASTM D 2216
OMC	--	13.9%	ASTM D 1557 (Modified)
MDD	kN/m ³	17.6	
LL	--	32%	ASTM D 4318
PL	--	22%	
PI	--	10%	
Soaked CBR	--	6.74%	AASHTO T 193
Gravel: Sand: Silt: Clay in %	--	0: 2.70: 73.2: 24.1	ASTM D 421 and D 422

2.2 MIXING OF THE SOIL SAMPLE

The collected soil sample was first air and oven dried and then powdered manually. This powdered sample was then sieved through #4 sieve which were mixed with QD and lime as well as with RHA and lime at varying mixing proportions. Then, the mixing samples were mixed with various percentage of water to get OMC and MDD of stabilized soil.

2.3 PREPARATION OF STABILIZED SOILS

In the laboratory, the stabilized soils were prepared at varying mixing proportions of QD as 0, 10, 20, 30, 40 and 50%; lime of 2, 4 and 6% with varying curing periods of 0, 7 and 28 days. Moreover, the admixtures of RHA with 0, 4, 8, 12 and 16%; lime of 0, 3, 4 and 5% was used to stabilize soil with RHA and lime. The stabilized samples were curing for 0, 7 and 28 days to get CBR of stabilized soils. In addition, for CBR test, samples were prepared by using 6 inch diameter and 7 inch height compaction mold. In addition, a spacer disk height and collar height was considered as 60 and 40mm, respectively. The soil samples were prepared for mixing with QD and lime as well as RHA and lime. Thereafter, same quantity of OMC was added in soil prepared with QD and lime as well as in soil prepared with RHA and lime to make ready for blows.

2.4 COMPACTION OF SAMPLES FOR CBR TEST

The prepared soil samples were compacted using modified proctor test. At first all the measurement and weight were taken before the compaction. The spacer disk was placed on the base plate and a filter paper kept on the spacer disk. Then the mold was placed over the spacer disk as well as a collar was fixed up on the mold. Later sample was poured in the mold of five layers and the compaction conducted per layer was 10, 30 and 65 blows, respectively. But the mold was clamped with base plate tightly during compaction. After compaction of five layers in each mold, it was level its top surface. Then the mold was removed from the base plate and spacer disk to take the weight of sample and mold. Further this sample was ready for curing periods of 0, 7 and 28 days.

2.5 CURING OF SAMPLES FOR CBR TEST

Total 54 samples for QD and lime as well as 60 samples for RHA and lime were curing for 0, 7 and 28 days. The samples were kept in water for curing. The water used in the curing was as the room temperature. The water temperature varies from 32 to 35°C.

2.6 CBR TEST OF SAMPLES

The curing samples were kept in open dry condition after removing the surcharge. When the molds become saturated dry, then the molds were untying its clamp for weighting of cured sample and mold. Later it was placed under the loading machine for CBR test. CBR machine is a gradual loading machine

which measures load with respect to deformation. Three molds were placed in the CBR testing machine to fix by wooden pieces for the tight hardly of sample. Then a collar and 4.70 kg of surcharge were placed on the mold. A deformation dial gauge was attached with the machine. By making the loading in dial gauge as zero, the load was gradually applied. The deformation was recorded for 0, 0.25, 0.50, 1.00, 1.25, 1.50, 2.00, 2.50, 3.00, 3.50, 3.75, 4.00, 4.50, 5.00, 6.00, 7.50, 10.00 and 12.50 mm, respectively and at the same time, the corresponding load was recorded. After the loading completed on sample, the mold was removed from the machine and the same procedure were repeated for the other samples.

2.7 SOFT COMPUTING SYSTEMS

In this study, to predict CBR of stabilized soil, the soft computing systems such as SLR and MLR through MS excel was performed. In addition, ANN with the different algorithm through MATLAB was implemented. Moreover, SVM with the different kernel functions was also performed and hence discussed in the following articles.

2.7.1 SIMPLE AND MULTIPLE LINEAR REGRESSIONS

The relationship between dependent variable CBR and other independent variables such as lime (%), QD (%) or RHA (%), curing period, CP (days), OMC (%) or MDD (kN/m^3) was established using SLR and MLR as well as R^2 was carried out. The dependent variable of SLR technique can be predicted by using the following Equation 1.

$$y = a + bx \quad (1)$$

Where y is dependent variable and x is the independent variable as well as b is the slope of the line and a is the intercept, where the line cuts the y axis. Moreover, values of a and b can obtain as constant after the analysis of SLR technique. In addition, the dependent variable of MLR technique can be predicted by using the following Equation 2.

$$Y = a + b_1X_1 + b_2X_2 + b_3X_3 + b_4X_4 + b_5X_5 + \dots + b_nX_n \quad (2)$$

Where Y is a dependent variable and $X_1, X_2, X_3, X_4, X_5, \dots, X_n$ are the independent variable as well as a is the coefficient of intercept and $b_1, b_2, b_3, b_4, b_5, \dots, b_n$ are coefficient of independent variables, respectively. Independent variables become two or more input values at the curing period of 0, 7 and 28 days.

2.7.2 ARTIFICIAL NEURAL NETWORK

In this analysis, the back-propagation ANN with different algorithms like Levenberg-Marquardt neural network (LMNN), bayesian regularization neural network (BRNN) and scaled conjugate gradient neural network (SCGNN) was implemented for the prediction of CBR of stabilized soils. In ANN analysis, to select the best model, the MSE, R^2 and OR were considered. Best model can be declared then, when R^2 is almost close to 1 with its best OR value is also close to 1.

2.7.3 SUPPORT VECTOR MACHINE

In this analysis, support vector machine (SVM) with different kernel functions like linear SVM (SVM-L), quadratic SVM (SVM-Q) and cubic SVM (SVM-C) was used to prediction the CBR of stabilized soil using different admixture at varying proportion. In SVM analysis, lime (%), QD (%) or RHA (%), CP (days), OMC (%) and MDD (kN/m^3) as well as CBR (%) were selected as input and target, respectively. In SVM analysis, to select the best model, the RMSE, R^2 and MAE were considered. When R^2 value is the near about 1, root mean square error (RMSE) and mean absolute error (MAE) value is near about zero, then it can call best fitted model of SVM.

3.0 RESULTS AND DISCUSSIONS

The soft computing systems like SLR, MLR and SVM with different kernel function are SVM-L, SVM-Q and SVM-C were performed for the prediction of CBR of stabilized soils and hence discussed in the following articles.

3.1 STABILIZED SOILS WITH ADMIXTURES

In the laboratory, the stabilized soils were prepared using QD with lime and RHA with lime at varying mixing proportions and hence discussed in the following articles.

3.1.1 QUARRY DUST WITH LIME

The variation of dry density in relation to the changing of moisture content of stabilized soil with QD and lime is shown in Figure 1. Figure 1 depicts that dry density increases with the increasing of QD and lime content in soil at a certain amount of moisture content. For a particular amount of QD like 50%, the stabilized soil with 6 % lime content showed comparatively the higher values of dry density due to more additive power of admixtures than that of stabilized soil with other less amount of QD content as shown in Figure 1(c).

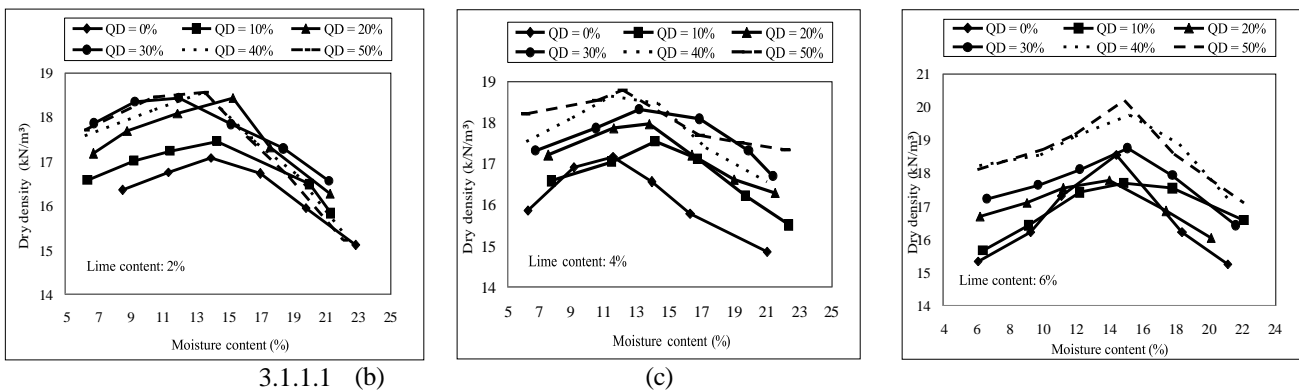


Figure 1: Effect of QD content on compaction curve for (a) 2% lime content, (b) 4% lime content and (c) 6% lime content

Figure 2 shows the variation of MDD of stabilized soil with different percentages of QD and lime. MDD is an important parameter to calculate the CBR of stabilized soils.

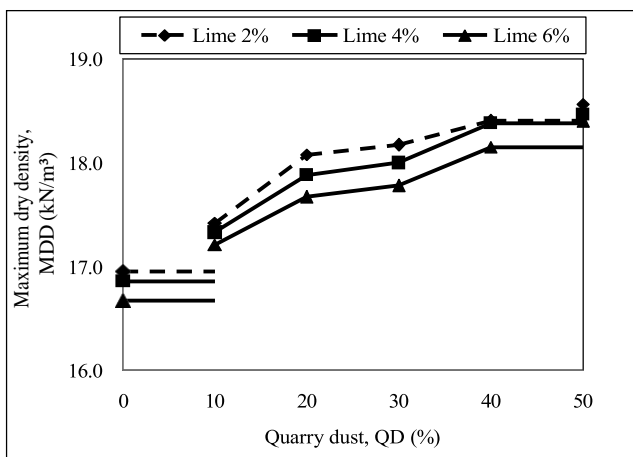


Figure 2: Variation of MDD with QD and lime content.

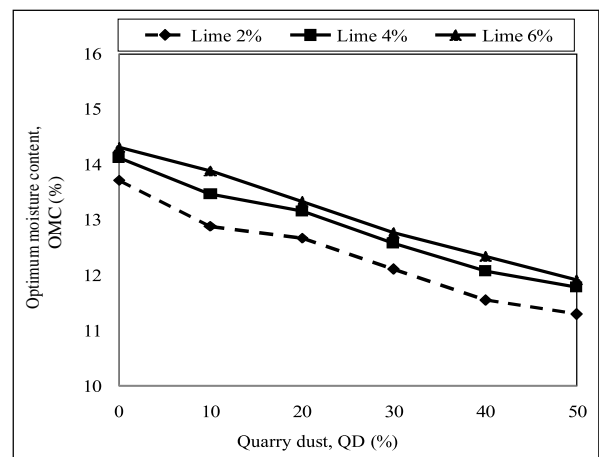


Figure 3: Variation of OMC with QD and lime content.

The MDD of stabilized soil decreases with the increasing of lime content as shown in Figure 2. In addition, MDD increases in relation to the increasing of QD content in soil. Figure 2 also shown that for a particular

mixing content of QD (30%), the value of MDD decreases with the increasing of lime content. Moreover, for a particular amount of lime content (6%), the value of MDD increases in relation to the adding of QD in stabilized soil. In addition, Figure 3 shows the variation of OMC of stabilized soil with different percentages of QD and lime. OMC is an important parameter to determine the CBR of stabilized soils. The OMC of stabilized soil increases with the increasing of lime content as shown in Figure 3. In addition, OMC decreases in relation to the increasing of QD content in stabilized soil. Figure 3 also shown that for a particular mixing content of QD (30%), the value of OMC increases with the increasing of lime content. Moreover, for a particular mixing amount of lime content (6%), the value of OMC decreases in relation to the adding of QD in stabilized soil.

The deviation of MDD and OMC in stabilized soil with QD (0 to 50%) and lime 2% is shown in Figure 4. The OMC decreases, while MDD increases with the increasing of QD content with a particular amount of lime (2%) as shown in Figure 4. A research conducted by [15] and stated that MDD decreases, while OMC increases with the increasing of admixture like RHA in soil. In this study, OMC and MDD of stabilized soil with QD showed the inverse behavior of stabilized soil with RHA due to the inherent properties of admixtures of QD and RHA. The findings in this study agreed well with the results postulated by [15].

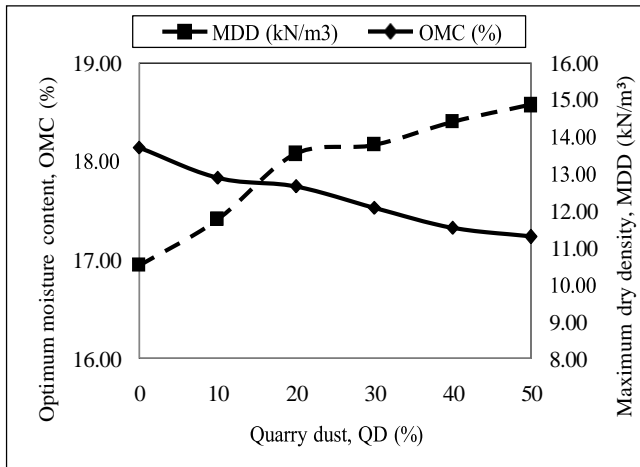


Figure 4: Variation of MDD and OMC with QD (%) and 2% lime.

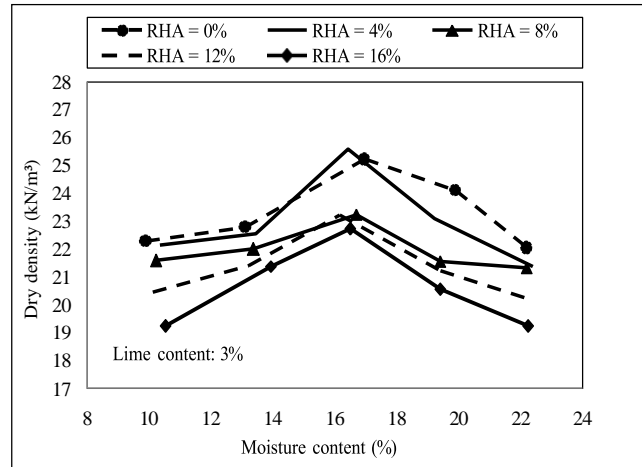


Figure 5: Effect of RHA content on dry density and moisture content.

3.1.2 RICE HUSK ASH WITH LIME

The effect of RHA content with 3% lime on the compaction curve of stabilized soil with RHA and lime is shown in Figure 5. Figure 5 reveals that dry density decreases for the increasing of RHA content with soil at certain amount of moisture content and then decreases. According to [16] the dry density values with moisture contents for soil samples with different percentage of additives are varied. The findings of this study are agreed well with the results by [16].

The MDD of stabilized soil decreases with the increasing of lime content as shown in Figure 6 (a). In addition, MDD decreases in relation to the increasing of RHA content in soil. Figure 6 (a) also shows that for a particular mixing content of RHA (8%), the value of MDD decreases with the increasing of lime content. Moreover, for a particular mixing amount of lime content (5%), the value of MDD decreases in relation to the adding of RHA in stabilized soil. Moreover, the OMC of stabilized soil increases with the increasing of lime content as shown in Figure 6 (b). In addition, OMC increases in relation to the increasing of RHA content in stabilized soil. Figure 6 (b) also shows that for a particular mixing content of OMC (8%), the value of OMC increases with the increasing of lime content. Moreover, for a particular

mixing amount of lime content (5%), the value of OMC increases in relation to the adding of RHA in

stabilized soil. So, Figure 6 (c) illustrates the deviation of MDD and OMC in stabilized soil with RHA (0 to 16%) and lime of 4%. The MDD decreases while OMC increases with the increasing of RHA.

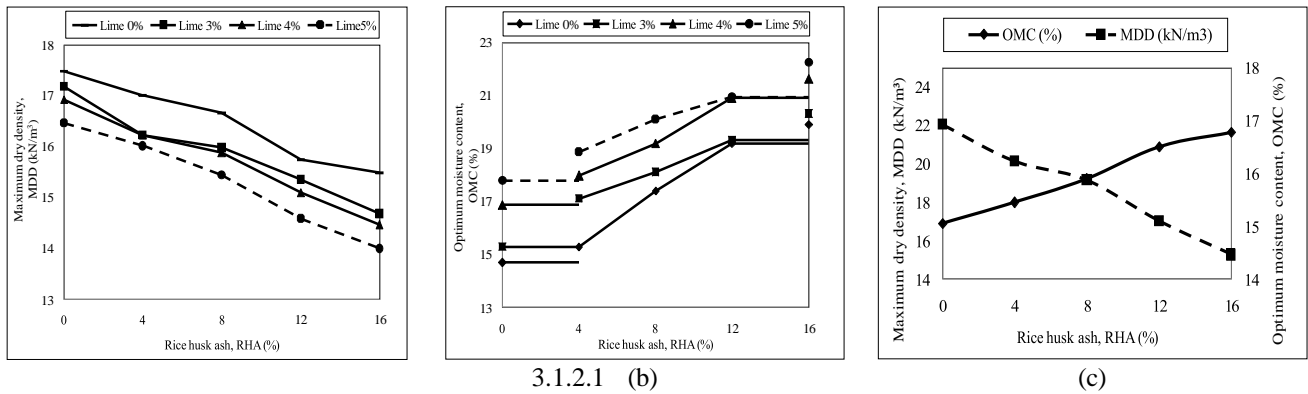


Figure 6: (a) Variation of MDD with RHA and lime (b) Variation of OMC with RHA and Lime (c) Variation of MDD and OMC with RHA (%) and 4% lime

3.1.3 VARIATION OF CALIFORNIA BEARING RATIO WITH ADMIXTURES

In the laboratory, stabilized soil with different admixtures like QD and RHA at varying mixing proportions and curing period was prepared. The CBR of stabilized soils was measured and the results of CBR of stabilized soils are hence discussed in the following articles.

3.1.3.1 Stabilized Soil with Quarry Dust and Lime

The results of CBR of stabilized soil with different mixing content of QD and lime at varying curing period of 0, 7 and 28 days is provided in Table 2.

Table 2: Results of CBR of stabilized soil with QD and lime at varying curing periods

QD content (%)	Lime content (%)	CBR (%) for different curing period (days)		
		0	7	28
0	2	28.70	33.34	57.66
10	2	32.92	40.21	69.30
20	2	35.17	45.32	73.20
30	2	38.86	51.31	78.65
40	2	42.82	61.10	87.25
50	2	40.36	56.64	81.89
0	4	29.03	44.67	62.12
10	4	30.12	46.21	73.55
20	4	39.80	53.78	79.00
30	4	53.68	62.32	87.81
40	4	77.54	83.27	98.26
50	4	66.35	74.50	91.22
0	6	28.87	39.80	59.89
10	6	31.52	41.14	71.50
20	6	37.48	44.77	76.22
30	6	46.27	59.55	83.50
40	6	60.18	74.19	91.75
50	6	53.35	69.13	87.21

Figure 7 shows the variation of CBR with different percentage of QD and lime at the curing period 0 days. It is observed that CBR goes on increasing up to 4% of lime, further decreases with adding lime. For a particular amount of lime, CBR increases with the increasing of QD in soil. The CBR increases up

to 40% of QD, further addition of QD decreases the values of CBR irrespective of the percentage of lime. The CBR increases to 77.54% from 28.70%, when the percentage of lime is 4%, QD is 40% and curing period is 0 days (Figure 7). The decline in CBR after a peak value at 40% QD may be connected with the decrease in the clay proportions which plays the role of the bonding agent at the lower percentage of QD. In addition, Figure 8 shows the variation of CBR with different percentage of QD and lime at the curing period of 7 days. It is observed that CBR goes on increasing up to 4% of lime, further decreases with adding lime with soil. For a particular mixing amount of lime content, CBR increases with the increasing of QD content. The CBR increases up to 40% addition of QD, further addition of QD decreases the CBR irrespective of the percentage of lime. The CBR increases to a value of 83.27% from 33.34%, when the percentage of lime is 4%, QD is 40% and curing period is 7 days.

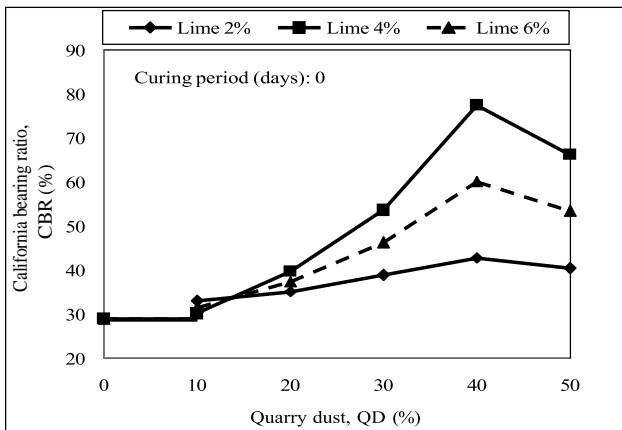


Figure 7: Stabilized soil with QD and lime at curing period of 0 days

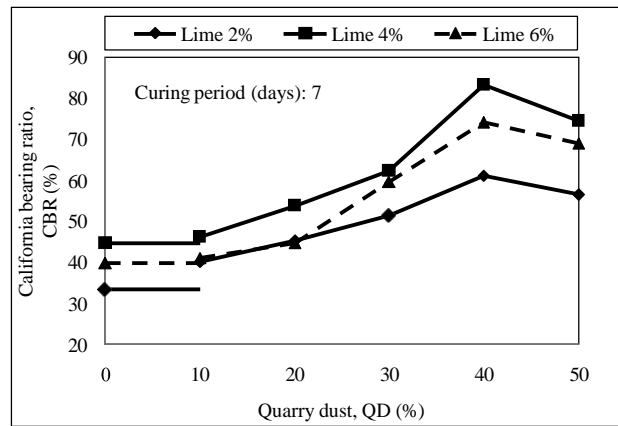


Figure 8: Variation of CBR of stabilized soil with QD and lime at curing period of 7 days.

3.1.3.2 Stabilized Soil with RHA and Lime

Figure 9 shows the variation of CBR of stabilized soil with different percentage of RHA and lime at the curing period of 0 days. It observed that CBR of stabilized soil goes on increasing up to 4% of lime, further decreases with adding lime with soil. For a particular mixing amount of lime content, CBR increases with increasing of RHA content in soil. The CBR increases up to 12% addition of RHA, further addition of RHA decreases CBR irrespective the percentage of lime. The CBR increases to a value of 50.1% from 5.1%, when the percentage of lime is 4%, RHA is 12% and curing period is 0 days as shown in Figure 9. The reason for increment in CBR may be because of the gradual formation of lime compounds in the soil by the reaction between the RHA and some amounts of CaOH present in soil and lime present. The decrease in CBR at RHA content of 16% may be due to extra RHA that could not be mobilized for the reaction which consequently occupies spaces within the sample. A research conducted by [12] stated that the CBR increases in relation to the increasing of RHA content in soil up. The result of this study agreed well with the researcher [12]. Figure 10 shows the variation of CBR of stabilized soil with different percentage of RHA and lime at the curing period of 28 days. It observed that CBR of stabilized soil goes on increasing up to 4% of lime, further decreases with adding lime with soil. For a particular mixing amount of lime content, CBR increases with the increasing of RHA content in stabilized soil. The CBR increases up to 12% addition of RHA, further addition of RHA decreases the CBR values irrespective of the percentage of lime. The CBR increases to a value of 58.41% from 13.43%, when the percentage of lime is 4%, RHA is 12% and curing period is 28 days as shown in Figure 10. The results of CBR of stabilized soil with RHA and lime depicted that the optimum content of RHA 12% was considered to get better CBR of stabilized soil for any curing period. The reason for increment in CBR may be because of the gradual formation of lime compounds in the soil by the reaction between the RHA and some amounts of Ca (OH)₂ present in soil and lime present.

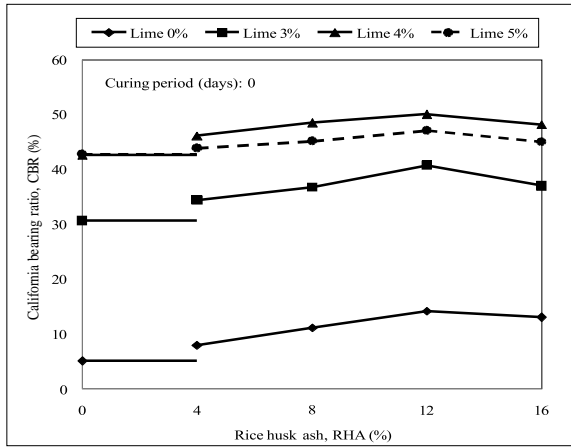


Figure 9: Variation of CBR of stabilized soil with RHA and lime at curing period of 0 days.

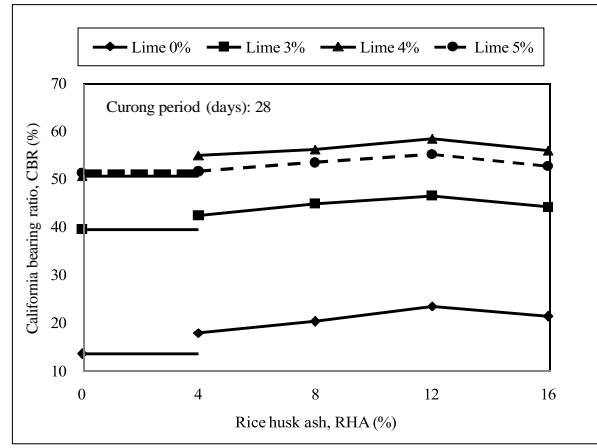


Figure 10: Stabilized soil with RHA and lime at curing period of 28 days

3.2 SOFT COMPUTING SYSTEMS

The soft computing systems like simple linear regression (SLR), multiple linear regressions (MLR), different algorithms of Levenberg-Marquardt neural network (LMNN), Bayesian regularization neural network (BRNN) and scaled conjugate gradient neural network (SCGNN) of ANN's back propagation as well as support vector machine (SVM) with different kernel functions like linear SVM (SVM-L), quadratic SVM (SVM-Q) and cubic SVM (SVM-C) applied for the prediction of CBR values of stabilized soils and hence discussed in the following articles.

3.2.1 SIMPLE LINEAR REGRESSION

In simple linear regression (SLR) analysis, QD (%), lime (%), CP (days), OMC (%) or MDD (kN/m³) as well as observed CBR considered as independent and dependent variables, respectively, of stabilized soil with QD and lime at different curing period of 0, 7 and 28 days. Moreover, RHA (%), lime (%), CP (days), OMC (%) or MDD (kN/m³) as well as observed CBR considered as independent and dependent variables, respectively, of stabilized soil with RHA and lime at different curing period of 0, 7 and 28 days.

3.2.1.1 Stabilized Soil with QD and Lime

In SLR analysis, QD (%), lime (%), CP (days), OMC (%) or MDD (kN/m³) as well as observed CBR considered as independent and dependent variables, respectively, at different curing period of 0, 7 and 28 days. After analysis, the value of R² was found at different curing periods depicted in Table 3. In Table 3, it is observed the best R² of 0.596 when independent variable of QD (%) and dependent variable as observed CBR (%) for curing period of 0 days. The best R² was found to be 0.722 when independent variable was QD (%) and dependent variable as observed CBR (%) for curing period 7 days. Similarly, for curing period 28 days, the best R² was found to be 0.798 with independent variable QD (%) and dependent variable as observed CBR (%).

Table 3: Performance analysis of SLR for stabilized soil with QD and lime at various curing period

Group	Dependent variable	Independent variables	R ² at varying curing period (days)		
			0	7	28
A	Observed CBR	lime (%)	0.037	0.04	0.018
B		QD (%)	0.596	0.722	0.798
C		OMC (%)	0.411	0.505	0.64
D		MDD (kN/m ³)	0.507	0.602	0.768

The predicted CBR of stabilized soil was correlated with all the variables independently and it was observed that CBR increases in relation to the increasing of QD (%) shown in Figure 11. The SLR analysis provided the best R^2 was 0.798 (shown in Group B) for curing period 28 days when QD (%) have taken as an independent variable. A researcher [7] stated that all the test results consisting of gravel, sand, fine grained, liquid limit, plastic limit, OMC or MDD as independent variable and CBR is dependent variable that's analyzed by statistical method of least regression. The best linear fitting approximation equations having maximum R^2 values are determined. Where independent variable used as FG, G and MDD separately on one dependent variable is CBR for different equations and plots. The findings of this study are agreed well with the results published by researcher [7].

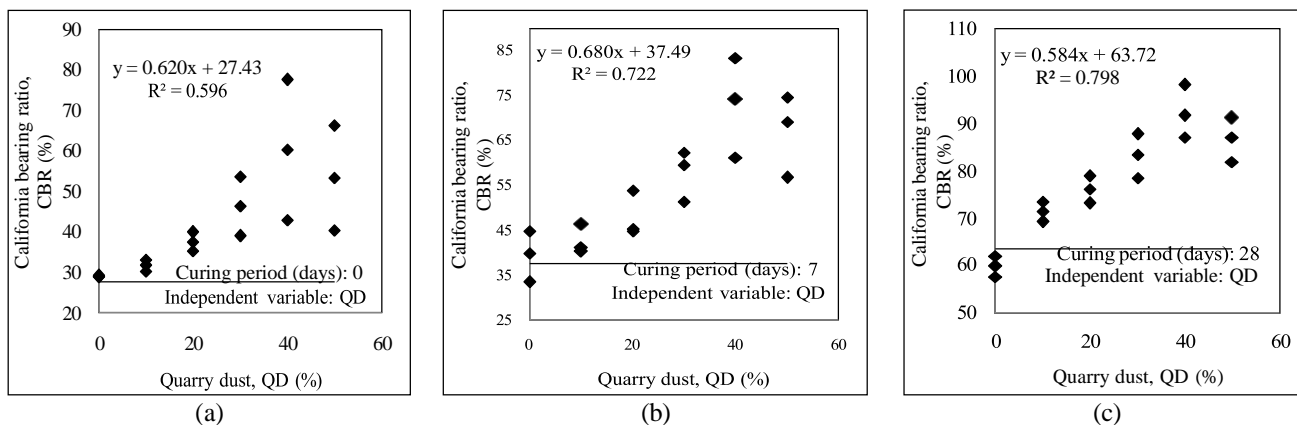


Figure 11: Changes of CBR with the variation of QD (%) in stabilized soils.

Table 4: Developed equations for predicting CBR of stabilized soils with QD and lime at varying curing periods

Correlation of predicted CBR	Equation No.	R^2	Curing period (days)	Figure No.
$CBR = 0.62 QD + 27.43$	3	0.596	0	Figure 11 (a)
$CBR = 0.68 QD + 37.48$	4	0.722	7	Figure 11 (b)
$CBR = 0.584 QD + 63.72$	5	0.798	28	Figure 11 (c)

In SLR analysis, the best linear fitting approximation equations having maximum value of R^2 were determined from the curing periods of 0, 7 and 28 days and can be expressed in Equations 3, 4 and 5, respectively. After analysis of SLR, the developed equations were selected as best based on R^2 for predicting CBR of stabilized soil with QD at varying curing periods provided in Table 4. From Table 4, it is clear that since best R^2 was found to be 0.798 by SLR analysis, therefore the best prediction of CBR at 28 days curing period can be determined by the Equation 5 where QD (%) has taken as an independent variable.

3.2.1.2 STABILIZED SOIL WITH RHA AND LIME

In SLR analysis, RHA (%), lime (%), CP (days), OMC (%) or MDD (kN/m^3) as well as observed CBR considered as independent and dependent variables, respectively at different curing period 0, 7 and 28 days. After analysis, the value of R^2 was found at different curing periods shown in Figure 12. From Figure 12 it is observed that, for 0 days curing the best R^2 is found to be 0.905 when independent variable is lime (%) and dependent variable as observed CBR (%). For curing period of 7 days, the best R^2 was found to be 0.901 when independent variable is Lime (%) and dependent variable as observed CBR (%). For curing period of 28 days, the best R^2 was found to be 0.908 when independent variable is Lime (%) and dependent variable as observed CBR (%).

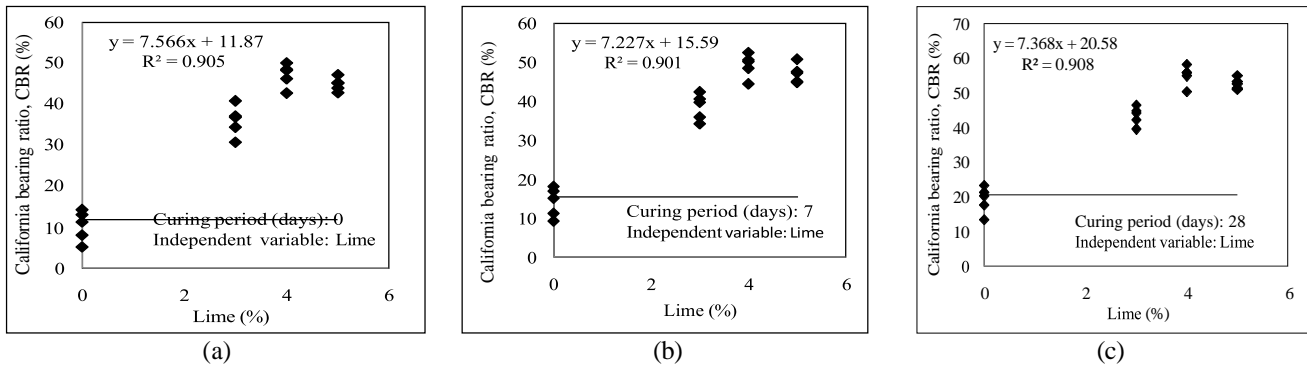


Figure 12: Changes of CBR with the variation of Lime (%) in stabilized soils.

In this study, in SLR analysis the best linear fitting approximation equations having maximum value of R^2 were determined from the curing periods of 0, 7 and 28 days and can be expressed in Equations 6, 7 and 8 respectively. After analysis of SLR, the developed equations were selected as best based on R^2 for predicting CBR of stabilized soil with RHA at varying curing periods provided in Table 5. Equation (8) can be taken as satisfactory for the prediction of CBR and more reliable equations need to be evolved for best values of R^2 .

Table 5: Developed equations for predicting CBR of stabilized soils with QD and lime at varying curing periods

Correlation of predicted CBR	Equation No.	R^2	Curing period (days)	Figure No.
$CBR = 7.566 \text{ Lime} + 11.87$	6	0.905	0	Figure 12 (a)
$CBR = 7.566 \text{ Lime} + 15.59$	7	0.901	7	Figure 12 (b)
$CBR = 7.566 \text{ Lime} + 20.58$	8	0.908	28	Figure 12 (c)

3.2.2 MULTIPLE LINEAR REGRESSION

In multiple linear regression (MLR) analysis, QD (%), lime (%), CP (days), OMC (%) and MDD (kN/m^3) as well as observed CBR considered as independent and dependent variables, respectively of stabilized soil with QD and lime at different curing period of 0, 7 and 28 days. Moreover, RHA (%), lime (%), CP (days), OMC (%) and MDD (kN/m^3) as well as observed CBR considered as independent and dependent variables, respectively of stabilized soil with RHA and lime at different curing period of 0, 7 and 28 days. The analysis of MLR for stabilized soils is described in the following articles.

3.2.2.1 STABILIZED SOIL WITH QD AND LIME

In MLR analysis, QD (%), lime (%), CP (days), OMC (%) and MDD (kN/m^3) as well as observed CBR considered as independent and dependent variables, respectively at different curing period of 0, 7 and 28 days. The results of R^2 by MLR analysis are provided at different curing period in Table 6.

Table 6: Performance analysis of MLR for stabilized soil with QD and lime at various curing period

Group	Dependent variable	Independent variables	R^2 at varying curing period (days)		
			0	7	28
A	Observed CBR	QD, lime, CP, OMC, MDD	0.663	0.787	0.872
B		QD, lime, OMC, MDD	0.663	0.787	0.871
C		Lime, OMC, MDD	0.628	0.741	0.870
D		QD, OMC, MDD	0.663	0.786	0.853
E		QD, lime, OMC	0.651	0.781	0.82
F		QD, lime, MDD	0.640	0.766	0.863
G		QD, lime,	0.633	0.763	0.817
H		OMC, MDD	0.533	0.619	0.792

The values of 0.663, 0.787 and 0.872 were found for R^2 at curing period of 0, 7 and 28 days for the independent variables in group A (QD, lime, CP, OMC, MDD). After that the independent variables were eliminated one or more and rearranged successively at various combination of variables designated as group B, C, D, E, F, G and H to get best R^2 of stabilized soils with QD and lime (Table 6). The MLR analysis was carried out by taking all the independent variables in consideration at first and thereafter eliminating one or more forming various combinations to get the best R^2 .

From Table 6, the selected best R^2 was 0.872 at curing period of 28 days in group A (QD, lime, CP, OMC, MDD) as compared to other groups of B, C, D, E, F, G and H. In addition, predicted model for CBR containing five variables and giving significant value of R^2 derived by MLR analysis is given by Equation (9), where MDD is in (kN/m³) and all other parameters are in %.

$$CBR = -262.723 + 2.322 * Lime - 0.333 * QD + 0 * CP - 0.214 * OMC + 18.839 * MCD \quad (9)$$

when R^2 is 0.872.

Equation (9) can be taken as satisfactory for the prediction of CBR and more reliable equations need to be evolved for better values of R^2 . Moreover, the best prediction of CBR at curing period of 28 days can be determined by use this equation.

3.2.2.2 STABILIZED SOIL WITH RHA AND LIME

In MLR analysis, RHA (%), lime (%), CP (days), OMC (%) and MDD (kN/m³) as well as observed CBR considered as independent and dependent variables, respectively at different curing period of 0, 7 and 28 days. The results of R^2 by MLR analysis are provided at different curing period in Table 7. The values of 0.949, 0.950 and 0.946 were found for R^2 at curing period of 0, 7 and 28 days for the independent variable in group A (RHA, lime, CP, OMC, MDD). After that the independent variables were eliminated one or more and rearranged successively at various combination of variables designated as group B, C, D, E, F, G and H to get best R^2 of stabilized soils with RHA and lime (Table 7).

Table 7: Performance analysis of MLR for stabilized soil with RHA and lime at various curing period

Group	Dependent variable	Independent variables	R ² at varying curing period (days)		
			0	7	28
A	Observed CBR	RHA, lime, CP, OMC, MDD	0.949	0.950	0.946
B		RHA, lime, OMC, MDD	0.949	0.949	0.946
C		lime, OMC, MDD	0.925	0.925	0.926
D		RHA, OMC, MDD	0.79	0.79	0.795
E		RHA, lime, OMC	0.93	0.931	0.927
F		RHA, lime, MDD	0.947	0.948	0.946
C		RHA, lime	0.928	0.929	0.927
D		OMC, MDD	0.34	0.351	0.331

From Table 7, selected the best R^2 is 0.95 for curing period of 7 days shows as group A (RHA, lime, CP, OMC and MDD) as compared to other B, C, D, E, F, G and H. In addition, the predicted model for CBR containing five variables and giving significant value of R^2 derived by MLR is given by Equations (10), where MDD is in (kN/m³) and all other parameters are in %.

$$CBR = -228.643 + 10.516 * Lime - 2.582 * RHA + 0 * CP - 0.366 * OMC + 13.918 * MCD \quad (10)$$

when R^2 is 0.95.

Equation (10) can be taken as satisfactory for the prediction of CBR and more reliable equations need to be evolved for best values of R^2 . Moreover, the best prediction of CBR at curing period of 7 days can be determined by use this equation.

3.2.3 ARTIFICIAL NEURAL NETWORK

In this study, ANN was performed on stabilized soil with different admixtures at varying curing periods. The ANN was implemented to select the best fitted model such as Levenberg-Marquardt neural network (LMNN), Bayesian regularization neural network (BRNN) and scaled conjugate gradient neural network (SCGNN). The number of hidden layers and neurons were varied to find out the best structure of ANN modeling. In order to compute the most appropriate ANN architecture for modeling, the number of neurons in the hidden were tried to predict the best CBR of stabilized soils. The number of hidden neurons in hidden layer was varied as 2, 4, 6, 8, 10, 12, 15, 20, 25 and 30. In this study, the hidden layer ranges from 2 to 30 provided the good results of R^2 . Moreover, when increased the number of neurons in hidden layer from 2 to 10 in interval 2, then increase R^2 consequently and hence discussed in the following articles.

3.2.3.1 STABILIZED SOIL WITH QD AND LIME

In this study, the algorithms of LMNN, BRNN and SCGNN through ANN model has been evaluated based on R^2 and OR to predict the CBR of stabilized soil with QD and lime. In ANN analysis, QD (%), lime (%), CP (days), OMC (%) and MDD (kN/m^3) as well as CBR (%) were considered as independent and dependent variable, respectively. To get the best performance of LMNN, BRNN and SCGNN, it has been eliminated one or more independently and rearranged at various combinations. The results of OR and R^2 of LMNN analysis are provided in Table 8. The values of 1.231 and 0.987 were found for OR and R^2 , respectively, for the independent variable in group A (QD, lime, CP, OMC, MDD). In addition, the values of 0.769 and 0.966 were found for OR and R^2 respectively, for the independent variables in group B (QD, lime, OMC and MDD). After that the independent variables were eliminated one or more and rearranged successively at various combination of variables designated as group C, D, E, F, G and H to get best R^2 of stabilized soils with QD and lime (Table 8).

Table 8: Performance of LMNN for stabilized soil with QD and lime

Group	Dependent variable	Independent variables	Mean square error (MSE)		Over fitting ratio (OR)	Determination coefficient (R^2)
			Training	Testing		
A	Observed CBR	QD, lime, CP, OMC, MDD	8.415	12.750	1.231	0.987
B		QD, lime, OMC, MDD	5.937	3.510	0.769	0.966
C		lime, OMC, MDD	4.218	3.293	0.884	0.945
D		QD, OMC, MDD	5.972	3.612	0.778	0.984
E		QD, lime, OMC	2.198	2.882	1.145	0.992
F		QD, lime, MDD	1.857	2.566	1.175	0.987
G		QD, lime	12.937	4.681	0.602	0.961
H		OMC, MDD	10.091	27.968	1.665	0.840

From Table 8, it can be observed that the group E (QD, lime and OMC) showed the best R^2 with 0.992 which is almost close to 1 with its best OR 1.145 (also close to 1). Therefore, group E (QD, lime and OMC) was considered as best of LMNN as compared to other groups of A, B, C, D, F, G and H. A research conducted by [17] stated that in the five different models the number of input as independent variables changes from seven to two and the target (dependent variable) was CBR as observed CBR. As well as the best model select depend on its OR and R^2 . The findings of this study are agreed well with the results postulated by [17].

3.2.3.2 STABILIZED SOIL WITH RHA AND LIME

The results of OR and R² of BRNN analysis are provided in Table 9. The values of 1.103 and 0.998 were found for OR and R², respectively, for the independent variable in group A (RHA, lime, CP, OMC, MDD). After that the independent variables were eliminated one or more and rearranged successively at various combination of variables designated as group B, C, D, E, F, G and H to get best R² of stabilized soils with RHA and lime (Table 9). From Table 9, it can be observed that the group A (RHA, lime, CP, OMC, MDD) showed the best R² with 0.998 which is almost close to 1 with its best OR 1.103 (also close to 1). Therefore, group A (RHA, lime, CP, OMC, MDD) is considered as best of LMNN as compared to B, C, D, E, F, G and H.

Table 9: Performance of BRNN for stabilized soil with RHA and lime

Group	Dependent variable	Independent variables	Mean square error (MSE)		Over fitting ratio (OR)	Determination coefficient (R ²)
			Training	Testing		
A		RHA, lime, CP, OMC, MDD	2.32	2.823	1.103	0.998
B		RHA, lime, OMC, MDD	4.564	3.441	0.868	0.996
C	Observed CBR	lime, OMC, MDD	1.849	2.83	1.237	0.992
D		RHA, OMC, MDD	12.398	6.847	0.743	0.948
E		RHA, lime, OMC	7.458	5.160	0.832	0.997
F		RHA, lime, MDD	7.117	4.268	0.774	0.969
G		RHA, lime	7.4	4.174	0.751	0.969
H		OMC, MDD	10.034	4.226	0.649	0.444

3.2.4 SUPPORT VECTOR MACHINE

The support vector machine (SVM) analysis is also an important part for the prediction of CBR of stabilized soil using two or more independent variable such as QD (%), lime (%), CP (days), OMC (%) and MDD (kN/m³) at different curing period of 0, 7 and 28 days. Other independent variable such as RHA (%), lime (%), CP (days), OMC (%) and MDD (kN/m³) as well as dependent variable CBR (%) (as observed CBR) at different curing period of 0, 7 and 28 days were also considered in SVM analysis. The SVM modeling was implemented to select the best fitted like Linear support vector machine (SVM-L), Quadratic support vector machine (SVM-Q) Cubic support vector machine (SVM-C). The analysis of SVM is discussed in the following articles.

3.2.4.1 STABILIZED SOIL WITH QD AND LIME

In this study, the performance of different kernel functions like SVM-L, SVM-Q and SVM-C through SVM model has been evaluated based on RMSE, R² and MAE. In SVM analysis, QD (%), lime (%), CP (days), OMC (%) and MDD (kN/m³) as well as CBR (%) were considered as independent and dependent variables (as observed CBR), respectively. To get the best performance of SVM-L, SVM-Q and SVM-C, it has been eliminated one or more independent variables and rearranged at various combination. The results of RMSE, R² and MAE of SVM-L analysis are provided in Table 10. The values for RMSE, R² and MAE were found as 5.38, 0.77 and 4.53, respectively, for the independent variables in group A (QD, lime, CP, OMC, MDD). In addition, the values of 5.34, 0.77 and 4.48 were found for RMSE, R² and MAE, respectively, for the independent variables in group B (QD, lime, OMC and MDD).

After that the independent variables were eliminated one or more and rearranged successively at various combination of variables designated as groups C, D, E, F, G and H to get best R² of stabilized soils with QD and lime (Table 10). From Table 10, it can be observed that the group E (QD, lime and MDD) showed the best R² with 0.79 which is almost close to 1 with its best RMSE 5.19 (lowest value) and MAE 4.24 (lowest value). Therefore, group E (QD, lime and MDD) was considered as best of SVM-L as compared to other groups of A, B, C, D, F, G and H.

Table 10: Performance of SVM-L for stabilized soil with QD and lime

Group	Dependent variable	Independent variables	RMSE	R ²	MAE
A	Observed CBR	QD, lime, CP, OMC, MDD	5.38	0.77	4.53
B		QD, lime, OMC, MDD	5.34	0.77	4.48
C		lime, OMC, MDD	5.25	0.78	4.32
D		QD, OMC, MDD	5.57	0.75	4.51
E		QD, lime, MDD	5.19	0.79	4.24
F		QD, lime, OMC	5.28	0.78	4.36
G		QD, lime	5.96	0.72	4.85
H		OMC, MDD	5.86	0.73	4.73

3.2.4.2 STABILIZED SOIL WITH RHA AND LIME

From analysis SVM-C, the results of RMSE, R² and MAE of SVM-C analysis are provided in Table 11. The values of 2.37, 0.97 and 2.00 were found for RMSE, R² and MAE, respectively, for the independent variable in group A (RHA, lime, CP, OMC, MDD). After that the independent variables were eliminated one or more and rearranged successively at various combination of variables designated as group B, C, D, E, F, G and H to get best R² of stabilized soils with RHA and lime (Table 11). From Table 11, it can be observed that the group A (RHA, lime, CP, OMC, MDD) showed the best R² with 0.97 which is almost close to 1 with its best RMSE 2.37 (lowest value) and MAE 2.00 (lowest value). Therefore, group A (RHA, lime, CP, OMC, MDD) is considered as best of SVM-Q as compared to B, C, D, E, F, G and H.

Table 11: Performance of SVM-C for stabilized soil with RHA and lime

Group	Dependent variable	Independent variables	RMSE	R ²	MAE
A	Observed CBR	RHA, lime, CP, OMC, MDD	2.37	0.97	2.0
B		RHA, lime, OMC, MDD	2.64	0.97	2.23
C		lime, OMC, MDD	2.41	0.97	2.17
D		RHA, OMC, MDD	8.93	0.62	7.42
E		RHA, lime, OMC	3.01	0.96	2.58
F		RHA, lime, MDD	2.94	0.96	2.32
G		RHA, lime	2.94	0.96	2.32
H		OMC, MDD	5.01	0.95	2.65

3.3 OPTIMUM CONTENT OF ADMIXTURES

In this study, the stabilized soils were prepared using QD with lime and RHA with lime. The values of maximum CBR for stabilized soil with QD (40%) and lime (4%) were obtained as 77.54, 83.27 and 98.26% at curing period of 0, 7 and 28 days respectively, provided in Table 12.

Table 12: Obtained results of CBR of stabilized soil with QD and RHA

Stabilized soils with	Optimum content of admixtures		CBR (%) at varying curing period (days)		
			0	7	28
QD and lime	QD (40 %)	Lime (4 %)	77.54	83.27	98.26
RHA and lime	RHA (12 %)	Lime (4 %)	50.1	52.5	58.41

Moreover, the values of maximum CBR were obtained of 50.1, 52.5 and 58.41% for stabilized soil with RHA (12%) and lime (4%) at curing period of 0, 7 and 28 days, respectively. The maximum CBR (98.26%) was found for stabilized soil with QD and lime at curing period 28 days than other mixing

content and curing periods used in this study. Therefore, the higher CBR was found for stabilized soil with QD and lime than that of stabilized soil with RHA and lime.

3.4 FINAL SELECTION OF MODEL OF THIS ANALYSIS

The values of R^2 were found as 0.798, 0.872, 0.995 and 0.90 for SLR, MLR, ANN and SVM, respectively, for prediction of CBR of stabilized soil with QD and lime (Table 13). Moreover, the values of R^2 were found as 0.908, 0.95, 0.998 and 0.97 for SLR, MLR, ANN and SVM, respectively, for prediction of CBR of stabilized soil with RHA and lime.

From stabilized soil with QD and lime, the best R^2 was found 0.995 from ANN analysis as compared to SLR, MLR and SVM analysis. Moreover, from stabilized soil with RHA and lime, the best R^2 was found 0.998 by ANN as compared to SLR, MLR and SVM analysis. Therefore, ANN modeling gets its superior priority as the best performer to predict CBR of stabilized soil using QD and lime as well as RHA and lime. A research conducted by [18, 19, 20] as well as found the best model of ANN as compared to SLR, MLR and SVM. That means, the findings of this study was near about the findings of both researchers. Finally, the findings of this research are clearly agreed with these research that conducted by [18, 19, 20].

Table 13: Final models for analysis of stabilized soil with admixtures

Admixture	R ² of SLR		R ² of MLR		R ² of ANN		R ² of SVM		Selected model	
	Present study	Literature	Present study	Literature	Present study	Literature	Present study	Literature	Present study	Literature
QD and lime	0.798	--	0.872	0.933	0.995	0.981	0.90	0.98	ANN	ANN
RHA and lime	0.908	0.624	0.95	0.882	0.998	0.985	0.97	--	ANN	ANN
Reference of literature	-	Bhatt et al., 2014	--	(Sabat, 2013) and (Bhatt et al., 2014)	--	(Sabat, 2013) and (Ali et al., 2016)	--	Sabat, 2015	--	Sabat, 2013

4.0 CONCLUSION

Result reveals OMC of stabilized soil with QD and lime decreases, while, OMC increases in case of stabilized soil with RHA and lime. In addition, MDD of stabilized soil with QD and lime increases, while, MDD decreases in case of stabilized soil with RHA and lime. The optimum content 40% and 4% was found for QD and lime, respectively, at varying curing periods to obtain better CBR of stabilized soil with QD and lime. Moreover, the optimum content of RHA was found 12% and lime of 4% at varying curing periods to obtain better CBR of stabilized soil with RHA and lime. The optimum contents of QD and RHA with lime can be used to stabilize soils with further trial. The result of ANN analysis reveals that QD, lime and OMC were the best independent variables for the stabilization of soil with QD, while, RHA, lime, CP, OMC and MDD for stabilized soil with RHA. In addition, SVM proved QD and lime as well as RHA, lime, CP, OMC and MDD were the best independent variables for the stabilization of soil with QD and RHA, respectively. The observed CBR and selected independent variables can be expressed by a series of developed equation of reasonable degree of accuracy and judgement from SLR and MLR

analysis. The model ANN showed comparatively the better values of CBR with satisfactory values of prediction parameters as compared to SLR, MLR and SVM for the prediction of CBR of stabilized soils. Therefore, the selected optimum content of admixtures and newly developed techniques of soft computing systems will further be used of other researchers to stabilize soil easily and then predict CBR of stabilized soils.

5.0 ACKNOWLEDGEMENT

The authors gratefully acknowledged the financial, logistics and technical support provided by Khulna University of Engineering & Technology (KUET), Khulna, Bangladesh for the completion of this research successfully. Special thanks to Engr. Animesh Chandra Roy, Post-graduate student, Department of Civil Engineering, KUET, for his valuable time and kind efforts throughout the research periods.

REFERENCES

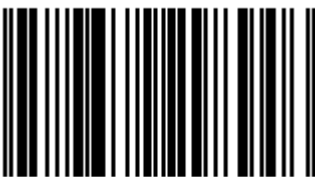
- [1] Venkatasubramanian, C. and Dhinakaran, G. 2011. ANN Model for Predicting CBR from Index Properties of Soils, *International Journal of Civil and Structural Engineering*, Integrated Publishing Association (IPA), 2 (2): 605- 611.
- [2] Joel, M. and Agbedi, I. 2011. Mechanical-Cement stabilization of laterite for use as flexible pavement material, *Journal of Material in Civil Engineering*, Vol.23, No.2, pp.146-152.
- [3] Hebib, S. and Farrell, E.R. 1999. Some Experiences of Stabilizing Irish Organic Soils. *Proceeding of Dry Mix Methods for Deep Soil Stabilization* (pp. 81-84).
- [4] Rajasekaran, G., and Narasimha Rao, S. 2000. Strength characteristics of lime-treated marine clay. *Proceedings of the Institution of Civil Engineers-Ground Improvement*, 4(3), 127-136.
- [5] Dash, S. K. and Hussain, M. 2011. Lime stabilization of soils: reappraisal. *Journal of materials in civil engineering*, 24(6), 707-714.
- [6] Taskiran, T. 2010. Prediction of California bearing ratio (CBR) of fine grained soils by AI methods, *Advances in Engineering Software*, Vol.41:886-892.
- [7] Bhatt, S., Jain, P. K., & Pradesh, M. 2014. Prediction of California Bearing Ratio of Soils Using Artificial Neural Network. *American International Journal of Research in Science, Technology, Engineering & Mathematics*, 156-16.
- [8] Sudhir, B. and Pradeep, K. J. 2014a. Prediction of California Bearing Ratio of Soils Using Artificial Neural Network. *American International Journal of Research in Science, Technology, Engineering & Mathematics*. ISSN (Print): 2328-3491, ISSN (Online): 2328-3580, ISSN (CD-ROM): 2328-3629.
- [9] Sudhir, B. and Pradeep, K. J. 2014b. Prediction of California Bearing Ratio of Soils Using Artificial Neural, *Transportation Research Record* (1219), 56-67.
- [10] Samui, P., Das, S. K. and Sabat, A. K. 2011. Prediction of field hydraulic conductivity of clay liners using an artificial neural network and support vector machine. *International Journal of Geomechanics*, 12(5), 606-611.
- [11] Afrin, H. 2017. A Review on Different Types Soil Stabilization Techniques. *International Journal of Transportation Engineering and Technology*, 3(2), 19.
- [12] Jay, p., Kusum. K. and Vijay, K. 2017. Stabilization of Soil Using Rice Husk Ash. *International Journal of Innovative Research in Science, Engineering and Technology*, Vol. 6, Issue 7, July 2017.
- [13] Rakaraddi, P. G., and Gomarsi, V. 2015. Establishing relationship between CBR with different soil properties. *International journal of research in engineering and technology*, 4(2), 182-188.
- [14] Smarten, (2018). The SVM Classification Analysis and How Can It Benefit Business Analytics. (Source, <https://www.elegantjbi.com/blog/what-is-svm-classification-analysis-and-how-can-it-benefit-business-analytics.htm>, October 16, 2018).
- [15] Rajkumar, C. and Meenambal, T. (2017). Artificial neural network modelling and economic analysis of soil subgrade stabilized with flyash and geotextile. *Indian journal of GEO Marine Science*. Vol. 46 (07), July 2017, 1454-1461.
- [16] Sarapu, D. 2016. Potentials of Rice Husk Ash for Soil Stabilization, *International Journal of Geomechanics*, 12(5), 606-611.
- [17] Al-Joulani, N. 2012. Effect of stone powder and lime on strength, compaction and CBR properties of fine soils. *Jordan Journal of Civil Engineering*, 6(1), 1-16.
- [18] Sabat, A. K. 2013. Prediction of California bearing ratio of a soil stabilized with lime and quarry dust using artificial neural network. *Electronic Journal of Geotechnical Engineering*, 18, 3261-3272.
- [19] Sabat, A. K. 2015. Prediction of California bearing ratio of a stabilized expansive soil using artificial neural network and support vector machine. *Electron. J. Geotech. Eng*, 20, 981-991.
- [20] Ali, B., Rahman, M. A., and Rafizul, I. M. 2016. Prediction of California Bearing Ratio of Stabilized Soil using Artificial Neural Network. *Proceedings of the 3rd International Conference on Civil Engineering for Sustainable Development (ICCESD 2016)*, (ISBN: 978-984-34-0265-3).

The book is based on scientific and technological advances in various Geotechnical and Geoenvironmental Engineering areas of Civil Engineering. It nurtures therefore the exchange of discoveries among research workforces worldwide including those focusing on the vast variety of facets of the fundamentals and applications within the Geotechnical and Geoenvironmental Engineering area. To offer novel and rapid developments, this book contains original contributions covering theoretical, physical experimental, and/or field works that incite and promote new understandings while elevating advancement in the Geotechnical and Geoenvironmental Engineering fields. Works in closing the gap between the theories and applications, which are beneficial to both academicians and practicing engineers, are particularly of interest to this book that paves the intellectual route to navigate new areas and frontiers of scholarly studies in Geotechnical and Geoenvironmental Engineering area.



UNIMAS
UNIVERSITAS Negeri Semarang
PUBLISHER

e ISBN 978-967-2298-94-6



9 7 8 9 6 7 2 2 9 8 9 4 6